ACKNOWLEDGMENTS

I would like to express my genuine appreciations to both of my supervisors Assoc. Prof. Dr. Nadim Copty and Assoc. Prof. Dr. Ali Kerem Saysel who have guided, supported and encouraged me during every stages of this study. I am really indebted to them for sharing generous time and vast knowledge with me.

I would like to thank my jury members Prof. Dr. Barış Mater, Prof. Dr. Orhan Yenigün and Assoc. Prof. Dr. Ömer Kara for their valuable comments and contributions on my thesis. I also acknowledge Assoc. Prof. Dr. Ömer Kara for all his generous support during both the field and laboratory work.

I would like to thank Dr. Abdurrahim Aydın from The Western Black Sea Forestry Research Institute, İlyas Bolat and Hüseyin Şensoy from Bartın University, Prof. Dr. Ali Ünal Şorman from Middle East Technical University, Assoc. Prof. Dr. Ömer Lütfi Şen, Dr. Abdusselam Altunkaynak, Dr. Erkan Bozkurtoğlu and Deniz Bozkurt from İstanbul Technical University, Assist. Prof. Dr. Orhan Sevgi, Dr. Barış Tecimen and Dr. Hasan Özdemir from İstanbul University, Mehmet Ali Küçüker from Boğaziçi University, Dr. Mehmet Çalıkoğlu from South West Anatolia Forestry Research Institute, Kemal Avşaroğlu and Serhat Sugeçti from Ulus Forestry Administration, Fatih Keskin and Selami Güzel from State Hydraulic Works, Yılmaz Aksoy from Private Administration of Karabük Province, Ali Yaşar and Osman Tüfekçi from Bartın Municipality who have helped me during the computational, field, laboratory and data gathering stages of this study.

The Research Fund of Boğaziçi University (B.A.P. 06HY102D) is acknowledged for the financial support.

I would like to thank my parents for their endless support over my whole education period. This study would have been difficult without them.

ABSTRACT

The Bartın spring watershed located in northwestern Turkey supplies the water needs of the Bartın, Amasra and İnkumu city centers. Although the water is presently adequate for the spring, autumn and winter seasons, the city centers suffer water scarcity in summer seasons.

It is widely recognized that land use changes have a significant impact on the water budget of a watershed. The purpose of this study is to model the land use and hydrological processes within the Bartın spring watershed and simulate the water yield under different future land use scenarios. For this purpose, a coupled land use-hydrodynamics model was developed. The land use dynamic simulation model was built using STELLA dynamic simulation platform while the MIKE SHE computer program was used to simulate the hydrodynamics of the watershed. The link between the two models is through the Leaf Area Index (LAI) and Root Depth (RD) parameters which are generated in the land use model and supplied to the hydrodynamics model.

The dynamic land use model represents several forest stand groups and land use categories with their respective acreages and their conversions. The model was structurally validated and analyzed through a series of sensitivity tests. It was calibrated with respect to the historical geographical data and the calibration results are quite satisfactory.

The calibration target for the hydrodynamics model was the river discharge at the downstream end of the watershed, while the calibration parameters were the saturated hydraulic conductivity of the deeper soil, the threshold melting temperature values and the RD value. The optimal simulation produced correlation coefficients, R=0.72 and R^2=0.52 with a mean error of 0.01 m^3/s. Sensitivity analyses of the hydrodynamics model indicate that it is quite sensitive to the land use type; complete agricultural cover would yield 25-33% higher discharge compared to a completely forested watershed. The hydrodynamics model is also sensitive to the LAI up to a value of 3 and becomes insensitive for higher values. The model however, is not strongly sensitive to hydraulic conductivity of the saturated zone.

To evaluate the impact of land use change on the water budget of the watershed, the calibrated land use-hydrodynamics model was used to simulate six different future land use scenarios over the period from 2006 to 2026. These six scenarios are the base case which assumes no change in current land use practices, agriculture to forest, forest to agriculture, deciduous and mixed to coniferous, coniferous and deciduous to mixed and coniferous and mixed to deciduous conversions. The conversion of coniferous and deciduous to mixed scenario is predicted to yield the highest average discharge with 5.19 m^3/s and the lowest evapotranspiration ratio of 66%. On the other hand, the conversion of agricultural areas to forest scenario is predicted to lead to the lowest average discharge of 4.54 m^3/s and highest evapotranspiration ratio of 71%. The monthly discharge lower than 1 m^3/s was assumed to be an indicator of low discharge. The scenario of agriculture to forest predicts that 52% of the dry summer months (August, September and July) have low discharge, whereas for the coniferous and deciduous to mixed scenario, only 27% of the dry summer months are predicted to have low discharge.

A long term simulation covering the years from 2026 to 2060 was also performed to assess the impact of global climate change on the water budget. The climate data which were generated using RegCM3 climate model predict a mean annual precipitation and temperature about 5.3% and 7.6% higher than the base case simulation. Results of the integrated land use-hydrodynamics model indicate an increase in the river discharge of about 15% and a decrease in the evapotranspiration of about 5% compared to the base case. In addition, higher maximum discharges and lower minimum discharges are also predicted indicating the watershed will be more susceptible to extreme discharge conditions in the future.

ÖZET

Türkiye'nin kuzeybatısında yer alan Bartın memba havzası, Bartın, Amasra ve İnkumu şehir merkezlerinin su ihtiyacını karşılamaktadır. Su, hâlihazırda ilkbahar, sonbahar ve kış mevsimleri için yeterli olmasına rağmen, şehir merkezleri yaz mevsimlerinde su kıtlığı çekmektedir.

Arazi kullanım değişimlerinin bir havzanın su bütçesi üzerinde önemli etkisi olduğu bilinmektedir. Bu çalışmanın amacı, Bartın memba havzası içerisinde arazi kullanım ve hidrolojik süreçleri modellemek ve geleceğe ait farklı arazi kullanım senaryoları altında su verimini tahmin etmektir. Bu amaçla, bütünleşik bir arazi kullanım-hidrodinamik modeli geliştirilmiştir. Arazi kullanım dinamik simülasyon modeli, STELLA dinamik simülasyon platformu kullanılarak oluşturulmuştur. MIKE SHE bilgisayar programı, havzanın hidrodinamiğini modellemek için kullanılmıştır. İki model arasındaki bağlantı, arazi kullanım modelinde üretilen ve hidrodinamik modele sağlanan LAI (Yaprak Alan İndisi) ve RD (Kök Derinliği) parametreleri sayesindedir.

Dinamik arazi kullanım modeli, çeşitli orman meşcere gruplarını ve arazi kullanım kategorilerini, yüzölçümleri ve dönüşümleri ile birlikte temsil etmektedir. Model yapısal olarak gerçeklenmiş ve bir dizi hassasiyet testleri ile analiz edilmiştir. Model, geçmiş coğrafik veriler dikkate alınarak kalibre edilmiştir ve kalibrasyon sonuçları oldukça tatmin edicidir.

Hidrodinamik model için kalibrasyonun hedefi, havzanın en son noktasındaki nehir debisidir. Kalibrasyon parametreleri ise alt toprak katmanlarının doygun hidrolik iletkenliği, eşik erime sıcaklığı değerleri, hava sıcaklığı ve kök derinlik değeridir. En uygun simülasyon, R=0.72 ve R^2=0.52 korelasyon katsayıları ve 0.01 m^3/s ortalama hata sonuçlarını üretmiştir. Hidrodinamik model ile yapılan hassasiyet analizleri, modelin arazi kullanım tipine oldukça hassas olduğunu göstermektedir. Şöyle ki, tamamen tarım alanları ile kaplı arazi kullanımı tamamen orman ile kaplı arazi kullanımına göre %25-33 daha fazla debi oluşturmaktadır. Hidrodinamik model, 3'e kadar olan Yaprak Alan İndisi (LAI) değerlerine hassasiyet göstermekte fakat daha yüksek değerlere karşı hassasiyetini

yitirmektedir. Bununla birlikte model, doygun bölgedeki hidrolik iletkenliğe karşı çok hassas değildir.

Arazi kullanım değişiminin havzanın su bütçesi üzerinde etkisini değerlendirmek için, kalibre edilmiş arazi kullanım-hidrodinamik modeli, geleceğe ait altı değişik arazi kullanım senaryosunu, 2006'dan 2026'ya kadar olan dönem için simüle etmek için kullanılmıştır. Bunlar, hâlihazır arazi kullanım uygulamalarında herhangi bir değişikliğin olmadığını kabul eden ana durum senaryosu, tarımdan ormana, ormandan tarıma, yapraklı meşcere ve karışık meşcereden ibreliye, ibreli meşcere ve yapraklı meşcereden karışığa ve ibreli meşcere ve karışık meşcereden yapraklıya dönüşüm senaryolarıdır. İbreli meşcere ve yapraklı meşcereden karışığa dönüşüm senaryosunun, 5.19 m^3/s ile en yüksek ortalama debiye ve %66 ile en düşük evapotranspirasyon oranına neden olduğu öngörülmektedir. Diğer taraftan, tarımdan ormana dönüşüm senaryosunun, 4.54 m^3/s ile en düşük ortalama debiye ve %71 ile en yüksek evapotranspirasyon oranına neden olduğu öngörülmektedir. Ortalama aylık debinin 1 m^3/s'nin altında kalması düşük debi işareti olarak kabul edilmiştir. Tarımdan ormana dönüşüm senaryosunun toplam kurak yaz aylarının (Ağustos, Eylül ve Temmuz) %52'sinde düşük debiye sahip olduğu öngörülürken, bu oranın ibreli meşcere ve yapraklı meşcereden karışığa dönüşüm senaryosunda sadece %27 olduğu öngörülmektedir.

Küresel iklim değişiminin su bütçesi üzerinde etkisini değerlendirmek için, 2006'dan 2060'a kadar olan yılları kapsayan bir uzun dönem simülasyonu gerçekleştirilmiştir. Bu dönem için, RegCM3 iklim modeli kullanılarak üretilen iklim verileri, ortalama yıllık yağışın yaklaşık %5.3 ve ortalama yıllık sıcaklığın yaklaşık %7.6 oranlarında ana durum tahmininden daha fazla olacağını öngörmektedir. Bütünleşik arazi kullanım-hidrodinamik model sonuçları, ana durum tahminine kıyasla, ortalama debinin yaklaşık %15 artacağını ve evapotranspirasyon oranının %5 azalacağını öngörmektedir. Bununla beraber, daha yüksek maksimum ve daha düşük minimum debiler öngörülmektedir. Bu da, gelecekte havzanın ekstrem akım koşullarına daha fazla maruz kalacağına işaret etmektedir.

TABLE OF CONTENTS

LIST OF FIGURES

LIST OF TABLES

1. INTRODUCTION

The sustainable management of a watershed is essential for the maintenance and protection of its water resources. The analysis and modeling of the hydrological processes that govern the fate and transport of water within a watershed is fundamental for achieving the sustainability of a watershed. As a result of the rapid development in computational methods and hardware, mathematical models that can simulate the hydrological processes occurring within a watershed and their interrelation have become valuable tools towards realizing this goal (Singh and Frevert, 2006).

The spatial and temporal dynamics of land use are important factors that strongly influence the hydrological processes within a watershed. Most of the mathematical models simulating the hydrological processes within the watershed involve land use and its dynamics. Until recently simple empirical expressions describing the relation between land use type and evapotranspiration have been typically incorporated in hydrodynamic models. These relationships often do not adequately represent the spatial, seasonal and long term variations of the land use changes and their impact on the watershed hydrology.

In this study, we develop a framework for the integration of land use dynamics with a spatially distributed surface-subsurface hydrological model. The model is developed for the Bartın spring watershed, a small rural watershed located in the northwestern Turkey. The model is used to evaluate present conditions as well as various future scenarios that account for different land use conversions, global climatic change, and forest management practices.

1.1. Watershed and the Hydrological Cycle

A watershed is an area of land that captures water in any form, such as rain, snow or dew, and drains it to a common water body such as a river, stream, lake or groundwater (DeBarry, 2004). The boundary of a watershed is principally defined by the water allocator lines which are mostly the crests of the hills surrounding the watershed (Özhan, 2004). The

forms of the watersheds differentiate based on the characteristics of the water resource, topography and the geology.

The physical components of a watershed include particularly the climatic conditions (precipitation, temperature etc.), land use types, soil properties, geological formations and water resource characteristics. Precipitation is mainly in the form of rainfall or snow. The land use components of a watershed may either be vegetation such as agriculture, forest and pasture or settlement such as urban and village or the extreme case an industry. The soil characteristics are principally defined by the geological formations of the watershed. The stream, pond and groundwater are the forms of the water body within the watershed.

The interaction between the atmosphere, land and the ocean generates the hydrological cycle. The watershed hydrological processes are precipitation, interception, evapotranspiration, overland flow, infiltration, subsurface flow, groundwater flow and the stream flow. Precipitation in the form of rainfall, snow and dew makes contact first with the vegetation or the land surface. The direct precipitation on the land surface is referred to as the throughfall (Raudkivi, 1979). The precipitation on the vegetation either evaporates from the leaves or drips down reaching ultimately the land surface. At the land surface, precipitation may infiltrate, evaporate or flow overland. The infiltration into the soil lasts until the soil is saturated which then leads to overland flow. The topography, soil and the land cover characteristics are the key factors controlling the infiltration and overland flow processes. Overland flow may either reach to a surface water body such as gully, stream, pond or sea or infiltrate into the unsaturated soil. The vegetation uptakes part of the soil water and transfer it to the atmosphere by transpiration. The soil water may also evaporate directly to the atmosphere. The evaporation from the soil surface and the canopy surface together with the vegetation transpiration is known as evapotranspiration. The soil water flowing in vertical and horizontal directions ultimately contributes to water resources such as stream, pond and groundwater (Chow et al., 1988).

1.2. Aim of the Study

Bartın spring watershed located in northwestern Turkey covers approximately 287 km^2 area. The watershed is draining into a spring water reservoir located on the 34^{th} km of

the Bartın-Safranbolu road. This spring water reservoir is supplying the water demand of the city centers of Bartın, Amasra and İnkumu. The spring water reservoir is the main water resource feeding the city centers of Bartın, Amasra and İnkumu.

The aim of this study is to determine the present water yield and simulate the possible future water yield capacity of the watershed. The hydrological evaluation and scenario analysis for the improvement of this capacity is the main target of this study. A comprehensive hydrodynamic model that considers the main physical characteristics of the watershed will support the hydrological evaluation and scenario analyses. For these purposes, an integrated land use-hydrological model for the Bartın spring watershed is developed.

The spatial hydrodynamic model is constructed using the MIKE SHE software (Refsgaard, 1997). The land use is one of the most significant physical components of hydrological cycle affecting the interception and evapotranspiration within the watershed. For this reason, the developed model considers the hydrodynamic processes together with the land use dynamics. Land use is modeled using the STELLA software (H.P.S., 2001). Both models are supported by a Geographical Information Systems (GIS) framework produced by Arc-Info 9.1 software (ESRI, 2005).

1.3. Watershed Land Use and Hydrology

Land use is one of the most important physical components that influence the hydrological processes within the watershed. The possible land use types within a watershed are generally forest, agriculture, pasture, settlement. These land use types determine the characteristics of interception, evapotranspiration, infiltration, overland flow, subsurface flow and consequently the stream channel flow and groundwater flow.

The land cover may be in the form of vegetation, bare surface or impervious surface. Forests, agricultural crops, pastures are examples of vegetation, whereas urban and village settlements or industrial buildings are examples of impervious surface. Also there may be bare surfaces among vegetation which may have been formed as a result of degradation of the vegetation cover such as forest open spaces. Agricultural crops and pastures intercept

part of the precipitation by their leaves and stems and contribute to the evapotranspiration processes during their growing seasons. The evergreen coniferous and broadleaf forests intercept precipitation over the whole year. Therefore, they contribute to the loss of water to the atmosphere by evaporation of intercepted precipitation and transpiration. However they reduce soil water evaporation by shading the soil with their canopy. The deciduous needleleaf and broadleaf forests, on the other hand have a seasonal impact on the interception, evaporation and transpiration processes. In this respect, deciduous forests are similar to agricultural crops and pastures.

The vegetation cover supports water infiltration into the soil both by reducing the impact velocity of precipitation with their canopy and by increasing the porosity of soil through their root systems. The slowed precipitation reaches the land surface at intervals delaying the rapid saturation of soil. The increased infiltration decreases the overland flow and consequently the stream channel flow. On the other hand, hard surface is a bare surface where precipitation directly reaches without being intercepted or slowed. The evaporation from impervious surface is like the evaporation from the open water source. Since infiltration almost does not occur, overland flow rapidly starts, leading to a water resource such as a stream or pond. Therefore urban or village settlements and industrial areas pose considerable risks for the rapid concentration of stream flows. The stream flow runs off to rivers and seas.

The significant role of land use within the hydrological cycle makes it a key component in water resources problems such as water yield estimation, watershed hydrologic modeling studies, rainfall-runoff and stream channel studies. Over the past decade Remote Sensing (RS) and Geographical Information Systems (GIS) techniques have developed important tools that can assist the spatial and temporal analysis of existing land use and land use change. GIS and RS have also become widely supplementary tools for the spatial description and analysis of watersheds and the development of hydrological models.

1.4. Literature Review

The purpose of this study is to evaluate the impact of the land use dynamics on the spring watershed hydrology. The analysis of this impact together with the future scenario simulations are achieved by development of an integrated land use-hydrologic model. In this section, relevant studies are reviewed. These studies are classified in three groups:

- Studies that focus on the impact of land use and its changes on the watershed hydrology.

- Studies that use MIKE SHE model.

- Studies that use a system dynamics approach for the water resources management problems.

1.4.1. Impact of Land Use on Hydrology

During the last ten years, several studies have investigated the relation between land use and hydrological processes. Most of them focus on the land use influence on watershed hydrology. Some of these studies evaluate the effect of existing land use while others investigate the effect of land use change on the watershed hydrology. In this section, most relevant studies are briefly described. These studies can be broadly divided into two groups: those which assessed the impact of land use on watershed hydrology through field observations and those involving numerical modeling studies.

Beighly and Moglen (2002) evaluated the effect of urbanization on the annual maximum discharges in the urbanizing watersheds of the U.S.A. They observed that the urbanized watersheds had led to increase in the annual maximum discharges.

Several published studies have analyzed the impact of land use change on the watershed hydrology. For example, Costa et al. (2003) studied the effect of land use change between 1949 and 1998 on the stream discharge in Southeastern Amazon. The ratio of the agricultural areas within the cropland and pasture basin increased from 30% to 49%.

This increment led to the 24% increment of mean annual discharge and to the 3.4% decrease of mean annual evapotranspiration.

Wissmar et al. (2004) analyzed the effect of forest decrease and impervious surface increase on discharge rates of a river in U.S.A between 1991 and 1998. They pointed out to the larger discharge rates in urban watersheds which lost part of the forests (range between 3-24%) and gained (range between 4-27%) impervious surfaces. The discharge rates also increased in rural areas which lost part of the forest (range between 4-14%) and gained (38-60%) impervious surfaces.

Wei et al. (2005) studied the impact of forest practices such as clear cutting and reforestation on the hydrology of Chinese forest. They reviewed the key findings of the measurements over the past 20 years in China such as rainfall interception, stream flow, stemflow, evapotranspiration and the impacts of forest management practices. Reducing the coverage of oak stands from 90% to 60% by thinning decreased the interception from 20% to 15.2%. The oak stemflow was 15.5% while the fir stemflow was less than 1%. The evapotranspiration was in the range of 40 to 90%. Forest harvesting increased peak stream discharges by 50% in small basins and 100% in large basins.

Yue and Hashino (2005) analyzed the impact of forest growth on stream flow in Japan for the period between 1953 and 1994. They found that the annual maximum daily flow, annual minimum five-day flow and annual total runoff decreased by 55.8, 75.8 and 39.6% respectively. However the annual precipitation and temperature did not increase. These results show that the forest growth is responsible for the decrease in the flow regimes.

Zhang and Schilling (2006) analyzed the effect of land use change on the stream flow and baseflow in Mississippi River since 1940s. They observed that the conversion of perennial vegetation to seasonal row crops such as soybeans had reduced the evapotranspiration, increased the groundwater recharge and thus increased baseflow and stream flow.

Molina et al. (2007) used a rainfall simulator to analyze the surface runoff response of land use types to intense rainfall. The degraded and abandoned lands produced surface runoff within a few minutes while surface runoff was rare for the arable and rangelands.

Buytaert et al. (2007) studied the effect of afforestation and cultivation in two catchments in southern Ecuador and compared the results with the natural grassland catchments. The water yield reduced 50% in the afforested catchment whereas the water yield from the cultivated catchment was similar to that of the natural grassland catchments. However, faster response of flow and loss of baseflow occurred in the cultivated catchment compared to the natural grassland catchments.

Chaves et al. (2008) analyzed the effects of forest clearing and conversion to cattle pasture in the lowland of Amazon region. For the forest watersheds, the throughfall, groundwater and soil water was 57%, 24% and 19% of the stream flow respectively. The througfall, groundwater and soil water was 60%, 35% and 5% of the stream flow respectively for the pasture watersheds.

Recently a number of studies developed numerical models to evaluate the impact of land use on the watershed hydrology. These hydrological models differ based on their spatial aggregation levels such as lumped, semi distributed and fully distributed. The hydrological models also vary according to their complexity such as simple, semi integrated and fully integrated.

The studies by Sun et al. (1998), Karvonen et al. (1999) and Liu et al. (2006) used simple hydrological models to investigate the impact of actual land use on the watershed hydrology. These simple hydrological models are generally lumped or semi distributed.

Sun et al. (1998) developed a model, FLATWOODS, evaluating the hydrological effects of forest management. They applied this model to flatwood sites in the US under three harvesting treatments (cypress wetlands harvesting, pine uplands harvesting and wetlands+uplands harvesting) and three climate years (dry, wet and normal). The simulations demonstrated that under any climate year, runoff increased the most under wetlands+upland harvesting. Under the normal and wet years, runoff increased the least for

pine upland harvesting and under dry year, runoff increased the least for cypress wetland harvesting. A similar response was also observed for the groundwater table rise except that pine upland harvesting had the least under any climate year. The evapotranspiration reduction occurred the most for wetland+upland harvesting except under the wet year while the least for upland harvesting under any climate year.

Karvonen et al. (1999) developed a simple hydrological model which predicted the land use influence on rainfall-runoff processes. Their model is based on subdivision of the catchment into hydrologically similar units which aggregate areas with similar land use, soil, slope and vegetation characteristics. They tested and calibrated their model for a catchment in Finland targeting daily river flow. The coefficient of determination was 0.74 and 0.70 for two and three years of calibration periods respectively.

Similarly, Liu et al. (2006) applied a grid-based physical-conceptual hydrological model, WetSpa to a river basin in Luxembourg. They simulated the storm runoff contributions from land use types such as urban, forest, pasture and agriculture. The surface runoff from urban, agriculture and pasture was 39.1%, 11.6% and 9.0% of the total storm runoff respectively whereas interflows from forest, pasture and agriculture was 16.7%, 8.8% and 7.5% of the total storm runoff respectively. Surface runoff from water surfaces and forest areas was 7.2% of the total storm runoff.

Kim et al. (2005) developed a conceptual grid-based hydrological model to analyze the impact of land use change on stream flow in South Korea. Therefore they used three Landsat TM satellite images belonging to 1986, 1994 and 2002. The increase in urban areas was 5.4% while the decrease in the paddy fields and forest was 4.6% and 3.4% respectively. According to the results of the simulation, the runoff generation change ratios were 14.3%, -9.8% and -6.7% for the urban areas, paddy fields and forest respectively.

Siriwardena et al. (2006) studied the impact of conversion of forest to grassland and cropland on the runoff generation in a large river catchment in Australia. They used a simple conceptual daily rainfall-runoff model SIMHYD for this purpose. According to the simulation results, the clearance of the forest had generated 40% increase in the runoff.

Notter et al. (2007) used a simple semi distributed grid-based water balance model NRM3 to predict the discharge in mesoscale catchment in Kenya. According to their scenario simulation with the model, the conversion of the forest area to cropland and grassland led to 11% and 59% increase in annual runoff respectively.

Besides these simple hydrological models, some researches used more complex semi-distributed and distributed models during their analysis of the land use impact on the watershed hydrology. Some of these studies are based on the influence of actual land use while the others are on the effect of land use change on the watershed hydrology. The studies by Fleischbein et al. (2006) and Costa-Cabral et al. (2008) focused on the actual land use impact on the watershed hydrology. The studies by Luijten et al. (2000), Wang et al. (2008), Choi and Deal (2008), Cuo et al. (2008), are examples of the studies which investigated the effect of land use change on the watershed hydrological processes.

Fleischbein et al. (2006) calculated the water budgets of three small catchments on the slope of montane forest in Ecuador between 1998 and 2002. They used field measurements indicating that the average annual precipitation, interception, throughfall, and stemflow was 2504 mm, 1006 mm, 1473 mm and 25 mm respectively. Based on these measured data surface flow was calculated by a semi-distributed catchment model, TOPMODEL as 1039mm. The resulting was the mean evapotranspiration as 1466 mm of which 32% (471) was transpiration.

Costa-Cabral et al. (2008) used the VIC hydrological model to simulate the influence of land cover on the hydrological processes in a river basin in China. According to the results of their study, the rainfall interception and evapotranspiration rates were higher for the forests which had high LAI compared to the agricultural and grassland areas.

Luijten et al. (2000) developed the Spatial Water Budget Model (SWBM) to analyze the water availability within a river basin in Colombia. The basin is mainly composed of forest, bushes, crops and pasture. They simulated the impact of the land cover changes on stream water availability. According to their simulation results, compared to the actual land use simulation, the evapotranspiration was 4.6% lower and consequently the water yield increased nearly 5% for the complete cropland simulation. In the complete forest

simulation, the annual evapotranspiration increased about 13% and average river flow decreased about 15%. For the complete bare soil simulation, the annual evapotranspiration reduced about 45% while the average river flow increased about 49%.

Wang et al. (2008) used the Soil and Water Assessment Tool (SWAT) model to analyze three different land use and climate change scenarios. According to the results of the first scenario which assumed the conversion of all the current grassland into forest land, the mean annual stream flow reduced by 6.9 mm (2.3%). The second scenario assumed that 25% of the current grassland would be shifted to forest land. The mean annual stream flow declined by 0.2 mm (0.01%). The third scenario considered that all the current forest land would be converted into grassland which led to the 3.4% increase in the stream flow.

Choi and Deal (2008) connected a cellular, dynamic, spatial urban growth model (LEAMluc) with the semi-distributed continuous hydrology model using the Hydrological Simulation Program-Fortran (HSPF). Their aim was to predict the impact of the urban growth on the stream flow in a river basin in U.S.A. According to their simulation results, they hardly could recognize an increase in the mean runoff and mean surface flow.

Vanshaar et al. (2002) conducted a study within four catchments of the Columbia river basin using the Distributed Hydrology-Soil Vegetation Model (DHSVM). They simulated the hydrologic effects of land cover changes for the period between 1900 and 1990. The vegetation became younger during this period as a result of logging, fires and grazing. The deciduous trees disappeared during the 90 years. Consequently, the LAI apparently increased within the 90 years except for one catchment. Relatively the stream flow generally decreased while the evapotranspiration plus the snow vapour flux increased.

Similarly, Thanapakpawin et al. (2006) analyzed the effects of the land use change on the hydrology of a river basin in Thailand using the DHSVM model. They developed future scenarios of expansion of forest to crop areas and a scenario of crop to forest reversal for the period between 1989 and 2000. According to the results of their scenario analysis, the expansion of the croplands increased the dry-season flow by about 4% and

slightly increased the wet season flow. On the other hand, the wet and dry season flows diminished under the scenario of cropland conversion to forests.

Cuo et al. (2008) used the DHSVM model to predict the effect of urbanization on the average daily peaks for a creek watershed in U.S.A. for a period between 1915 and 2002. According to the results of their study, the annual maximum daily flow increased about 3.1 fold for the urbanized watershed in between 1915 and 2002.

The literatures investigating the impact of either the actual land use or the land use change on the watershed hydrology using simple, conceptual, discrete, lumped, semi-distributed or fully distributed generally agree that the forest cover lead to less stream flow and higher evapotranspiration compared to other land use types such as agriculture, pasture, grassland and urban areas. However, it is hard to make an apparent distinction between the land use types for their influence on groundwater because of the variable effects of the evapotranspiration on the groundwater. On the other hand, among the land use types of agriculture, pasture and grassland, the order of the stream flow generation capacity changes based on the vegetation types and species of these lands. Urban areas are very sensitive to the generation of the stream flow because of the relatively abundance of bare surfaces.

Few of the hydrological models integrate both the surface and groundwater conditions. MIKE SHE is one of the few physical and spatially fully distributed models which integrate both the surface and the subsurface hydrological processes. MIKE SHE was developed and improved by the Danish Hydraulic Institute. It is a common and widely used alternative of its class (DHI, 2005). Many researches used MIKE SHE modeling system during their hydrological modeling studies. The relatively most relevant studies with MIKE SHE modeling system are discussed in the next subsection.

1.4.2. Hydrological Modeling Using MIKE SHE

Several studies have tested the physical distributed hydrological model, MIKE SHE for the investigation of the hydrological processes. Some of these studies focused on the parameterization, calibration and validation of the model such as by Refsgaard (1997),

Madsen (2003) and Henriksen et al. (2003) while others have done sensitivity tests with the model such as by Vazquez and Feyen (2007).

Refsgaard (1997) calibrated and validated the MIKE SHE code by applying it to a mesoscale catchment in Denmark. The calibration and validation target of his modeling study was the observations of the catchment discharge sites and the piezometric heads. The calibration and validation was satisfactory indicating that the R^2 of the observed and simulated discharges range between 0.68 and 0.78. The simulated piezometric heads were also consistent with the observed ones. The results also suggested that the maximum grid resolution for the interpolation of the model parameters should be 1000 m.

A similar study was conducted by Madsen (2003) for the same catchment in Denmark. He tried to formulate a consistent framework for the estimation of the MIKE SHE model parameters using automatic calibration. According to the results of his simulations, the Pareto optimum solution provided better runoff simulations compared to the manual expert calibration. The same performance was not valid for the simulations of the groundwater level.

Henriksen et al. (2003) summarized the methodology for the construction, calibration and validation of a hydrological model for the whole of Denmark. They chose a grid resolution of 1 km^2. They briefly described the modeling processes together with the problems associated.

Vazquez and Feyen (2007) investigated the effect of digital elevation models (DEM) gridding on the basin runoff predictions. The authors used coarse DEMs with a 600 m resolution and gridded from a set of elevation points geographically distributed with a much finer resolution. They tried to assess the effects of DEM generation methods on model parameter values, model global prediction accuracy and evaluation of internal state predictions. They applied three types of gridding methods. The first method was based on the MIKE SHE bilinear interpolation tool. The second method considered the input elevation data which were distributed about the centre of the gridded DEM cells. For the third method, they used TOPOGRID algorithm which involves landscape features.

According to the results of their simulations with the three methods, the accuracy order of the methods was second, third and the first.

There are also some other studies which used MIKE SHE modeling system for the discrete modeling processes. In the literatures, MIKE SHE modeling system was also used for the prediction of the evapotranspiration which is necessary for the agro-hydrological and cropping purposes. The studies by Boegh et al. (2004) and Islam et al. (2006) are some of the examples.

Boegh et al. (2004) investigated the soil water balance and vegetation growth relationship by coupled MIKE SHE with a vegetation-SVAT model (Daisy) which simulates the soil, vegetation and atmosphere together with the plant structure and function. According to the results of their model coupling, the modeling units which are homogeneous with respect to the Leaf Area Index (LAI) necessitate disaggregation of the land use classes with respect to the temporal development of the vegetation cover.

To analyze the effects of the cropping practices on water balance variables such as evapotranspiration and recharge, Islam et al. (2006) conducted experimental study in U.S.A. together with the hydrological model MIKE SHE. According to the results of their experimental study, the cropping practices did not significantly influence soil water content compared to the crop rotation and soil spatial variability. However, the simulation results indicated that winter cover cropping would not be useful in semiarid regions.

Some studies applied the MIKE SHE program for the analysis of case studies. Sahoo et al. (2006) applied the MIKE SHE modeling system to a stream watershed in Hawaii. They used the stream flow data collected at 15 minute intervals for the calibration of their model. They used the single-valued hydraulic conductivity for the saturated zone. According to the results of their calibration, the correlation coefficients were greater than 0.7. The shape of the flood peaks were mainly affected by both the vertical and horizontal conductivities. Changing the Manning's roughness M from 60 to 10 reduced the peak stream flow by about 1 m^3/s.

McMichael and Hope (2007) investigated the effects of fire size on seasonal and annual stream flow for a mesoscale basin in the U.S.A. They used the MIKE SHE model calibrated and tested with GLUE (Generalized Likelihood Uncertainty Estimation) methodology. They made model simulations for wet and dry regimes. According to the results of their study, both the seasonal and annual stream flow increased almost linearly with fire size under both wet and dry regimes. Large fires led to more stream flow than smaller fires. Total cumulative stream flow under the dry weather regime was lower than for the wet regime for all fire size scenarios. After the fire, the stand age and consequently the LAI increased and stream flow decreased.

To quantify the accumulated hydrologic effects of watershed management in China, Zhang et al. (2008) evaluated the performance of MIKE SHE. They simulated the basin runoff, calibrated and validated the model using the observed stream runoff for the periods between 1983 and 1985 and between 1989 and 1991 respectively. According to the results of their calibration and validation, the correlation coefficient for the first calibration period and the second validation period were 0.83 and 0.63 respectively.

Mernild et al. (2008) applied the MIKE SHE model to simulate the annual discharge from the snow and glacierized mesoscale river basin in Greenland. They coupled snow modeling system (SnowModel) to the MIKE SHE program. Three discharge simulations were conducted for the periods between 1997 and 2001 (calibration), 2001 and 2005 (validation) and 2071 and 2100 (scenario). The simulation results were generally in accordance with the observed data (R^2=0.58). However, there were discrepancies between the simulated and observed discharge hydrographs. For the future simulations, the mean annual runoff was expected to be 1.5 orders of the magnitude greater than from today.

A number of studies used the MIKE SHE modeling system for groundwater simulations and irrigation planning. Jayatilaka et al. (1998) analyzed the hydrological processes influencing the surface drainage and groundwater levels within a small experimental irrigation site in Australia. For this purpose, they used MIKE SHE model and calibrated the model with the observed piezometric levels, drain flow and soil moisture for the 19 month period between 1991 and 1992. The correlation coefficient R^2 for the piezometric levels changed between 0.86 and 0.92. However, the model was inadequate in

simulating the rapid flow through the macropores due to soil cracking and swelling properties.

Singh et al. (1999) used the MIKE SHE model to simulate the water balance of a small watershed in India for the main cropping season between July and October and second cropping season between November and February. Their target was to construct an irrigation plan for the watershed. As a result of their simulation, for the first main cropping season, they determined the necessity of irrigation which is 490 mm for the upstream and 340 mm for the downstream. For the second cropping season, there was excess water that could be stored in the tank and would possibly be used for the supplemental irrigation.

Demetriou and Punthakey (1999) developed a hydrogeological model with MIKE SHE for simulating the temporal and spatial dynamics of the water table in an irrigation district of Australia. The target was to propose sustainable water management policies for the district. They analyzed the scenarios for the management options such as on-farm recycling pond application with laser leveling, deep-rooted perennials, tree planting, installation of deep groundwater pumps and shallow groundwater pumping. According to the result of the scenario simulations, they concluded that the best management option was shallow groundwater pumping.

There are published studies which integrated MIKE 11, a hydraulic modeling tool with the MIKE SHE program. The integration of the two models allow more detailed representation of the channel flow together with the hydraulic structures such weirs, gates, bridges and culverts. For example, Thompson et al. (2004) coupled MIKE SHE and MIKE 11 for a wet grassland in England. They analyzed the impact of the wetland management and restoration. They calibrated and validated the integrated model with the observed data of groundwater and ditch water levels. The calibration and validation results of the model were consistent with the observed data. According to the results of the integrated model simulations, they found that the topographic depressions were significant for the flood initiation.

Liu et al. (2007) investigated the overland flow response to the groundwater and topography. They calculated the average water balance by conducting a simulation with

the integrated MIKE SHE/MIKE 11 model. They developed a hybrid fractal-wavelet method to explain the recharge response associated with overland flow, distance from midstream, topography and flooding depth. According to the results of the model simulations, they concluded that the hybrid fractal-wavelet method was suitable for simulating the groundwater response. Also they found that the groundwater levels reacted quickly to the overland flow depth change during the flooding events.

1.4.3. System Dynamics Approach to Water Resources Management

Studies that adopt system dynamics approach in watershed management aim to understand the system structure that causes behavior patterns in watershed variables such as climate, surface water, groundwater, soil, population, aquatic life and etc. They are well suited for policy and socio-economic scenario analysis. On the other hand, modeling and simulation of some systemic problems particularly require spatial representations of several elements of the system's structure. Land use change as related to hydrodynamics is a typical example where a spatial dynamic modeling approach can be more useful compared to a non-spatial, over-simplified dynamic systems model.

This section reviews some of the recent literature on the use of a system dynamics approach to water resources management. For example, Saysel and Barlas (2001) developed a dynamic model of salt accumulation on irrigated lands. They simulated the rootzone salinization integrating four major sub-processes; irrigation, drainage, groundwater discharge and groundwater intrusion. The study projected the long-term processes of salt accumulation in lowlands under continuous irrigation practice. Their scenario assumed that the irrigated lands annually increased. The simulation period consisted 32 years beginning from 1998 till 2030. They investigated the conditions which would increase the rootzone salinity to critical levels and the strategies to prevent this accumulation. In situations where the mixing of drainage water into irrigation water supplies is high, rootzone salinity quickly reaches alarming levels. Thus, the typical strategy of increasing the drainage in order to control the salinity level yields unprecedented, growing salinity levels, a catastrophic result for the agriculture. The model was constructed to represent the basin wide salinization process on different geographical settings in agricultural development.

The previous study was part of a more comprehensive study done by Saysel and his colleagues (2002). They developed a system dynamics simulation model (GAPSIM) as an experimental platform for policy analysis. They analyzed the potential long term environmental problems of the South East Anatolian Project (GAP). These problems were concentrated on water resources, land use, land degradation, agricultural pollution and demography.

Simonovic (2002) developed a model of the global world water resources using a system dynamics approach. Water resources sector (quantity and quality) was integrated with five sectors that drive industrial growth: population; agriculture; economy; nonrenewable resources; and persistent pollution. He developed a WorldWater model on the basis of the last version of World3 model. According to his simulations of world water dynamics with WorldWater, there was a strong relationship between the world water resources and future industrial growth of the world. He also showed that the water pollution is the most important future water issue on the global level.

Stave (2002) illustrated the process of building a strategic-level system dynamics model using the case of water management in Las Vegas, Nevada. The purpose of the model was to increase public understanding of the value of water conservation in Las Vegas. The effects of policies on water supply and demand in the system were not straightforward because of the structure of the system. Multiple feedback relationships led to the somewhat counterintuitive result that reducing residential outdoor water use has a much greater effect on water demand than reducing indoor water use by the same amount. The model output showed this effect clearly. The author described the use of the model in research workshops and discussed the potential of this kind of interactive model to stimulate stakeholder interest in the structure of the system, engaged participant interest more deeply, and built stakeholder understanding of the basis for management decisions.

In order to evaluate the sustainability of the water resource system in the study area, Xu et al. (2002) used an object-oriented system dynamics approach to develop a model for the water resources system in the Yellow River basin. Their model is referred to as Water Resources System Dynamics (WRSD) model. Their aim was to simulate a water resource system and capture the dynamic character of the main elements affecting water demand

and supply in the study area. They acquired projection results of different scenario analysis.

Simonovic and Rajasekaram (2004) developed a system dynamics model, CanadaWater which allows for an intensive study of different feedbacks between human activities, environmental change, ecosystem integrity, and social and economic factors. They developed this model to address important water issues including: a) climate variability and change (floods and droughts) b) bulk water export c) water pollution d) urban water management e) institutional arrangements and f) aging infrastructure for water supply and drainage. The use of CanadaWater model was planned to help in identifying water-related issues of national priority and can assist policy makers in evaluating various sustainable solutions for Canadian 'troubled' waters.

Güneralp and Barlas (2003) conducted a dynamic ecosystem modeling of a shallow freshwater lake where fishing is a major commercial activity and high nutrient loading occur. From this perspective, they analyzed the potential sustainable management policies for the ecosystem. According to their results, the eutrophication was not at a level to lead to algal blooms in the near future. However, the population increase was the main threat for the welfare of the inhabitants. Their different scenario applications showed that the lake would have become eutrophic with algal dominance, if the crayfish population did not collapse due to a fungus disease in 1986. Their crayfish recovery scenario demonstrated the increase in crayfish harvest leading to improvement of the social conditions. Only one of their alternative policies which were based on the improvement of the agricultural techniques led to better social conditions.

Tidwell et al. (2004) employed system dynamics modeling to assist in community-based water planning for a three-county region in north-central New Mexico. The planning region is centered on a ~165 km reach of the Rio Grande that includes the greater Albuquerque metropolitan area. Their challenge was to balance a highly variable water supply among the demands posed by urban development, irrigated agriculture, river/reservoir evaporation and riparian/in-stream uses. The third objective of the model was to engage the public in the water planning process. Their first modeling objective was to build a quantitative platform for exploring alternative water management strategies in

terms of costs and water savings. They developed a system dynamics model that incorporates 24 conservation alternatives and a “no action” alternative. Another reason for them to develop the model was to educate the public about the complexity of the regional water system. At the highest level, the model effectively conveyed the basic elements of the water budget.

Fernandez and Selma (2004) developed a dynamic model developed to analyze the key socio-economic and environmental factors driving the whole system. Their dynamic model, New Irrigated Lands included five sectors: Irrigated Lands, profitability, available space, water resources and pollution. They simulated the environmental effects regarding water consumption by reference to aquifer levels, natural outflows through springs, piezometric levels and aquifer water salinity. The exploration of their scenarios showed that current policies based on the increase in the water resources did not eliminate the water deficit problem because the feedback loops of the system lead to a further increase in irrigated land and continuation of the water deficit. The total area of irrigated lands is the true driving factor of the system. Therefore, any policy aiming to reduce or eliminate the water deficiency problem should be based on the stabilization of the irrigated lands.

Ahmad and Simonovic (2004) developed a new approach named as spatial system dynamics to model the feedback based temporal and spatial dynamic processes. They supported this new approach with GIS assistance. They applied this approach for flood management in a river basin in Canada. The coupled model was able to analyze the impacts of dike sizing and breach. The model was also able to calculate the damage and the impacts of flood of different magnitude.

Elshorbagy et al. (2005) developed a system dynamics watershed model (SDWM) to simulate one of the reconstructed watersheds and assess its ability to provide common watershed functions. Their preliminary results pointed to the potential of the system dynamics approach in simulating watersheds and testing different scenarios. Their tested reclamation strategy seems to be satisfactory within a certain range of hydrologic conditions. Further validation of the SDWM is required, however, before relying on its results for decision support with regard to reclamation strategies.

Many researchers tried to analyze the impact of physical and social components of a watershed on the water resources such as stream, pond and groundwater. They focused on the watershed system to determine these impacts. They chose different tools for their analysis. Some of them preferred conceptual approaches while the others constructed deterministic models. Although the spatial and temporal aggregation levels of these studies differed, most of them concentrated on simplified and aggregated models.

There have been few studies investigating the impact of land use system on the water resources system considering both the spatial and the temporal dynamics of these two systems. Mostly, the spatial and temporal resolution consistency could not have been achieved between the land use and water resources systems. Consequently, the models generated based on the spatial and temporal dynamics of the two systems could succeed to a certain level in determining existing condition and the future simulations. Therefore the results of the scenario analyses have been also questionable. This required the more complex models which have integrated the two land use and water resources systems to some extent. The integrated land use-hydrodynamics model developed in this study attempts to be a part of such initiative studies whose aim is to evaluate different management options for the sustainability of the watershed.

2. METHODOLOGY

This chapter describes the numerical models developed to simulate the land use dynamics and the hydrodynamics of the Bartın spring watershed. The land use dynamics were modeled using the STELLA program (H.P.S., 2001) while the watershed hydrodynamics were modeled using the MIKE SHE computer model (D.H.I., 2005). Arc Info 9.1 was used as a Geographical Information Systems (GIS) tool for the representation of the spatial databases for both the land use dynamics and the hydrodynamics models. The materials and the methods of the field and the laboratory works are also described briefly in this chapter.

2.1. Land Use Dynamics Model

There are several alternative methods for building a model that describes land use dynamics of a region. One option is to use visual and statistical interpretation of land use maps and satellite data by Geographical Information Systems (GIS) and Remote Sensing Another option is to develop numerical models that simulate the processes responsible for land use changes (Lambin, 2004). While in principle this numerical modeling approach can account for full spatial distribution, in practice most applications tend to be spatially lumped. The land use model developed for the Bartin spring watershed is a dynamic simulation model which to some extent allows combining the GIS techniques and dynamic simulation.

Ford (1999) defined the 'system' as a combination of two or more elements that are interconnected for some purpose. From this perspective, system dynamics can be described as the time dependent analysis method of the system components. These components are the stocks, flows, and converters. Here stocks are the important accumulations over time. Flows represent the rate of change of stocks (Barlas, 2002). Converters are the intermediate variables and calculations used to determine the flow variable values.

There are many multipurpose simulation softwares for building dynamic system models such as STELLA, POWERSIM (Powersim Corp., 1996) and VENSIM (Ventana,

1996) to name a few. STELLA which was developed by the High Performance Systems (H.P.S., 2001) is preferred as the software tool for building land use dynamics model. The practical usage of the STELLA software for modeling the land use changes was the preference reason.

STELLA has three different levels on which the user can work. These levels show alternative levels of model complexity, details and organization. These three levels are (Deaton and Winebrake, 2000):

1) The high-level mapping layer: High-level system maps can be designed and model dynamics can be explored by the user.

2) The model construction layer: A system diagram which displays the stocks, flows, converters and connecters can be sketched by the user. In addition, the model construction layer is used to specify the mathematical relationships that are used to in the model.

3) The equations layer: The underlying equations in the model can be viewed and modified by the user. For example, *Coniferous maturation (Flow) = Young Coniferous Stand (Stock) / average coniferous maturation time (converter).*

2.2. Hydrodynamics Model

Hydrodynamics modeling is the simulation of the spatial and temporal movement of the hydrological cycle in a watershed. Hydrodynamics modeling must generally involve the spatial and temporal variability of surface and subsurface processes of the hydrological cycle.

The three-dimensional hydrological model MIKE SHE was chosen for modeling the watershed hydrology. The simple schematic representation of the hydrodynamics model is demonstrated in Figure 2.1.

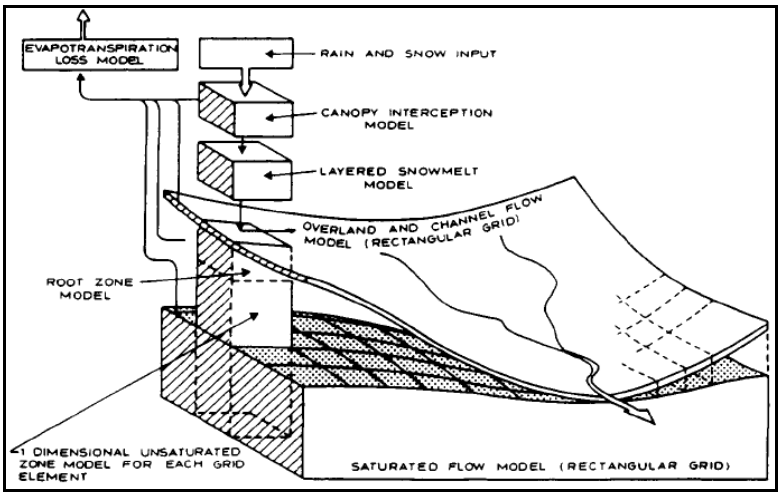

Figure 2.1. Schematic representation of the hydrodynamics model (Refsgaard and Storm, 1995)

The reason for the preference of MIKE SHE tool for hydrological modeling of our watershed is that it is the only fully distributed hydrological model for the simulation of a watershed integrating both the surface and ground layers of the watershed. It allows also the analysis of the land use parameters which have significant impact on the watershed hydrology. Another attractive feature is that MIKE SHE also allows for the use of GIS which will facilitate the interaction between the hydrodynamic and land use models. As described in Chapter 1, the different components of MIKE SHE have been extensively tested and applied in numerous studies.

2.2.1. Modules and Model Components

The MIKE SHE tool allows the simulation of the hydrological components such as evapotranspiration, overland flow, river and lakes flow, unsaturated zone flow and saturated zone flow. The calculation of these flows is based on a number of physical watershed and hydrological parameters such as the model domain and the grid resolution, topography, precipitation, land use, evapotranspiration, overland flow, river flow, unsaturated zone flow and the saturated zone flow. It allows some alternative calculation methods for each of those hydrological components. The alternative calculation methods are discussed below by presenting the key equations and the parameters needed for these

calculations stressing on the relevant parameters and equations of the selected calculation methods.

2.2.1.1. Model Domain and Grid. The first input of the hydrodynamics model is the definition of the model domain. Generally the model domain is the boundary of the studied watershed. The watershed boundary is introduced to the model with a shape file prepared separately using GIS. The alternative method is the separately definition of a grid file which introduces the inner and the outer watershed grids to the model. The model also requires the definition of the three-dimensional grid cell resolution upon which the calculations will be made.

2.2.1.2. Topography. The definition of the topography is necessary for the overland flow and the river flow components of the model. MIKE SHE allows for three different alternatives for the definition of the watershed topography. The altitude of the watershed may be assumed as uniform throughout the model domain, representing the average altitude of the watershed. Second, the spatial distribution of the topography data may be supplied to the model by either the triangular or the bilinear interpolation methods choices. The point data in the form of the separately prepared GIS based shape or the text file is interpolated based on a flexible search radius. The third alternative is the definition of the altitude value of each grid by a separately prepared grid file.

2.2.1.3. Precipitation. The model provides the option of making the precipitation data spatially uniform or distributed, and temporal or constant in time. The spatial distribution of the precipitation data may be supplied at selected meteorological stations or fully distributed over the entire model domain. The former requires either a GIS based shape file or a grid file where the flexible influence area of the meteorological station can be defined. The latter necessitates the precipitation data to be defined for all the model grids. The separately prepared flexible time series files allow the temporal dynamics of the precipitation data. These files may be in the form of annual, monthly and daily time series.

The model permits to include the snowmelt component to the precipitation. According to the snowmelt theory (D.H.I., 2005), the snow storage reduces by melting based on the equation below (2.1):

$$q_{snow} = DegreeDayFactor \times (AirTemperature - ThresholdMeltingTemperature) \times \Delta t \quad (2.1)$$

Here, degree day factor (mm snow/day/°C) is the amount of snow that melts per day for every degree temperature above the threshold melting temperature. The threshold melting temperature is the temperature at which the snow starts to melt. The model allows defining these two parameters as snowmelt constants. The air temperature data may be uniform or spatially distributed and constant or time varying. The spatial and temporal distribution options for precipitation data are also valid for air temperature data.

2.2.1.4. Land Use. The land use is one of the significant components of the hydrodynamics model. The vegetation definition of the model land use component aims to determine the values of the two land use parameters; Leaf Area Index (LAI) and Root Depth (RD). The LAI is the ratio of the surface area of one side of the leaves to the projected crown area of the vegetation (Ward and Robinson, 2000). The RD is the maximum length of the roots below the ground surface (D.H.I., 2005). These are the two key parameters that control the amount of evapotranspiration. The precise estimation of these two parameters will potentially assist the estimation of the evapotranspiration and consequently the river flow.

Similar to the previous physical parameters, the model provides an opportunity to define the land use as uniform or spatially distributed. The spatially distributed land use may be in the form of a grid file or the GIS based shape file. Also the parameter values may be temporal or constant in time. The temporal values of the vegetation parameters may be defined in a time series file similar to the precipitation or the vegetation property files.

Besides these two vegetation parameters, there are also evapotranspiration parameters which are vegetation constants and necessary for the calculation of the actual evapotranspiration. These are C_1, C_2, C_3, C_{int} (mm) and *Aroot* (1/m) constants and they are briefly defined in the evapotranspiration subsection.

2.2.1.5. Evapotranspiration. Evapotranspiration consists of two major hydrological processes; evaporation and transpiration. Evaporation occurs both from the soil surface and from the vegetation surface. Transpiration, on the other hand, occurs from the leaves of the

vegetation. Evapotranspiration is one of the most significant hydrological processes that directly influences the watershed water budget since in most climates a large portion of the precipitation either in the form of rainfall or snow is lost back to the atmosphere by evapotranspiration. Therefore, proper computation of evapotranspiration is essential for the accurate estimation of the water budget.

The hydrodynamics model calculates the actual evapotranspiration from the potential evapotranspiration which is the amount of water lost to the atmosphere from a surface with an unlimited amount of water (D.H.I., 2005). There are several methods to calculate the potential evapotranspiration. The Penman (Penman, 1948), Thornthwaite (Thornthwaite, 1948), Blaney-Criddle (Usul, 2001), Priestly-Taylor (Priestly and Taylor, 1972) are some of the common potential evapotranspiration calculation methods found in the literature. In this study the Penman method which is commonly used in Turkey (Dumlu et al., 2006) was selected. The method is described briefly in this subsection.

The Penman method (Penman, 1948) combined the turbulent transfer and the energy-balance approaches. Penman then proposed modified forms of the model in 1952, 1954, 1956 and 1963 (Ward and Robinson, 2000). The simplified equation for the Penman model is as follows (2.2) (Dumlu et al., 2006):

$$E_p = \frac{(A \times H) + (0.27 \times E_a)}{A + 0.27} \tag{2.2}$$

E_p = Daily potential evaporation (mm.day^{-1}).

A = Gradient of saturation vapor pressure at air temperature (t) (mmHg/°C) (equation 2.3).

$$\text{If temperature } (t) = 0°\text{C-}20°\text{C} \rightarrow A = 0.75 - \left[0.67\left(1 - e^{0.057t}\right)\right] \tag{2.3}$$

$$(t) = 21°\text{C-}30°\text{C} \rightarrow A = 0.17t - 1.3$$

H = Net amount of radiation remaining at the free water surface (mm.day^{-1}) (equation 2.4).

$$H = R_C - R_B \tag{2.4}$$

R_C = Solar energy reached the evaporation surface (converted to mm.day^{-1}) (equation 2.5).

$$R_C = R_A \times (1 - r) \times \left(0.18 + 0.55 \frac{n}{N} \right) \quad (2.5)$$

R_A = Monthly mean solar energy above atmosphere (converted to mm.day^{-1})

r =The reflection coefficient of the evaporation surface (Albedo)

R_B = Net long wave radiation of the earth (converted to mm.day^{-1}) (equation 2.6).

$$R_B = B \times \left(0.56 - 0.92\sqrt{e_d}\right) \times \left(0.1 + 0.9 \frac{n}{N} \right) \quad (2.6)$$

B = The value that defines the relation between the Boltzman constant and the air temperature. This value can be simplified as following equation (2.7) (Yalçın, 1992).

$$B = 0.2t + 11 \quad (2.7)$$

e_d = Saturation vapor pressure of air at dew point (mm.Hg) (equation 2.8).

$$e_d = R_H e_a \quad (2.8)$$

R_H = Monthly mean relative moisture value of air (dimensionless)

e_a =Saturation vapor pressure of air (mm.Hg) at monthly mean temperature (t) (equation 2.9) (Yalçın, 1992).

$$e_a = 4.579 + 0.333512t + 1.069 \times 10^{-2} t^2 + 1.879 \times 10^{-4} t^3 + 3.081 \times 10^{-6} t^4 \quad (2.9)$$

E_a =Evaporation due to mass transfer of vapor (mm.water.day^{-1}) (equation 2.10).

$$E_a = 0.35 \times (e_a - e_d) \times (1 + 0.0098 U_2) \quad (2.10)$$

U_2 =Monthly mean wind velocity at 2m height (m/s).

The model has two alternative methods of calculating the actual evapotranspiration using potential evapotranspiration. One of them is the Kristensen and Jensen method (Kristensen and Jensen, 1975) and the other is the simplified evapotranspiration for the two layer water balance method (Yan and Smith, 1994). The simplified evapotranspiration for the two layer water balance method is particularly useful for areas with shallow groundwater table. This method considers the entire unsaturated zone to consist of two layers representing average conditions in the unsaturated zone. Since the Kristensen and Jensen method was used in this study, it is briefly described in this subsection.

The Kristensen and Jensen method was developed at the Royal Veterinary and Agricultural University (KVL) in Denmark. In this model, the actual evapotranspiration and the actual soil moisture status in the root zone is calculated from the potential evaporation rate, along with maximum root depth and leaf area index for the plants. The empirical equations in the model are based on actual measurements or assumptions. The model generally assumes the temperature to be above 0°C and hence, precipitation does not occur as snow (Kristensen and Jensen, 1975; D.H.I., 2005).

The first hydrological process after the precipitation is introduced to the vegetation is the canopy interception. The interception is calculated based on interception storage. The interception storage must be saturated before stemflow or leaf drip to the ground surface processes occurs. The size of the interception storage capacity, I_{max} (L), depends on the vegetation type and its stage of development, which is characterized by the interception coefficient, C_{int} (L) and the leaf area index, LAI (m^2/m^2). The equation for I_{max} is given below (2.11).

$$I_{\max} = C_{\text{int}} \times LAI \quad (2.11)$$

The values of *LAI* and C_{int} parameters are defined at the model land use component and called from that component. A typical value of C_{int} is about 0.05 mm (D.H.I., 2005).

The evaporation from the canopy storage, E_{can} (LT^{-1}) is equal to the potential evapotranspiration, E_p (LT^{-1}) during a time step length of the simulation (Δt), if sufficient water has been intercepted on the leaves. The equation for E_{can} is given below (2.12).

$$E_{can} = \min\left(I_{\max}, E_p \Delta t\right) \tag{2.12}$$

The actual evapotranspiration is the total of actual transpiration and the actual soil evaporation. The actual transpiration from the vegetation canopy (E_{at}) is calculated using the potential evapotranspiration and three different functions. The first is the function based on the LAI, ($f_1(LAI)$). The second is based on the soil moisture content in the root zone, ($f_2(\theta)$). The third is the Root Distribution Function (*RDF*). The equation is described below (2.13).

$$E_{at} = f_1\left(LAI\right) \times f_2\left(\theta\right) \times RDF \times E_p \tag{2.13}$$

The LAI based function is calculated with the following equation which considers also two empirical constants, C_1 and C_2 (2.14).

$$f_1\left(LAI\right) = C_2 + \left(C_1 \times LAI\right) \tag{2.14}$$

The values of C_1 and C_2 parameters are defined at the model land use component and called from that component. C_1 is plant dependent. For agricultural crops and grass, C_1 has been estimated to be about 0.3. For agricultural crops and grass, grown on clayey loamy soils, C_2 has been estimated to be about 0.2 (D.H.I., 2005).

The function based on the soil moisture content in the root zone is calculated with the following equation which considers volumetric moisture content at field capacity (θ_{FC}), volumetric moisture content at the wilting point (θ_W), actual moisture content (θ), potential evapotranspiration and the empirical constant, C_3 (LT^{-1}) (2.15).

$$f_2(\theta) = 1 - \left(\frac{\theta_{FC} - \theta}{\theta_{FC} - \theta_W} \right)^{\frac{C_3}{E_p}} \tag{2.15}$$

The empirical parameter, C_3 may depend on soil type and root density. A typical value for C_3 is 20 mm/day (D.H.I., 2005). Higher values of C_3 will lead to higher values of transpiration, which means that the soil will dry out faster, assuming all other factors constant.

The root extraction is assumed to vary logarithmically with depth. The root extraction at depth z (log$R(z)$) is dependent upon the root extraction at the soil surface (log$R(0)$) and *Aroot* (1/L) parameter. The deriving equation is stated below (2.16).

$$\log R(z) = \log R(0) - Aroot \times z \tag{2.16}$$

Aroot parameter defines how the water extraction is distributed with the depth. The actual transpiration becomes more uniformly distributed as *Aroot* approaches 0 while it tends to become smaller for higher values of *Aroot* because most of the water is drawn from the upper layer, which subsequently dries out faster (D.H.I., 2005).

The Root Distribution Function (*RDF*) in each layer is calculated by dividing the amount of water extracted in that layer by the total amount of water extracted by the roots. The equation is (2.17),

$$RDF_i = \int_{z_1}^{z_2} R(z)dz \Big/ \int_{0}^{RD} R(z)dz \tag{2.17}$$

where the numerator is the total amount of water extracted in layer i bounded above by z_1 and below by z_2 and the denominator is the total amount of water extracted by the roots between the ground surface and the maximum root depth, *RD*. The values of *Aroot* and *RD* parameters are defined at the model land use component and called from that component.

The actual soil evaporation, E_s, occurs from the upper part of the unsaturated zone and consists of a basic amount of evaporation, $E_p \times f_3(\theta)$, plus additional evaporation from excess soil water as the soil saturation reaches field capacity (D.H.I., 2005). This can be described by the following function (2.18).

$$E_s = \left[E_p \times f_3(\theta)\right] + \left[\left(E_p - E_{at} - \left(E_p \times f_3(\theta)\right)\right) \times f_4(\theta) \times \left(1 - f_1(LAI)\right)\right] \tag{2.18}$$

Functions $f_3(\theta)$ and $f_4(\theta)$ are given by the equations below where θ_r is residual moisture content (2.19 and 2.20).

$$f_3(\theta) = \begin{cases} c_2 \, for \, \theta \geq \theta_w \\ c_2 \dfrac{\theta}{\theta_w} \, for \, \theta_r \leq \theta \leq \theta_w \\ 0 \, for \, \theta \leq \theta_r \end{cases} \tag{2.19}$$

$$f_4(\theta) = \begin{cases} \dfrac{\theta - \dfrac{\theta_w + \theta_{FC}}{2}}{\theta_{FC} - \dfrac{\theta_w + \theta_{FC}}{2}} \, for \, \theta \geq \dfrac{\left(\theta_w + \theta_{FC}\right)}{2} \\ 0 \, for \, \theta < \dfrac{\left(\theta_w + \theta_{FC}\right)}{2} \end{cases} \tag{2.20}$$

The hydrodynamics model allows defining the potential evapotranspiration data uniform or distributed and temporal or constant. Such as for the precipitation component of the model, the spatial distribution of the potential evapotranspiration data may be station based or fully distributed. The station based distribution requires a GIS based shape file or a grid file where the flexible influence area of the meteorological station can be defined. The fully distribution of the potential evapotranspiration data is achieved by defining the data for all the model grids. The temporal dynamics of the potential evapotranspiration data is supplied by preparing time series files separately and then introducing them to the model.

The two important land use parameters, LAI and RD and the evapotranspiration constants C_1, C_2, C_3, C_{int} (mm) and *Aroot* (1/m) are the other necessary data for the

calculation of the actual evapotranspiration using potential evapotranspiration. The values of these parameters are provided as part of the land use component of the input

2.2.1.6. Overland Flow. When the net rainfall rate exceeds the infiltration capacity of the soil, the excess water forms ponds on the soil surface. This excess water contributes to the evaporation and/or may lead to overland flow towards the river system based on the topography and the flow resistance conditions.

The model offers two alternative methods of calculating the overland flow. The first is finite difference method and the second is the simplified overland flow routing method. The simplified overland flow routing method assumes the hillslope equations as lumped across a catchment. The finite difference method on the other hand allows for spatially distributed computation of overland flow based on the topography. Therefore, the finite difference method was used during this study, and hence is briefly described below.

The finite difference method applies the diffusive wave approximation adapted to the Saint Venant equation, ignoring the momentum loss due to local and convective acceleration and lateral inflows perpendicular to the flow direction.

The ultimate simplified representation of the diffusive wave approximation is given below (2.21 and 2.22).

$$uh = K_x\left(-\frac{\partial z}{\partial x}\right)^{1/2} h^{5/3} \tag{2.21}$$

$$vh = K_y\left(-\frac{\partial z}{\partial y}\right)^{1/2} h^{5/3} \tag{2.22}$$

uh = Discharge per unit length along the cell boundary in the x direction (L^3/T)
vh = Discharge per unit length along the cell boundary in the y direction (L^3/T)
K_x = Strickler roughness coefficient in the x direction ($L^{1/3}/T$)
K_y = Strickler roughness coefficient in the y direction ($L^{1/3}/T$)

h = Flow depth (L)

z = Ground surface level + flow depth (L)

The Strickler roughness coefficient (K) is equivalent to the Manning's m. The value of m is typically in the range of 10 ($m^{1/3}/s$) (thickly vegetated channels) to 100 ($m^{1/3}/s$) (smooth channels).

In the model, the parameters to be defined are the Manning's m, detention storage and the initial water depth. These parameters can be defined as uniform or spatially distributed. The spatial distribution files may be in the form of a grid or a GIS based shape file. The spatial distribution of the overland flow parameter values may be supplied to the model by either the triangular or the bilinear interpolation methods choices. The point data in the form of the separately prepared GIS based shape or the text file is interpolated based on a flexible search radius. The third alternative is the definition of the values of each grid by a separately prepared grid file.

2.2.1.7. River Flow. The fully dynamic Saint Venant equations are used for one dimensional simulation of the river flows and the water levels. The first equation is the conservation of mass and the second is the conservation momentum equation. The conservation of mass and momentum equations are given below respectively (2.23 and 2.24) (Turan, 2002).

$$\frac{\partial Q}{\partial x} + \frac{\partial A}{\partial t} = q \tag{2.23}$$

$$\frac{\partial Q}{\partial t} = \frac{\partial\left(\alpha \frac{Q^2}{A}\right)}{\partial x} + gA\frac{\partial h}{\partial x} + \frac{gQ|Q|}{C^2 AR} = 0 \tag{2.24}$$

q= Lateral inflow (L^2/T)

g= Gravitational acceleration (L/T^2)

Q= River discharge (L^3/T)

h= Stage above datum (L)

A= Flow area (L^2)

α= Momentum distribution coefficient

t= time (T)

C= Chezy resistance coefficient ($L^{1/2}/T$)

x= Distance (L)

R= Hydraulic or resistance radius (L)

The Chezy resistance coefficient is equal to the $R^{1/6}m$ where m is the Manning's roughness coefficient of the stream or channel (Chow et al., 1988).

The model considers a river simulation file which is prepared separately. The river simulation file includes the components files. These are river network, cross sections, boundary and hydrodynamic parameters files. The river network file includes the main river chainage together with the river branch chainages. The model allows digitizing these chainages from rectified map. The locations of the cross sections may also be defined on these chainages. The cross sections file includes the cross sections of the river network together with their physical characteristics such as their roughness coefficients and their upper and lower nodes. The boundary file defines the boundary conditions of the river network. The discharge or the water level boundaries of the initial and the ultimate point of the river network are defined in this file. The hydrodynamic parameters file includes the flexible hydrodynamic characteristics of the river network such as the initial discharge and water level values, flood plain resistance, bed resistance, wind and heat conditions and etc.

2.2.1.8. Unsaturated Zone Flow. The model has three options for calculating vertical flow in the unsaturated zone. They are the full Richards equation, the simplified gravity flow method and the simple two-layer water balance method (Yan and Smith, 1994). Simplified gravity flow procedure assumes a uniform vertical gradient and ignores the capillary forces while simple two-layer water balance method is only for shallow water tables.

The hydrodynamic model developed for the Bartın spring watershed calculates the unsaturated zone flow using the Richards equation (Richards, 1931; Jury and Horton,

2004) which is considered the most accurate of the three methods. However, numerically it is the most complex computationally demanding to solve.

According to the Richards equation the change in the pressure head (ψ) in time is dependent upon the unsaturated hydraulic conductivity ($K_{(\theta)}$) and the gravitational head (z). The one-dimensional Richards equation in the vertical direction is given below (2.25).

$$\frac{\partial \psi}{\partial t} = \frac{\partial}{\partial z}\left(K_{(\theta)} \frac{\partial \psi}{\partial z} \right) + \frac{\partial K_{(\theta)}}{\partial z} \tag{2.25}$$

The model offers soil profile definitions option to define all of these soil parameters either as spatially uniform or horizontally and/or vertically distributed. The horizontal distribution of the soils is supplied either by grid files or GIS based shape files. The vertical distribution of the soil profiles is achieved by defining the flexible depth intervals. The soil property files are defined for each of these depth intervals. In these soil property files, initially the methods for the calculation of the unsaturated hydraulic conductivity and the water retention curve and subsequently the parameters attributed to those methods are defined.

The unsaturated hydraulic conductivity is calculated based on the saturated hydraulic conductivity values. The Van Genuchten, Averjanov, Campbell/Burdine and tabulated are the methods to calculate the unsaturated hydraulic conductivity from the saturated hydraulic conductivity. The Van Genuchten method (Van Genuchten, 1980) was used to calculate the unsaturated hydraulic conductivity from the saturated hydraulic conductivity and the equation is expressed below (2.26).

$$K_{(\theta)} = K_S \frac{\left(\left(1 + \left|\alpha\theta\right|^n\right)^m - \left|\alpha\theta\right|^{n-1} \right)^2}{\left(1 + \left|\alpha\theta\right|^n\right)^{m(l+2)}} \tag{2.26}$$

Besides the soil characteristics such as saturated hydraulic conductivity (K_s), there are some empirical constants that are dependent on soil type and may be measured or defined based on literature data. These empirical constants are water retention parameters, α (1/L),

n, *m* and shape factor, *l*. They all are defined in the soil profile files in the MIKE SHE model.

The Van Genuchten, Campbell and tabulation are the methods to calculate the dynamic soil moisture content. The soil moisture content is also calculated based on Van Genuchten retention curve formula as given below. The soil moisture content is calculated based on the saturated moisture content (θ_s), the residual moisture content (θ_r), the pressure head (ψ) and again the water retention parameters, α, *n*, *m* (2.27).

$$\theta_{(\psi)} = \theta_r + \frac{(\theta_s - \theta_r)}{\left[1 + (\alpha\psi)^n\right]^m} \tag{2.27}$$

The saturated moisture content is basically equal to the porosity of the soil. Such as for the hydraulic conductivity parameters, the water retention curve parameters are also defined in the soil profile files in the model.

2.2.1.9. Saturated Zone Flow. The model offers two methods to calculate the flow in the saturated zone. One of them is the 3D Finite Difference method and the other is the linear reservoir method. In the linear reservoir method, the entire catchment is subdivided into a number of subcatchments. Within each subcatchment, the saturated zone is represented by a series of interdependent, shallow interflow reservoirs and a number of separate, deep groundwater reservoirs that contribute to stream baseflow (D.H.I., 2005).

The 3D Finite Difference method was selected for the Bartın spring watershed because it is considered the more accurate. The governing flow equation for three-dimensional saturated flow in saturated porous media is as follows (2.28).

$$\frac{\partial}{\partial x}\left(K_{xx}\frac{\partial h}{\partial x}\right) + \frac{\partial}{\partial y}\left(K_{yy}\frac{\partial h}{\partial y}\right) + \frac{\partial}{\partial z}\left(K_{zz}\frac{\partial h}{\partial z}\right) - Q = S\frac{\partial h}{\partial t} \tag{2.28}$$

K_{xx} = Saturated hydraulic conductivity along the x axes of the model (L/T)
K_{yy} = Saturated hydraulic conductivity along the y axes of the model (L/T)
K_{zz} = Saturated hydraulic conductivity along the z axes of the model (L/T)

h = Hydraulic head (L)

Q = Source/sink term (1/T)

S = Specific storage coefficient (1/L).

Two special features of this elliptic equation should be noted. First; the equations are non-linear when flow is unconfined and, second, the storage coefficient is not constant but switches between the specific storage coefficient for confined conditions and the specific yield for unconfined conditions (D.H.I, 2005).

The saturated hydraulic conductivity, storage coefficient and the specific yield parameters may be defined for the flexible number of soil layers and for each layer, they may be either uniform or spatially distributed in the model. The spatial distribution may be supplied either by grid files or GIS based shape files as described for the previous model components.

2.3. Geographical Information Systems (GIS)

Geographical Information Systems (GIS) are worldwide accepted and used techniques for any study involving spatial analysis. GIS are supplementary tools for the spatial description and analysis of watersheds. Recently there are also many applications of GIS to the hydrological models due to the new inventions on both these GIS modules and the hydrological models.

ArcGIS is a Geographical Information System software developed by the ESRI company. ArcGIS provides a scalable framework for implementing GIS for users on desktops, in servers, over the Web, and in the field. ArcGIS is an integrated collection of GIS software products for building a complete GIS. It consists of a number of frameworks for deploying GIS. One of these frameworks is the ArcGIS Desktop which is an integrated suite of professional GIS applications and serves as a productivity tool for authoring, sharing, managing, and publishing geographic knowledge. ArcGIS Desktop includes a suite of integrated applications; ArcCatalog, ArcMap, ArcGlobe, ArcToolbox, and ModelBuilder which together supply the user perform any GIS task, from simple to advanced, including mapping, geographic analysis, data editing and compilation, data

management, visualization, and geoprocessing. ArcGIS desktop is available to the user at three functional levels; ArcView, ArcEditor and ArcInfo (ESRI, 2005).

ArcInfo supplies full geoprocessing and analysis tools besides all the capabilities of Arc View and ArcEditor. Because of this, ArcInfo is a complete, professional GIS desktop containing comprehensive GIS functionality for data management, visualization, modeling, and analysis, including rich geoprocessing tools. The optional extensions may be integrated to the ArcInfo to complement the geoprocessing for special needs such as the three dimensional watershed spatial analysis. For such an analysis, the extensions ArcGIS 3D and the ArcGIS Spatial Analyst must be used. ArcGIS 3D Analyst enables effective visualization and analysis of surface data supplying the user to view a surface from multiple viewpoints, query a surface, determine what is visible from a chosen location on a surface, and produce a realistic perspective image by draping raster and vector data over a surface. ArcGIS Spatial Analyst provides a broad range of powerful raster modeling and analysis features that allow users to produce, query, map, and analyze cell-based raster data. ArcGIS Spatial Analyst also allows integrated raster-vector analysis (ESRI, 2005).

2.4. Field and Laboratory Analyses

A number of field and laboratory analyses were conducted to define some of the parameters necessary for both the land use dynamics and the hydrodynamics models. In general, the field works consist of photographing the vegetative cover for the estimation of the LAI and soil sampling. For the definition of the LAI, the hemispherical photographs of the forest stands are taken with the photographic equipments such as camera and fisheye lense. In total 92 photographs were taken to cover 30 different forest stand types.

Soil sampling was conducted to determine the soil type, moisture, porosity and saturated hydraulic conductivity, of the top soil about 20 cm depth. These parameters were determined from distributed and undisturbed soil samples. In total 100 undisturbed and 100 disturbed soil samples were taken from the field. 50 undisturbed and disturbed samples from each 0-10 cm and 10-20 cm depths were collected respectively.

The location of the forest stands to be photographed and the soil sampling points are defined based on the digitized map analysis with the GIS. The coordinates of those points are noted and found by Geographical Positioning Systems (GPS).

2.4.1. Leaf Area Index (LAI) Measurement

The Leaf Area Index (LAI) is one of the key parameters necessary for the land use dynamics and hydrodynamics model. As described earlier, the LAI is the ratio of the surface area of one side of the leaves to the projected crown area of the vegetation (Ward and Robinson, 2000).

There are many methods of measuring the LAI. These are grouped as direct and indirect methods. The direct methods include the leaf collection and some leaf area determination techniques such as planimetric and gravimetric techniques (Daughtry, 1990). One of the indirect measurements is the inclined point quadrat method which involves piercing a vegetation canopy with a long thin needle (point quadrat) under known elevations and azimuth angles and counting the number of contacts of the point quadrat with green canopy elements (Wilson, 1960). The LAI is then determined by simple equations. Another indirect measurement is the allometric techniques for forests which rely on relationships between leaf area and any dimensions of the woody plant element carrying the green leaf biomass such as stem diameter, tree height and crown base height (Jonckheere et al., 2004). The indirect non-contact methods are generally based on the measurement of light transmission through canopies. DEMON (Welles and Cohen, 1996) Ceptometer (Jonckheere et al., 2004), LAI-2000 and TRAC (Chen, 1996) are some of the instruments used for such measurements. Remote Sensing techniques are used also within this concept. The studies by Cohen et al. (2003), Fang and Liang (2005), Berterretche et al. (2005), Shabanov et al. (2005), Pisek and Chen (2007), all analyzed the Leaf Area Index using satellite data and Remote Sensing techniques.

The hemispherical canopy photography is a common indirect non-contact method of measuring LAI. The integration of digital or film cameras with 180° angle fisheye lenses is a widely used method for this purpose. The photographs taken with such instruments are analyzed by software packages such as Hemiwiew (Hale and Edwards, 2002), SCANOPY

(North et al., 2004), GLA (Frazer et al., 2001), EYE-CAN (Jonckheere et al., 2004) and HEMISFER (Schleppi et al., 2007).

2.4.1.1. Photographic Equipment and Usage. For the LAI measurement, the hemispherical canopy photography method was used in this study. This method is easier and cheaper compared to the other methods described above. However the results are quite satisfactory as cited in the literatures (Demarez et al., 2008, Schelppi et al., 2007).

The photographic equipment chosen for such a measurement is Canon EOS 3 Film camera with Sigma 8 mm Fisheye Lense. The fisheye lense has 180° angle of vision. The fisheye lense is mounted to the camera and the reverse canopy photographs are taken. During the photographing process, the camera and the lense is stabled to be 90° to the ground surface. Direct sunlight should be avoided from the vision.

2.4.1.2. Photograph LAI Analysis. The software Hemisfer 1.4 version was used during the analysis of the photographs. The software is designed to estimate the LAI from hemispherical (or wide angle) photographs. The software works on image files in BMP, GIF and JPEG formats. The software takes the ground slope into account during the analysis. It also corrects the canopy clumping. Several literature method alternatives are used during the calculation of the LAI (Schleppi et al., 2007, Nobis and Hunziker, 2005, Chen, 1996) and the correction (Schleppi et al., 2007, Chen and Cihlar, 1995) procedures.

2.4.2. Soil Analysis

The soil type, moisture, porosity and hydraulic conductivity parameters were measured during the soil analysis. The disturbed soil samples were taken into sealed plastic bags. These disturbed soil samples were used during the soil type and moisture analysis. The undisturbed soil samples were taken with the iron cylinders and covered. These undisturbed soil samples were used during the soil porosity and hydraulic conductivity analysis.

2.4.2.1. Soil Type. The standard Bouyoucos hydrometer method (Bouyoucos, 1936) is used for the definition of the soil type. This soil is mixed with 200 ml water and shaked.

The lime solvent is added to this mixture to avoid the clogging of the clay particles. The ultimate mixture stays 18-20 hours before processing. The soil suspension in water is poured into a mixer and shaked for 5 minutes. The mixture is then poured into the Bouyoucus hydrometer cylinder glass (Figure 2.2). Water is added to the mixture until the total volume reaches 1000 ml and again shaked vertically in the cylinder. The Bouyoucos scale is put into the mixture. After 4 minutes and 48 seconds, first reading of the hydrometer scale (H_1) is done and the temperature is measured also. The second reading of the hydrometer scale (H_2) is done after 2 hours and the temperature is again measured. The two hydrometer scale readings were corrected based on the temperature measurements. The following formulas are used to calculate the particle size distribution where the *SW* represents the soil weight without hygroscopic moisture (2.29 and 2.30) (Gülçur, 1974). The type of the soil sample is determined using the soil type triangle based on the international particle size classes (Kantarcı, 2000).

$$Silt(\%) + Clay(\%) = \frac{H_1}{SW} \times 100 \tag{2.29}$$

$$Clay(\%) = \frac{H_2}{SW} \times 100 \tag{2.30}$$

Figure 2.2. Bouyoucos hydrometer cylinder glass

2.4.2.2. Soil Moisture. The soil moisture is defined by measuring the gravimetric water content of the soil (Çepel, 1985). Ten grams of disturbed soil samples in the sealed plastic bags are weighted immediately to avoid evaporation. These ten grams of soil samples are then oven-dried at 105°C. The difference in the weight is the mass of water (M_w). The mass of water over the dry mass of the soil (M_{ds}) gives the moisture content of that soil. The equation for calculation of the percentage soil moisture content (θ_g) is given below (2.31).

$$\theta_g = \frac{M_w}{M_{ds}} \times 100 \tag{2.31}$$

2.4.2.3. Soil Porosity. The undisturbed soil samples taken using iron cylinders are saturated with water and weighted. These saturated soil samples are then oven-dried at 105°C and the volume of the soil (V_s) is acquired. The difference in the volume over the entire volume of the iron cylinders (V) gives the porosity of that soil (Çepel, 1985). The equation for calculation of the percentage soil porosity (ϕ) is given below (2.32).

$$\phi = \frac{V - V_s}{V} \times 100 \tag{2.32}$$

2.4.2.4. Soil Permeability. The undisturbed soil samples were taken from the field using the iron cylinders with 50 mm height and 50 mm diameter. These undisturbed soil samples were used to measure the soil permeability and saturated hydraulic conductivity. The soil samples are first saturated with water. The saturation time of the samples lasts at least a day or under extreme hard soil conditions a week. Soil permeability is measured by the laboratory soil permeameter (Figure 2.3).

Figure 2.3. Soil permeability measurement instrument

The laboratory soil permeameter instrument forms difference in water pressure on both ends of the saturated soil sample and measures the resulting water flow. The water is pumped from a storage cistern using a circulation pump. The inflow water is then led to an adjustable level regulator through a filter. The regulator is connected to a plastic and has a pipe to lead back surplus water to the storage cistern. The undisturbed saturated soil samples inside the iron cylinders are placed in a ringholder. The ringholder is placed into the container. The plastic siphons are placed on saturated soil samples. These siphons lead the water oozing from the samples to the burettes (Eijkelkamp, 2008).

The instrument allows two methods each of which is valid for soil samples with different soil textures. The constant head method is used for any soil sample except the poorly permeable ones such as clay and peat. The falling head method is used to measure low permeable soil samples like clay and peat. With the constant head method, a constant level difference should be maintained inside and outside the ringholder. The ultimate discharge burette cock is closed. The level difference inside the burette in a unit of time gives the saturated hydraulic conductivity of that sample after some basic calculations as given in equation 2.33 (Eijkelkamp, 2008). On the other hand, with the falling head method, the water level in the ringholder is reduced with a pipette to a level that is just above the sample. This level is measured with an electronic measuring bridge. The level is measured after a certain period of time. The water level difference is used in the calculation of the saturated hydraulic conductivity by the equation 2.34 (Eijkelkamp, 2008).

$$K_s = \frac{V \times L}{a \times t \times h} \tag{2.33}$$

K= Saturated hydraulic conductivity (L/T)

V= Volume of water flowing through the soil sample (L^3)

L= Length of the soil sample (L)

a= Surface of the soil sample cross section (L^2)

t= time between beginning and end of the measurement (T)

$$K_s = \frac{A \times L}{a \times t} \times \ln \frac{h_1}{h_2} + \frac{x \times A \times l}{a \times \sqrt{(h_1 \times h_2)}} \tag{2.34}$$

l= Length of the soil sample (L)

L= Length of the sample ringholder (L)

a= Surface of the soil sample cross section (L^2)

A= Surface of sample ringholder cross section (L^2)

h_1 and h_2= Water level difference inside and outside the ringholder at the beginning and end of the measurement respectively (L)

t= time between beginning and end of the measuring (T)

3. MODEL DEVELOPMENT

3.1. Site Characteristics

In this section, the site characteristics which constitute the infrastructure of both the land use dynamics and the hydrodynamics models are briefly discussed. The site characteristics include the spring water reservoir which is used to supply water to the cities of Bartın, Amasra and İnkumu and the watershed characteristics such as the location, climate, topography, slope, aspect, geology, soil, forest and agricultural vegetation and the settlement situation. The spatial watershed characteristics are presented in terms of maps which were prepared using the Geographical Information Systems (GIS). The Arc Info module of ArcGIS 9.1 version together with the Spatial Analyst and the 3D Analyst extensions (ESRI, 2005) were used for digitizing and visualization of the maps. These site characteristics form the basis of the model input data as described in Section 3.3.

3.1.1. Spring Water Reservoir

The spring water reservoir forms the downstream end of the Bartin spring watershed which is the focus of this study. The Bartın spring water serves the Bartın city center and the sub-province of Amasra and İnkumu town. It first appears as surface water in Bahçecik Village at Ulupınar Location, on the 34th km of Bartın-Safranbolu road (Figure 3.1). The spring water collecting pool has an average 60 m diameter and 50 m depth (İller Bankası, 1998).

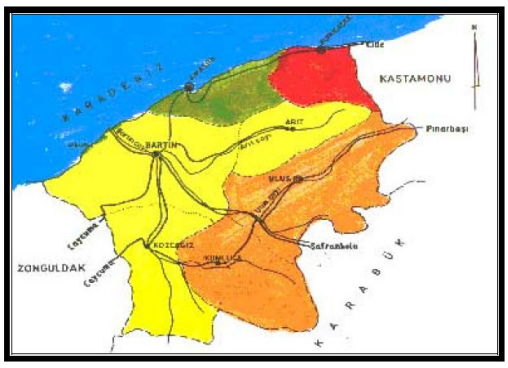

Figure 3.1. The road from Bartın to Safranbolu (Bartın Valiliği, 2003)

The bottom of the surface pond is overlain by 1.5 m coarse gravel layer which is overlain by a 1.5 m fine gravel layer (Figure 3.2). Nine perforated pipes with 600 mm diameter are located between these coarse and fine gravels. The fine gravel layer is covered with a membrane where then 1 m soil was located on. The water in the pool is rising from this 50 m depth till the 1.5 m coarse gravels and then drained with the 9 perforated pipes into a 150 m^3 reservoir with 2.5 m height, 2 m width and 30 m length. The reservoir was constructed in 1985 according to the project prepared by The Banks of the Provinces (İller Bankası, 1985). The excess flow is drained either to the river or to the old mill about 100 m downstream of the reservoir. The perspective view of the spring water reservoir with the collecting pool is shown in Figure 3.2.

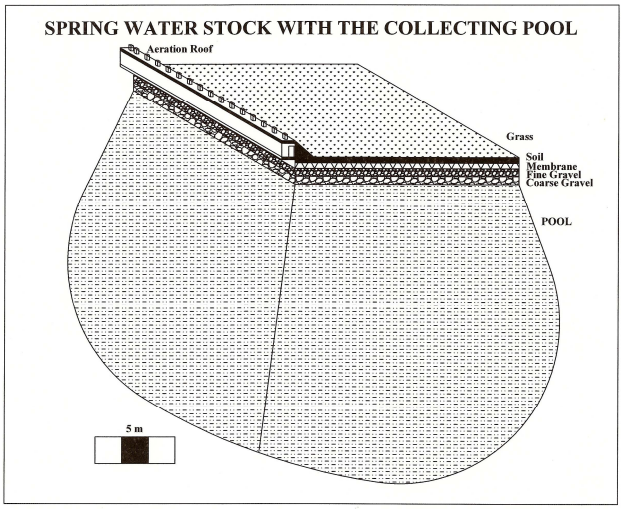

Figure 3.2. Perspective view of the spring water reservoir with the collecting pool

The water is then transported from the reservoir to Bartın by asbestos and steel pipes with initial diameter of 700 mm that eventually decrease to 600 mm. The water first comes to Orduyeri Location in Bartın and then is distributed to the other reservoirs located at various points in Bartın city center, İnkumu town center and Amasra city center. The water is used only in the central districts of Bartın, İnkumu and Amasra; it is not distributed to the villages of Bartın and Amasra, which supply their own water needs.

The average flow of the water at the reservoir is about 750 L/s of which 230-250 L/s is served to Bartin. The project flow capacity of the pipe is 218 L/s. Bartın is sharing almost 18% of its water or about 35-40 L/s with Amasra. The flow of the water at the

reservoir reaches a maximum level of about 2000 L/s, and declines down to the levels of 110 L/s in summer (1994 Summer) leading to the water interruption in the center of Bartın, İnkumu and Amasra. The flow of the water is 1500-1750 L/s at average in winter and declines to 500-600 L/s in summer. The 2001 water discharges are shown in Figure 3.3.

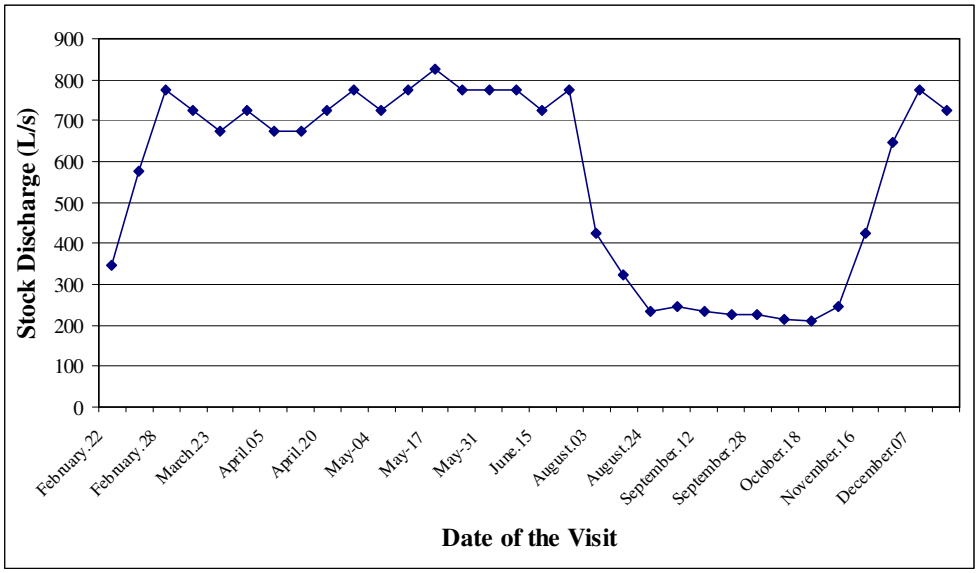

Figure 3.3. Stock water discharges in 2001

3.1.2. Location

The drainage area of the Bartın spring is approximately 287 km^2. The spring watershed is at the north-western of Turkey (Figure 3.4). It extends into the Black Sea Region of Turkey. The larger part of the watershed belongs to Karabük Province while the smaller part of the watershed belongs to Bartın Province. The watershed is located between 41° 21' and 41° 34' northern latitudes and between 32° 35' and 32° 60' eastern latitudes. The ultimate drainage point of the watershed where the spring originates is at the western part of the watershed. This point is the 34^{th} km of the Bartın-Safranbolu road in Bahçecik village. The southern edge of the watershed leads up to the 64 km of the Bartın-Safranbolu road. The north-eastern side of the watershed leads to Uluyayla Plain.

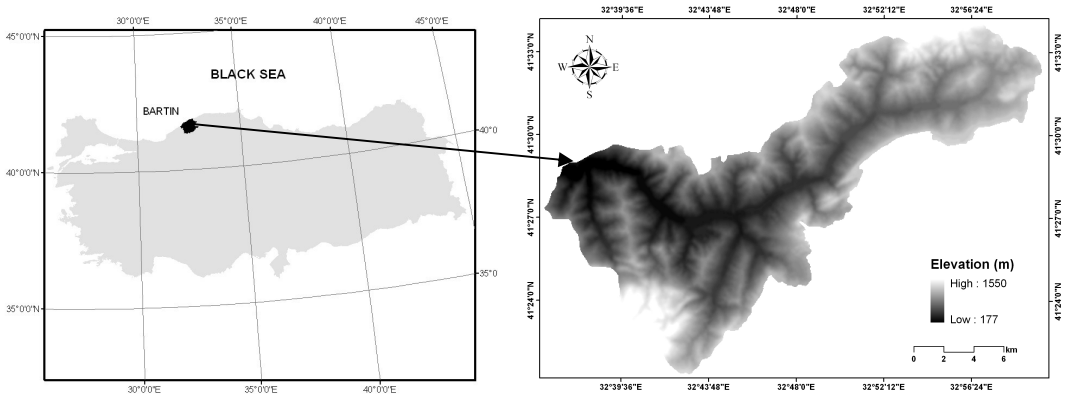

Figure 3.4. Location map of the Bartın-Ulupınar watershed

3.1.3. Climate

The climate of the watershed belongs to the Ulus Meteorological station 12 km away from the ultimate discharge point of the watershed. The altitude of the Ulus Meteorological station is 171 m. There are also two close stations to the watershed at Safranbolu and Eflani regions. However the data of these two stations are not consistent throughout the 21 years between 1986 and 2006. The annual Penman water budget calculations were prepared based on the meteorological data between 1986 and 2006 at the Ulus station (D.M.İ., 2007). The average annual precipitation is 988.87 mm and the average potential evaporation value is 951.96 mm in the watershed area. The monthly total rainfall data of Ulus Meteorological station between 1986 and 2006 are demonstrated in Figure 3.5. According to the data, the highest rainfall occurred in May 1998 when a destructive flood occurred. Although the rainfall is distributed throughout almost the whole year, the rainiest month is November. The least rainy month is July. The monthly mean temperature data of Ulus Meteorological station between 1986 and 2006 are shown in Figure 3.6.

The hottest month was August 2006 with the mean temperature of 24.6°C. In general, the hottest month is July with the mean temperature of 22.5°C. The coldest month is January with the mean temperature of 3.4°C.

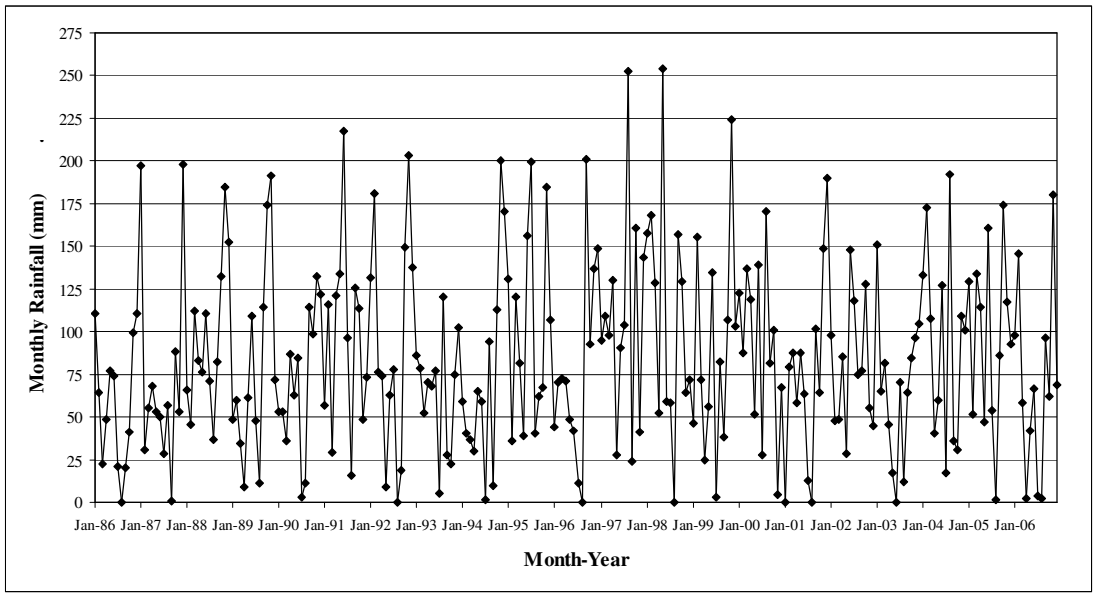

Figure 3.5. Monthly rainfall between 1986 and 2006

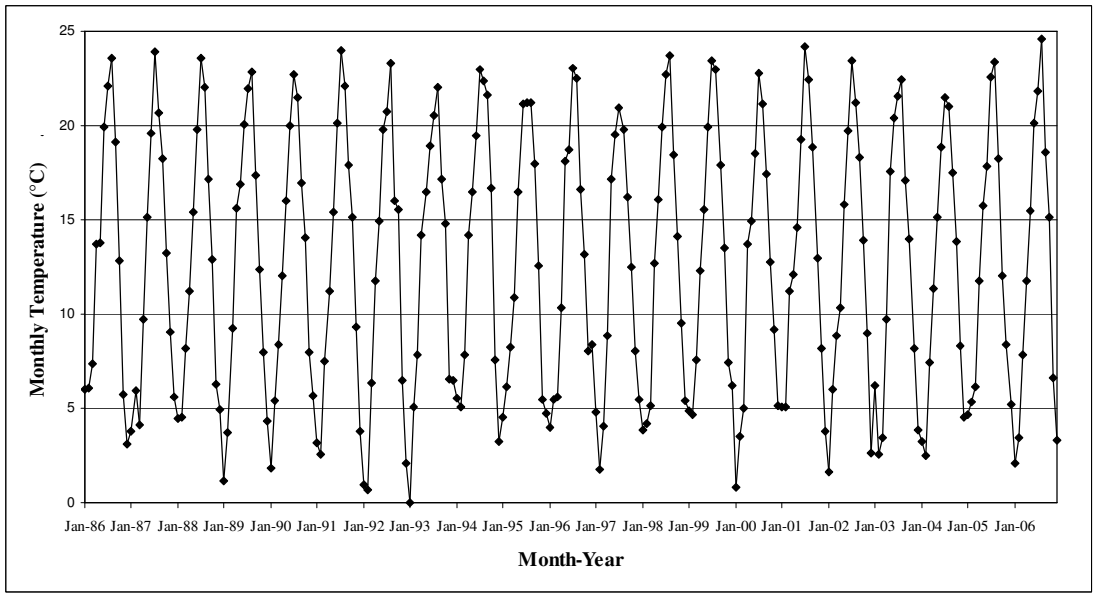

Figure 3.6. Monthly mean temperature between 1986 and 2006

3.1.4. Topography, Slope and Aspect

The topography of the spring watershed was defined based on the 1/100000 scaled topography map of Turkey which was acquired from the General Command of Mapping. The spring water pool is the lowest point of the watershed with the altitude of 177m. The

highest altitude within the watershed is 1550 m. Figure 3.7 shows the topography of the watershed together with the four subwatersheds. The four subwatersheds were defined based on the topography as defined in the Section 3.2. The average altitude of the watershed is 751 m. The altitude of the watershed increases from west to east. The altitudes of the crests of the hills in the watershed range between 350-1550 m. The altitude of the Ahmetusta Mountain Pass is 1300 m (Figure 3.7). The altitude of the stream ranges between 177 m and 550 m. The altitude range of the watershed and the ratio of these ranges within the watershed are presented in Table 3.1. These ratios were estimated using the Spatial Analyst extension of the ArcGIS 9.1 (ESRI, 2005). The altitude range between 650 and 800 meters covers the largest area compared to the other ranges. The spring watershed together with the entire Bartın watershed is shown in Figure 3.8. The entire Bartın watershed covers approximately 2060 km^2 area (Turoğlu and Özdemir, 2005). The average altitude of the entire Bartın watershed is 520 m.

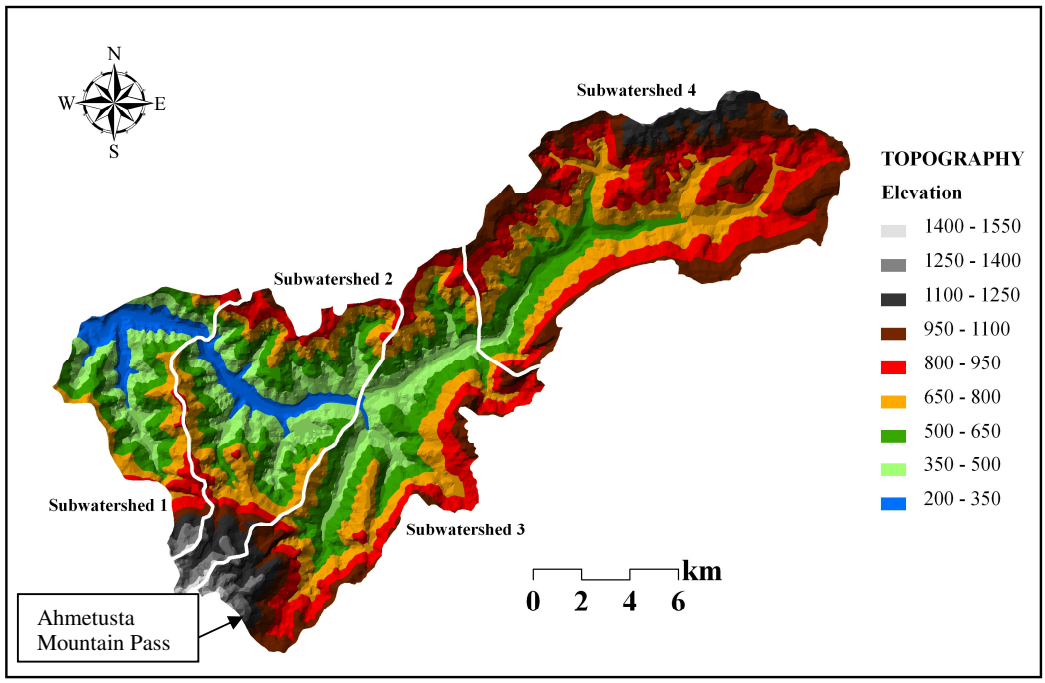

Figure 3.7. Topography of the Bartın spring watershed boundary

Table 3.1. The altitude range of the watershed and the ratio of these ranges within the watershed

Altitude Range (m)	Area (km^2)	Ratio (%)
177-350	12.4	4.3
350-500	37.2	13.0
500-650	54.9	19.2
650-800	62.6	21.9
800-950	58.9	20.6
950-1100	40.4	14.1
1100-1250	11.5	4.0
1250-1400	6.5	2.3
1400-1550	2.1	0.7

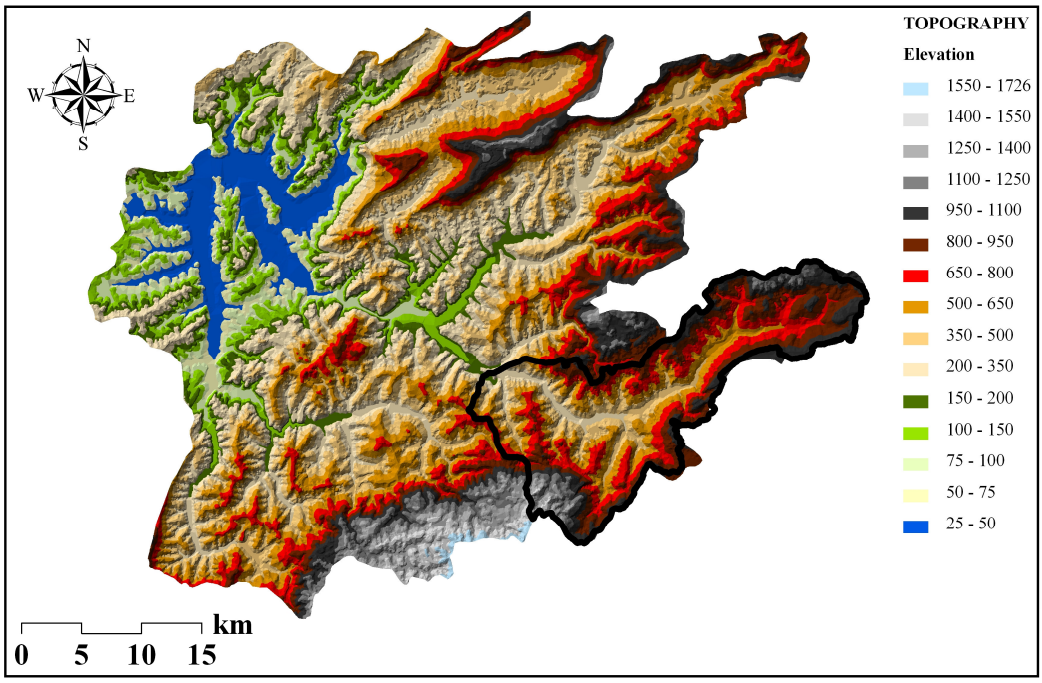

Figure 3.8. The spring watershed together with the entire Bartın watershed

Figure 3.9 shows the slope of the watershed. The average slope of the watershed is 28%. The slope distribution together with the ratios within the watershed is stated on the Table 3.2. These ratios were estimated using the Spatial Analyst extension of the ArcGIS 9.1 (ESRI, 2005). The watershed is generally covered with steep hills and mountains. However, the slope range between 0% and 5% covers the largest area compared to the other ranges. These flat areas exist primarily around the river channel.

Table 3.2. The slope range of the watershed and the ratio of these ranges within the watershed

Slope Range (%)	Area (km^2)	Ratio (%)
0-5	48.1	16.8
5-15	5.3	1.8
15-25	46.2	16.1
25-30	41.3	14.4
30-35	38.1	13.3
35-40	30.6	10.7
40-45	22.7	7.9
45-50	16.5	5.8
50-	37.6	13.1

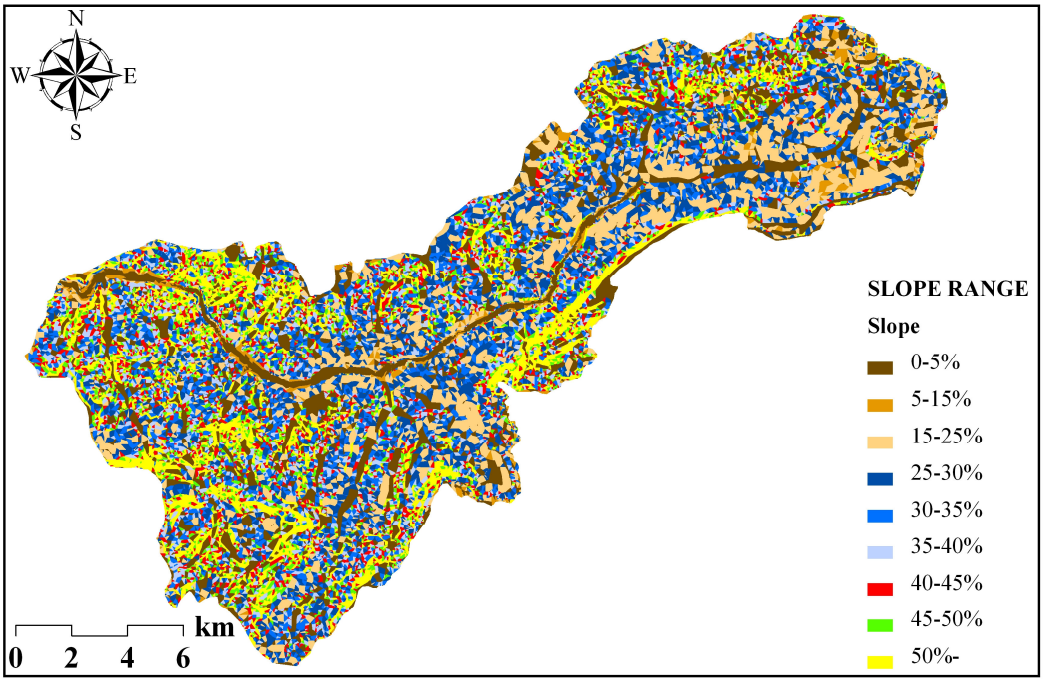

Figure 3.9. Slope of the watershed

The aspect of the spring watershed is displayed on the Figure 3.10. The weighted averages of the aspect distribution are defined in Table 3.3. These averages were estimated using the Spatial Analyst extension of the ArcGIS 9.1 (ESRI, 2005). According to the figure and the table, the dominant aspect within the watershed is flat one. On the other hand, the second dominant aspect within the watershed is the north-west direction.

Table 3.3. The aspects and their ratios within the watershed

Aspect	Area (km^2)	Ratio (%)
Flat	45.6	15.9
North	29.5	10.3
North-East	23.6	8.2
East	30.8	10.8
South-East	30.3	10.6
South	31.8	11.1
South-West	24.0	8.4
West	30.5	10.7
North-West	40.4	14.1

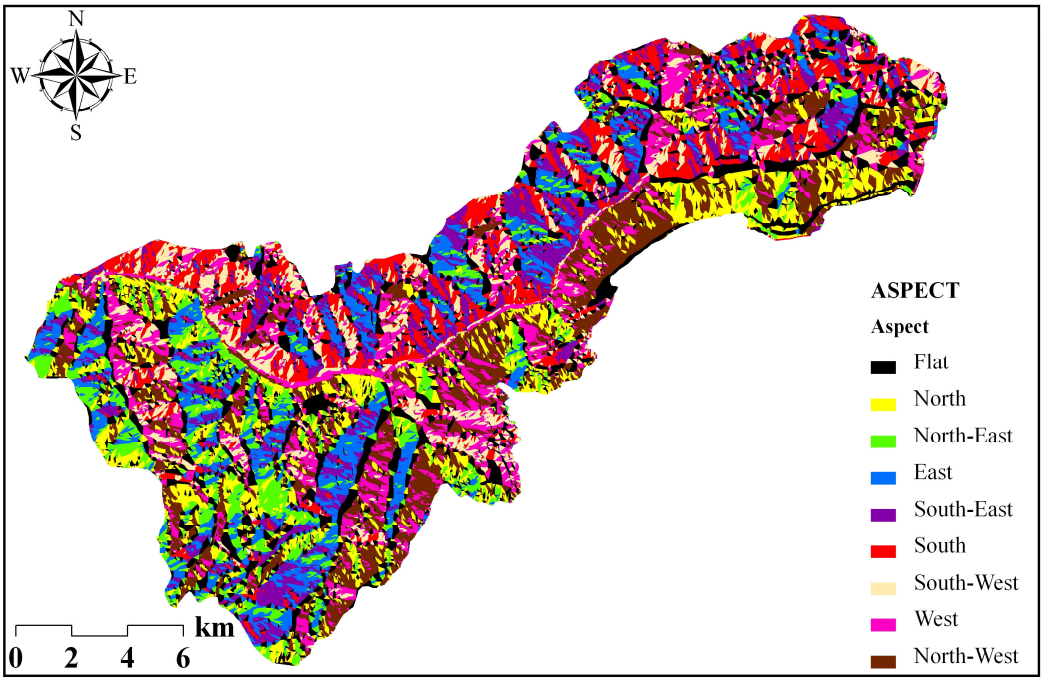

Figure 3.10. Aspect of the watershed

3.1.5. Stream Network

The watershed includes a complex surface water network. The stream collecting water from the upland of the watershed (Ahmetusta Mountain Pass) connects to the stream coming from the foots of Uluyayla Mountain in Ovacuma Town and flows about seven kilometers until another stream (Kara Stream together with Şimşirli Stream) merges with

them about one kilometer away from the spring water reservoir in Ulupınar (Öztürk et al., 2007). The location of the main streams within the watershed can be seen in Figure 3.7.

3.1.6. Geology

The general geological formation units of the study area are presented in Figure 3.11 (M.T.A, 2002). The geology of the watershed varies from Ereğli formation to the alluvial along the main watershed stream. The permeable layer of the watershed is the weathered part of the Ulus formation. The upper layer of this formation has been affected by the weathering processes and the porous layers formed (M.T.A., 2002). The thickness of the weathered layer ranges from 2 m at the northeastern part to 14.5 m at the southwestern part of the watershed while the thickness of the alluvion reaches up to 30 m (Karabük İl Özel İdaresi, 2006). There are numerous springs with small discharges within the watershed but the main discharge point is a karstic one developed in the limestones of the Ereğli formation at the southeastern part of the watershed. The discharge of this spring water ranges between 280 and 1100 L/s. The distance from the spring to the furthest border of the watershed is approximately 30 km where the limestone of the Safranbolu formation spread on the land (M.T.A., 2002).

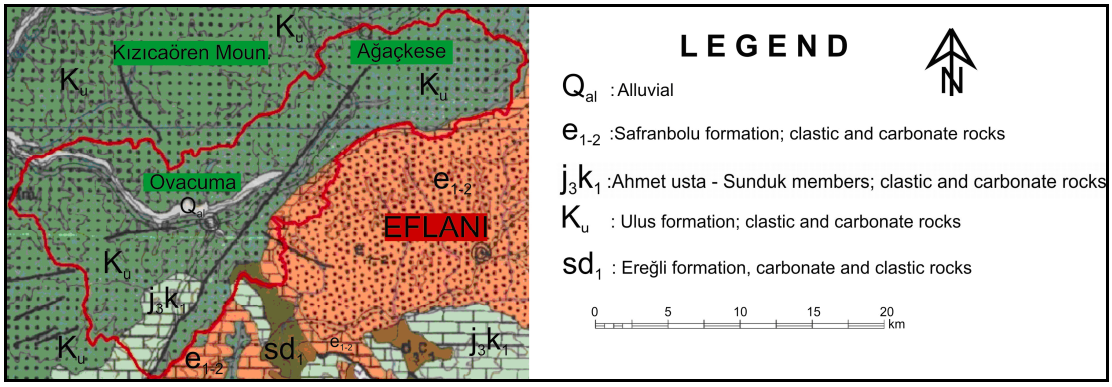

Figure 3.11. Geological formation units of the area (M.T.A., 2002)

The Ordovician age Ereğli formation is the basement of the study area. This formation consists of shale, sandstone and limestone. It is overlaid by the Cretaceous age Ulus formation consisting sandstone, shale, conglomerate, limestone, granite and marble blocks. Ulus formation has two members; Ahmet Usta and Sunduk which are conglomerate and

limestone respectively. The Ulus formation is overlaid by the Tertiary age Safranbolu formation which contains limestone with nummulites, marl and clastic rocks (M.T.A., 2002). The geology of the top layer is shown in Figures 3.11 and 3.12.

The structure of the basin is interrupted by the faults as a result of the tectonic movements during the geological processes. Safranbolu and Ulus formations face each other through the fault between the Bağcıyaz and Soğucak direction (Figure 3.11). The uplifted side of the fault Ulus formation faces Safranbolu formation and the karstification was developed among these two formations by environmental effects during the geological processes. Moreover; a physical connection is also possible between the limestones of the Ereğli formation under the Ulus formation so that the karstic structures developed between these geological units may be extending towards the Kastamonu – Pınarbaşı regions.

Table 3.4. Geological formations and their ratios within the watershed

Geological Formation	**Area (km^2)**	**Ratio (%)**
Alluvion	7.3	2.6
Sandstone-Mudstone	223.3	77.9
Limestone	33.9	11.8
Gravel	19.2	6.7
Sandstone-Mudstone-Limestone	2.5	0.9
Rhyodacite	0.3	0.1

Figure 3.12 shows the different formations within the watershed. The geological formations within the watershed are alluvion, gravel, limestone, rhyodacite, sandstone-mudstone mixtures and the sandstone-mudstone-limestone mixtures. The distribution of these formations and their ratios within the watershed are given in Table 3.4. These ratios were estimated using the Spatial Analyst extension of the ArcGIS 9.1 (ESRI, 2005). According to the figure and the table, the dominant geological formation is sandstone and mudstone which cover almost 78 % of the watershed.

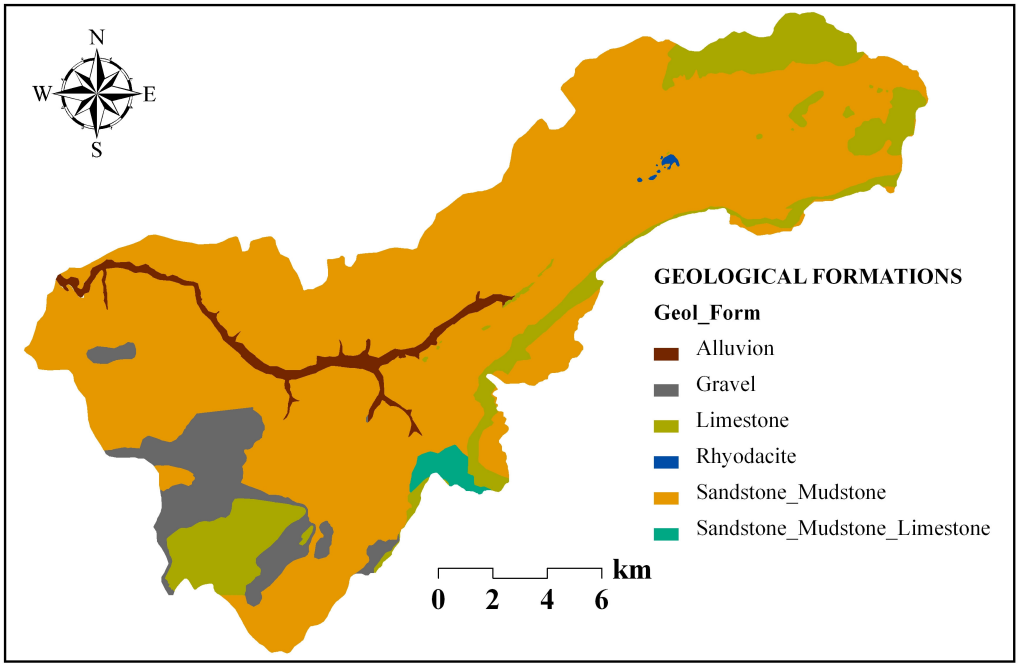

Figure 3.12. Geological formations in the watershed

3.1.7. Soil

The major soil groups within the watershed are presented in Figure 3.13. The major soil groups within the watershed are alluvial soil, brown forest soil, colluvial soil, grey brown podsolic soil and the limeless brown forest soil. The major soil groups and their ratios within the watershed are listed also in Table 3.5. According to the Table 3.5, the dominant major soil group within the watershed is grey brown podsolic soil which covers almost half of the watershed. The second dominant major soil group is the brown forest soil (A.P.K., 2005).

Table 3.5. Major soil groups and their ratios within the watershed

Major Soil Group	**Area (km^2)**	**Ratio (%)**
Alluvial	7.9	2.7
Colluvial	1.6	0.6
Grey Brown Podsolic	138.4	48.3
Brown Forest	106.4	37.1
Limeless Brown Forest	31.1	10.8
Settlement	1.2	0.4

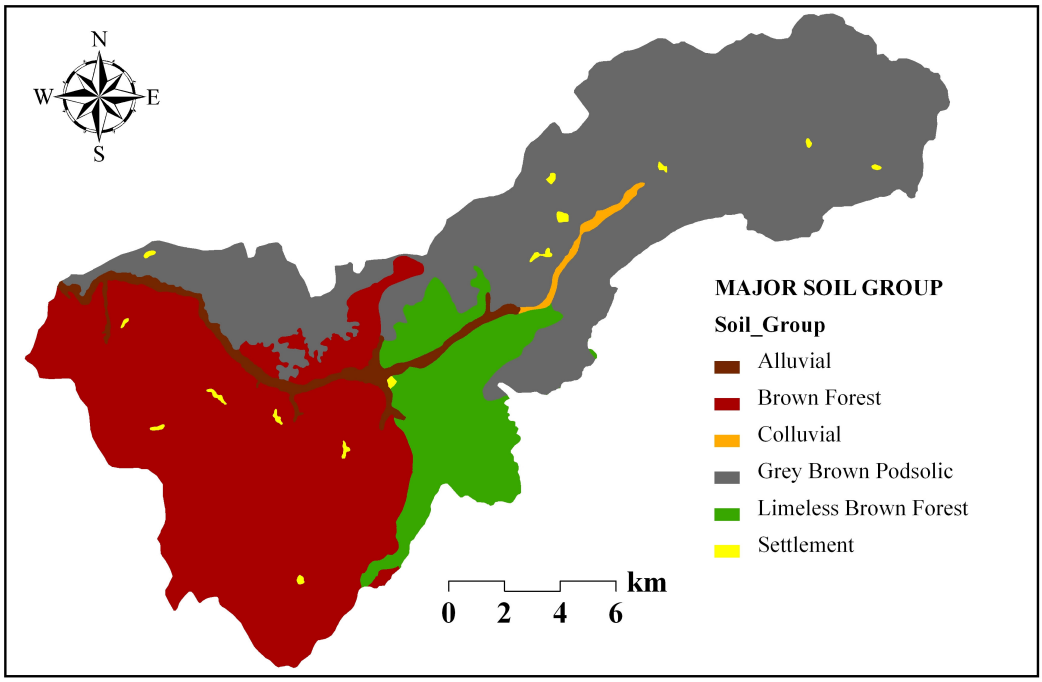

Figure 3.13. Major soil groups within the watershed (A.P.K., 2005)

The depth ranges of these soils and their ratios within the watershed are shown in Figure 3.14 and Table 3.6. These ratios were estimated using the Spatial Analyst extension of the ArcGIS 9.1 (ESRI, 2005). These depths represent the actual soil depth up to the parent material and the rock. The soil with the depth range of 20 cm and 50 cm cover almost half of the watershed. In other words, the half of the watershed is covered with shallow soils. The depth of the alluvial and the colluvial soils exceed 5 meters.

Table 3.6. Soil depth ranges and their ratios within the watershed

Soil Depth Range (cm)	Area (km^2)	Ratio (%)
0-20	57.3	20.0
20-50	141.8	49.5
50-90	76.8	26.8
500+	9.4	3.3
Settlement	1.2	0.4

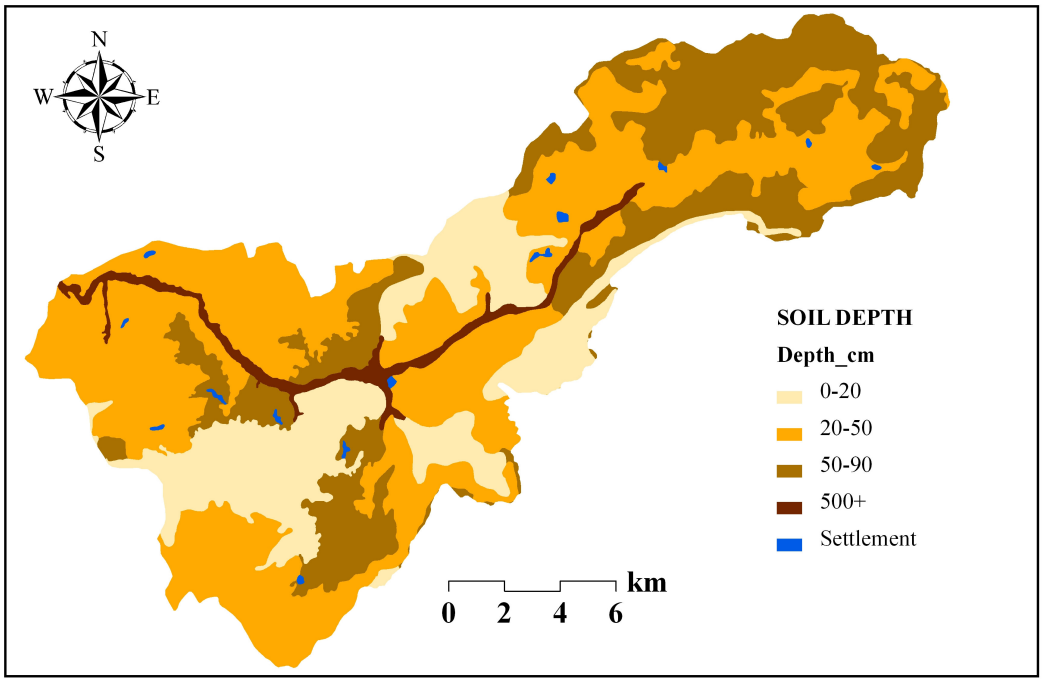

Figure 3.14. Soil depth ranges within the watershed (A.P.K., 2005)

The physical characteristics of the soil such as the soil type, porosity and the vertical hydraulic conductivity are described in Section 3.3.1.8, the Unsaturated Zone Flow subsection of the hydrodynamics model. These physical characteristics of the soil together with the corresponding values are based on the field sampling and laboratory analysis that were performed as part of this study. The sampling and the measurement methods are also discussed in the Field and Laboratory works subsection (2.4) of the Methodology chapter.

3.1.8. Forest and Agricultural Vegetation

The vegetation in the watershed is in the form of agriculture and forest. The forest vegetation is defined according to the plant type. The area and the ratio of the land uses are given in Table 3.7 (O.G.M., 2006). These ratios were estimated using the Spatial Analyst extension of the ArcGIS 9.1 (ESRI, 2005).

Table 3.7. The area and ratio of the land uses within the watershed

Stand Group	Land Use	Area (km^2)	Ratio (%)
	Agriculture	99.2	34.6
	Settlement	4.8	1.7
	Forest Open Space	2.2	0.8
Coniferous	Fir	20.0	7.0
	Fir-Pine	3.5	1.2
	Pine	32.6	11.4
Deciduous	Beech	26.0	9.1
	Beech-Hornbeam	4.3	1.5
	Beech-Oak	3.3	1.1
	Oak	23.2	8.1
	Oak-Hornbeam	16.3	5.7
	Hornbeam	7.1	2.5
	Plane	0.4	0.2
Mixed	Fir-Beech	24.9	8.7
	Fir-Oak	5.2	1.8
	Fir-Hornbeam	2.0	0.7
	Pine-Oak	7.3	2.6
	Pine-Hornbeam	4.1	1.4

The agricultural areas cover more than 1/3 of the watershed. The deciduous forests cover the largest forest area which is almost 28% of the watershed. The coniferous and the mixed forests cover almost 20% and 15% of the watershed, respectively. The settlement and the forest open space together consist of only 2.5% of the watershed. The dominant deciduous, coniferous and mixed forest stands are generally the beech, pine and fir-beech. The distribution of these forest stands within the watershed is presented in Figure 3.15.

Table 3.8 shows the area and ratio distribution of the land use types for different altitude ranges. Table 3.9 groups these land use types under wider altitude ranges. The relation of land use types to elevation are also shown in Figure 3.16.

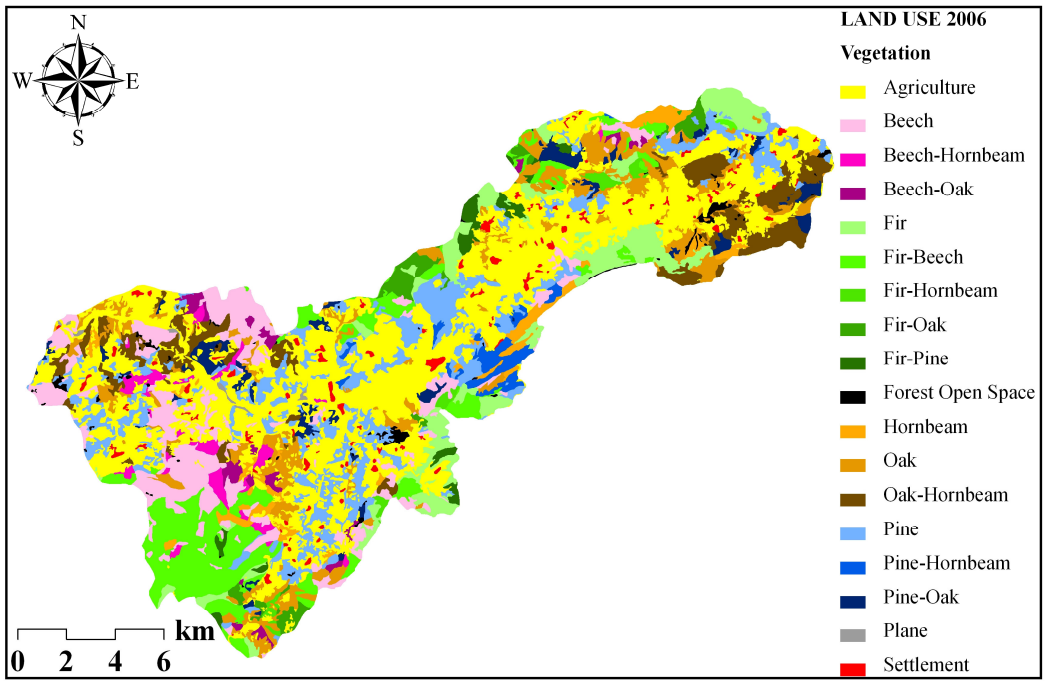

Figure 3.15. Land use map of 2006 (O.G.M., 2006)

The agricultural vegetation is mainly composed of wheat and corn. The areas covered by wheat are distributed within the watershed while the corn is cultivated on the areas close to the settlements. The agricultural areas cover more than 1/3 of the watershed. Almost 75% of these agricultural areas are located at the altitude range between 350 m and 800 m (Table 3.9) which is relatively low compared to the general altitude ranges of the watershed. However almost 19% of the agricultural areas are located within the altitude ranges of 800 m and 1100 m. These areas are close to the upland settlements within the watershed.

Table 3.8. Area and ratio distribution of the land use types for different altitude ranges

Altitude Range / Vegetation	200-350		350-500		500-650		650-800		800-950		950-1100		1100-1250		1250-1400		1400-1550	
	Area (km^2)	Ratio (%)	Area (km^2)	Ratio (%)	Area (km^2)	Ratio (%)	Area (km^2)	Ratio (%)	Area (km^2)	Ratio (%)	Area (km^2)	Ratio (%)	Area (km^2)	Ratio (%)	Area (km^2)	Ratio (%)	Area (km^2)	Ratio (%)
Agriculture	6.9	7.0	21.2	21.4	28.3	28.5	24.4	24.6	14.8	14.9	3.6	3.6	0.01	0.01	0.01	0.01	0.01	0.01
Settlement	0.1	3.0	0.9	19.6	1.5	30.5	0.9	19.5	1.0	21.0	0.3	6.4	×	×	×	×	×	×
Forest Open Space	0.2	10.4	0.2	7.4	0.6	26.6	0.8	36.2	0.2	8.3	0.2	10.0	0.02	1.1	×	×	×	×
Fir	×	×	×	×	0.5	2.4	3.3	16.7	6.7	33.5	7.0	35.3	1.5	7.5	0.6	3.1	0.3	1.6
Fir-Pine	×	×	×	×	×	×	0.3	7.3	1.2	34.9	1.5	44.3	0.3	9.0	0.2	4.5	×	×
Pine	0.5	1.6	5.6	17.1	10.7	32.7	8.1	24.7	4.9	15.1	2.3	7.2	0.5	1.6	0.01	0.02	×	×
Beech	1.3	5.1	2.1	8.0	3.8	14.5	8.2	31.7	6.8	26.3	2.3	8.9	1.1	4.3	0.3	1.0	0.1	0.3
Beech-Hornbeam	0.2	3.8	0.7	16.6	1.1	25.3	1.6	36.0	0.6	13.6	0.1	1.2	0.01	0.2	0.1	2.9	0.02	0.4
Beech-Oak	×	×	0.2	6.4	0.5	16.4	1.1	34.3	0.8	24.8	0.2	7.5	0.3	9.8	0.02	0.7	×	×
Oak	1.1	4.9	1.4	6.0	2.4	10.1	5.1	21.9	6.5	27.8	6.1	26.3	0.6	2.7	0.1	0.3	×	×
Oak-Hornbeam	1.4	8.4	2.2	13.7	2.0	12.4	2.0	12.5	3.4	20.5	5.3	32.5	×	×	×	×	×	×
Hornbeam	0.2	3.3	0.5	6.4	0.8	10.9	0.9	12.4	1.2	16.9	2.1	29.1	0.9	13.1	0.5	7.5	0.04	0.5
Plane	0.4	94.1	0.03	5.9	×	×	×	×	×	×	×	×	×	×	×	×	×	×
Fir-Beech	×	×	0.04	0.2	0.9	3.7	2.5	10.0	5.4	21.7	5.0	20.1	5.0	20.2	4.4	17.8	1.6	6.4
Fir-Oak	×	×	×	×	0.2	3.3	0.9	16.6	2.0	39.2	1.0	19.9	0.9	16.8	0.2	4.2	×	×
Fir-Hornbeam	×	×	×	×	×	×	0.4	19.0	1.0	50.7	0.6	30.3	×	×	×	×	×	×
Pine-Oak	0.3	3.7	1.6	21.2	1.0	13.0	1.2	16.7	1.6	21.8	1.5	21.1	0.2	2.4	×	×	×	×
Pine-Hornbeam	×	×	0.2	6.0	0.5	12.6	1.0	24.3	1.4	33.8	0.9	22.8	0.02	0.4	×	×	×	×

Table 3.9. The generalized area of the land uses and the ratio of this area within the watershed altitude ranges

Vegetation-Altitude	**Area (km^2)**	**Ratio (%)**
Agriculture-350-800	73.9	74.5
Agriculture-800-1100	18.4	18.5
Settlement-350-800	3.3	69.7
Settlement-800-1100	1.3	27.4
Forest Open Space-200-800	1.8	80.6
Forest Open Space-800-1250	0.4	19.4
Fir-650-1100	17.1	85.5
Fir-1100-1550	2.4	12.2
Fir-Pine-800-1100	2.7	79.1
Fir-Pine-1100-1250	0.5	13.5
Pine-350-650	16.2	49.9
Pine-650-1100	15.3	47.0
Beech-200-500	3.4	13.1
Beech-500-950	18.8	72.4
Beech-950-1250	3.4	13.1
Beech-Hornbeam-200-500	0.9	20.4
Beech-Hornbeam-500-950	3.3	74.9
Beech-Oak-350-650	0.7	22.8
Beech-Oak-650-950	1.9	59.1
Beech-Oak-950-1250	0.6	17.3
Oak-200-650	4.9	21.0
Oak-650-1100	17.7	76.0
Oak-Hornbeam-200-500	3.6	22.1
Oak-Hornbeam-500-800	4.1	24.9
Oak-Hornbeam-800-1100	8.7	53.0
Hornbeam-500-800	1.6	23.2
Hornbeam-800-1100	3.2	46.0
Hornbeam-1100-1400	1.5	21.1
Plane-200-350	0.4	94.1
Fir-Beech-650-1100	12.9	51.8
Fir-Beech-1100-1550	11.0	44.4
Fir-Oak-500-800	1.0	19.9
Fir-Oak-800-1100	3.1	59.1
Fir-Oak-1100-1400	1.1	21.1
Fir-Hornbeam-650-950	1.4	69.7
Fir-Hornbeam-950-1100	0.6	30.3
Pine-Oak-200-500	1.8	24.9
Pine-Oak-500-800	2.2	29.8
Pine-Oak-800-1100	3.1	42.9
Pine-Hornbeam-350-650	0.8	18.6
Pine-Hornbeam-650-950	2.4	58.2
Pine-Hornbeam-950-1250	1.0	23.3

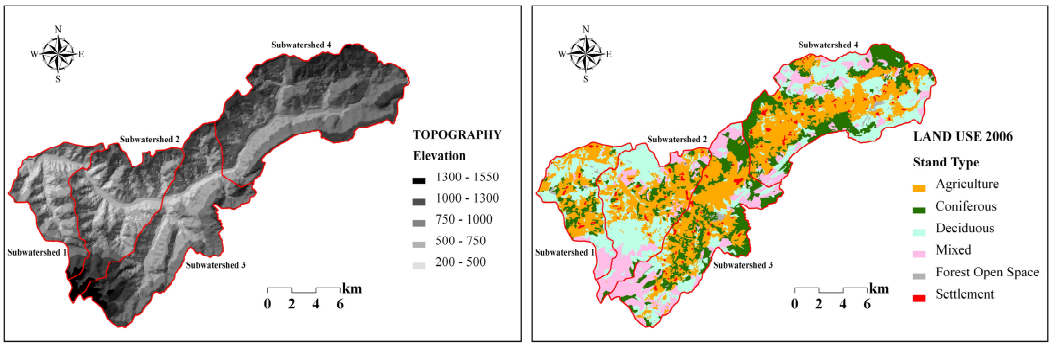

Figure 3.16. Land use altitude relations within the watershed

The Black Pine (*Pinus nigra*), Calabrian Pine (*Pinus brutia*), Scots Pine (*Pinus sylvestris*) and Turkish Fir (*Abies bornmülleriana*) constitute the coniferous stands in the watershed, while the deciduous stands are mainly composed of Oriental Beech (*Fagus orientalis*), Oaks (*Quercus sp.*), Oriental Hornbeam (*Carpinus orientalis*) and Oriental Plane (*Platanus orientalis*).

The pure Turkish firs dominate especially the hills within the watershed particularly between the altitudes of 650 m and 1100 m. The range of the altitudes where Turkish fir optimum grows is between 1000 m and 2000 m (Saatçioğlu, 1976). The Turkish Fir and the Oriental Beech exist together as mixtures at some hills ranging between 650 and 1550. Particularly at the range of 800 m and 1100 m altitudes, the Turkish Fir exists as mixtures with oaks also. At that altitude range, Oriental Hornbeams also accompany the Turkish Firs.

The Black Pines mainly grow on the relatively lower altitudes compared to the Turkish Firs. The optimum growth altitude for the Black Pines in the Western Black Sea is 400 m and 1400 m (Saatçioğlu, 1976). Almost half of the pure Black Pines occur at the altitude range of 350 m and 650 m while the other half occurs at the altitude range of 650 and 1100 m in the watershed. They particularly make mixtures with Turkish Firs at the range of 800 and 1100 m. Within this range, they also mix with the oaks and the Oriental Hornbeams.

Although the optimum spread range of the Oriental Beeches is 1100 and 1500 m (Saatçioğlu, 1976), they particularly (72%) occur as pure stands in the range of 500 and 950 m altitudes within the watershed. At that range, they also make mixture stands with oaks and Oriental Hornbeams. As mentioned, the Turkish Firs accompany them at the higher altitude ranges such as 650 and 1550 m.

Similar to the Turkish Fir, the pure oak stands occur particularly at the altitude range of 650 m to 1100 m within the watershed. Different species of the oaks are found at different altitude ranges in the Western Black Sea Region. They mix with particularly Oriental Hornbeams at the altitude range of 800 and 1100 m. They also mix with almost all the other plants within the watershed such as the Oriental Beeches, Turkish Firs and the Black Pines at different altitudes.

The pure Oriental Hornbeams grow at the altitude range of 800 m to 1100 m within the watershed. The Oriental Hornbeams are generally found as mixtures with other plants mainly with oaks. They also mix with almost all the other plants within the watershed such as the Oriental Beeches, Black Pines and Turkish Firs. The oriental planes dominate especially the stream banks of the watershed where the altitude ranges between 200 and 350 m.

3.1.9. Settlement

Settlements within the low laying areas of the study area are sparse mainly in the form of villages. The population density increases at higher altitudes of the area, primarily within the town municipality of Ovacuma. The density of the agricultural areas also is dependent upon the settlement; being sparse at the downland and relatively dense at the upland close to Ovacuma Town Municipality.

3.2. Land Use Dynamics Model

The input data for the land use dynamics model and the hydrodynamics model were defined based on the site characteristics described in the previous section. This section

describes the database used in the land use dynamics model. The input data of the hydrodynamics model are described in the Section 3.3

The land use model was built to simulate the temporal dynamics of the land use change in the Bartın-Ulupınar watershed. The digitized land use maps of 1986 and 2006 were used for conceptualization and calibration of land use model (Figures 3.17 and 3.18). The 1986 map was digitized using the GIS software Arc-Info 9.1 and used as the initial model parameter data. The digitized forest management map for the year 2006 was acquired from the Ulus Forestry Administration and used as the model target data.

3.2.1. Land Use Dynamics Model Database

Based on the land use existing within the study area, three general land use types were defined in the land use dynamics model: Forest, agricultural area, settlement and forest open space. The digitized maps obtained from The General Directorate of Forestry (O.G.M., 2006) give the coverage of land use types, detailed forest stand types, age categories and crown closures. From this information, the forest was classified into forest stand categories based on the stand types, age categories and crown closures:

- The Stand types were grouped as *coniferous*, *deciduous* and *mixed*. The Latin and common names and the symbols of the forest trees together with their stand type groups are shown in Table 3.10.

- The age categories of the stand types based on their DBH (Diameter at Breast Height) are presented in Table 3.11.

- The crown closure ranks of the stand types are defined according to their closure percentages as in Table 3.12.

Table 3.10. Latin and common names and the symbols of coniferous and deciduous trees in the watershed (O.G.M., 2006)

	Symbol	**Latin Name**	**Common Name**
Coniferous	Ab	*Abies bornmülleriana*	Turkish Fir, Bornmuller's Fir
	Pb	*Pinus brutia*	Turkish Pine
	Pn	*Pinus nigra*	European Black Pine, Austrian Pine
	Ps	*Pinus sylvestris*	Scots Pine
Deciduous	Qp	*Quercus sp.*	Oak Species
	Fo	*Fagus orientalis*	Oriental Beech
	Co	*Carpinus orientalis*	Oriental Hornbeam
	Po	*Platanus orientalis*	Oriental Plane

Table 3.11. The growth periods of the forest stands based on their DBH Class Boundaries and the symbols attributed to these growth periods (O.G.M., 2006)

Growth Period	**DBH Class Boundary (cm)**	**Symbol**
juvenile-intense	≤7,9	a
pole-post	8,0-19,9	b
slender tree	20,0-35,9	c
average tree	36,0-51,9	d
thick tree	52,0≤	e

Table 3.12. Stand crown closure ranks based on their closure percentages (O.G.M., 2006)

Crown Closure Class	**Closure Percentage**	**Symbol**
Almost Empty	≤10%	0
Sparse	11-40%	1
Moderate	41-70%	2
Dense	71%≤	3

The categories shown in Table 3.11 and Table 3.12 were aggregated with respect to their hydrological parameters in order to avoid increment of the model magnitude and complexity with the land categories that exist on the maps. As to growth period categories in Table 3.11, juvenile-intense and pole-post were aggregated together under “ab” considering them as *young*. The subsequent three growth periods; slender tree, average tree and thick tree were aggregated under “cd” considering them as *mature*. The multi-aged stand types were aggregated under “abcd”. The “e-thick tree” period was included into the “d-average tree” period, following the convention by General Directorate of Forestry (G.D.F.). For the *mixed* multi-aged stand types, the first two age symbols represent the *coniferous* stands within the mixture while the second two represent the deciduous ones.

For example, "*Mixed cdab*" stand category represents Mature Coniferous trees together with the Young Deciduous ones. As to crown closure categories in Table 3.12, the stands with closure 0 were treated as almost empty spaces. The formation of an aggregated model stand category may be summarized with an example of the mixed stand symbolized as Pnd/Mb3 on the map. As stated in Table 3.10, 'Pn' symbolizes the *coniferous* tree; *Pinus nigra*, European Black Pine and 'd' symbolizes that it is average tree being *mature*. Similarly 'Mb' symbolizes the *deciduous* tree; *Quercus sp.*, Oak species and 'a' symbolizes that it is juvenile tree being *young*. The symbol '3' indicates that the stand crown closure is *dense*. Therefore the mixed stand with the map symbol of Pnd/Mb3 was aggregated as *Mature Coniferous Young Deciduous 3* stand category in the land use model.

Besides all these forest stand categories, there are also multi-aged dense stands within the watershed. The age category of these stand types with multi-aged trees are symbolized with capital letters A, B, C and D as accepted by the General Directorate of Forestry (O.G.M., 2006). The letter symbols and their corresponding age groups are stated in Table 3.13.

Table 3.13. The letter symbols and their corresponding age groups.

A	Mature trees are dominant
B	Young trees are dominant
C	Mature and Young trees are almost equal
D	Mixture combination of previous three groups

According to the summarized characteristics (Table 3.13) of the multi-aged stands, the stands symbolized with any of those capital letters were included in the most relevant stand category.

The watershed was then divided into four subwatersheds for spatial disaggregation of the land use dynamics model. The boundaries of the subwatersheds were defined based on topography. The higher number of subwatersheds would complicate the land use dynamics model while the less would simplify too much. The land use maps of 1986 and 2006 showing the map and model forest stand categories together with the four subwatersheds are shown in Figures 3.17, 3.18, 3.19 and 3.20 respectively.

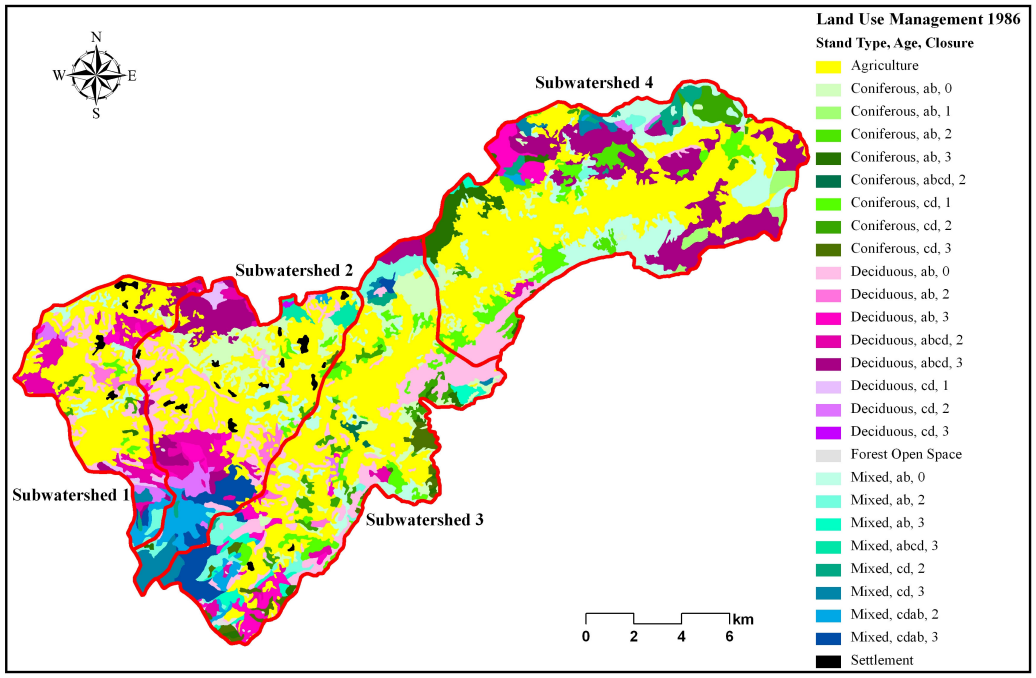

Figure 3.17. Land use map of 1986 with map categories

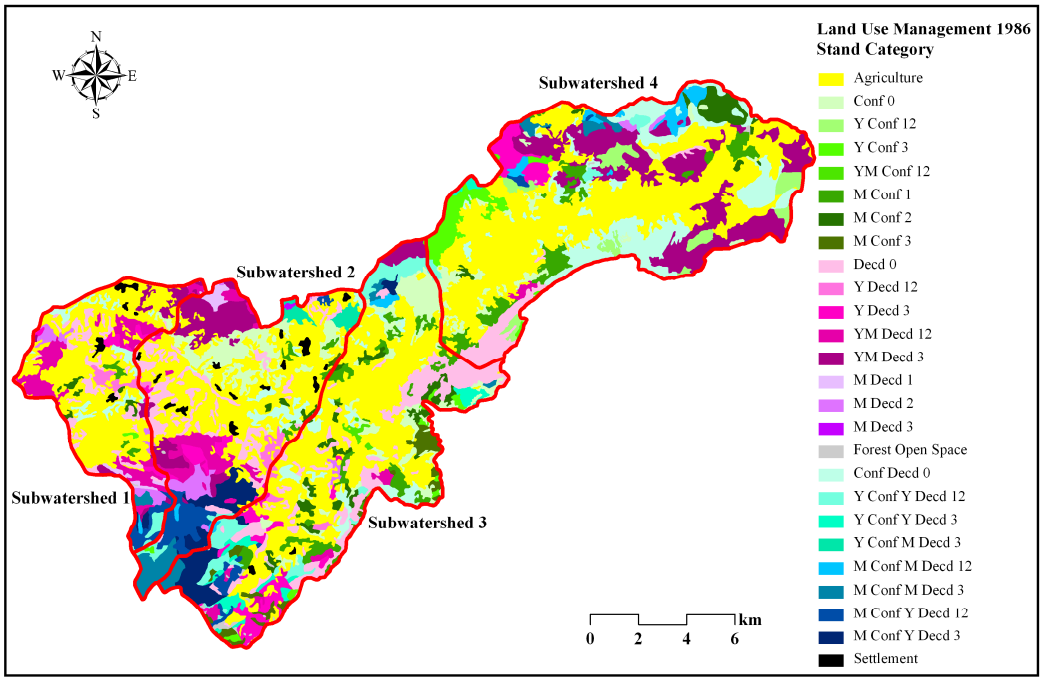

Figure 3.18. Land use map of 1986 with model categories

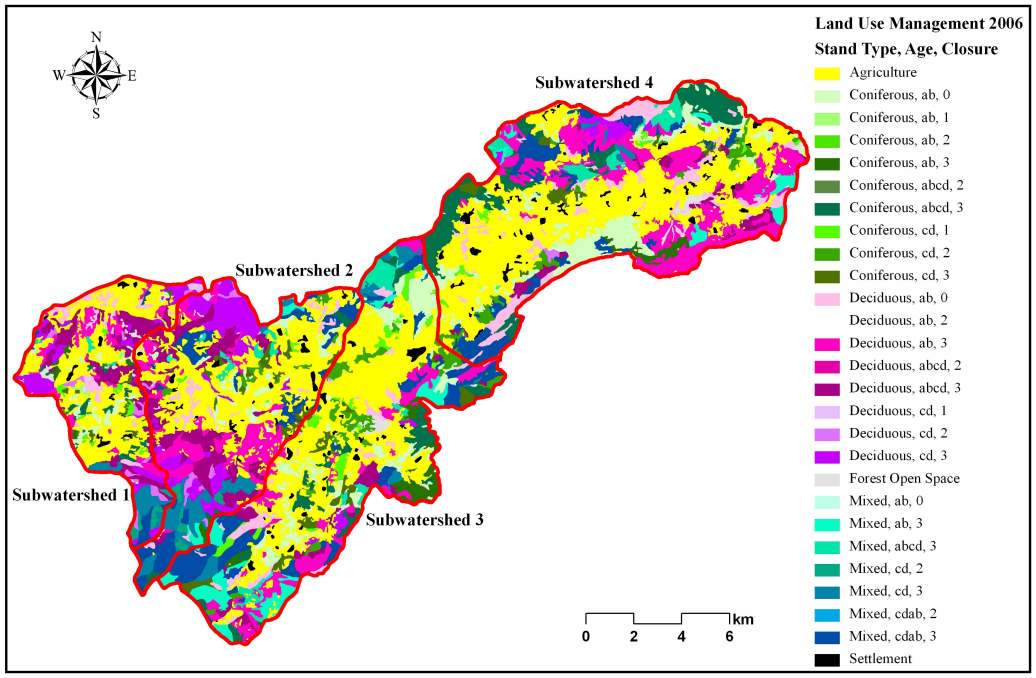

Figure 3.19. Land use map of 2006 with map categories

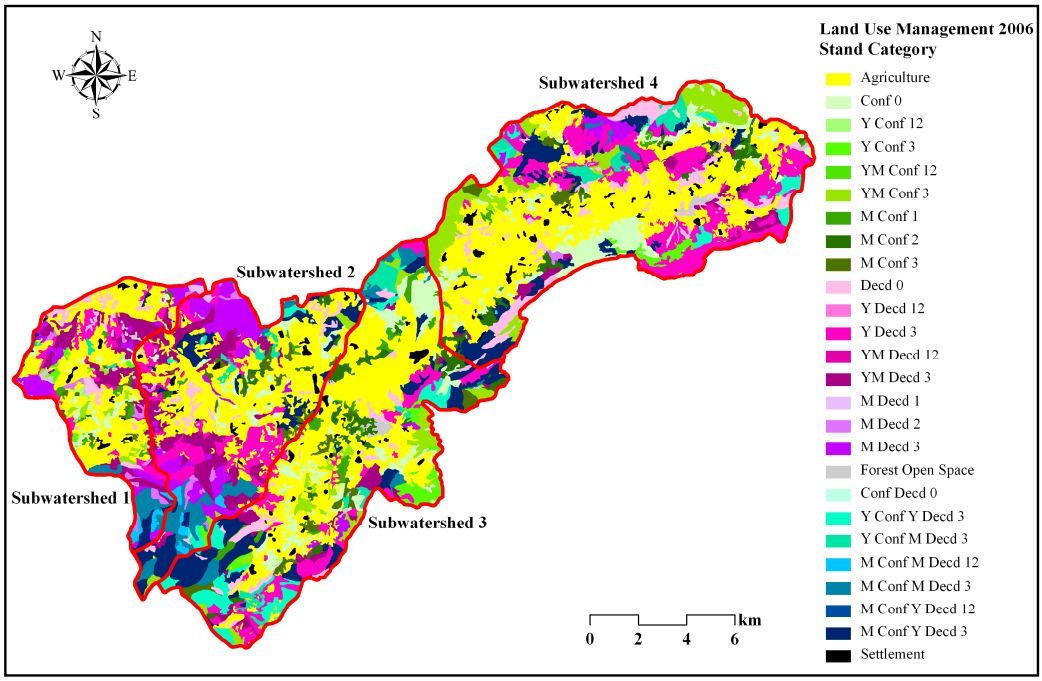

Figure 3.20. Land use map of 2006 with model categories

3.2.2. Land Use Transformation

Table 3.14 presents the model stand categories and their correspondence to aggregated geographical data. These stand categories are the model state variables. They were represented by the rectangles (stock variables) as illustrated in Figure 3.21.

Table 3.14. Stand categories for the 1986 and 2006 land use maps and the model state variables

1986 Map	Model	2006 Map
Coniferous ab 0	Coniferous 0	Coniferous ab 0
Coniferous ab 1	Young Coniferous 12	Coniferous ab 1
Coniferous ab 2		Coniferous ab 2
Coniferous ab 3	Young Coniferous 3	Coniferous ab 3
Coniferous abcd 2	Young-Mature Coniferous 12	Coniferous abcd 2
	Young-Mature Coniferous 3	Coniferous abcd 3
Coniferous cd 1	Mature Coniferous 1	Coniferous cd 1
Coniferous cd 2	Mature Coniferous 2	Coniferous cd 2
Coniferous cd 3	Mature Coniferous 3	Coniferous cd 3
Deciduous ab 0	Deciduous 0	Deciduous ab 0
Deciduous ab 2	Young Deciduous 12	Deciduous ab 2
Deciduous ab 3	Young Deciduous 3	Deciduous ab 3
Deciduous abcd 2	Mature-Young Deciduous 12	Deciduous abcd 2
Deciduous abcd 3	Mature-Young Deciduous 3	Deciduous abcd 3
Deciduous cd 1	Mature Deciduous 1	Deciduous cd 1
Deciduous cd 2	Mature Deciduous 2	Deciduous cd 2
Deciduous cd 3	Mature Deciduous 3	Deciduous cd 3
Mixed ab 0	Coniferous-Deciduous 0	Mixed ab 0
Mixed ab 2	Young Coniferous-Deciduous 12	
Mixed ab 3	Young Coniferous-Deciduous 3	Mixed ab 3
	Young Coniferous Mature Deciduous 12	
Mixed abcd 3	Young Coniferous Mature Deciduous 3	Mixed abcd 3
Mixed cdab 2	Mature Coniferous Young Deciduous 12	Mixed cdab 2
Mixed cdab 3	Mature Coniferous Young Deciduous 3	Mixed cdab 3
Mixed cd 2	Mature Coniferous-Deciduous 12	Mixed cd 2
Mixed cd 3	Mature Coniferous-Deciduous 3	Mixed cd 3
Agriculture	Agriculture	Agriculture
Forest Open Space	Forest Open Space	Forest Open Space
Settlement	Settlement	Settlement

Above model stand categories were modeled as state (stock) variables (rectangles in Figure 3.21). The natural transformations that occur between these state variables are *maturation*, *intensification*, *degradation, regeneration*, and *regrowth* while the

anthropogenic transformations are unusual cuts, stand removal, and conversion between agricultural areas, forest areas, settlement and forest open spaces. These transformations are the rate of change of associated state variables and are illustrated by the "pipes with valves" in Figure 3.21. Stella software the version 7.0.1 Research was used to model the land use dynamics (H.P.S., 2001). These transformations are briefly discussed below.

3.2.2.1. Natural Transformations.

Maturation. The maturation is the alteration of the stages ab (young) up to stages cd (mature). The maturation time for both the coniferous and the deciduous forest is assumed to be 50 years (Kalıpsız, 1998). According to the land use model, the coniferous stand groups Y Conf 3 and YM Conf 3 mature to be the stand group M Conf 3. The deciduous stand groups Y Decd 3 and YM Decd 3 mature to be the stand group M Decd 3. The mixed stand groups Y Conf Y Decd 3, Y Conf M Decd 3 and M Conf Y Decd 3 mature to be M Conf M Decd 3.

Intensification. The intensification is the alteration of the stand group from less stand closure to higher stand closure. The intensification time both for the coniferous and deciduous stands is 5 years (interpreted from Genç, 2004). According to the model, the coniferous stand groups Y Conf 12 and YM Conf 12 intensify to be Y Conf 3 and YM Conf 3 respectively while the deciduous stand groups Y Decd 12 and YM Decd 12 intensify to be Y Decd 3 and YM Decd 3 respectively. Among the mixed stand groups, Y Conf Y Decd 12, M Conf Y Decd 12 and Y Conf M Decd 12 intensify to be Y Conf Y Conf 3, M Conf Y Decd 3 and Y Conf M Decd 3 respectively.

Degradation. The forest stands begin to degrade as they grow older. Based on the principle that the average life of a tree is 150-200 years (Saatçioğlu, 1976), the 50-60 years old mature stands degrade in almost 100-120 years. During the degradation, the stand closure also diminishes gradually. According to the model, the M Conf 3 degrades to be M Conf 2 in 40 years and M Conf 2 degrades to be M Conf 1 in 40 years. The degradation time for M Conf 1 to be Conf 0 is 20 years. The situation is the same for the deciduous stand groups such as M Decd 3 degrades to be M Decd 2 in 40 years and M Decd 2 degrades to be M Decd 1 in 40 years. The degradation time for M Decd 1 to be Decd 0 is 20 years. The

mixed stand group M Conf M Decd 3 degrades to be M Conf M Decd 12 in 40 years while M Conf M Decd 12 degrades to Conf Decd 0 in 20 years.

Regeneration. Regeneration is the introduction of the seedlings into the stands where the ecological conditions are available. The sources of the seeds for seedlings are the mature trees (Genç, 2004). The new generations of young coniferous grow beneath the mature ones. The introduction of the young seedlings may be either natural or artificial due to forestry management practices. In this model, the natural and the artificial regeneration processes are separately evaluated naming the natural regeneration as regeneration and the artificial as regrowth. The regeneration time is assumed to be 50 years for any stand group. The coniferous stand groups, M Conf 1 and M Conf 2 regenerate to become YM Conf 12. The same situation is valid for the deciduous stand groups, M Decd 1 and 2 and for the mixed stand group, M Conf M Decd 12.

Regrowth. The artificial regeneration process, regrowth, is actually the regeneration itself but, since it occurs within the handicapped (stand closure 0) stand groups, it is named as regrowth for distinction. The artificial treatment involves not the plantation practices but the management practices such as the soil improvement, seed spreading and removal of the living covers. As a result of such management practices, there is still a possibility that regrowth may not occur. According to the land use model, a fraction of the handicapped stands regrow into the young stands. This fraction was determined based on the interpretation of the land use difference between the maps of 1986 and 2006. Also the regrowth could occur in one subwatershed while it could not in another.

The handicapped coniferous stand Conf 0 in subwatersheds 1 and 3 regrow into Y Conf 12 with the fractions of 0.005 and 0.01 respectively. The 0.005 and 0.02 of the Conf 0 also regrows to be YM Conf 12 in subwatersheds 3 and 4 respectively. The 0.01, 0.01 and 0.03 of the Conf 0 regrows to be M Conf Y Decd 12 in subwatersheds 2, 3 and 4 respectively. The 0.005 of the Conf 0 regrows to be Y Conf Y Decd 12 in subwatershed 3. The 0.05 of the Conf 0 regrows to be Y Decd 12 in subwatershed 2.

The handicapped deciduous forest group, Decd 0 regrows to be Y Decd 12 with the fraction of 0.04, 0.05 and 0.04 in subwatersheds 1, 2 and 3 respectively. The 0.02 and 0.01

of the Decd 0 regrows to be YM Decd 12 in subwatersheds 2 and 3 respectively. Also 0.005 and 0.02 of the Decd 0 regrows to be Y Conf M Decd 12 in subwatersheds 1 and 3.

The handicapped mixed forest group; Conf Decd 0 regrows to be M Conf Y Decd 12 with the fraction of 0.06 and 0.04 in subwaterheds 2 and 3 respectively. The 0.05 of the Conf Decd 0 regrows to be Y Conf 12 in subwaterhed 3. The 0.04 and 0.01 of the Conf Decd 0 regrows to be Y Conf Y Decd 12 in subwaterheds 2 and 4 respectively. The 0.01 of the Conf Decd 0 regrows to be YM Decd 12 in subwatershed 1. The 0.008, 0.06 and 0.005 of the Conf Decd 0 regrow to be YM Conf 12 in subwatersheds 1, 3 and 4 respectively. The 0.05, 0.02 and 0.1 of the Conf Decd 0 regrow to be Y Decd 12 in subwatersheds 2, 3 and 4 respectively. The 0.05 of the Conf Decd 0 regrow to be Y Conf M Decd 12, in subwatershed 4.

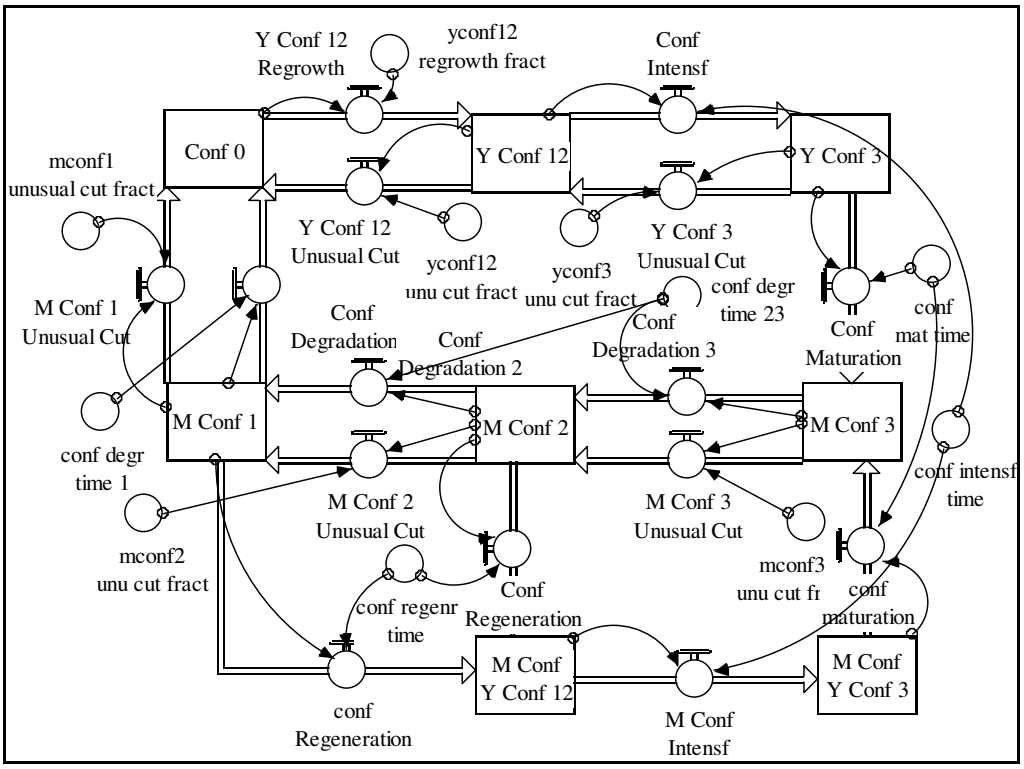

Figure 3.21. Stock-flow structure of the coniferous stand categories (Y: Young; M: Mature, Conf=Coniferous; numbers represent the stand closure)

Figure 3.21 is a section of the model representing land categories (stock variables) and land transformation (flow variables) for coniferous forests. For example, it illustrates

that, *young coniferous moderately close forests* (Y Conf 12) are intensified to *young coniferous dense forests* (Y Conf 3) through *coniferous intensification* transformation in *average coniferous intensification time* and this process is linearly approximated by the equation:

$$\textit{coniferous intensification} = \text{Y Conf 12} / \textit{average coniferous intensification time} \quad (3.1)$$

Similarly, *mature coniferous dense forests* (M Conf 3) are degraded to *mature coniferous moderately close forests* (M Conf 2) through *coniferous degradation* transformation in *average degradation time* and this transformation is linearly approximated by the equation:

$$\textit{coniferous degradation} = \text{M Conf 3} / \textit{average coniferous degradation time} \quad (3.2)$$

3.2.2.2. Anthropogenic Transformations. Most of the anthropogenic processes occurring within the forest area are based on the forest management practices conducted by the local forestry administration. The annual reports on the conducted forest management practices show that these practices particularly include nursing, regenerating, selection, illumination, spacing and unusual cut. None of these practices are intended to alter the stand age category, canopy closure and consequently the stand category except for unusual cut processes which generally occur based on some natural damages such as insects and wind knockdown (O.G.M., 2006). The unusual cut processes alter the stand category by decreasing the canopy closure. As a result of the unusual cut, the canopy closure of a stand part decreases to a lower closure state altering the category of that stand to one state lower closure category. In the model equations, the fraction of the unusual cut is defined based on the annual reports of the forest management practices. As an example, the *mature mixed moderately close stand* (M Conf M Decd 12) was cut unusually altering a definite fraction of that stand to *handicapped mixed stand* (Conf Decd 0). The equation for this transformation is linearly approximated by the equation:

$$\textit{M Conf M Decd 12 unusual cut} = \text{M Conf M Decd 12} \times \textit{unusual cut fraction} \quad (3.3)$$

The stand removal also occurs as a result of unusual cut in multi-aged stands but changes the category of that stand by sweeping the mature ones out of that stand. Consequently the new category of that stand becomes pure young stand category. The equation for the removal of mature deciduous trees from the *multi-aged deciduous dense stand* (YM Decd 3) is below:

$$M\ Decd\ removal = \text{YM Decd 3} \times removal\ fraction \tag{3.4}$$

The anthropogenic land use change within the watershed also includes the land conversions between agricultural areas, forest areas, settlement and forest open spaces. The rate of these processes is approximated with respect to the observed difference when the 1986 and 2006 maps are superimposed for comparison. In the model equations, it is assumed that the observed transformation occurs with respect to constant fractional change. For example, the conversion of agricultural area to young coniferous forest by introduction of the young coniferous seedlings is linearly approximated by the equation:

$$Agriculture\ to\ Y\ Conf\ 12 = \text{Agricultural area} \times agriculture\ to\ y\ conf\ 12\ fraction \tag{3.5}$$

Model fractions are calibrated so as to generate a fit between simulated and real land use stocks. Model runs are illustrated briefly in Chapter 4.

3.3. Hydrodynamics Model

The components of the hydrodynamics model were described in the Chapter 2. In this Section, the development of the hydrodynamics model is briefly described. The development of the hydrodynamics model involves supplying the model parameters for each model component.

3.3.1. Hydrodynamics Model Database

The hydrodynamics model database generally consists of the model parameters that are generally spatially uniform over the entire domain or in the form of GIS based files and associated time series values. The model input data consist of model domain and grid

resolution, topography, precipitation, land use, evapotranspiration, overland flow, river flow, unsaturated zone flow, saturated zone flow components.

3.3.1.1. Model Domain and Grid. The model covers the entire area of the watershed which covers approximately 287 km^2 (Figure 3.4). The boundaries of the watershed were identified in the form of a shape file using Geographical Information Systems (GIS). The horizontal grid resolution used in the model was selected as 100 x 100 m. The number of the grids is almost 28700.

3.3.1.2. Topography. The topography of the model was determined by a 1/100000 scaled contour map which was acquired from the General Command of Mapping. Therefore the contours of the map generally represent 50 m intervals of the altitude. The contour map was introduced to the model in the form of a GIS based shape file (Figure 3.7). The triangular interpolation method was used to distribute the point data horizontally. The search radius was defined as 100 m.

3.3.1.3. Precipitation. The spatially uniform, daily precipitation data were used for the model data based on the climate data of the Ulus Meteorological station between 1986 and 2006 (Figures 3.5 and 3.6) (D.M.İ., 2007). The station is 12 km away from the ultimate discharge point of the watershed. The altitude of the Ulus Meteorological station is 162 m. There are also two close stations to the watershed at Safranbolu and Eflani regions. However the data of these two stations are not consistent throughout the 21 years between 1986 and 2006.

The average altitude of the study area is 752 m. The raw air temperature data of the Ulus Meteorological Station were adjusted for the study area based on the correlation between the altitude and the air temperature. According to Erol (2004), for 100 meters altitude difference, the air temperature changes between 0.35°C and 0.75°C for mountainous regions. Therefore, an average lapse rate of 0.4°C was assumed in this study. Since the maximum altitude difference is 590 meters, the daily mean air temperature was dropped 2.36°C. The daily rainfall and altitude-adjusted temperature data are supplied to the model as time series files.

The hydrodynamics model also included a snowmelt component. The snowmelt component considers the degree day factor constant as 2mm/day/°C. The threshold melting temperature values of 0 and 1°C were treated as a calibration parameter.

The future values of the precipitation and the temperature were included in the model based on the simulations of the regional climate model RegCM3 (Bozkurt et al., 2008). The details of this simulation are briefly discussed in the Chapter 5.

3.3.1.4. Land Use. As described in the previous chapter, the definition of the land use component of the hydrodynamic model focuses on two key land use parameters; LAI and RD and the evapotranspiration constants; C_1, C_2, C_3, C_{int} (mm) and Aroot (1/m). The evapotranspiration constants; C_1, C_2, C_3, C_{int} (mm) and Aroot (1/m) were assumed to be 0.3, 0.2, 20, 0.05 and 0.25 respectively (D.H.I., 2005). The LAI values of each stand category were determined by the analysis of the hemispherical photographs as described in the previous chapter. The hemispherical photographs of the main forest stand categories were taken during the summer of 2007. The symbol of the forest stands where the photographs were taken and their corresponding forest stand categories, the number of the photographs, the corresponding LAI values and the mean LAI value of that stand category are described in Tables 3.15, 3.16 and 3.17. The symbols define the species, age groups and closure of that stand (as defined by Tables 3.10, 3.11 and 3.12). The hemispherical photograph taken from a multi aged *Fagus orientalis*-Oriental Beech stand (YM Decd 3) is shown in Figure 3.22. The LAI value of this photograph was computed as 2.26.

Figure 3.22. Hemispherical photograph of multi-aged *Fagus orientalis* stand (YM Decd 3)

Table 3.15. The coniferous stand symbol, category, corresponding LAI values and mean coniferous stand category LAI values

Coniferous Stands			
Symbol	**Type**	**LAI**	**Mean**
Pn0	Conf 0	0.78	
Ab0	Conf 0	1.01	0.74
Ab0	Conf 0	0.43	
Pba1	Y Conf 12	1.07	
Pba1	Y Conf 12	0.84	1.01
Pba1	Y Conf 12	1.11	
AbB3	Y Conf 3	1.85	
AbB3	Y Conf 3	1.95	
AbB3	Y Conf 3	1.59	1.48
AbB3	Y Conf 3	1.32	
AbB3	Y Conf 3	0.88	
AbB3	Y Conf 3	1.31	
Pnd1	M Conf 1	1.18	
Pnd1	M Conf 1	1.09	1.13
Pnd1	M Conf 1	1.11	
Pbcd2	M Conf 2	1.20	
Pbcd2	M Conf 2	1.32	1.26
Pbcd2	M Conf 2	1.27	
AbA	M Conf 3	1.70	
AbA	M Conf 3	1.81	
AbA	M Conf 3	1.98	1.87
AbA	M Conf 3	1.96	
AbA	M Conf 3	1.89	
Pnbc2	YM Conf 12	1.18	
Pnbc2	YM Conf 12	1.26	1.60
AbD2	YM Conf 12	2.02	
AbD2	YM Conf 12	1.93	
AbD3	YM Conf 3	1.70	
AbD3	YM Conf 3	1.71	
AbD3	YM Conf 3	1.59	
AbD3	YM Conf 3	1.72	1.83
AbD3	YM Conf 3	2.25	
AbD3	YM Conf 3	1.76	
AbPsD3	YM Conf 3	2.30	
AbPsD3	YM Conf 3	1.62	

Table 3.16. The deciduous stand symbol, category, corresponding LAI values and mean deciduous stand category LAI values

Deciduous Stands			
Symbol	**Type**	**LAI**	**Mean**
Os0	Decd 0	0.80	0.80
Osb1	Y Decd 12	1.41	
Foa2	Y Decd 12	1.91	1.74
Foa2	Y Decd 12	1.91	
Osb3	Y Decd 3	2.19	
Osb3	Y Decd 3	2.45	
Osb3	Y Decd 3	1.54	
Osb3	Y Decd 3	1.42	
Osb3	Y Decd 3	1.55	
Osb3	Y Decd 3	1.70	1.82
Osb3	Y Decd 3	1.54	
Osb3	Y Decd 3	1.81	
Osb3	Y Decd 3	1.43	
Osb3	Y Decd 3	1.81	
Osb3	Y Decd 3	1.42	
Osb3	Y Decd 3	1.77	
Foa3	Y Decd 3	2.34	
Foa3	Y Decd 3	2.47	
Fobc2	YM Decd 12	1.98	
Fobc2	YM Decd 12	2.28	2.15
Fobc2	YM Decd 12	2.18	
Fobc3	YM Decd 3	2.62	
Fobc3	YM Decd 3	2.26	2.40
Fobc3	YM Decd 3	2.31	
Fod1	M Decd 1	1.44	
Fod1	M Decd 1	1.86	1.52
Fod1	M Decd 1	1.26	
Pocd2	M Decd 2	1.35	
Pocd2	M Decd 2	1.47	
Pocd2	M Decd 2	1.13	
Pocd2	M Decd 2	2.26	1.76
Pocd2	M Decd 2	2.04	
Pocd2	M Decd 2	2.30	
FoHo3	M Decd 3	2.22	2.05
FoHo3	M Decd 3	1.87	

Table 3.17. The mixed stand symbol, category, corresponding LAI values and mean mixed stand category LAI values

Mixed Stands			
Symbol	**Type**	**LAI**	**Mean**
AbFoB2	Y Conf Y Decd 12	1.75	1.75
AbFoB	Y Conf Y Decd 3	2.03	
AbFoab3	Y Conf Y Decd 3	1.82	1.93
AbPsOsFo2	M Conf Y Decd 12	1.43	1.79
PnHo12	M Conf Y Decd 12	2.14	
PnOsbc3	M Conf Y Decd 3	1.10	
PsHobc3	M Conf Y Decd 3	2.65	2.01
PsHobc3	M Conf Y Decd 3	2.29	
AbFobc3	M Decd Y Conf 3	1.85	2.15
AbFobc3	M Decd Y Conf 3	2.44	
AbFoA	M Conf M Decd 3	2.19	
AbFoA	M Conf M Decd 3	1.84	
AbFoA	M Conf M Decd 3	1.78	
AbFoA	M Conf M Decd 3	1.88	
AbFoA	M Conf M Decd 3	2.15	
AbFoA	M Conf M Decd 3	2.12	
AbFoA	M Conf M Decd 3	1.76	2.01
AbFoA	M Conf M Decd 3	1.76	
AbFoA	M Conf M Decd 3	2.11	
AbFoHoc3	M Conf M Decd 3	2.11	
AbFoHoc3	M Conf M Decd 3	2.17	
AbHo3	M Conf M Decd 3	2.26	

As noted in Section 3.2, the watershed was divided into four subwatersheds in the land use dynamics model. The land use dynamics within each subwatershed was modeled and an average LAI value for each subwatershed for each year was produced. The seasonality of these annual values was achieved assuming that the 4 months (November, December, January and February) of a year were winter season and 6.5 months (March-16, April, May, June, July, August and September) were summer. According to this assumption, the leaves of the trees grow in 15 days between March 1 and 16 while they fall in 30 days of October. The seasonal dynamics of LAI were generated based on some assumptions about the winter values. Based on Fang (2008), it was assumed that the LAI values of the coniferous and mixed forests decrease almost 20% and 50% during the winter season respectively. The winter LAI value of the deciduous forest is 0. For the agricultural

areas, the winter and summer LAI values were assumed as 0 and 1 respectively (Fang, 2008). The transition between the summer and winter LAI values was defined gradually for each subwatershed. The LAI value is 0 throughout the year both for the settlement areas and forest open spaces. Ultimately, based on the summer, winter and the gradual transition values of the annual LAI, the daily time series of the LAI values were generated for each subwatershed and provided to the hydrodynamics model.

The weighted average value of the Root Depth (RD) parameter was used for each subwatershed as described for LAI parameter. The seasonality of the Root Depth (RD) parameter was defined by assuming the summer root depth of agricultural areas as 500 mm and the winter as 0 mm. The root depth of the forest trees was assumed to be 1000 mm, temporally constant over the entire watershed. The RD value is 0 mm throughout the year both for the settlement areas and forest open spaces. The summer, winter and the transition periods for Root Depth were assumed to be similar to the periods for LAI. The generated ultimate time series data of the RD parameter were provided to the hydrodynamics model.

The calibration results of the land use dynamics model together with the associated LAI and RD values are briefly described in the next chapter.

3.3.1.5. Evapotranspiration. The hydrodynamics model calculates the actual evapotranspiration using the potential evapotranspiration. The potential evapotranspiration was calculated using the Penman method (Penman, 1948). The actual evapotranspiration was calculated based on the Kristensen and Jensen (1975) method. These two methods for the calculation of the potential and actual evapotranspiration were briefly described in the previous chapter. The calculation of the actual evapotranspiration depends also on the value of the LAI and RD and the evapotranspiration constants C_1, C_2, C_3, C_{int} (mm) and Aroot (1/m) which were defined in the previous subsection.

The spatially uniform, daily potential data were used for the model data based on the climate data of the Ulus Meteorological station between 1986 and 2006 (D.M.İ., 2007). The raw station data were used during the calculation of the potential evapotranspiration. Associated with the potential evapotranspiration, the conceptual and lumped Penman water budgets were prepared including the actual evapotranspiration, flow, soil water etc. These

annual Penman water budget tables for the period between 1986 and 2006 are given in the Appendix A.

3.3.1.6. Overland Flow. As described in the previous chapter, the finite difference method was used during the calculation of the overland flow. The finite difference method applies the diffusive wave approximation adapted to the Saint Venant equation, ignoring the momentum loss due to local and convective acceleration and lateral inflows perpendicular to the flow direction.

In the hydrodynamics model, the uniform values of the overland flow parameters were used. The uniform value of 10 $m^{1/3}/s$ for the Manning's m, was used in the model (D.H.I., 2005). The detention storage and the initial water depth were assumed to be 0 mm and uniform for elsewhere of the watershed since there was no distributed data for the initial surface water.

3.3.1.7. River Flow. As described in the previous chapter, the hydrodynamics model considers a river simulation file which includes river network, cross sections, boundary and hydrodynamic parameters files. The river network file includes only the main river channel which was digitized from the previously rectified map. The length of the main river chainage which is 27274 meters was defined in terms of 18 points as shown in Figure 3.23. The profiles of these 18 cross sections were defined based on the topography file digitized by GIS. The roughness coefficient Manning's m was assumed to be 30 $m^{1/3}/s$ and uniform within all the cross sections (D.H.I., 2005). The upper and the lower nodes and the other critical points were also defined for each cross section.

Two boundary files were prepared for the definition of the river boundary conditions. The first boundary file was prepared for the upstream initial point of the river channel. The second boundary file was prepared for the downstream ultimate point of the watershed. The first boundary file (upstream boundary) was defined as an inflow (Q) data. The river discharge data supplied from the State Hydraulic Works (D.S.İ., 2001) for the period between 1985 and 2001 was used for defining the initial boundary inflow (Q). The watershed area of the discharge measurement station is 955 km^2. The watershed area of the initial boundary point is 71.4 km^2. Based on the weighted averages of the watersheds, the

inflow of the initial boundary point was defined for the period between 1986 and 2001. The daily data were prepared as time series file and introduced to the boundary file of the hydrodynamics model. The necessary boundary inflow data for the period between 2001 and 2027 were prepared based on the monthly regression curves between the precipitation and the flow (Q). Therefore the daily precipitation and the flow (Q) averages of each month between 1985 and 2001 were prepared. The regression curves between these two averages were drawn and the regression equations were defined. The future precipitation data are based on the simulations with the climate model RegCM3 which is described in the Chapter 5 (Bozkurt et al., 2008).

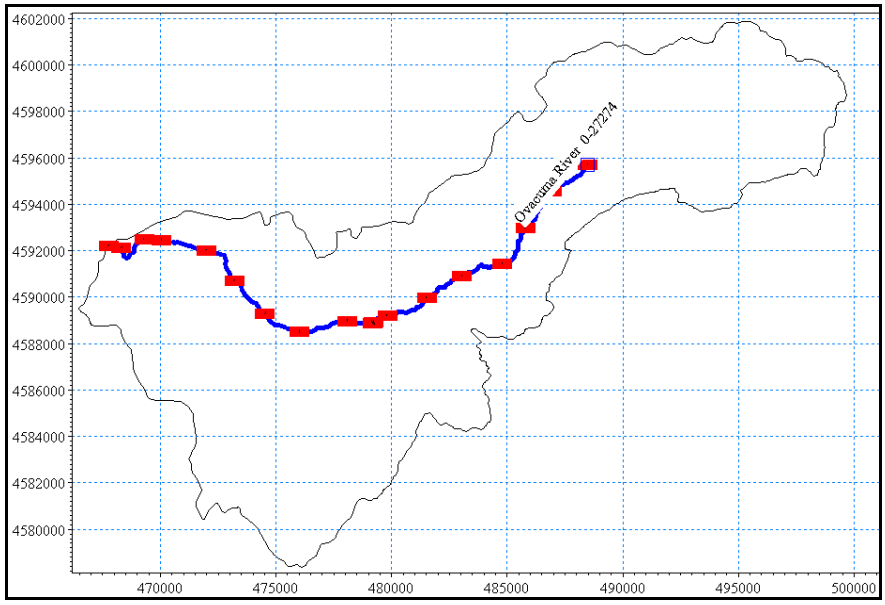

Figure 3.23. The network of the main river channel and the cross section points

The downstream ultimate boundary flow data were defined as discharge-water level (Q-h) relation based on the Manning's equation (3.6) (Linsley et al., 1975).

$$Q = \frac{1.49}{n} A R^{2/3} S^{1/2} \qquad (3.6)$$

Q= Discharge (L^3/T)

n= Manning's roughness coefficient ($T/L^{1/3}$) (inverse of Manning's m)

A= Flow area (L^2)

R= Hydraulic or resistance radius (L)
S= Slope of the channel

The resistance radius is the wetted perimeter of the ultimate downstream cross section. The Manning's m was assumed as 30 $m^{1/3}/s$ (D.H.I., 2005). The slope was calculated as 0.004. The Q-h relation is calculated automatically by the model based on this equation and the related parameter values. The initial discharge value and the associated water level value were defined by taking the average of the initial and ultimate boundary values.

3.3.1.8. Unsaturated Zone Flow. Richards equation (Jury and Horton, 2004) was used for the simulation of flow in the unsaturated zone. The Van Genuchten formulation (Van Genuchten, 1980) was selected for the calculation of the water retention and hydraulic conductivity relative to the soil moisture content. The parameters needed in the Van Genuchten model are: the saturated hydraulic conductivity (K_s), saturated moisture content (Q_s) parameters and the water retention parameters (Qr, n and α).

The saturated hydraulic conductivity and the saturated moisture content were measured from near surface soil samples, whereas the water retention parameters are based on the literature for the observed soil types and estimated hydraulic conductivity values (Carsel and Parish, 1988).

For the saturated hydraulic conductivity and soil type, 50 soil sampling points were defined within the watershed. The soil sampling was conducted between 1st and 15th of July 2007. The coordinates of the soil sampling points were defined on the digitized maps. The target was to collect soil samples from the entire watershed, as much as possible. At each location point, two undisturbed soil samples were taken from 0-10 and 10-20 cm depths by iron cylinders with 5 cm length and 5 cm diameter. The geometric mean of the saturated hydraulic conductivity of these two samples representing two depths was taken to get a mean value for the soil between 0-20 cm.

As described in the previous Methodology chapter, the saturated moisture content of these soil samples was measured by calculating the weight difference between the

saturated and the oven dried samples. This also supplied the porosity data for that sample. Also at least 100 grams of soil from each depth were taken into plastic bags. These bags were then sealed to prevent the evaporation of the sample moisture. 10 grams of these samples were used to determine the actual soil moisture while 50 grams were used for the determination of the soil texture and type. The particle size analysis were done with the 50 grams of soil using the Bouyoucos hydrometer method (Bouyoucos, 1936). The percentages of the particle sizes defined the soil type. The international soil texture triangle was used for this purpose (Kantarcı, 2000).

The soil sampling points, the saturated hydraulic conductivity values at the two depths and their geometric mean, the porosity, soil type and soil moisture of two depths are all presented in Table 3.18.

Geographical Information Systems (GIS) based kriging was used to estimate the saturated hydraulic conductivity at unsampled locations. Kriging was applied to the watershed area excluding the alluvial and colluvial soils along the banks of the stream. Thus only the geometric mean values of the saturated hydraulic conductivity of the first 38 soil samples were considered for kriging. As a result of the kriging process with GIS, four different ranges of saturated hydraulic conductivity values were defined for the entire watershed area except the alluvial and colluvial soils. The polygons corresponding to these four value ranges were also acquired using GIS. The geometric mean value of the five alluvial soils with the sample numbers of 39, 40, 41, 42 and 43 was used for the entire alluvial area. The saturated hydraulic conductivity value of the colluvial soil with the sample number 44 was used for the colluvial areas.

The horizontal and the vertical distribution of the soil parameters were supplied by kriging and averaging processes applied to the soil sample values. The location of the soil sample points within the subwatersheds of the entire watershed area and the polygons acquired from kriging and averaging processes are shown on the Figure 3.24.

Table 3.18. Saturated hydraulic conductivity, porosity, soil type and soil moisture of sampling points

No.	K_s (m/s)		K_{sgm} (m/s)	Porosity (%)		Soil Type		Soil Moisture (%)	
	0-10cm	10-20cm	0-20cm	0-10cm	10-20cm	0-10cm	10-20cm	0-10cm	10-20cm
1	2.82×10^{-5}	2.39×10^{-6}	8.21×10^{-6}	47.58	43.67	Loamy Clay	Silty Clay Loam	17.95	17.19
2	7.00×10^{-6}	8.33×10^{-8}	7.64×10^{-7}	51.86	48.67	Sandy Clay Loam	Loamy Clay	20.06	13.28
3	1.99×10^{-5}	4.36×10^{-6}	9.32×10^{-6}	51.74	56.01	Sandy Clay Loam	Sandy Loam	16.50	14.29
4	2.38×10^{-5}	3.39×10^{-6}	8.99×10^{-6}	54.01	55.18	Loamy Clay	Loamy Clay	3.96	8.51
5	5.00×10^{-6}	N-M	5.00×10^{-6}	63.57	N-M	Loamy Clay	Loamy Clay	18.99	13.39
6	3.50×10^{-6}	N-M	3.50×10^{-6}	42.56	N-M	Loamy Clay	Loamy Clay	12.18	11.5
7	3.97×10^{-6}	1.81×10^{-6}	2.68×10^{-6}	48.88	44.81	Loamy Clay	Loamy Clay	12.85	13.46
8	5.12×10^{-5}	N-M	5.12×10^{-5}	55.32	N-M	Sandy Clay Loam	Silty Loam	16.70	24.04
9	2.89×10^{-5}	N-M	2.89×10^{-5}	53.45	N-M	Loamy Clay	Clay	26.53	33.98
10	5.86×10^{-5}	N-M	5.86×10^{-5}	49.54	N-M	Sandy Loam	Sandy Clay	15.26	14.64
11	2.98×10^{-5}	N-M	2.98×10^{-5}	39.42	N-M	Sandy Clay Loam	Sandy Clay Loam	10.83	10.05
12	2.33×10^{-5}	5.72×10^{-6}	1.16×10^{-5}	53.05	62.20	Loamy Clay	Sandy Clay Loam	19.53	11.89
13	1.97×10^{-6}	2.22×10^{-7}	6.62×10^{-7}	48.59	51.57	Clay	Loamy Clay	N-M	6.73
14	N-M	5.56×10^{-8}	5.56×10^{-8}	N-M	51.82	Loamy Clay	Loamy Clay	8.75	8.83
15	9.74×10^{-5}	5.28×10^{-7}	7.17×10^{-6}	54.66	53.12	Clay	Loamy Clay	3.37	5.47
16	1.28×10^{-5}	4.31×10^{-6}	7.43×10^{-6}	53.01	52.16	Clay	Clay	6.43	2.54
17	2.60×10^{-5}	1.67×10^{-7}	2.08×10^{-6}	41.85	49.96	Loamy Clay	Loamy Clay	15.62	12.70
18	2.22×10^{-6}	5.56×10^{-7}	1.11×10^{-6}	49.71	50.71	Clay Loam	Loamy Clay	4.50	9.81
19	3.18×10^{-5}	6.39×10^{-7}	4.51×10^{-6}	49.62	65.44	Sandy Clay Loam	Loamy Clay	20.03	21.62
20	9.99×10^{-5}	1.46×10^{-5}	3.82×10^{-5}	39.44	41.66	Loamy Clay	Loamy Clay	6.55	7.48
21	1.43×10^{-5}	1.06×10^{-6}	3.88×10^{-6}	42.79	35.75	Sandy Clay Loam	Sandy Clay	22.94	14.38
22	9.25×10^{-6}	N-M	9.25×10^{-6}	52.73	N-M	Sandy Loam	Clay Loam	17.14	12.10
23	3.36×10^{-6}	1.14×10^{-6}	1.96×10^{-6}	46.98	56.12	Clay	Loamy Clay	7.49	8.85
24	3.64×10^{-5}	7.47×10^{-6}	1.65×10^{-5}	43.79	42.91	Clay	Loamy Clay	15.38	14.44
25	9.47×10^{-6}	1.50×10^{-6}	3.77×10^{-6}	22.05	35.14	Sandy Clay Loam	Sandy Loam	12.22	10.52
26	N-M	2.71×10^{-5}	2.71×10^{-5}	N-M	45.84	Loamy Clay	Clay	15.04	13.48
27	8.83×10^{-5}	6.78×10^{-6}	2.45×10^{-5}	21.87	53.22	Loamy Clay	Clay Loam	24.29	21.40
28	N-M	3.89×10^{-7}	3.89×10^{-7}	N-M	35.77	Loamy Clay	Loamy Clay	17.56	14.36
29	1.36×10^{-6}	1.11×10^{-7}	3.89×10^{-7}	45.67	42.92	Loamy Clay	Loamy Clay	13.53	13.56
30	6.09×10^{-5}	4.63×10^{-5}	5.31×10^{-5}	47.55	56.27	Clay Loam	Sandy Clay Loam	9.22	22.70
31	8.53×10^{-6}	3.06×10^{-7}	1.61×10^{-6}	44.38	43.19	Loamy Clay	Loamy Clay	9.65	9.43
32	1.87×10^{-5}	8.33×10^{-7}	3.96×10^{-6}	46.98	44.96	Loamy Clay	Loamy Clay	4.84	7.45
33	2.77×10^{-5}	1.33×10^{-6}	6.08×10^{-6}	52.91	45.96	Loamy Clay	Clay Loam	10.86	11.66
34	3.51×10^{-5}	1.31×10^{-6}	6.77×10^{-6}	49.41	49.48	Loamy Clay	Loamy Clay	22.47	19.56
35	1.64×10^{-6}	3.61×10^{-7}	7.69×10^{-7}	51.31	54.25	Silty Loam	Loamy Clay	23.03	22.40
36	9.81×10^{-6}	1.25×10^{-6}	3.50×10^{-6}	48.50	49.75	Loamy Clay	Loamy Clay	15.34	15.04
37	6.11×10^{-6}	2.86×10^{-6}	4.18×10^{-6}	48.85	50.81	Loamy Clay	Loamy Sand	15.94	14.73
38	2.03×10^{-6}	1.47×10^{-6}	1.73×10^{-6}	59.63	49.02	Loamy Clay	Silty Loam	14.53	18.71
39	5.97×10^{-6}	3.53×10^{-6}	4.59×10^{-6}	46.13	42.66	Loamy Sand	Loamy Sand	2.43	4.68
40	1.38×10^{-4}	8.89×10^{-7}	1.11×10^{-5}	41.46	49.66	Clay Loam	Sandy Clay Loam	3.20	1.88
41	5.11×10^{-6}	3.67×10^{-6}	4.33×10^{-6}	47.82	42.94	Loamy Clay	Loamy Clay	8.65	7.83
42	2.08×10^{-6}	2.78×10^{-7}	7.61×10^{-7}	46.55	46.69	Loamy Clay	Loamy Clay	4.88	7.41
43	7.25×10^{-6}	6.31×10^{-6}	6.76×10^{-6}	51.52	41.87	Sandy Loam	Sandy Loam	5.59	5.14
44	9.69×10^{-6}	1.36×10^{-6}	3.63×10^{-6}	39.09	49.64	Loamy Clay	Loamy Clay	4.00	7.92
45	1.42×10^{-6}	N-M	1.42×10^{-6}	62.72	N-M	Sandy Clay	Loamy Clay	19.98	19.20
46	N-M	N-M	N-M	N-M	N-M	Sandy Clay Loam	Loamy Clay	15.54	14.56
47	N-M	N-M	N-M	N-M	N-M	Sandy Clay	Loamy Clay	16.67	15.13
48	N-M	N-M	N-M	N-M	N-M	Loamy Clay	Loamy Clay	0.67	1.61
49	N-M	N-M	N-M	N-M	N-M	Sandy Loam	Loamy Clay	33.94	42.90
50	N-M	N-M	N-M	N-M	N-M	Loamy Sand	Sandy Loam	42.78	39.30

K_{sgm}: Geometric mean of the saturated hydraulic conductivity values of two depths
N-M: The soil sample parameter could not be measured due to disturbed soil samples

The horizontal distribution of these soils was through the GIS based shape file (Figure 3.24). The six saturated hydraulic conductivity values of these polygon areas together with their code numbers are also stated in the legend of the figure. The digital version of this map was provided to the unsaturated zone flow component of the hydrodynamic model for the automatic spatial definition of the saturated hydraulic conductivity values and the other Van Genuchten parameters.

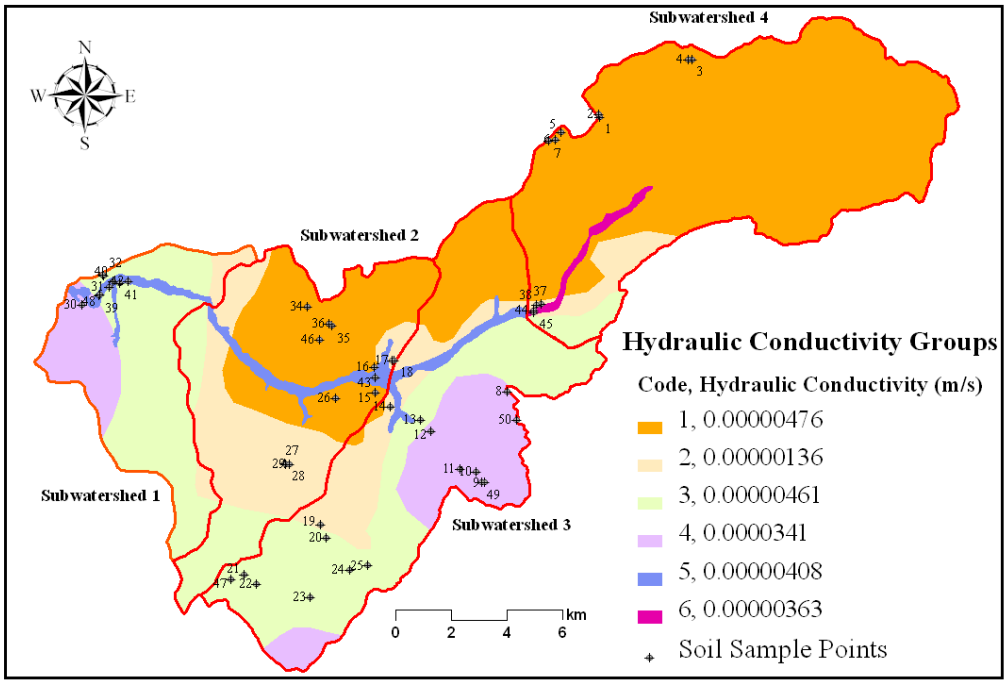

Figure 3.24. Soil sample points and the polygon areas of the saturated hydraulic conductivity values

The vertical distribution of the soil profiles was achieved by defining the flexible depth intervals changing between 20 cm and 30 m. The soil property files were defined for each of these depth intervals. In these soil property files, initially the methods for the calculation of the unsaturated hydraulic conductivity and the water retention curve and subsequently the parameters attributed to those methods were defined. The details of these processes are discussed below.

Because soil samples were limited to depths of 20 cm, the saturated hydraulic conductivity of the deeper soils were estimated from the measured values at depths (0-10

cm and 10-20 cm). At each location a regression expression of the saturated hydraulic conductivity as a function of depth was developed at each sampling location based on the measured data at depths (0-10 cm and 10-20 cm). Consequently, the saturated hydraulic conductivity values were generated for the depths between 20 cm and 20 m. The regression analysis was performed for each of the observation points. The hydraulic conductivity of the deeper soils was defined as the geometric mean of the curves falling with each of the soil groupings shown in Figure 3.24. The alluvial and colluvial areas were evaluated distinct from rest of the watershed area. According to the model, the deepest point of these alluvial and colluvial areas was assumed as 30 m.

The five soil sample points; 39, 40, 41, 42 and 43 were used for the alluvial soil whereas only point 44 was used to for the colluvial soil. The values of the ten sample points; 1, 2, 3, 4, 7, 15, 16, 34, 35 and 36 were used for the soil hydraulic conductivity group polygons coded 1. The soil group polygons with the code 2 used the soil sample values of the seven points; 17, 18, 19, 27, 29, 37 and 38. The values of the nine soil sample points; 13, 20, 21, 23, 24, 25, 31, 32 and 33 were used for the soil group polygons with the code 3 whereas the soil group polygons with the code 4 used the soil sample values of the two points; 12 and 30.

In addition to the saturated hydraulic conductivity, the Van Genuchten model parameters include: The saturated moisture content (Q_s), residual moisture content (Q_r), n and α which are used to define the capillary pressure in the soil as a function of moisture content. These values were estimated from the literature (Carsel and Parrish, 1988) based on the measured hydraulic conductivity values at each sampling location. The Van Genuchten parameter values; saturated hydraulic conductivity and saturated moisture content (Qs) for each soil group and each soil layer intervals are presented in Tables 3.19 and 3.20.

Table 3.19. The saturated hydraulic conductivity values for soil group and soil layer intervals

Soil Layer Interval (cm)	Ks (m/s)					
	1	**2**	**3**	**4**	**5**	**6**
0-20	4.76×10^{-6}	1.36×10^{-6}	4.61×10^{-6}	3.41×10^{-5}	4.08×10^{-6}	3.63×10^{-6}
20-100	3.72×10^{-7}	2.73×10^{-7}	3.88×10^{-7}	8.93×10^{-6}	8.51×10^{-7}	4.18×10^{-7}
100-500	1.49×10^{-7}	1.26×10^{-7}	1.44×10^{-7}	4.97×10^{-6}	4.82×10^{-7}	1.54×10^{-7}
500-1000	1.02×10^{-7}	9.30×10^{-8}	9.50×10^{-8}	3.70×10^{-6}	3.83×10^{-7}	9.92×10^{-8}
1000-1500	8.51×10^{-8}	8.07×10^{-8}	7.80×10^{-8}	3.18×10^{-6}	3.43×10^{-7}	8.03×10^{-8}
1500-2000	—	—	—	—	3.22×10^{-7}	7.06×10^{-8}
2000-2500	—	—	—	—	3.07×10^{-7}	6.46×10^{-8}
2500-3000	—	—	—	—	2.97×10^{-7}	6.03×10^{-8}

Table 3.20. The saturated moisture content values for soil group and soil layer intervals

Soil Layer Interval (cm)	Qs					
	1	**2**	**3**	**4**	**5**	**6**
0-20	0.47	0.45	0.47	0.52	0.47	0.47
20-100	0.47	0.47	0.47	0.47	0.47	0.47
100-500	0.48	0.48	0.48	0.47	0.50	0.48
500-1000	0.50	0.50	0.50	0.47	0.47	0.50
1000-1500	0.50	0.50	0.50	0.48	0.47	0.50
1500-2000	—	—	—	—	0.47	0.50
2000-2500	—	—	—	—	0.47	0.50
2500-3000	—	—	—	—	0.47	0.50

3.3.1.9. Saturated Zone Flow. As described in the previous chapter, the Finite Difference method was used to calculate the three-dimensional saturated zone flow in this hydrodynamics model. Uniform values of the saturated zone soil parameters were applied. Based on the site geology and the unsaturated zone observations and estimations, it was assumed that the saturated vertical hydraulic conductivity was in the range of 10^{-8} and 10^{-7} m/s while the saturated horizontal hydraulic conductivity was in the range of 10^{-7} and 10^{-6} m/s. Both parameters were adjusted during model calibration.

As part of the sensitivity analysis, spatially distributed values of the horizontal flow parameter of the saturated zone were also considered. The same GIS based shape file that was used for the unsaturated zone was also used for this saturated zone flow.

The saturated hydraulic conductivity, storage coefficient and the specific yield parameters were defined for one soil layer. The lower vertical boundary of that layer was

defined based on the previous sounding well observations (Karabük İl Özel İdaresi, 2006). The spatial distribution of the lower level was estimated by the depths to the impermeable rock at the six observation points. The two observation points inside alluvial deposits showed that the depth of the alluvial soil reached up to 30 meters (Karabük İl Özel İdaresi, 2006). Thus, the 30 m depth was assumed to be constant for both the alluvial and the colluvial areas.

For the rest of the watershed, the depth to the impermeable rock was assumed to be 2 meters at the north-eastern edge of the watershed. The other two observation points showed that the depth was in the order of 8 and 13 meters respectively (Figure 3.25). Based on these data it was assumed that the depth to the impermeable rock decreases linearly with distance upstream the watershed, starting from a maximum value of 14.5 m at the downstream of the watershed to a value of 2 m at the upstream end. These values were digitized for entry into the hydrodynamic model and the resultant map is shown in Figure 3.25.

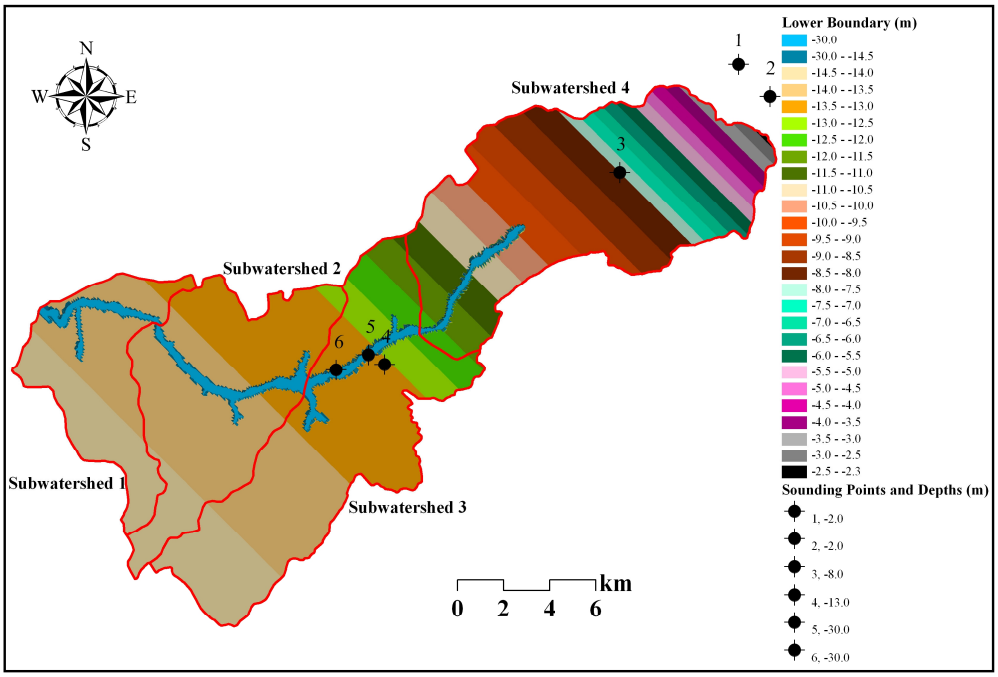

Figure 3.25. Sounding observation points and the bottom elevation map of the watershed

The specific yield value was assumed uniform with a value of 0.2, whereas the storage coefficient was assumed as 10^{-4} m^{-1} (D.H.I., 2005). The soil was assumed to be fully saturated at the beginning of the simulation being the initial potential head, zero relative to the ground.

4. MODEL CALIBRATION, VALIDATION AND SENSITIVITY ANALYSIS

This chapter presents the calibration, validation and sensitivity analysis of the two models; the land use model and the hydrodynamics model. In Section 4.1, model validity, validation, and types of model validation tests are described. The calibration of the land use model is discussed in Section 4.2, while the calibration of the hydrodynamics model is presented in Section 4.3. Section 4.4 presents the sensitivity of the hydrodynamics model to the land use parameters and the saturated zone soil parameters.

4.1. Validation and Sensitivity Analysis for Land Use Dynamics Model

According to Barlas (1996), the ultimate objective of system dynamics model validation is to establish the validity of the internal structure of the model. System dynamics model validation consists of two sequential steps. The first one is the validation of structure where the adequacy of the model structure in representing the real world problem is tested. After sufficient confidence is built in the validity of the structure, model behavior patterns are compared with real life data (Barlas, 2002). During the structural validation tests, the sufficient confidence in the structure of the model is sought (Barlas, 1996). The structure tests are grouped under two types. One is the direct structure tests and the other is the structure-oriented behaviour tests (indirect structure tests). The former evaluates the validity of the model structure by direct comparison with knowledge about real system structure (Barlas, 1996). The latter assesses the validity of the structure indirectly by applying certain behaviour tests on model-generated behaviour patterns (Barlas, 1996).

Extreme condition test is one of the structure oriented behavior tests. Extreme values are assigned to the selected parameters of the model. The model-generated behavior is compared with the observed or the anticipated behavior of the real system under the same extreme condition (Barlas, 1996). This extreme condition test is applied to part of the land use dynamics model. The natural dynamics of the coniferous stand groups without any anthropogenic treatment or practice except the regrowth process are exposed to the

extreme condition test. Figure 4.1 illustrates the structure representing regrowth, intensification, maturation and degradation processes on coniferous stands.

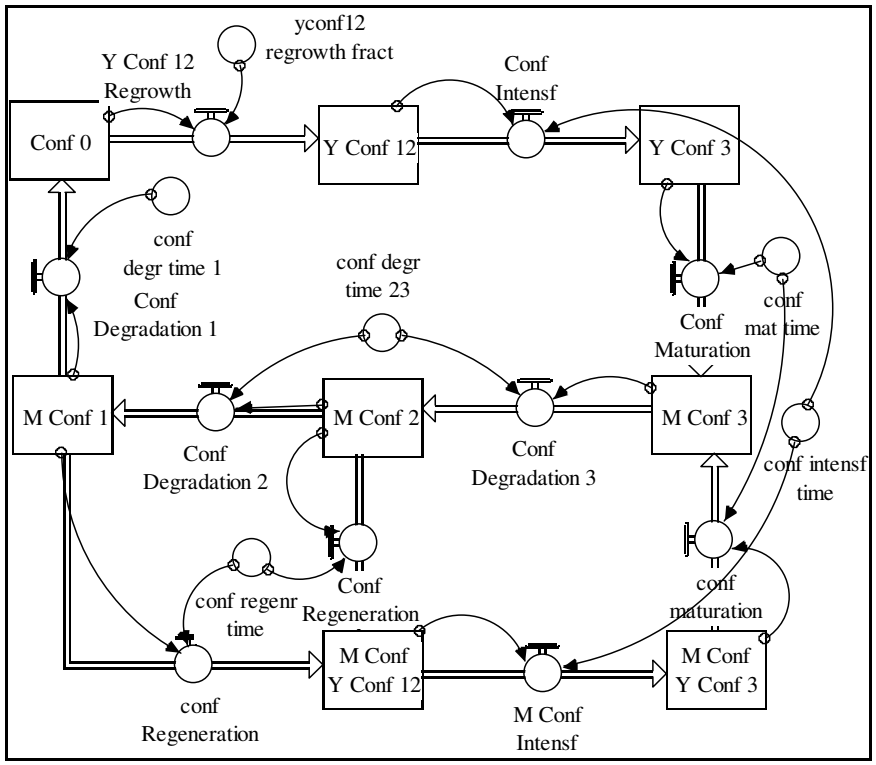

Figure 4.1. Natural processes of the coniferous stand groups

In this test, the extreme condition is the absence of any treatment and practice for the regrowth of the coniferous seedlings. Therefore, the regrowth fraction for the Young Coniferous 12 stand group is set to 0. The initial values of the coniferous stand groups (stock variables) are the areas of these stand group in 1986 measured in hectares of land. According to the management plans of the General Directorate of Forestry, the management period of the forest trees changes between 100 and 150 years (O.G.M., 2006). Hence, the natural dynamics of the coniferous stand groups over the 200 years between 1986 and 2186 were analyzed. Figures 4.2 and 4.3 demonstrate the dynamics of the coniferous stand groups over the 200 years.

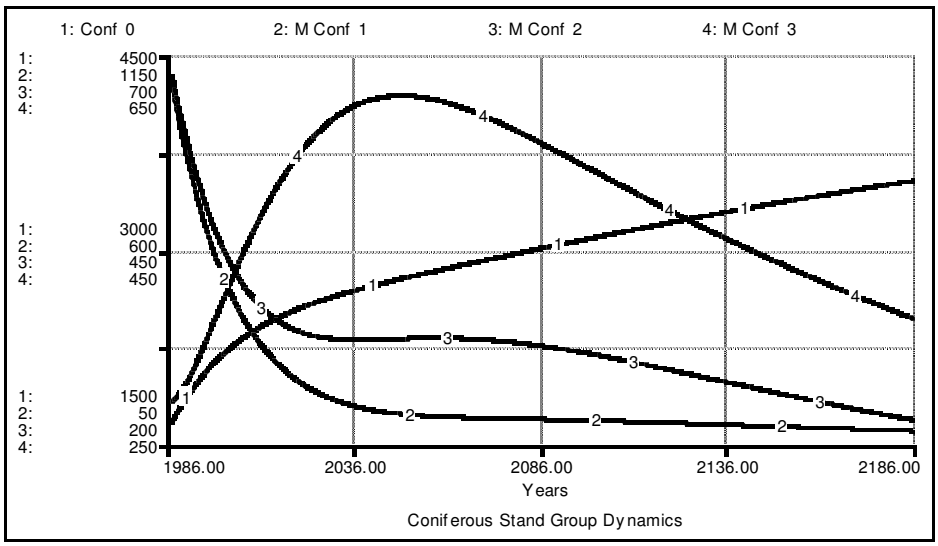

Figure 4.2. Model response to regrowth fraction set to 0

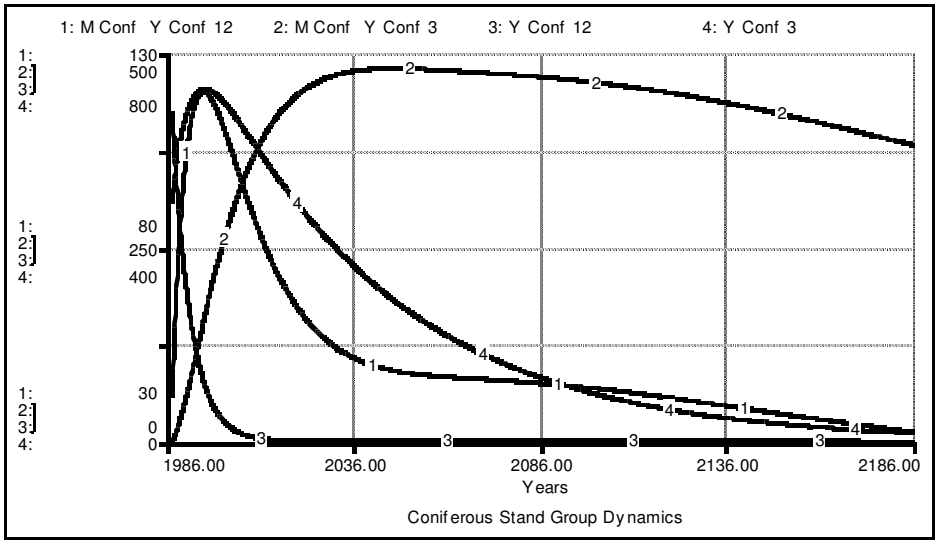

Figure 4.3. Model response to regrowth fraction set to 0

Based on the regeneration processes (Figure 4.2), the dense multi-aged coniferous stand group (M Conf Y Conf 3) increases over the first 50 years and then begins to decline due to its maturation to Mature Coniferous 3. All the other stand groups decline in time except the handicapped coniferous stand group (Conf 0). The increase in the handicapped coniferous stand group (Conf 0) continues over the 200 years due to the degradation of the mature coniferous stand groups. Since the regrowth fraction of the young coniferous seedling is set to 0, there is no outflow from the handicapped coniferous stand group (Conf 0). The same condition is true for the real forest lifecycle. In the region, the forest

vegetation is not the original vegetation of that region. They were introduced to the region gradually in time. If these forests are not treated according to the forest management plans such as plantation, nursing and field preparation for regrowth, they are exposed to degradation and consequently to elimination from the field.

Another structure oriented behavior test is the behavior sensitivity test. According to Barlas (1996), behavior sensitivity test involves the determination of the parameters to which the model is highly sensitive. This test investigates whether the real system responds to the corresponding parameters with the same high sensitivity or not. This behavior sensitivity test was also applied to the natural dynamics model of the coniferous stand groups.

First, the sensitivity of the model to the coniferous maturation time was analyzed. The regrowth fraction is set to 0.1 (1/year). The maturation times of 10, 20, 30, 40 and 50 were tested, respectively. The results are plotted on the graph shown in Figure 4.4. Figure illustrates, the higher the maturation time, the lower will be the equilibrium area of dense mature coniferous stands.

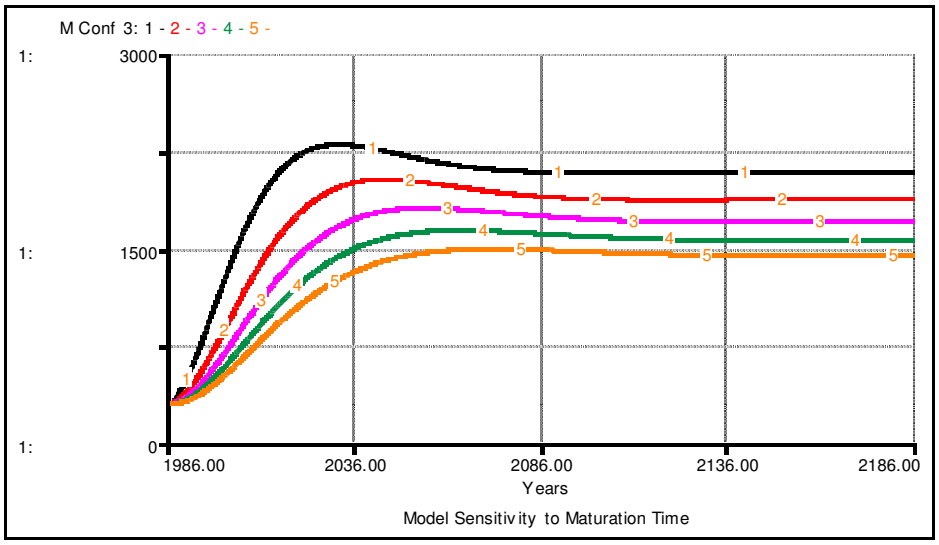

Figure 4.4. M Conf 3 sensitivity to maturation time parameter

In a second parameter sensitivity test, the degradation time for Mature Coniferous 2 and 3 was tested (Figure 4.5). Runs 1, 2, 3 and 4 are the behavior responses to degradation

times of 10, 20, 30 and 40 years, respectively. Since M Conf 3 degrade to M Conf 2 and then to M Conf 1, higher degradation time leads to lower values of Mature Coniferous 1.

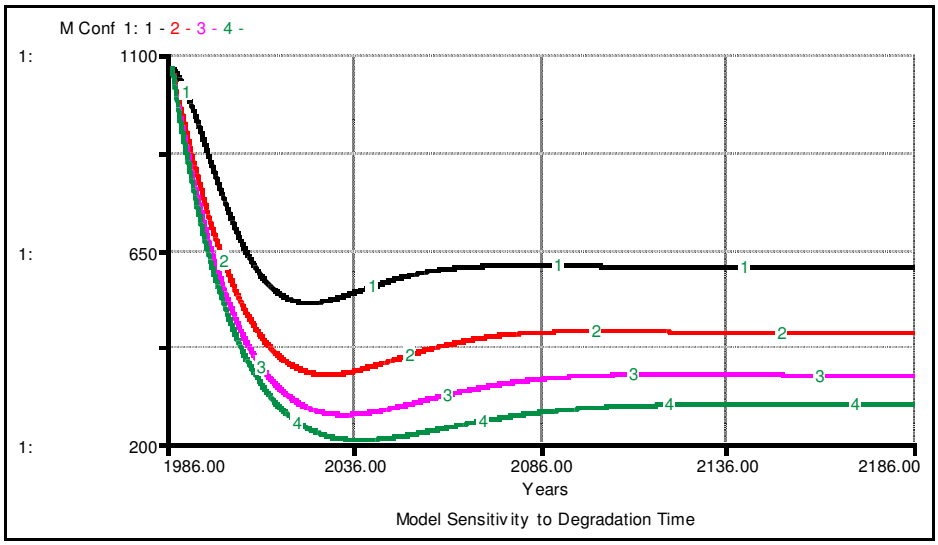

Figure 4.5. M Conf 1 sensitivity to degradation time parameter

The regeneration time was defined as 50 years. Figure 4.6 shows the model sensitivity to regeneration time parameter. Runs 1, 2, 3, 4 and 5 represent the response to regeneration time of 10, 20, 30, 40 and 50, years respectively. Higher regeneration time leads to lower values of multi-aged coniferous stand group (YM Conf 3).

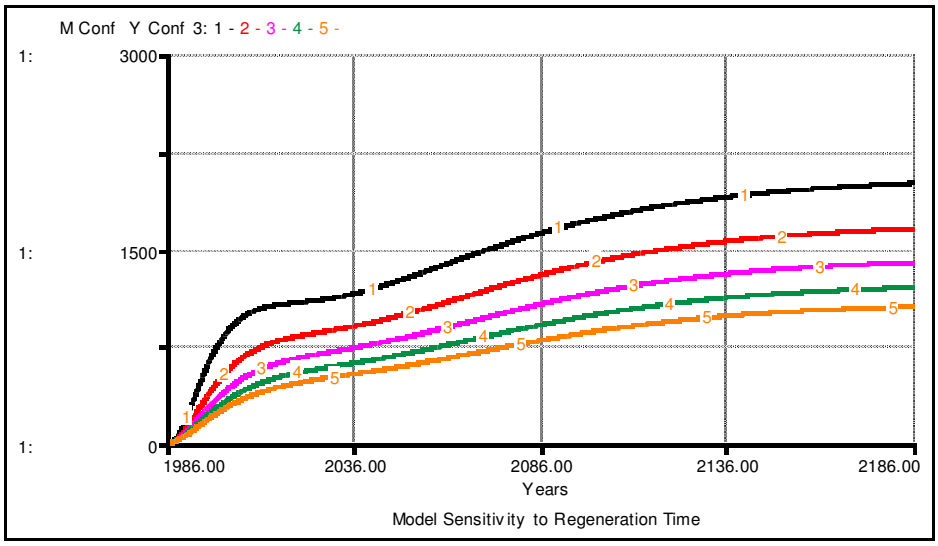

Figure 4.6. M Conf Y Conf 3 sensitivity to regeneration time parameter

The results of this sensitivity analysis are consistent with real life systems which are highly sensitive to the maturation, degradation and regeneration time parameters (Saatçioğlu, 1976). Namely, as discussed in Chapter 3, maturation is the increment of the tree Diameter at Breast Height (DBH) from thinner stages ‘ab’ to thicker stages ‘cd’ (Kalıpsız, 1998), degradation is the gradual reduction of the forest closure due to tree removal whereas the regeneration is the introduction of the tree seedlings into the stand (Genç, 2004). During an average lifetime, among the two forests, the forest in which the DBH of the trees increases in a shorter period is expected to have larger area of mature stands. However, the forest which more rapidly loses trees and therefore its closure is expected have larger area of sparse and handicapped stands. The forest which produces new seedlings faster is expected to have larger area of younger stands.

Finally the phase relationship test was applied to the land use model. The phase relationship test is another structure oriented behavior test. The phase relationships test assesses the phase relationships between the simulated behavior of pairs of model variables. The phase relationship between the two coniferous stand groups is demonstrated in Figure 4.7.

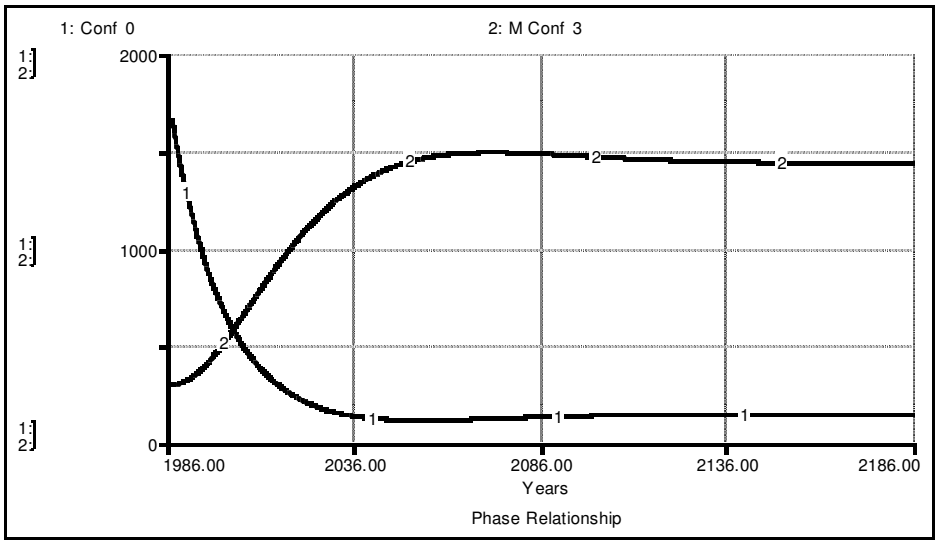

Figure 4.7. Phase relationship between Conf 0 and M Conf 3 stand groups

The Mature Coniferous 3 increases as the handicapped coniferous stand group (Conf 0) declines. They tend to stabilize after about 100 years, with an apparent difference between their values. This is a valid real life condition based on the regrowth of the young coniferous seedlings. In average, 60 years are needed for the regrowth of dense mature stands from handicapped stands. On the other hand, about 100 years are needed for the dense mature stands to degrade to handicapped stands. The difference between these periods leads to the initial increase in the M Conf 3 and the decrease in the Conf 0 along the 75 years. The equilibrium is reached in about 100 years when degradation process completed.

4.2. Calibration of Land Use Dynamics Model

In this section, the calibration of the land use dynamics model is presented. The model calibration target was the 2006 land use map data obtained from the General Directorate of Forestry (O.G.M., 2006) (Figure 3.18). The starting point of the simulations was the 1986 land use map and the conversion fractions were adjusted to fix the model predictions to that target. The area covered by the land uses of each of the four subwatersheds in 1986, 2006 and model simulation results are given in Table 4.1.

Table 4.1 shows that the total model simulation results are in agreement with the land use data of 2006. The agricultural area decreased in all the four subwatersheds while the forest area increased.

As an example, the change in coniferous stand categories of the Subwatershed 4 between 1986 and 2006 can be explicitly seen on the Figures 4.8 and 4.9. The change in the coniferous, deciduous and mixed stand categories of all the four subwatersheds are given in the figures of the Appendix B.

Table 4.1. The area (in hectares) covered by land uses of each subwatershed for 1986, 2006 and model simulation results

	Subwatershed 1			Subwatershed 2			Subwatershed 3			Subwatershed 4		
Land Use	**Data 1986**	**Data 2006**	**Model 2006**	**Data 1986**	**Data 2006**	**Model 2006**	**Data 1986**	**Data 2006**	**Model 2006**	**Data 1986**	**Data 2006**	**Model 2006**
Conf 0	20	158	151	615	246	217	718	750	708	319	909	920
Y Conf 12	0	22	11	0	0	0	0	3	39	424	1	15
Y Conf 3	10	51	56	8	28	5	89	230	175	390	120	114
YM Conf 12	0	0	13	0	0	6	42	0	76	0	0	132
YM Conf 3	0	95	84	0	64	20	0	429	320	0	859	405
M Conf 1	45	64	36	68	20	26	470	226	192	490	70	162
M Conf 2	64	8	38	39	81	34	317	359	231	256	239	131
M Conf 3	0	51	63	7	151	59	286	227	249	0	144	139
Decd 0	326	202	201	626	176	193	1045	286	298	337	696	629
Y Decd 12	78	0	46	98	0	167	50	0	105	0	0	119
Y Decd 3	84	283	280	137	700	738	336	716	600	248	1613	1464
YM Decd 12	497	0	29	371	0	65	115	0	26	35	0	8
YM Decd 3	164	539	545	594	811	841	120	237	251	1665	260	292
M Decd 1	57	22	41	68	10	58	0	0	9	0	0	13
M Decd 2	130	108	99	161	81	134	22	0	50	34	21	78
M Decd 3	0	338	231	12	688	420	0	66	225	0	137	372
Conf Decd 0	207	0	104	179	0	32	309	0	32	1453	1	9
Y Conf Y Decd 12	58	0	1	59	0	9	441	0	47	88	0	3
Y Conf Y Decd 3	0	0	37	0	80	80	218	504	484	35	199	112
Y Conf M Decd 12	0	0	6	0	0	6	0	0	46	0	0	17
Y Conf M Decd 3	0	21	25	157	81	122	5	252	178	0	238	168
M Conf Y Decd 12	122	3	4	305	0	37	106	0	54	28	0	162
M Conf Y Decd 3	25	93	109	298	566	542	311	819	462	1	665	478
M Conf M Decd 12	11	65	14	18	76	69	49	1	70	223	0	68
M Conf M Decd 3	35	164	69	202	357	345	108	204	372	109	53	212
Agriculture	1834	1444	1436	2178	2011	2010	3010	2735	2735	4101	3722	3726
Forest Open Space	3	51	49	5	15	9	47	64	67	12	92	90
Settlement	64	52	56	131	95	93	14	124	129	0	210	211
Total	3834	3834	3834	6337	6337	6337	8230	8230	8230	10249	10249	10249

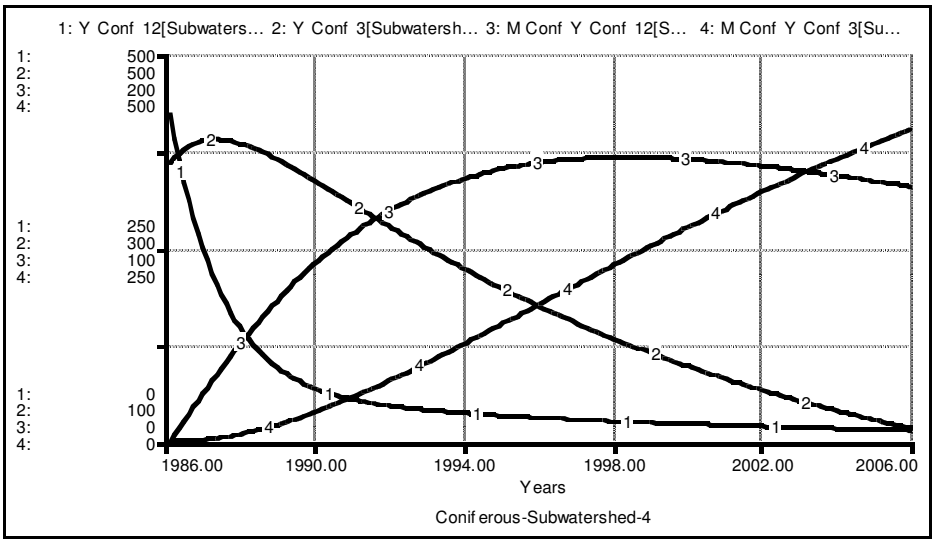

Figure 4.8. Simulation of the young coniferous stands, Subwatershed 4, 1986-2006

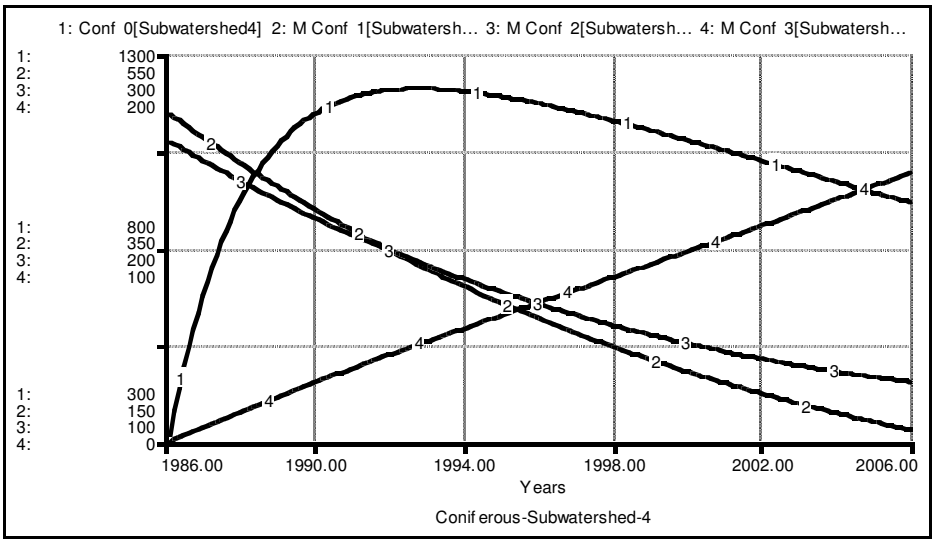

Figure 4.9. Simulation of the mature coniferous stands, Subwatershed 4, 1986-2006

Figures 4.8 and 4.9 show that *Young Coniferous 12* decreased and stabilized since it intensified to *Young Coniferous 3* and a fraction was cut degrading this *Young Coniferous 12* to *Coniferous 0*. This unusual cut led to the initial increase in *Coniferous 0*. The fraction of the unusual cut was defined based on the annual reports of the conducted forest management practices. These annual reports determine the number of the trees which were unusually cut. The number of the tree in one hectare is calculated based on the calculation tables of the forest management plans (O.G.M., 2006). Finally the fraction of the unusually cut stand area is determined (Chapter 3).

The later decline in *Coniferous 0* is due to the regrowth of *Mature Coniferous Young Deciduous 12* in *Coniferous 0*. The intensification of *Young Coniferous 12* to *Young Coniferous 3* increased *Young Coniferous 3* which eventually decreased due to its maturation to *Mature Coniferous 3*. This maturation process increased *Mature Coniferous 3*. This increase then stabilized due to the natural degradation of *Mature Coniferous 3* to *Mature Coniferous 2*. The degradation of *Mature Coniferous 2* to *Mature Coniferous 1* and *Mature Coniferous 1* degradation to *Coniferous 0* led to the decline both in *Mature Coniferous 1* and *2*. *Mature Coniferous 1* and *Mature Coniferous 2* regenerated to become *Mature Coniferous Young Coniferous 12*. This regeneration process together led to increase in *Mature Coniferous Young Coniferous 12*. The later decline in *Mature Coniferous Young Coniferous 12* was due to the intensification of *Mature Coniferous Young Coniferous 12* to *Mature Coniferous Young Coniferous 3*. Consequently, the *Mature Coniferous Young Coniferous 3* increased.

The Leaf Area Index (LAI) and Root Depth (RD in mm) are the two parameters that depend on land use and used for calculating actual evapotranspiration. As described in the previous chapters, the LAI was measured based on the hemispherical photograph analysis method (Schleppi et al., 2007) while the RD was estimated based on the assumption of average root depth, 1000 mm for forest and 500 mm for agriculture. The hemispherical photographs of the main forest stand categories were taken during the summer of 2007. The forest stand categories where the photographs were taken, corresponding LAI values and the mean LAI value of that stand category are briefly described in Tables 3.15, 3.16 and 3.17 in the previous Chapter 3.

The land use model generated the area occupied by different forest stands and land use categories for individual subwatersheds. For each subwatershed, a single LAI is calculated by weighing the average of individual stand groups' LAIs, with respect to the areas covered by these groups. The same procedure is applied to calculate a RD parameter for each subwatershed. According to the land use change between 1986 and 2006, the simulated annual summer and winter values of LAI and RD parameters are given in Tables 4.2 and 4.3.

Table 4.2. The average summer and winter LAI parameters between 1986 and 2006

	LAI-Summer				LAI-Winter			
	Subwatersheds				Subwatersheds			
Year	**1**	**2**	**3**	**4**	**1**	**2**	**3**	**4**
1986	1.29	1.34	1.20	1.28	0.11	0.25	0.37	0.26
1987	1.30	1.36	1.22	1.28	0.12	0.25	0.38	0.26
1988	1.32	1.38	1.23	1.28	0.13	0.25	0.38	0.27
1989	1.33	1.40	1.25	1.29	0.13	0.25	0.39	0.27
1990	1.34	1.42	1.26	1.29	0.14	0.25	0.39	0.27
1991	1.34	1.43	1.27	1.29	0.14	0.25	0.40	0.27
1992	1.35	1.45	1.28	1.29	0.14	0.25	0.40	0.27
1993	1.36	1.46	1.29	1.29	0.15	0.24	0.41	0.28
1994	1.37	1.48	1.30	1.30	0.15	0.24	0.41	0.28
1995	1.37	1.49	1.31	1.30	0.16	0.24	0.42	0.28
1996	1.38	1.50	1.32	1.30	0.16	0.24	0.42	0.28
1997	1.39	1.51	1.33	1.30	0.17	0.24	0.42	0.29
1998	1.39	1.52	1.34	1.30	0.17	0.24	0.43	0.29
1999	1.40	1.53	1.34	1.31	0.17	0.24	0.43	0.29
2000	1.40	1.53	1.35	1.31	0.18	0.24	0.43	0.29
2001	1.40	1.54	1.36	1.31	0.18	0.24	0.44	0.30
2002	1.41	1.55	1.36	1.31	0.19	0.24	0.44	0.30
2003	1.41	1.56	1.37	1.32	0.19	0.24	0.44	0.30
2004	1.42	1.56	1.37	1.32	0.19	0.24	0.45	0.30
2005	1.42	1.57	1.38	1.32	0.20	0.24	0.45	0.30
2006	1.43	1.57	1.38	1.32	0.20	0.24	0.45	0.31

Table 4.3. The average summer and winter RD parameters between 1986 and 2006

	RD-Summer (mm)				RD-Winter (mm)			
	Subwatersheds				Subwatersheds			
Year	**1**	**2**	**3**	**4**	**1**	**2**	**3**	**4**
1986	743	807	810	799	504	635	627	599
1987	746	808	810	793	509	636	628	599
1988	748	809	810	789	515	638	629	600
1989	750	809	809	788	520	640	629	600
1990	752	810	809	787	525	641	630	600
1991	755	811	809	787	530	643	631	601
1992	757	812	809	787	535	645	632	601
1993	759	813	809	788	540	646	633	602
1994	761	814	809	788	545	648	634	602
1995	763	815	809	788	549	649	635	603
1996	765	816	809	788	554	651	636	603
1997	767	817	809	789	559	653	636	603
1998	770	818	809	789	563	654	637	604
1999	772	818	809	789	568	656	638	604
2000	774	819	809	789	572	657	639	605
2001	776	820	809	788	577	659	640	605
2002	778	821	809	788	581	661	641	605
2003	779	822	809	788	586	662	641	606
2004	781	823	809	788	590	664	642	606
2005	783	824	809	788	594	665	643	607
2006	785	824	809	787	598	667	644	607

4.3. Calibration Results of Hydrodynamics Model

The calibration target of the hydrodynamics model was the river discharge observed by the Turkish State Hydraulic Works (D.S.İ., 2001). The calibration simulations were extended over two years; 1986 and 1987 since the observed data were most reliable for this period. After 1987, a dam was built close to the discharge measurement station which interfered with the river channel discharge data.

Table 4.4 summarizes the various parameter values considered in model calibration and the overall results of each run. The LAI values were seasonal for all the simulation runs whereas constant values of Root Depth (RD) parameter as well as seasonal values were also considered. The constant values tested for RD were 1000 mm and 500 mm. For

the saturated zone, four different values of saturated vertical (10^{-8}, 5×10^{-8}, 5×10^{-7} and 10^{-7} m/s) and horizontal hydraulic conductivity (10^{-7}, 5×10^{-7}, 5×10^{-6} and 10^{-6} m/s) were considered. The effect of the threshold melting temperature was also tested by applying the values 0ºC and 1ºC. The reference evapotranspiration was modified according to the modified air temperature values for the last three calibration runs.

Table 4.4. Parameter values and results of each calibration run

Model Parameters					Measured	Simulation Performance			
Run No:	**Tmt (°C)**	**RD (mm)**	**K_v (m/s)**	**K_H (m/s)**	**$Q_{m,av}$ (m^3/s)**	**$Q_{p,av}$ (m^3/s)**	**ME (m^3/s)**	**R (correlation)**	**R^2 (Nash-Sutcliff)**
1	0	1000	10^{-7}	10^{-6}	3.42	2.73	0.69	0.64	0.38
2	1	1000	10^{-7}	10^{-6}	3.42	2.75	0.65	0.64	0.38
3	0	500	10^{-7}	10^{-6}	3.42	3.49	-0.07	0.68	0.46
4	1	500	10^{-7}	10^{-6}	3.42	3.45	-0.03	0.66	0.43
5	0	1000	10^{-8}	10^{-7}	3.42	4.30	-0.88	0.72	0.38
6	1	1000	10^{-8}	10^{-7}	3.42	3.68	-0.26	0.75	0.54
7	0	500	10^{-8}	10^{-7}	3.42	3.54	-0.12	0.66	0.33
8	1	500	10^{-8}	10^{-7}	3.42	3.91	-0.49	0.63	0.22
9	0	1000	5×10^{-7}	5×10^{-6}	3.42	2.77	0.65	0.63	0.27
10	0	500	5×10^{-8}	5×10^{-7}	3.42	3.41	0.01	0.72	0.52
11	0	Seasonal	10^{-7}	10^{-6}	3.42	3.20	0.22	0.63	0.40
12	0	Seasonal	5×10^{-8}	5×10^{-7}	3.42	3.25	0.17	0.71	0.51
13*	0	Seasonal	10^{-7}	10^{-6}	3.42	3.25	0.17	0.68	0.45
14*	0	Seasonal	10^{-8}	5×10^{-7}	3.42	3.36	0.06	0.72	0.51
15*	0	Seasonal	5×10^{-8}	5×10^{-7}	3.42	3.41	0.01	0.72	0.52

Tmt: Threshold melting temperature for snow
RD: Root Depth
K_V: Vertical Hydraulic Conductivity of the Saturated Zone
K_H: Horizontal Hydraulic Conductivity of the Saturated Zone
$Q_{m,av}$: Average Measured Discharge
$Q_{p,av}$: Average Model-Predicted Discharge
*: Modified Reference Evapotranspiration values were used

For each of the simulated parameters three statistics which related the simulated values to the observed ones were computed. These are:

- the mean error (ME)

$$ME = \frac{\sum (Q_{mi} - Q_{pi})}{n} \tag{4.1}$$

- the correlation coefficient (R) (Devore and Farnum, 1999)

$$R = \frac{\sum (Q_{mi} - Q_{mav})(Q_{pi} - Q_{pav})}{\sqrt{\sum (Q_{mi} - Q_{mav})^2} \sqrt{\sum (Q_{pi} - Q_{pav})^2}} \tag{4.2}$$

- the Nash and Sutcliff (R^2) (Gupta et al., 2008):

$$R^2 = 1 - \frac{\sum (Q_{mi} - Q_{pi})^2}{\sum (Q_{mi} - Q_{mav})^2} \tag{4.3}$$

Q_{mi} and Q_{pi} in the above equations are the i^{th} measured and model predicted discharges, respectively. Q_{mav} and Q_{pav} are the average measured and model predicted discharges, respectively, i is 1, 2, …n and n is the number of observations. Values of R and R^2 close to 1, mean that the simulation results are close to the observed values, whereas small absolute values of the *ME* are indicative of good agreement between the simulated and observed values.

A summary of these statistics computed for each of the runs is shown in Table 4.4. In summary, all runs produced correlation coefficients (R) that are around 0.63-0.75 and Nash and Sutcliff R^2 around 0.22-0.54 while the Mean Error values ranged from 0.3% to about 26 % of the average observed flow rate.

The results in Table 4.4 indicate that higher vertical and horizontal hydraulic conductivity values lead to lower discharge peaks and higher overall discharge (Table 4.4). The 50% decrease of the RD increased the overall discharges. Decreasing the threshold melting temperature from 1°C to 0°C produced some improvement in the simulated average flow rate relative to the observed one.

Overall, the 15^{th} simulation, which considers the modified reference evapotranspiration data and seasonal RD values together with the moderate saturated hydraulic conductivity values, appears to be most consistent with the observed data. For the 15^{th} run, the predicted average discharge (Q_{pav}) is 3.41 m^3/s. The mean error (ME) is only 0.01 m^3/s. This run also leads to relatively high correlation coefficients, with R and R^2 values equal to 0.72 and 0.52, respectively. The results of Run 15 and the observed values

are displayed in Figure 4.10. Although the model tends to underestimate the peak river discharges, the results show that the model is capable of predicting the main discharge events.

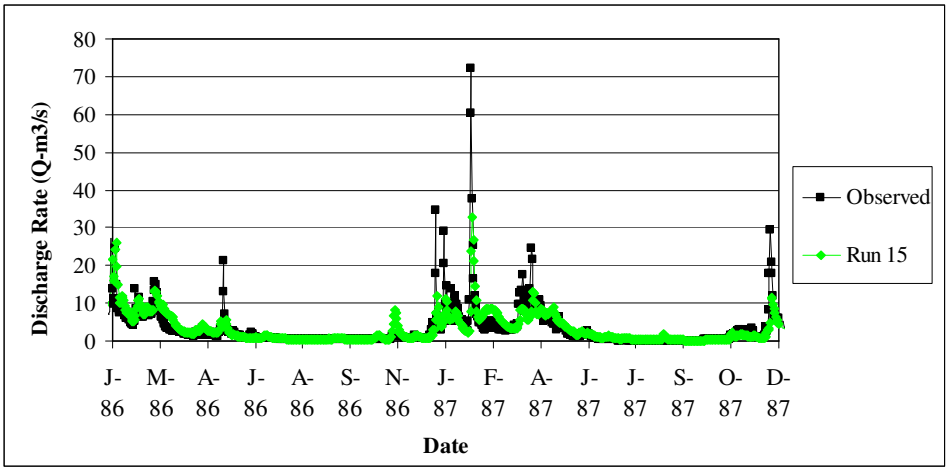

Figure 4.10. Comparison of simulation 15 with the observed discharge data

4.4. Sensitivity Analysis for the Hydrodynamics Model Parameters

The calibrated model was used next to simulate the water budget within the watershed for the 20-years historical period from 1986 to 2006. This run, referred to as the base case, is used to estimate the mean seasonal and annual watershed water budget as well as peak discharge values. The base case simulation is then used to assess the sensitivity of the hydrodynamics model to key parameters, namely: land use, Leaf Area Index (LAI), the Root Depth (RD), and the saturated hydraulic conductivity. The base case simulation will also be compared with the results of the future scenarios presented in Chapter 5.

4.4.1. Base Case Analysis

The daily water balance of the 20 years was generated with the water balance module of MIKE SHE computer program. The simulated results on monthly basis are presented on Figure 4.11 and the daily discharge from the ultimate point cross section of the stream is given in Figure 4.12. The year 1985 is also included in the simulation results.

The mean annual precipitation over the 20-year period is 1001 mm. The mean annual river flow is 355 mm. The mean annual evapotranspiration is 646 mm. For the winter months which extend over the period between October 1 and March 15, the mean precipitation, overland and baseflow to river and evapotranspiration are 545 mm, 430 mm and 115 mm respectively. For the summer months which cover the period between March 16 and September 30, the mean precipitation, overland and baseflow to river and evapotranspiration are 456 mm, -75 mm and 531 mm respectively.

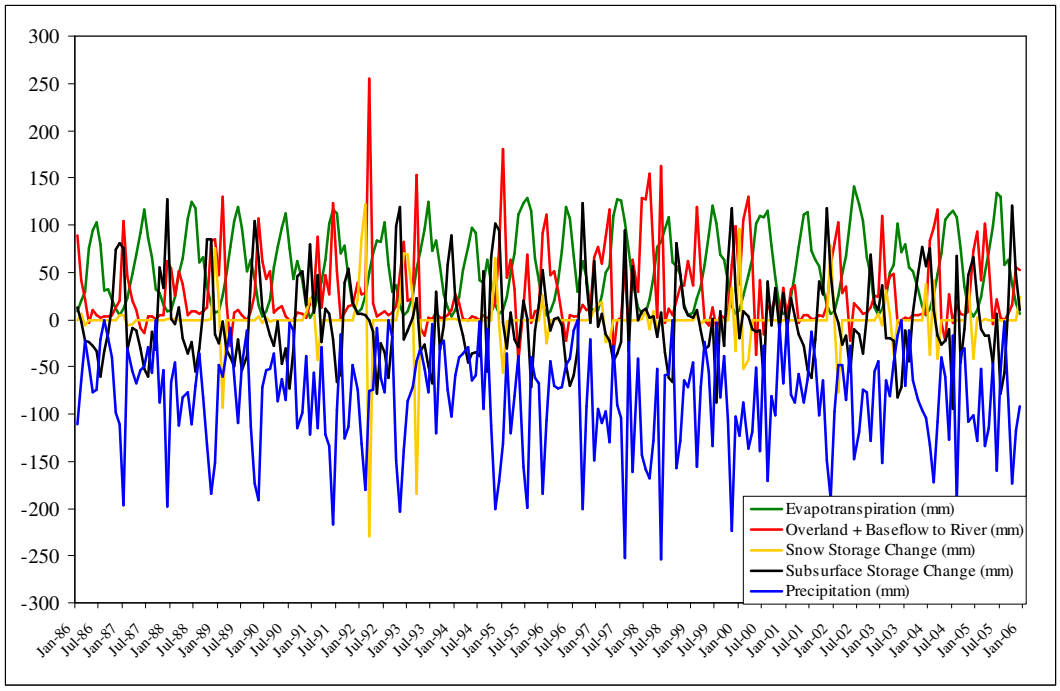

Figure 4.11. The monthly water balance profile of the 20 years of simulation

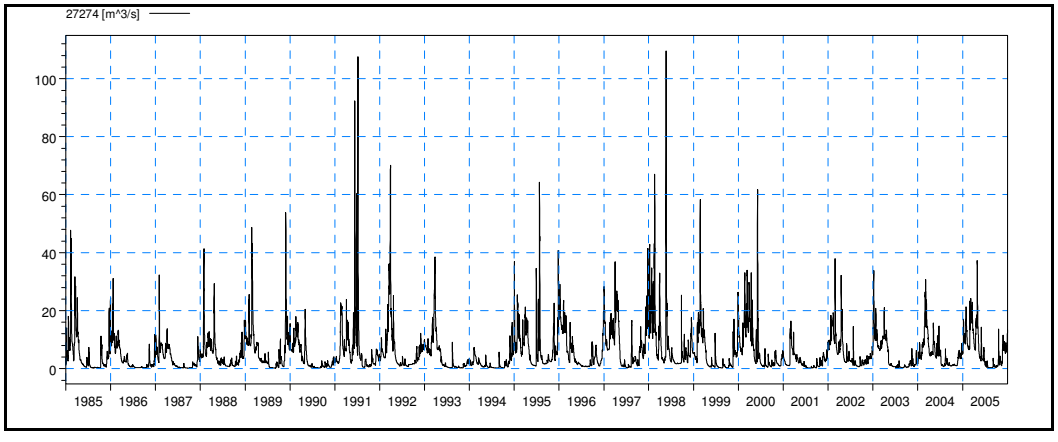

Figure 4.12. Daily discharge of the stream between 1985 and 2006

Inspection of the precipitation input data from 1986 to 2006 indicates that the highest daily precipitation was 254 mm which occurred in May 1998 when heavy rains led to flash flood in the city center and the vicinity of Bartın. The mean temperature on that day was 13.7°C. Model simulations show that almost 64% of the precipitation appears as river flow while only 33% of the precipitation is lost by evapotranspiration.

The mean precipitation over the winter (December, January and February), autumn (September, October and November), spring (March, April and May) and summer (June, July and August) months along the 20-year period are 98.9 mm, 94.5 mm, 70.2 mm and 70.1 mm respectively. On the other hand, the mean overland and baseflow to river in winter, autumn, spring and summer are 86 mm, 57 mm, -2 mm and -23 mm respectively. The mean winter, autumn, spring and summer evapotranspirations are 13 mm, 37 mm, 72 mm and 93 mm respectively.

The highest daily river flow predicted with the model occurred on March 1992 when the riverflow at the downstream point of the domain was almost 256 mm. The precipitation for this day was only 76 mm but the snowmelt contribution was almost 229 mm throughout the month which is consistent with the meteorological station data (D.M.İ., 2007). However the precipitation in February 1992 was relatively high; 181 mm and the snowmelt contribution is 122 mm. During especially the summer months, the overland and baseflow to river declines below 0 indicating that the entire precipitation appear as evapotranspiration or infiltration into the subsurface.

The highest subsurface water storage change occurred in December 1987 with monthly recharge of almost 127 mm. The precipitation for this period was relatively high equal to 198 mm while the evapotranspiration is only 4.4% of the precipitation. The mean monthly temperature is 3.2°C. However, the subsurface water discharges were 54 mm and 33 mm in previous months, October and November 1987 respectively. The highest monthly subsurface water discharge, 95 mm, occurred in July 2004. The precipitation for this period was only 17.3 mm and the evapotranspiration was 115 mm. The mean temperature was also high at 19.1 °C. However the precipitation was relatively high with 127 mm in the previous month, June 2004.

The highest evapotranspiration, 141 mm, occurred in June 2002 when the mean temperature was 17.3% and the precipitation was high for June with almost 148 mm. The lowest evapotranspiration, 2.5 mm, occurred in December 1990 when the mean temperature was 3.3°C and precipitation was 121.5 mm. However 18.4% of this precipitation was stored as snow and 65.4% infiltrated into the soil as recharge. The evapotranspiration was higher during the vegetation periods when the temperature was also higher.

The volumetric moisture content change between 1985 and 2006 in the unsaturated zone at the ultimate discharge of the watershed is shown on Figure 4.13. The change occurs only within the 3 meters depth from soil surface since the point is at almost the lowest altitude. However, the summer moisture content of the topsoil drops down to 5% which correlates with the measured values of summer 2007. The soil moisture does not drop below 15% at depth greater than 1 meter. The maximum (saturated) soil moisture content is the maximum porosity of that soil which varies between 45% and 52% within the watershed.

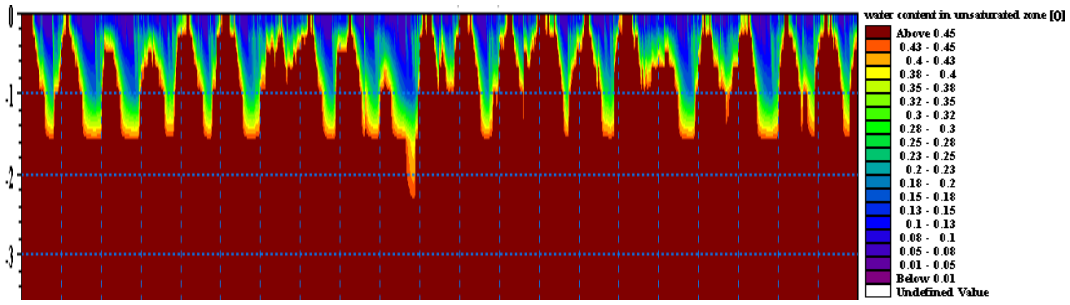

Figure 4.13. The change in the unsaturated zone between 1985 and 2006

4.4.2. Sensitivity of the Hydrodynamics Model to Land Use

Land use is one of the main parameters influencing the water budget of a watershed. To assess the sensitivity of the simulated water budget to land use, the calibrated hydrodynamics model was simulated for the period from 1986 to 2006 assuming the entire watershed is completely covered with agricultural areas, coniferous, deciduous and mixed forests, respectively. These are extreme scenarios that are used to evaluate the response of the hydrodynamics model. Mature Coniferous 3 (M Conf 3), Young-Mature Deciduous 3

(YM Decd 3) and Y Coniferous M Deciduous 3 (Y Conf M Decd 3) were selected from the coniferous, deciduous and mixed stand groups since these stand groups have the highest LAI values within their group. The summer LAI values of the agricultural area, M Conf 3, YM Decd 3 and Y Conf M Decd 3 are 1.0, 1.87, 2.40 and 2.15 (Tables 3.15, 3.16 and 3.17) respectively and their winter values are 0, 1.49, 0 and 1.07 respectively.

A comparison of the mean river discharges predicted with respect to these 4 scenarios and the actual river discharge are presented in Table 4.5. Since the water data were missing for years 1989 and 2000, those two years were excluded from the correlation statistics. The four scenario simulations and the calibrated model simulation are indicated with 1a, 2a, 3a, 4a and 5a respectively.

Table 4.5. The statistics of scenario and calibrated model simulations

Sim. No:	Land Use	$Q_{m,av}$ (m^3/s)	$Q_{p,av}$ (m^3/s)	ME
1a	Agriculture	4.99	5.61	-0.62
2a	M Conf. 3	4.99	4.49	0.50
3a	YM Decd. 3	4.99	4.22	0.77
4a	Y Conf. M Decd. 3	4.99	4.37	0.62
5a	Calb. Model	4.99	5.59	-0.60

$Q_{m,av}$: Average Measured Discharge
$Q_{p,av}$: Average Model-Predicted Discharge

The results of these simulations indicate that the calibrated model predicted a discharge value close to the measured one. The mean error is the highest for the third simulation. For the first scenario, the high values of stream discharges are basically due to the constant agricultural areas for the 20 years. Based on the difference between the land use maps of 1986 and 2006, the agricultural areas diminished approximately 10% due to the land abandonment. The calibrated model considers this change. Although the agricultural areas diminished, the calibrated model estimated an average discharge close to that of the first scenario. The reason for this result may be the higher loss of water by evaporation from the relatively open agricultural areas with lower LAI.

The hydrological impact of the four simulations may better be understood by a simple water balance model. The daily water balance model was also produced for the four scenarios. A simple water balance model consists of two main components; evapotranspiration and stream flow. Figure 4.14 visualizes the ratio of these two

components to the precipitation and allows a comparison between the calibrated model and the scenarios for the 20 years.

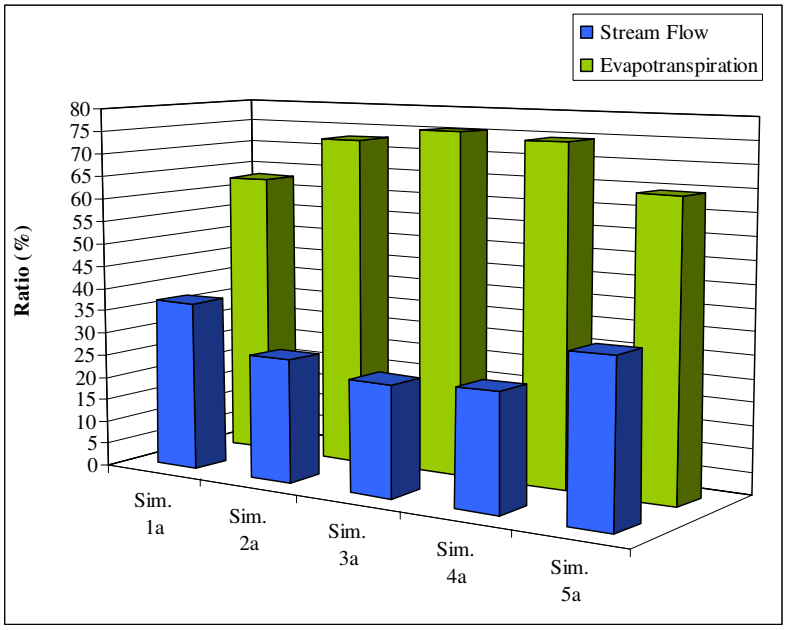

Figure 4.14. Water balance comparison between the scenario runs and the calibrated result

The water budget analysis shows that the stream flow ratios are 37.2%, 27.1%, 24.4%, 25.6% and 35.5% for the simulations 1a, 2a, 3a, 4a and 5a respectively while the evapotranspiration ratios are 62.8%, 72.9%, 75.6%, 74.4% and 64.5%. The scenario with the agricultural areas predicts the highest stream flow compared to the other three land use scenarios while YM Deciduous 3 forests yields the lowest stream flow. The evapotranspiration for YM Deciduous 3 is a bit higher than the Young Coniferous Mature Deciduous 3 and Mature Coniferous 3.

The sensitivity of the hydrodynamics model to extreme land use scenarios was evaluated in terms of average discharge and evapotranspiration. The results of these simulations indicate that the agricultural watershed leads to about 25-33% higher discharge and about 10-13% lower evapotranspiration compared to the forested watershed.

4.4.3. Sensitivity of the Hydrodynamics Model to the LAI and RD

The previous section discusses the sensitivity of the hydrodynamics model to the extreme land use scenarios which have specific seasonal LAI and RD parameter values. In this set of runs, the soil and climate parameters were fixed for the calibrated hydrodynamics model while the sensitivity of the model to the LAI and RD parameters was evaluated. The hydrodynamics model was run for 20 years from 1986 to 2006 for all the sensitivity tests. The water balance models of each simulation runs were estimated. For the first six simulations, RD parameter was fixed to 1000 mm, while the LAI values of 1, 2, 3, 5, 7 and 10 were tested by the model. For the next six simulations, RD parameter was fixed to 500 mm and the same values of the LAI were tested. Table 4.6 presents the stream flow and the evapotranspiration ratios of the simulation runs for the different LAI and RD values. Figure 4.15 and Figure 4.16 shows the effect of the LAI and the RD on the water balance of the watershed.

Table 4.6. Stream flow and the evapotranspiration ratios of the simulation runs for different LAI and RD values

Sim. No:	LAI	RD (mm)	Evapotranspiration (%)	Stream Flow (%)
1b	1	500	63.9	36.1
2b	1	1000	66.8	33.2
3b	2	500	68.6	31.4
4b	2	1000	73.6	26.4
5b	3	500	70.6	29.4
6b	3	1000	77.4	22.6
7b	5	500	70.5	29.5
8b	5	1000	77.5	22.5
9b	7	500	70.5	29.5
10b	7	1000	77.7	22.3
11b	10	500	×	×
12b	10	1000	77.7	22.3

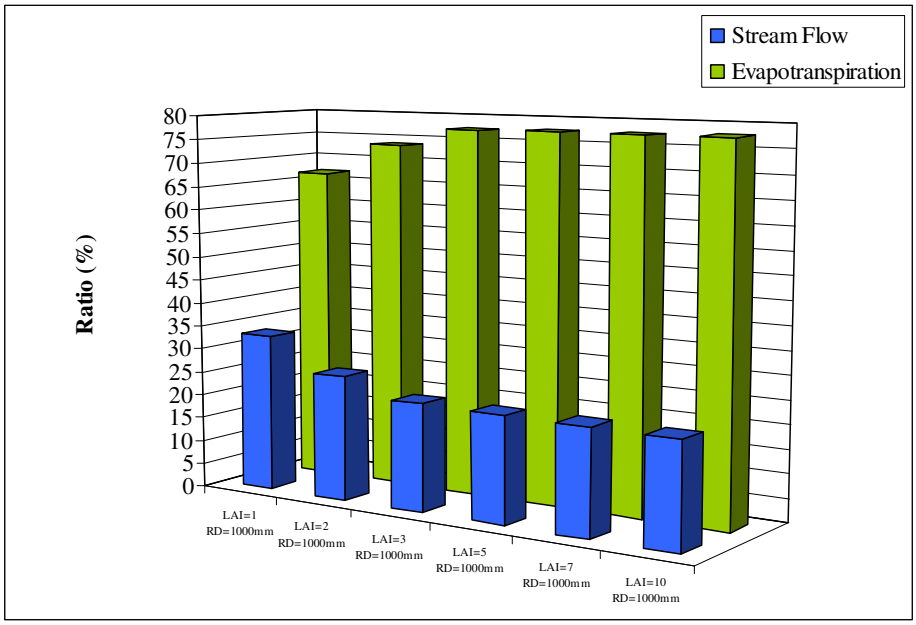

Figure 4.15. Water balance comparison for the LAI parameter values (RD=1000 mm)

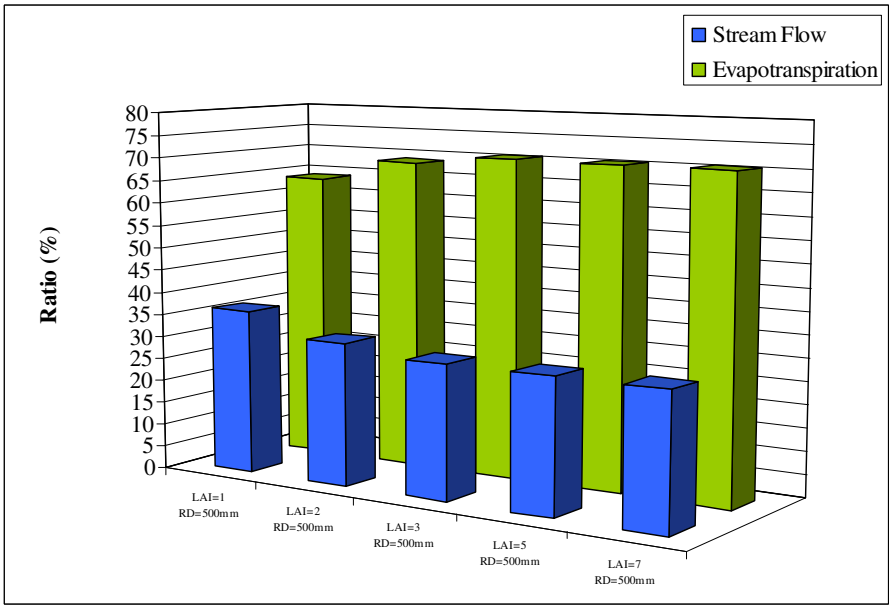

Figure 4.16. Water balance comparison for the LAI parameter values (RD=500 mm)

For a RD value of 1000 mm, increasing the LAI from 1 to 3 increases the evapotranspiration and decreases the stream flow by almost 11%. The water balance becomes insensitive to the LAI parameter greater than 3. The critical LAI value range for this watershed is between 1 and 3. For LAI values greater than 3, the increase in canopy

closure would balance the evapotranspiration by shading the soil against evaporation. The soil loses less water and faster generation of overland flow occurs. This overland flow balances the increment of the transpiration due to LAI increase. For a RD value of 500 mm, increasing the LAI from 1 to 3 increases the evapotranspiration and decreases the stream flow by almost 7%. As in the case of RD=1000 mm, the water balance is insensitive to LAI parameter greater than 3. Decreasing the RD from 1000 mm to 500 mm decreases the evapotranspiration while increasing the stream flow by the range of 3-7% which is dependent upon the LAI values.

The hydrodynamics model is highly sensitive to the impact of the different land uses. Particularly, the impacts of the agricultural areas and the forests are more distinct due to their different seasonal LAI and RD values. In addition, the hydrodynamics model is highly sensitive to the variable LAI and RD values. Therefore, the important role of the land use change on the hydrodynamics model re-emphasizes the need for integrating land use model with the hydrodynamics model.

4.4.4. Sensitivity Analysis for the Saturated Zone Soil Parameters

Another set of simulations were conducted to assess the sensitivity of the hydrodynamics model to the hydraulic conductivity values of the saturated zone. The subsurface flow module of the hydrodynamics model requires the definition of horizontal and vertical saturated hydraulic conductivity for saturated zone. These values were defined as calibration parameters in Section 4.3. The calibrated vertical saturated hydraulic conductivity value was found to be 5×10^{-8} m/s while the horizontal hydraulic conductivity value was 5×10^{-7} m/s (Table 4.4). Because the hydraulic conductivity typically exhibits wide variations in space, the sensitivity simulations considered non uniform values to assess the impact of heterogeneity on model predictions.

For this purpose, two simulation runs were conducted using non uniform vertical saturated hydraulic conductivity values equal to those defined for the unsaturated zone. The horizontal hydraulic conductivity values were set equal to 10 times the vertical hydraulic conductivity values. This anisotropy ratio is consistent with published values (Freeze and Cherry, 1979). The land use and climate parameters were kept unchanged as

defined in the calibrated hydrodynamics model (Table 4.4). The vertical saturated hydraulic conductivity values of the soil layer interval between 1 m and 5 m were tested during the first run. The vertical saturated hydraulic conductivity values of the soil layer interval between 10 m and 15 m were tested in the second run. The average horizontal hydraulic conductivity values for these two scenarios are 1.0×10^{-5} m/s and 6.4×10^{-6} m/s, respectively, while the average vertical hydraulic conductivity values for these two scenarios are 1.0×10^{-6} m/s and 6.4×10^{-7} m/s, respectively.

The relation between the simulated and observed data is shown in Table 4.7. Because the water data were missing for year 1989 and the years after 2000, those years were excluded out of the correlation statistics.

Table 4.7. The statistics of the two simulations and calibrated model

Sim. No:	$Q_{m,av}$ (m^3/s)	$Q_{p,av}$ (m^3/s)	ME
1c	4.99	5.48	-0.49
2c	4.99	5.56	-0.57
Calb. Model	4.99	5.59	-0.60

$Q_{m,av}$: Average Measured Discharge
$Q_{p,av}$: Average Model-Predicted Discharge

The model predictions show a slight decrease in the predicted mean discharge with the higher hydraulic conductivity values (Simulation 1c) because higher hydraulic conductivity values lead to higher percolation rather than to overland flow. However, overall, these simulations show that the river discharge for the Bartin watershed is not strongly sensitive to the hydraulic conductivity of the saturated zone. The saturated zone in the watershed is generally characterized by low permeability, making subsurface flow a small component of the overall water budget.

5. FUTURE SIMULATION AND SCENARIO ANALYSIS

The calibrated land use-hydrodynamics model was used to simulate the long term water budget of the Bartın spring watershed under different future scenarios. The purpose of these simulations is to assess the impact of future land use changes on the water yield of the watershed. These predictions can be used to develop plans to meet future water needs of the region.

Six simulations were made, each covering a 21-year period between 2006 and 2026. These six simulations are described in Table 5.1. The first simulation assumes that current land use conditions are unchanged. Hence, it serves as a base case scenario that will be used for comparison with the other scenarios. The second scenario assumes that all the handicapped forest areas and forest open spaces are converted to agricultural areas. The third scenario is about the conversion of the agricultural areas and forest open spaces to forest areas. The conversion of the handicapped deciduous and mixed stand groups to coniferous stand groups constitutes the fourth scenario. The conversion of the handicapped deciduous and coniferous stand groups to mixed stand groups constitutes the fifth scenario. The sixth simulation considers the conversion of handicapped coniferous and mixed stand groups to deciduous stand groups.

Table 5.1. List of scenarios

No.	**Simulation**
1	Base Case (unchanged land use)
2	Agriculture to Forest
3	Forest to Agriculture
4	Deciduous and Mixed to Coniferous
5	Coniferous and Deciduous to Mixed
6	Coniferous and Mixed to Deciduous

The precipitation and temperature data that were used for the simulation of these future scenarios are described in Section 5.1. The results of the base case scenario are discussed in Section 5.2. Sections 5.3 and 5.4 present the description of the different land use scenarios and the results obtained with these scenarios. The key parameters used to

compare the model predictions are the river discharge at the downstream end of the watershed and evapotranspiration from the entire watershed.

To predict the long term water budget of the watershed and to assess the impact of climatic change on the water yield, the base case scenario was prolonged to the period between 2027 and 2060. Section 5.5 discusses the results of this long term simulation.

5.1. Generation of Future Climatic Data

The daily climate data used in the future scenarios were obtained from the regional climate modeling study by the Institute of Eurasia Earth Sciences in İstanbul Technical University (İ.T.Ü) (Bozkurt et al., 2008). The data were generated using the RegCM3 regional climate model which was originally produced at the National Center for Atmospheric Research of U.S.A. (Elguindi et al., 2007). The model was adapted to Turkey using local conditions. The resolution of the model covering Turkey was increased to 27×27 km^2 grids. The model results were evaluated as part of the project titled "Climate Scenarios for Turkey" (Dalfes, 2008).

The RegCM model is used for regional climate simulations considering the greenhouse gas scenarios proposed by the International Panel on Climate Change (I.P.C.C.) (Bates et al., 2008). These scenarios are named as A1, B1, A2 and B2. The A1 and B1 scenarios assume a world economy dominated by global trade and alliances. According to these two scenarios, the global population is expected to increase from today's 6.6 billion and peak at 8.7 billion in 2050. On the other hand, the A2 and B2 scenarios project less globalization and co-operation. According to these two scenarios, global population is expected to increase until 2100, reaching 10.4 billion (B2) and 15 billion (A2) by the end of the century. A2 scenario considers the future economic situation as regionally oriented.

The results of the simulations conducted in this study for the Bartın watershed are based on the A2 scenario. The mean daily rainfall and mean daily temperature are the climatic parameters used from this regional climate model. The generated daily rainfall data were modified such that the mean monthly generated data matches the mean monthly

precipitation data observed at the Ulus Meteorological Station data from the years 1974 to 1990. (D.M.İ., 2007).

The mean annual temperature and precipitation trends covering both the observed (1986 and 2005) and the model generated data (2006 to 2060) are presented in Figures 5.1 and 5.2, respectively. The mean annual temperature exhibits an increasing trend starting around the year 2030. Although the mean annual precipitation increases over the entire 75-year period between 1986 and 2060, it does not exhibit a pronounced trend. Therefore, the results of the scenarios listed in Table 1, which extend over the period from 2006 to 2026, are not expected to reflect any consequences of global warming. On the other hand, the results of the long-term simulation which will extend to year 2060 will reflect the consequence of the warming trend observed in the simulated climatic data.

For the generated climatic data between 2006 and 2060, the mean annual precipitation is predicted to be 1034 mm. The maximum and minimum annual precipitations are predicted to be 1443 mm and 631 mm, respectively. The wettest month is predicted to be January with the mean precipitation of 141 mm. The driest month is predicted to be July with the mean precipitation of 36 mm. For this period, the mean annual temperature is predicted to be 11°C. The warmest month is predicted to be July with a mean temperature of 19.4°C. The coldest month is predicted to be January with a mean temperature of 3.5°C.

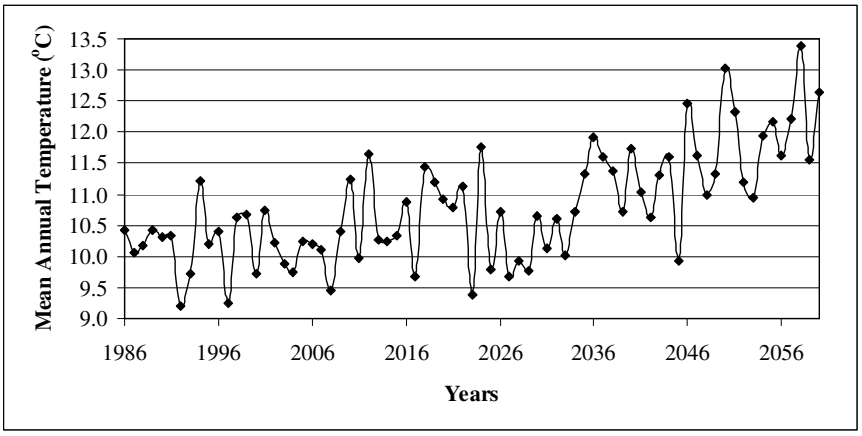

Figure 5.1. Mean annual temperature trends between 1986 and 2060

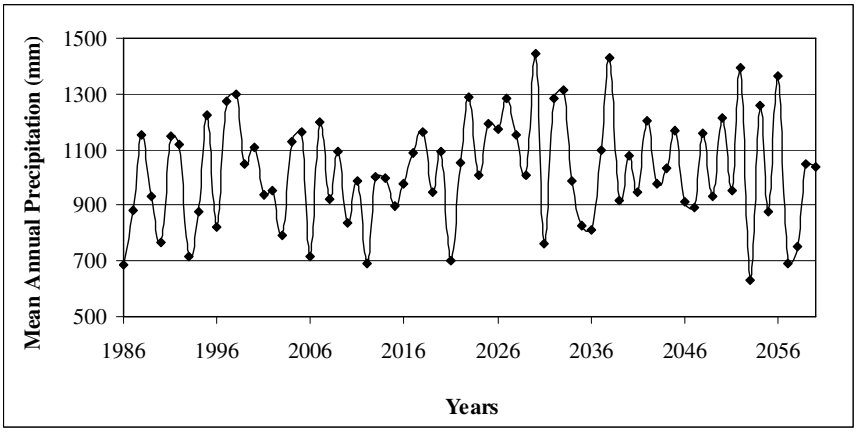

Figure 5.2. Mean annual precipitation trends between 1986 and 2060

5.2. Base Case Analysis

As part of model calibration, the land use-hydrodynamics model was used to match the 1986 and 2006 land use data. The base case simulation assumes that the land use change pattern and practices will continue unchanged until year 2026. To simulate the future land use for the study area, the land use model was run for 41 years between 1986 and 2026 assuming the same land use dynamics condition. From these simulations, the annual summer and winter values of the land use parameters; LAI and RD were computed and supplied to the hydrodynamics model.

The generated annual summer and winter LAI and RD parameters for the period between 2006 and 2026 are shown in Tables 5.2 and 5.3. The summer and winter LAI values of the subwatersheds are generally increasing over the 21-year period since the agricultural areas are decreasing while the forest areas are increasing (Section 4.4.2). On the other hand, the decrease of the summer RD values in some subwatersheds is due to the increment in the forest open spaces. The decrease in the agricultural areas and increment in the forest areas and forest open spaces are due to the continued land abandonment which occurred between 1986 and 2006.

Table 5.2. The annual summer and winter values of LAI parameters between 2006 and 2026.

	LAI-Summer				LAI-Winter			
	Subwatersheds				Subwatersheds			
Year	**1**	**2**	**3**	**4**	**1**	**2**	**3**	**4**
2006	1.43	1.57	1.38	1.32	0.20	0.24	0.45	0.31
2007	1.43	1.58	1.39	1.33	0.21	0.24	0.45	0.31
2008	1.43	1.58	1.39	1.33	0.21	0.24	0.45	0.31
2009	1.44	1.59	1.40	1.33	0.21	0.24	0.46	0.31
2010	1.44	1.59	1.40	1.33	0.22	0.24	0.46	0.31
2011	1.44	1.60	1.40	1.33	0.22	0.24	0.46	0.32
2012	1.44	1.60	1.41	1.34	0.22	0.24	0.46	0.32
2013	1.45	1.60	1.41	1.34	0.23	0.24	0.46	0.32
2014	1.45	1.61	1.41	1.34	0.23	0.24	0.47	0.32
2015	1.45	1.61	1.41	1.34	0.23	0.24	0.47	0.32
2016	1.46	1.62	1.42	1.34	0.24	0.24	0.47	0.33
2017	1.46	1.62	1.42	1.34	0.24	0.24	0.47	0.33
2018	1.46	1.62	1.42	1.35	0.24	0.24	0.47	0.33
2019	1.46	1.62	1.42	1.35	0.25	0.24	0.47	0.33
2020	1.47	1.63	1.43	1.35	0.25	0.24	0.47	0.33
2021	1.47	1.63	1.43	1.35	0.25	0.24	0.48	0.33
2022	1.47	1.63	1.43	1.35	0.25	0.24	0.48	0.33
2023	1.47	1.63	1.43	1.35	0.26	0.24	0.48	0.33
2024	1.48	1.64	1.43	1.35	0.26	0.24	0.48	0.34
2025	1.48	1.64	1.43	1.35	0.26	0.24	0.48	0.34
2026	1.48	1.64	1.44	1.35	0.27	0.24	0.48	0.34

Table 5.3. The annual summer and winter values of RD parameters between 2006 and 2026

	RD-Summer (mm)				RD-Winter (mm)			
	Subwatersheds				Subwatersheds			
Year	**1**	**2**	**3**	**4**	**1**	**2**	**3**	**4**
2006	785	825	810	789	598	667	644	607
2007	787	826	810	788	602	668	645	607
2008	789	827	810	788	606	670	645	608
2009	791	828	810	787	610	671	646	608
2010	793	829	810	787	614	673	647	609
2011	795	830	810	786	618	674	648	609
2012	796	830	810	786	622	676	649	609
2013	798	831	810	786	626	677	649	610
2014	800	832	810	785	630	679	650	610
2015	801	833	810	785	634	680	651	611
2016	803	834	810	784	637	682	652	611
2017	805	835	810	784	641	683	653	611
2018	806	835	810	783	645	685	653	612
2019	808	836	810	783	648	686	654	612
2020	810	837	810	782	652	688	655	612
2021	811	838	810	782	655	689	656	613
2022	813	839	810	782	659	690	656	613
2023	814	839	810	781	662	692	657	614
2024	816	840	810	781	665	693	658	614
2025	817	841	810	780	669	695	659	614
2026	819	842	810	780	672	696	659	615

The mean annual precipitation is predicted to be 1001 mm for the 21-year period between 2006 and 2026. For this period, the maximum and minimum annual precipitations are predicted to be 1287 mm and 692 mm. The mean annual temperature is predicted to be 10.5°C.

The monthly water balance of the 21 years was generated with the water balance module of MIKE SHE computer program. The simulated results are presented on monthly basis in Figure 5.3. Figure 5.4 also shows the simulated results on annual basis.

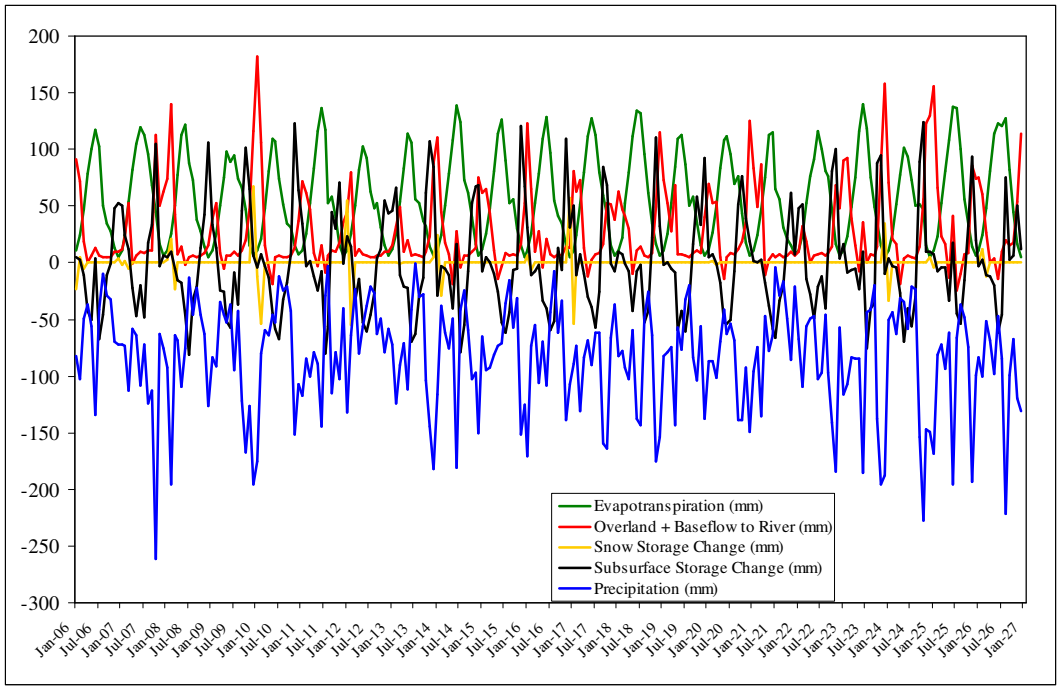

Figure 5.3. The monthly water balance for the years 2006 and 2026-Base case scenario

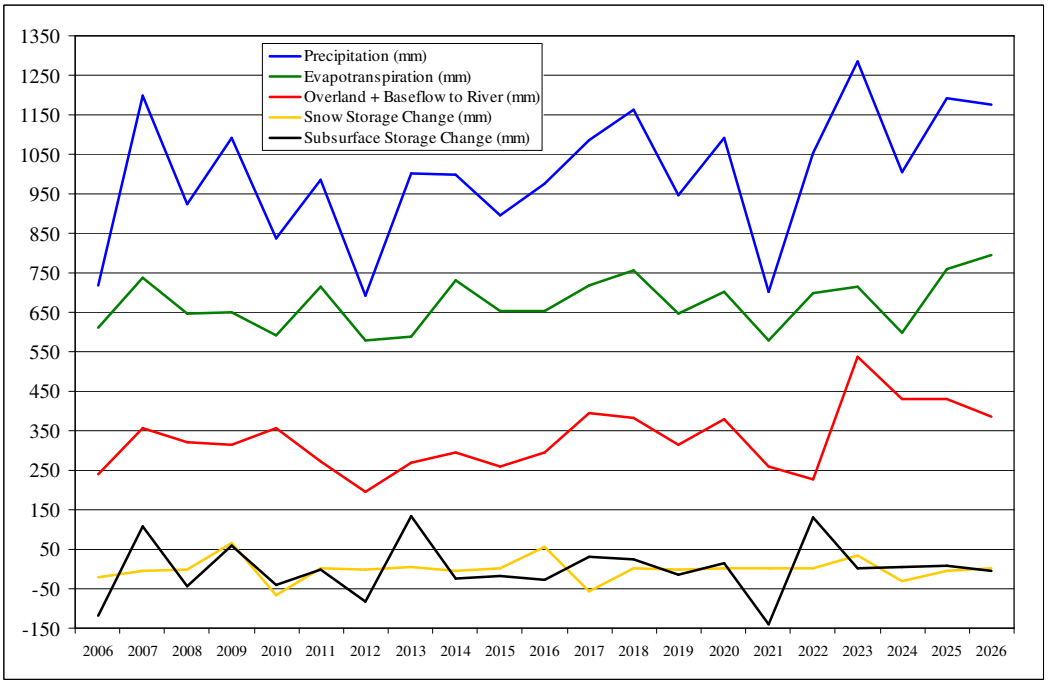

Figure 5.4. The annual water balance for the years 2006 and 2026-Base case scenario

The average annual evapotranspiration over the 21 year period from 1986 to 2006 is predicted to be almost 67% of the total precipitation while the river flow is predicted to be

33% of the total precipitation. The fractions of evapotranspiration and river flow are predicted to be 64.5% and 34.5%, respectively. This slight increase in the evapotranspiration may be attributed to the increment of the LAI and RD values due to the regrowth of the forest in the abandoned agricultural areas. On annual basis, the water balance components are predicted to show no increasing or decreasing trend for the 21-year period.

The highest monthly overland and baseflow to river is predicted to occur in January. The mean precipitation and evapotranspiration for this month are predicted to be 7.6 % and 1.1 % of the mean annual precipitation. The lowest monthly overland and baseflow to river is predicted to occur in May. It is about -0.2% of the mean annual precipitation indicating that the precipitation infiltrated only into the soil rather than flowing as overland. In May, the evapotranspiration is predicted to be 10.8% of the mean annual precipitation.

The highest monthly subsurface water recharge is predicted to occur in November equal to the 6.6% of the mean annual precipitation. The evapotranspiration for this month is predicted to be only 1.5% of the mean annual precipitation. The highest monthly subsurface water discharge is predicted to occur in July being the 5.4% of the mean annual precipitation. In July, the evapotranspiration is predicted to be 9.8% of the mean annual precipitation.

The highest monthly evapotranspiration is predicted to occur in June, equal to 11.9% of the mean annual precipitation. In June, the overland and baseflow to river is predicted to be only 1.0% of the mean annual precipitation. The lowest monthly evapotranspiration which is predicted to occur in December is only 0.6% of the mean annual precipitation. In December, the overland and baseflow to river is predicted to be 6.5% of the mean annual precipitation.

The volumetric moisture content change in the unsaturated zone of a point close to the ultimate discharge of the watershed is shown in Figure 5.5. The change is predicted to occur only within the top 3 meters of soil since the point is at almost the lowest altitude. However, the summer moisture content of the topsoil is predicted to drop down to 5%. The soil moisture content remains mostly above 15% below the depth of 1 meter. The

maximum (saturated) soil moisture content is the maximum porosity of that soil which varies between 45% and 52% within the watershed.

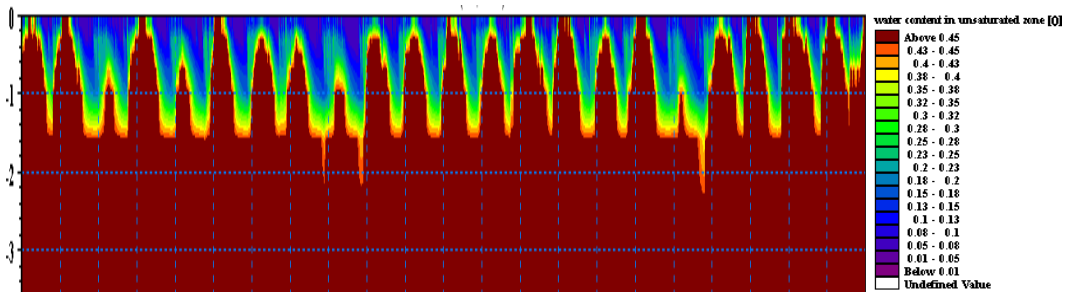

Figure 5.5. The water content change in the unsaturated zone between 2005 and 2026

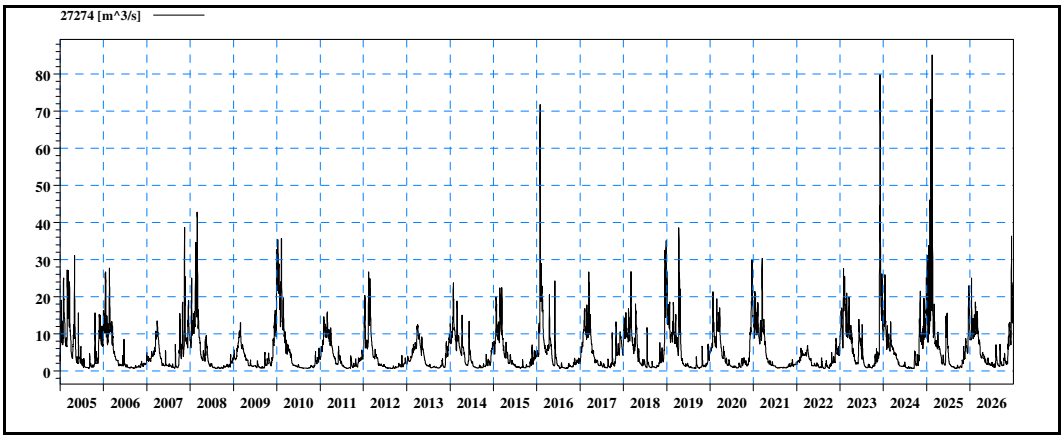

Figure 5.6. Predicted daily river discharge-Base case analysis

The daily discharge at the downstream end of the stream is shown in Figure 5.6. The average daily discharge at the downstream discharge point is predicted to be almost 5.00 m^3/s for the period between 2006 and 2026. The average daily discharge is 5.59 m^3/s for the period between 1986 and 2006. The predicted decrease in the discharge is in part due to the increase in the LAI and RD which were computed using the land use model assuming unchanged land use practices. The difference is also due to differences in the precipitation patterns of these two periods.

The comparison of the future base case analysis and the different scenarios will be based on the annual water budget for the entire watershed and a number of statistics describing the watershed's response to extreme conditions (Section 5.4). These peak (maximum/minimum) values are presented below for the base case analysis.

For the 21-year period from 2006 to 2026, the number of the years which are predicted to have average daily discharge less than the 21-year average daily discharge is 10. The maximum and minimum annual discharges are predicted to be 7.89 m^3/s and 2.80 m^3/s respectively. The maximum and minimum daily discharges are predicted to be 85.12 m^3/s and 0.68 m^3/s respectively.

The highest daily discharge is predicted to occur in February with monthly average of 12.1 m^3/s. January and March are the other two months which are predicted to have the second and third highest daily discharges with monthly averages of 10.8 m^3/s and 9.1 m^3/s respectively. The lowest daily discharge is predicted to occur in August with monthly average of 1.0 m^3/s. September and July are the other two months which are predicted to have the second and third lowest daily discharges with monthly averages of 1.3 m^3/s and 1.4 m^3/s respectively.

In this study, it was assumed that the daily river discharge below 1.0 m^3/s indicated a low discharge. This corresponds to about 6.6% of the average annual precipitation reaching the watershed. The three months with the lowest river discharge are predicted to be in the following order: August, September and July. That is consistent with the water balance results of the overland flow and baseflow to river. During the summer months, the overland and baseflow to river declines below 0 mm indicating the precipitation contributed to subsurface to meet the subsurface water deficiency.

For the base case analysis, 38.1% of the summer months (July, August and September) are predicted to have low discharge. Out of the 21 August, September and July months (covering the period from 2006 to 2026), the percentages of the August, September and July months with low discharges are predicted to be 66.7%, 33.3% and 14.3% respectively (Figure 5.17). The average monthly evapotranspiration for August, September and July are predicted to be 7.0%, 5.5% and 9.8% of the mean annual precipitation respectively. The generated mean monthly temperatures for July, August and September are 18.4°C, 19.8°C and 14.8°C, respectively.

5.3. Land Use Simulation for the Future Scenarios

This section describes the five future scenarios that were simulated with the land use-hydrodynamics model. A list of these simulations is given in Table 5.1. As in the base case, the simulations cover 21 years from 2006 to 2026. The land use model was first simulated for each of these scenarios in order to estimate the LAI and RD time series for the 21-year period. These values were then incorporated in to the hydrodynamics model to simulate the watershed budget.

The predicted results of the land use model are presented in this section. A discussion of the results of the hydrodynamic model are presented in Section 5.4

5.3.1. Conversion of Agricultural Areas to Forest

In this scenario, the agricultural areas and forest open spaces were assumed to be converted to the forest stand groups. It was also assumed that the agricultural areas and the forest open spaces were equally planted with the young coniferous, deciduous and mixed forest stand groups (Y Conf 12, Y Decd 12 and Y Conf Y Decd 12) with gradually increasing fraction beginning with 0.05 in 2006 and reaching 0.25 for each of the 3 forest stand groups in 2010. All the other anthropogenic transformations were assumed to be diminished gradually beginning in 2006 and ending by 2010.

The generated seasonal (summer and winter) LAI and RD values of the four subwatersheds were simulated using the land use model for the 21-year period. From the simulated time series for each of the four subwatersheds, the weighted averages of the LAI and RD were calculated for the entire watershed. The averaged summer and winter values of the LAI and RD were plotted for each of the scenario for the 21-year period. Figure 5.7 and Figure 5.8 present the summer and winter LAI values for each of the scenarios respectively including the base case simulation. Figure 5.9 and Figure 5.10 present the summer and winter RD values for each of the scenarios respectively.

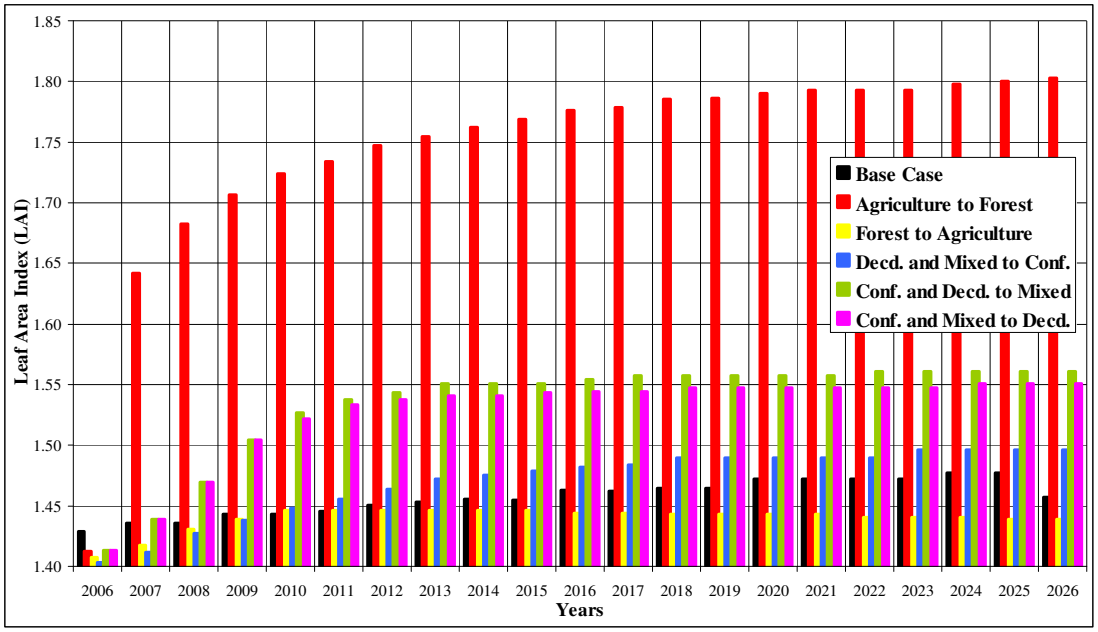

Figure 5.7. Average summer LAI values for the base case and future scenarios

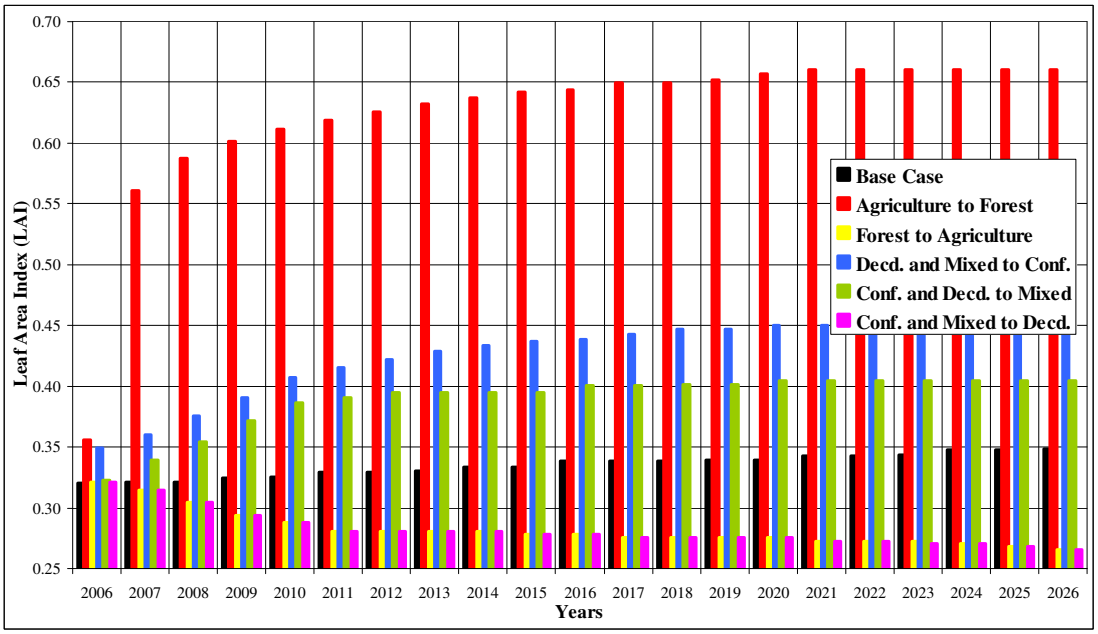

Figure 5.8. Average winter LAI values for the base case and future scenarios

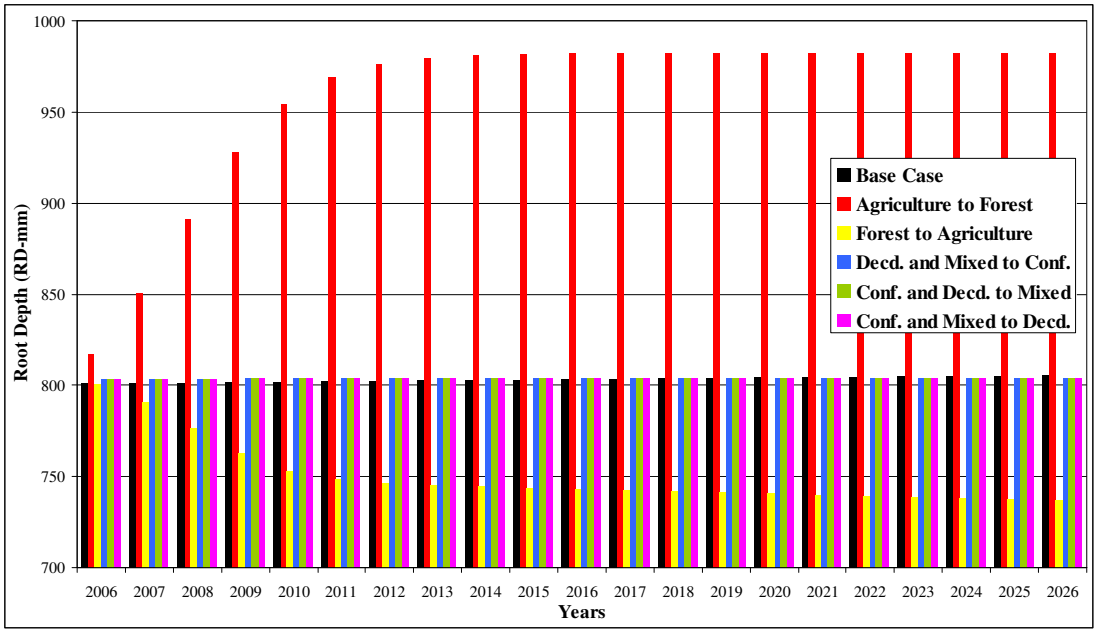

Figure 5.9. Average summer RD values for the base case and future scenarios

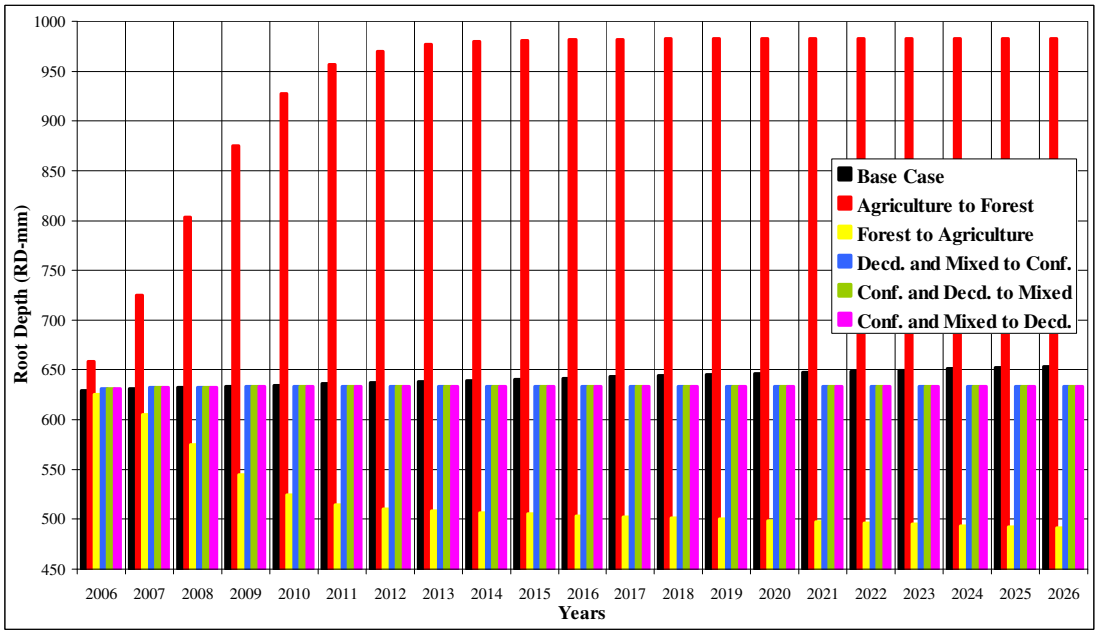

Figure 5.10. Average winter RD values for the base case and future scenarios

For this scenario (conversion of agricultural areas to forest), the decrease of the agricultural areas and the forest open spaces and the increment in the forest stand group areas leads to the gradual increment in both the summer and winter LAI (Leaf Area Index) and RD (Root Depth) parameter values.

5.3.2. Conversion of Forest to Agricultural Areas

For this scenario, the handicapped forest stand groups and forest open spaces were assumed to be converted to agricultural areas. As discussed in the Model Development chapter, the handicapped forest stand groups are the handicapped coniferous (Conf 0), deciduous (Decd 0) and mixed (Conf Decd 0) stand groups. They are referred to as handicapped stand groups because their canopy closure has dropped below 10%. Besides the handicapped forest stand groups, forest open spaces were also assumed to be converted to agricultural areas.

For the purpose of estimating the LAI and RD using the land use model, it was assumed that the handicapped forest stand groups and the forest open spaces were converted to agricultural areas with a gradually increasing fraction beginning with 0.1 in 2006 and reaching 1 in 2010. That is, almost all the handicapped forest stand groups and the forest open spaces were assumed to be converted to the agricultural areas by the end of 2010. All the other anthropogenic transformations were assumed to diminish gradually beginning in 2006 and ending by 2010.

As a result of the increment in the agricultural areas and the decrease in the forest stand group areas and forest open spaces, an initial gradual increase in the summer LAI and a slight gradual decrease in the winter LAI are predicted (Figures 5.7 and 5.8). On the other hand, the conversion of forest to agricultural areas leads to a decrease in both the summer and winter RD values (Figures 5.9 and 5.10).

5.3.3. Conversion of Deciduous and Mixed Stands to Coniferous Stands

The deciduous and mixed stand groups for this scenario were assumed to be converted to the coniferous stand groups. It was specifically assumed that the handicapped coniferous, deciduous and mixed stand group areas were replaced with young coniferous seedlings (Y Conf 12) with gradually increasing fraction beginning with 0.1 in 2006 and reaching 1 in 2010. Almost all the handicapped coniferous, deciduous and mixed stand group areas were assumed to be planted with the young coniferous seedlings by the end of

2010. All the other anthropogenic transformations were assumed to diminish gradually beginning in 2006 and ending by 2010.

The decrease in the deciduous and mixed stand groups and the increment in the coniferous stand groups leads to the slight gradual increase in both the summer and winter values of LAI (Figures 5.7 and 5.8). On the other hand, both the summer and winter RD values are practically constant over the entire 21-year period (Figures 5.9 and 5.10).

5.3.4. Conversion of Coniferous and Deciduous Stands to Mixed Stands

This future scenario is the reverse of the previous one whereby the coniferous and deciduous stand groups were assumed to be converted to the mixed stand groups. It was assumed that the handicapped coniferous, deciduous and mixed stand group areas were planted with the young mixed seedlings (Y Conf Y Decd 12) with gradually increasing fraction beginning with 0.1 in 2006 and reaching up to 1 in 2010. That is, almost all the handicapped coniferous, deciduous and mixed stand group areas were assumed to be planted with the young mixed seedlings by the end of 2010. All the other anthropogenic transformations were assumed to diminish gradually beginning in 2006 and ending by 2010.

The decrease in the coniferous and deciduous stand groups and the increase in the mixed stand groups leads to the gradual increase in both the summer and winter values of LAI (Figures 5.7 and 5.8). On the other hand, both the summer and winter RD values are almost constant along the 21-year period (Figures 5.9 and 5.10).

5.3.5. Conversion of Coniferous and Mixed Stands to Deciduous Stands

The fifth future scenario assumed that the coniferous and mixed stand groups were converted to the deciduous stand groups. The handicapped coniferous, deciduous and mixed stand group areas were assumed to be planted with the young deciduous seedlings (Y Decd 12) with gradually increasing fraction beginning with 0.1 in 2006 and reaching up to 1 in 2010. Almost all the handicapped coniferous, deciduous and mixed stand group areas were assumed to be planted with the young deciduous seedlings by the end of 2010.

All the other anthropogenic transformations were assumed diminished gradually beginning in 2006 and ending by 2010.

The decrease in the coniferous and mixed stand groups and the increment in the deciduous stand groups leads to the gradual increase in the summer LAI values and to the gradual decrease in winter values of LAI (Figures 5.7 and 5.8). The winter values of the deciduous stand groups are low since they peel their leaves in winter. On the other hand, both the summer and winter RD values are almost constant over the 21-year period (Figures 5.9 and 5.10).

5.4. Discussion of the Scenario Simulations

This section presents the results of the coupled land use-hydrodynamics model obtained for each of the future scenarios. The discussion primarily focuses on the two parameters of the water budget: river discharge and evapotranspiration. The predictions obtained with the future scenarios are compared against each other and the base case scenario presented in Section 5.2.

5.4.1. Overall Water Balance

The first set of results focus on the river discharge and evapotranspiration average over the entire simulation period. The average river discharge for the base case and five future scenarios are presented in Table 5.4. Figure 5.11 presents the annual river discharges and precipitation data over the simulation period. The fraction of the average stream flow and average evapotranspiration relative to mean precipitation are shown in Table 5.5. These fractions are also shown graphically in Figure 5.12.

Table 5.4. Average river discharge predicted for the base case and future scenarios

Simulation	**Discharge (m^3/s)**
Base Case	5.00
Agriculture to Forest	4.54
Forest to Agriculture	5.01
Deciduous and Mixed to Coniferous	4.92
Coniferous and Deciduous to Mixed	5.19
Coniferous and Mixed to Deciduous	4.87

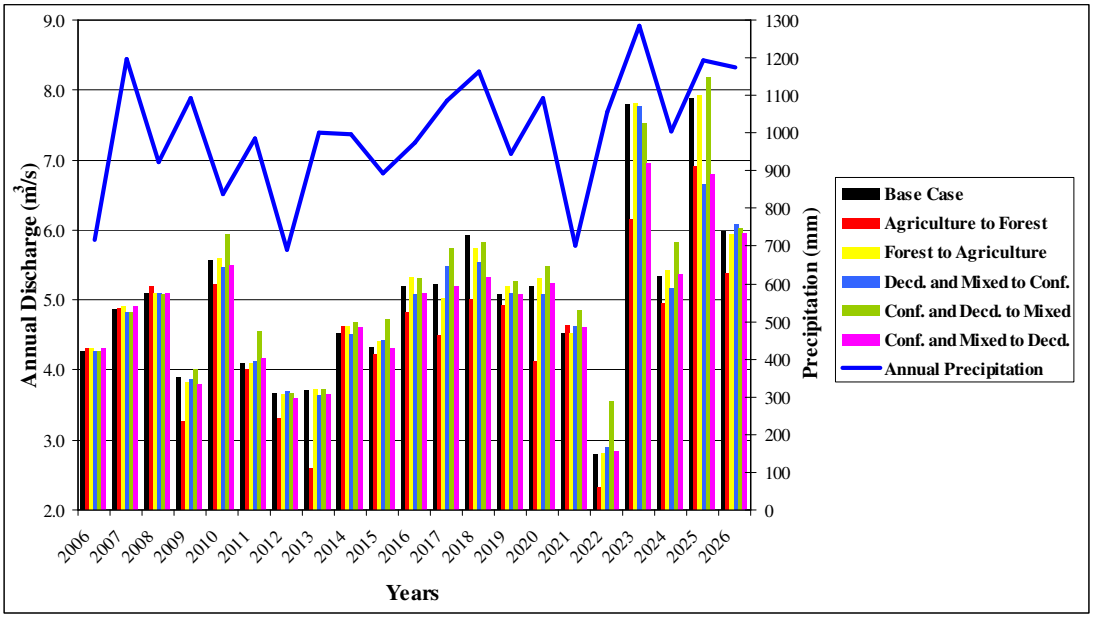

Figure 5.11. Annual river discharges and precipitations

Table 5.5. Stream flow and the evapotranspiration ratios of the future base and the five scenario simulations

Simulation	Evapotranspiration (%)	Stream Flow (%)
Base Case	67.2	32.8
Agriculture to Forest	70.8	29.2
Forest to Agriculture	67.2	32.8
Deciduous and Mixed to Coniferous	67.4	32.6
Coniferous and Deciduous to Mixed	66.2	33.8
Coniferous and Mixed to Deciduous	67.7	32.3

It is predicted that the conversion of the agricultural areas to young forest stand group areas would lead to the largest decrease in the discharge to 4.54 m^3/s. This scenario is also predicted to have the lowest annual discharges which exceed 71% (Figure 5.11). The scenario of coniferous and deciduous stands conversion to mixed stands is predicted to have the highest annual discharges over the 62% of the entire simulation period (Figure 5.11) with the highest average discharge of 5.19 m^3/s. The total evapotranspiration for this scenario is predicted to be almost 70.8% of the total precipitation while the river flow is predicted to be 29.2% of the total precipitation. As mentioned earlier, the difference in these values between the future base simulation and the agriculture to forest conversion scenario simulation are attributed to the predicted change in LAI and RD values (Figures 5.7, 5.8, 5.9 and 5.10).

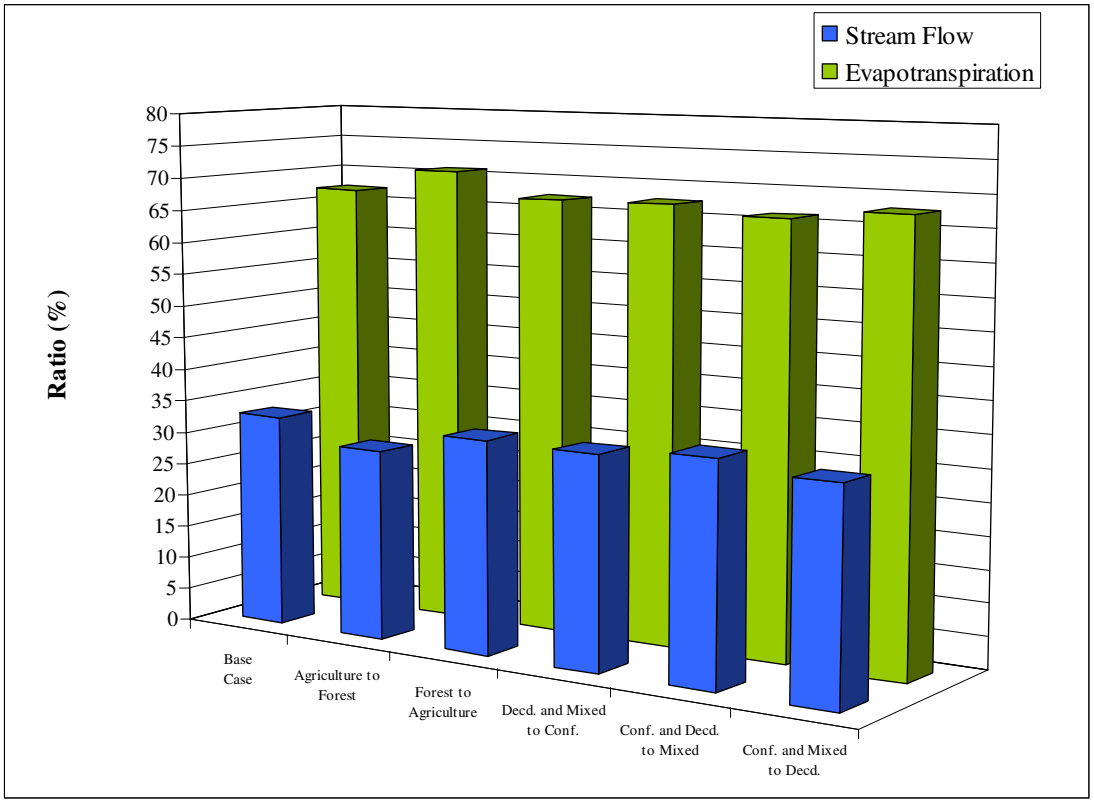

Figure 5.12. Water balance ratios of the future base and the five scenario simulations

Examination of the results for the other future scenarios shows that the predicted 21-year average discharge and evapotranspiration ratio would not significantly change when the forest stands are changed to agricultural areas. When the forest stands are shifted to coniferous only or deciduous only there would be a slight decrease in the river discharge and a corresponding increase in the evapotranspiration ratio, with a slightly lower discharge value and higher evapotranspiration ratio for the case of deciduous forest stands. The higher summer values of the LAI for these scenarios compared to the LAI values predicted for the base case are the primary factors for the decrease in the average discharge and increase in the evapotranspiration ratio.

On the other hand, the discharge is predicted to increase and the evapotranspiration ratio to decrease somewhat when the forest is converted to mixed stands. One of the reasons could be the balance between the summer and winter LAI values since higher LAI triggers the increase in transpiration but prevents the evaporation. Another reason could be the relatively constant RD values compared to the future base case simulation (Figures 5.9

and 5.10). These results are consistent with the computed LAI and RD time series discussed in the previous section (Figures 5.7, 5.8, 5.9 and 5.10).

5.4.2. Histogram and Extremes of Daily River Discharge

Figure 5.13 presents the histogram of the daily discharge ranges of the six scenario simulations over the 21-year period. The maximum and minimum daily discharges of these scenarios are shown in Figure 5.14.

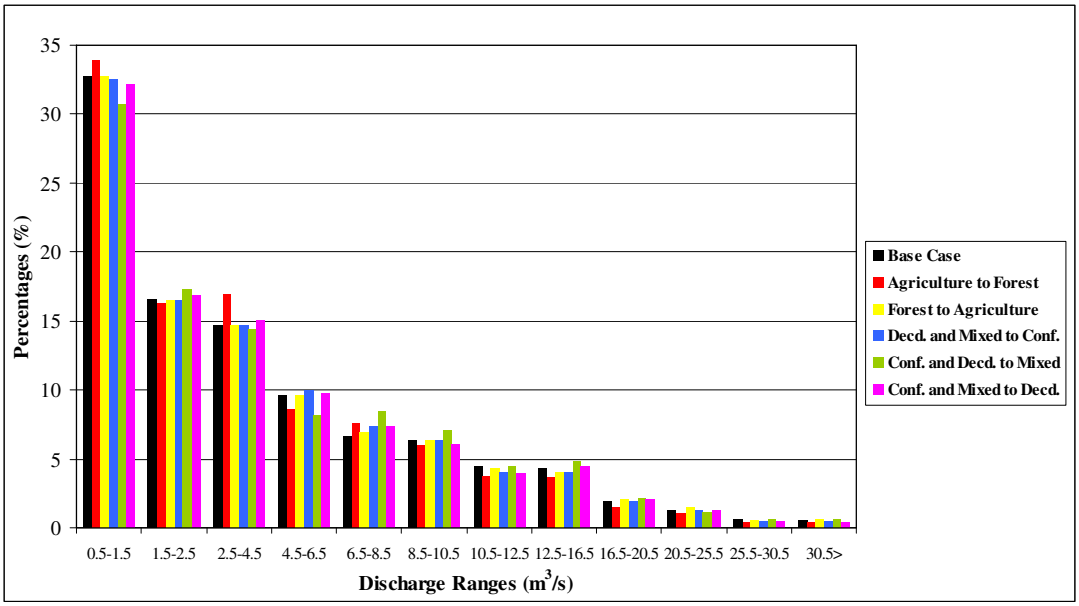

Figure 5.13. Histogram of daily discharge for the different scenarios

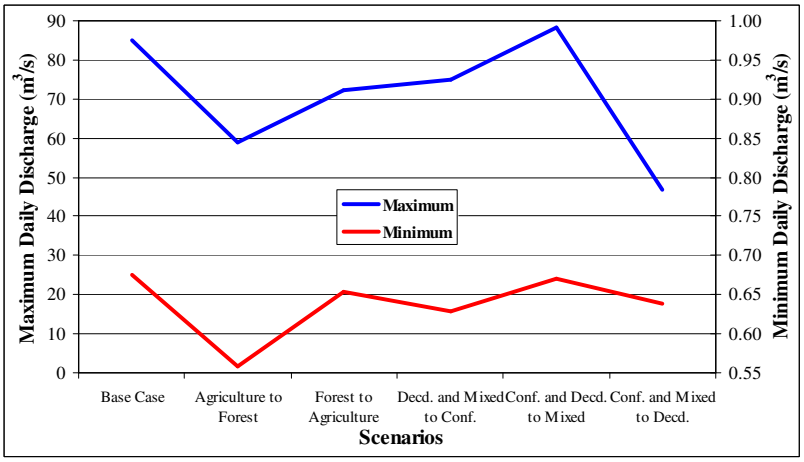

Figure 5.14. Maximum and minimum daily discharges for the different scenarios

Almost 1/3 of all the scenario simulations are predicted to have daily discharges between 0.5 m^3/s and 1.5 m^3/s. The agricultural areas conversion to forest scenario is predicted to have higher percentage of this range. Also, daily discharge values greater than 8.5 m^3/s are predicted to occur in lower percentages for this conversion scenario compared to the others. The maximum daily discharge for this scenario is predicted to be 58.8 m^3/s whereas the minimum daily discharge is predicted to be 0.56 m^3/s over the 21-year simulation period (Figure 5.14). These results are consistent with the predicted average annual discharge values which show the lowest value for this scenario (Table 5.4).

The scenario of coniferous and deciduous stands conversion to mixed stands is predicted to have the lowest percentage of daily discharges between 0.5 m^3/s and 1.5 m^3/s compared to the other scenarios. The daily discharge values greater than 6.5 m^3/s are predicted to occur in higher percentages for this conversion scenario compared to the others. The maximum daily discharge for this scenario is predicted to be 88.3 m^3/s which is the highest of all the six scenarios (Figure 5.14). These high daily values are consistent with the average annual discharge value which is predicted to be the highest for this scenario (Table 5.4). As a result the potential for flooding is highest for this scenario. On the other hand, the minimum daily discharge for this scenario is predicted to be 0.67 m^3/s (Figure 5.14).

Although the coniferous and mixed stands conversion to deciduous stands scenario is predicted to yield an average annual discharge that is close to the base case and the forest to agricultural areas and deciduous and mixed to coniferous, the maximum daily discharge is predicted to be quite lower than the other cases. The maximum daily discharge over the 21-year period is predicted for this case to be 46.9 m^3/s, while the maximum daily discharges for the base case, forest to agricultural areas and deciduous and mixed to coniferous conversion scenarios are predicted to be 85.1 m^3/s, 72.3 m^3/s and 74.9 m^3/s respectively.

The base case, forest to agricultural areas conversion and deciduous and mixed to coniferous conversion scenarios are predicted to have histograms of the daily discharges that are close to each other. The scenario of forest conversion to agricultural areas is predicted to lead less water yield compared to the scenario of coniferous and deciduous

stands conversion to mixed stands. The evaporation part of the evapotranspiration for the agricultural areas would possibly be higher than for the mixed forest stands leading to higher water loss and lower discharge.

5.4.3. Monthly Variations in Water Balance

Differences in the monthly average values of the discharge and evapotranspiration ratio for the different scenarios are discussed in this section. Figure 5.15 presents the monthly average of the river discharge together with their maximum and minimum ranges for the six scenarios. For comparison, the annual average and annual maximum/minimum values are also shown. Figure 5.16 presents the corresponding average monthly evapotranspiration ratios as percentages of the mean monthly precipitation together with their maximum and minimum ranges.

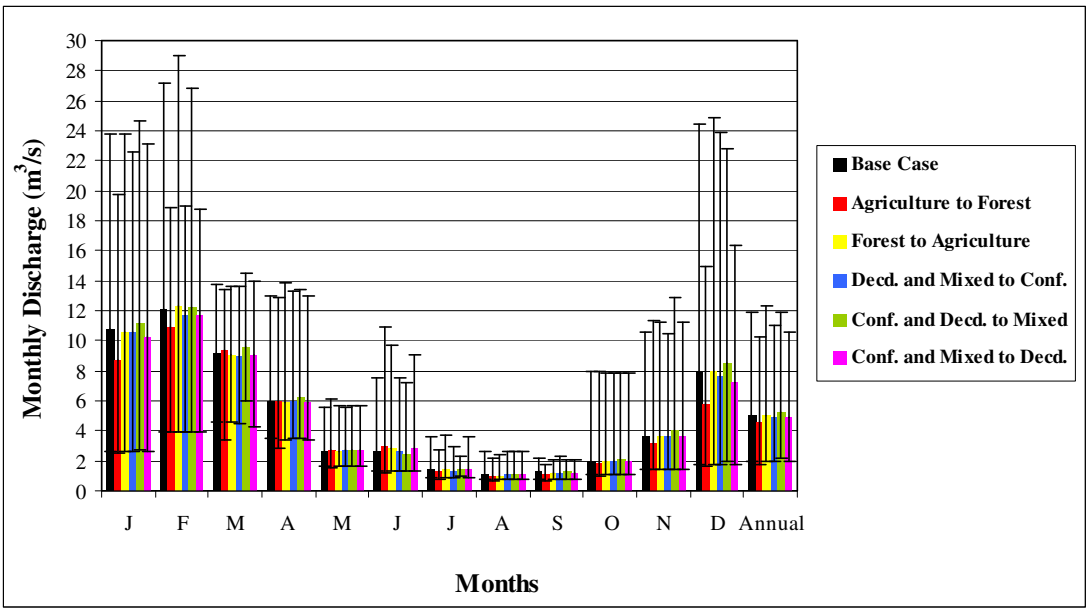

Figure 5.15. Simulated monthly average of the river discharge along with the maximum and minimum ranges for the six scenarios

For all six scenarios, the monthly average discharges are predicted to be highest in February and lowest in August. However, the monthly evapotranspiration ratio is predicted to be highest in late spring (May and June) and lowest in winter (December and January). Except the four months; February, May, June and July, the coniferous and deciduous

stands conversion to mixed stands scenario is predicted to have the highest monthly average discharges. The scenario of agricultural areas conversion to forest is predicted to have the highest average monthly evapotranspiration ratios except for the month of April. The scenario of coniferous and deciduous stands conversion to mixed stands is predicted to have the lowest average monthly evapotranspiration ratios.

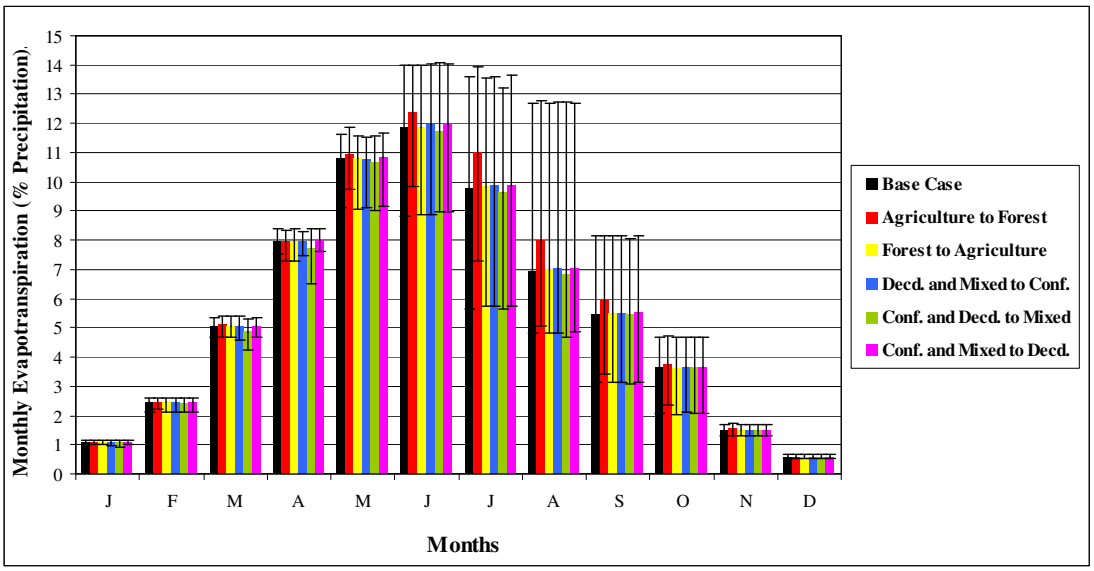

Figure 5.16. Simulated average monthly evapotranspiration ratios for six scenarios

Figure 5.17 shows the standard deviation of monthly average of the river discharge normalized by the respective monthly averages for the six scenario simulations together with the mean monthly precipitation. Figure 5.18 presents the standard deviation of monthly average of the evapotranspiration ratio (as a fraction of mean monthly precipitation) along with the mean monthly temperature. The mean annual values are also shown in these two figures for comparison. A large standard deviation for a particular scenario is indicative that that scenario is associated with more variability from one year to the other.

The standard deviation of the monthly average discharge is predicted to be higher for June, October, November and December compared to the other months. The mean monthly precipitations are also higher for these months compared to the others. The high standard deviations for the summer months are due the low average monthly values which are used

in the normalization. The standard deviation of the monthly average discharge is predicted to be lowest for March.

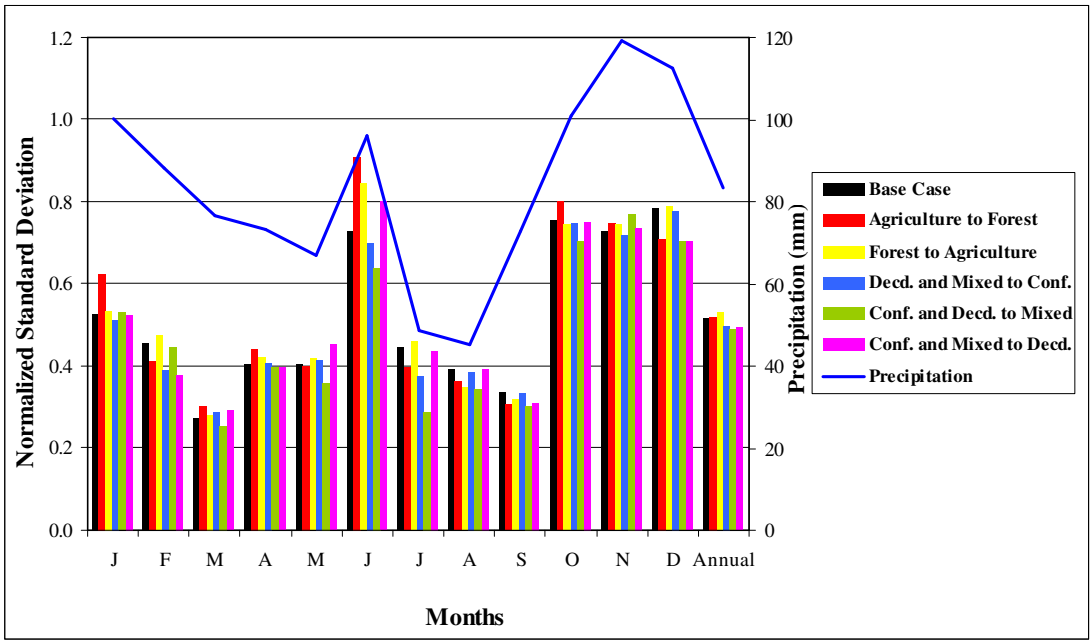

Figure 5.17. Standard deviation of monthly average of the river discharge for six scenarios along with the mean monthly precipitation

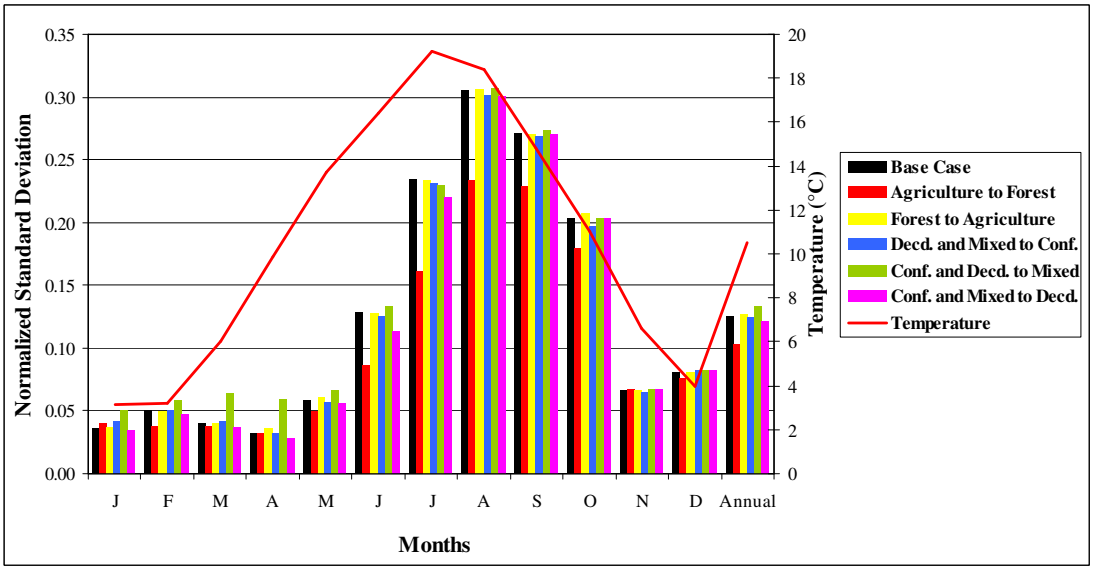

Figure 5.18. Standard deviation of monthly average of the evapotranspiration ratios for the six scenarios together with the mean monthly temperature

The monthly standard deviation of the evapotranspiration ratios is predicted to be highest for the summer months June, July, and August, and for September and October. This situation arises from the increment of both the mean temperature and the land use parameters; LAI and RD along these summer months. The monthly standard deviation of the mean evapotranspiration ratio is predicted to be lowest for April except for the scenario of coniferous and deciduous stands conversion to the mixed stands.

The scenario of forest conversion to agricultural areas is predicted to have the highest average annual standard deviation. This is followed by the scenario of agricultural areas to forest. On the other hand, the scenario of coniferous and deciduous stands conversion to mixed stands is predicted to have the lowest average annual standard deviation of the evapotranspiration ratios.

The scenario of coniferous and deciduous stands conversion to mixed stands is predicted to have the highest average annual evapotranspiration ratios. This is followed by the scenario of forest conversion to agricultural areas. The scenario of agricultural areas conversion to forest is predicted to have the lowest average annual standard deviation of the evapotranspiration ratios.

5.4.4. Low Discharges

As discussed in the Section 5.2 (Base Case Analysis), the daily discharge below 1.0 m^3/s which corresponds to 6.6 % of the annual precipitation was assumed to be the indicator of “low discharge”. The percentage of summer months within the 21-year simulated period with low discharge are shown in Figure 5.19.

The scenario of agricultural areas conversion to forest is predicted to have the highest percent of low discharge months, with almost 52% of all the dry summer months. The low discharge is predicted for almost 81% of all the August months and for 43% of all the September months and for 33% of all the July months.

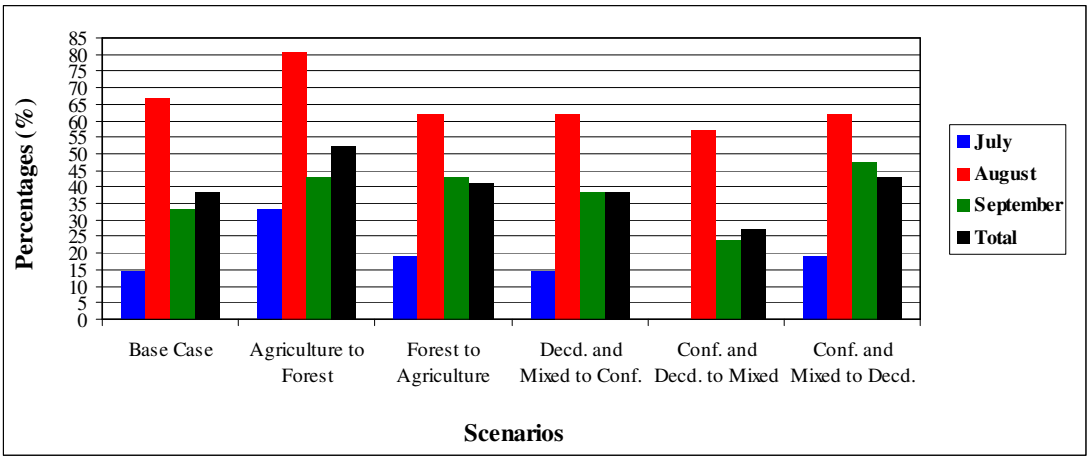

Figure 5.19. Percentage of summer months with low discharge

The scenario of coniferous and deciduous stands conversion to mixed stands is predicted to have the lowest percent of low discharge months, with almost 27% of all the dry summer months. The low discharge is predicted to be valid for only 57% of all the August months and for only 24 % of all the September months. Low discharge is not predicted for any of the July months.

The other scenarios susceptible to low river discharges in the summer months are predicted to be coniferous and mixed stands conversion to deciduous stands scenario, forest to agricultural areas scenario, deciduous and mixed stands conversion to coniferous stands scenario and base case scenario respectively. The percent of summer months with low discharges are predicted to be 43%, 41%, 38% and 38% for these four scenarios respectively.

Among the five scenario simulations discussed, the plantation of the handicapped coniferous, deciduous and mixed stand group areas with the young mixed seedlings seems to be more satisfactory from the point of the river discharge and consequently the water yield. The average daily discharge is predicted to be relatively high and the average evapotranspiration ratio is predicted to be relatively low. The summer periods that are predicted to experience low river discharge are less compared to the other scenario simulations and the future base simulation.

In summary, the conversion of the agricultural and forest open spaces to the forest scenario is predicted to lead to the lowest river discharge and consequently the water yield. The average daily discharge is predicted to be relatively low and the average evapotranspiration ratio is predicted to be relatively high. The summer periods that are predicted to suffer low river discharge are predicted to be highest for this scenario compared to all the other scenarios. However, flooding is less likely to occur with this scenario.

5.5. Long-term Variations in Water Budget

To assess the long term variations in water budget of the Bartın watershed associated with climate change, the base case simulation was extended to cover a total of 55 years from 2006 to 2060. As discussed in Section 5.1, the climatic data were generated using the RegCM3 model based on the A2 greenhouse gas emission scenario proposed by the International Panel on Climate Change (I.P.C.C.) (Bates et al., 2008). The summer and winter values of the LAI and RD of the watershed up to year 2060 were first computed using the land use dynamics model assuming land use change practices would continue as in the years from 1986 to 2006. The LAI and RD time series were then incorporated, along with the generated climatic data, into the hydrodynamics model to simulate the hydrological budget of the watershed.

The generated annual summer and winter land use parameter values, LAI and RD for the period between 2027 and 2060 were presented in Tables 5.6 and 5.7. The average summer and winter values of LAI and RD parameters for the entire watershed between 2006 and 2060 are also presented in Figures 5.20 and 5.21 respectively. Except the summer LAI values of the subwatershed 4, the summer and winter LAI values of the three subwatersheds are generally increasing over the 34-year period since the agricultural areas are decreasing while the forest areas are increasing. On the other hand, the decrease of the summer RD values in subwatershed 4 is due to the increment in the forest open spaces. The decrease in the agricultural areas and increment in the forest areas and forest open spaces are due to the assumed continued land abandonment at the same rate that occurred between 1986 and 2006.

Table 5.6. The annual summer and winter values of LAI parameters for years 2027 to 2060

	LAI-Summer				LAI-Winter			
	Subwatersheds				Subwatersheds			
Year	**1**	**2**	**3**	**4**	**1**	**2**	**3**	**4**
2027	1.48	1.64	1.44	1.35	0.27	0.24	0.48	0.34
2028	1.48	1.64	1.44	1.35	0.27	0.24	0.48	0.34
2029	1.48	1.64	1.44	1.35	0.27	0.24	0.49	0.34
2030	1.49	1.65	1.44	1.35	0.28	0.24	0.49	0.34
2031	1.49	1.65	1.44	1.35	0.28	0.24	0.49	0.34
2032	1.49	1.65	1.44	1.35	0.28	0.24	0.49	0.34
2033	1.49	1.65	1.44	1.35	0.28	0.24	0.49	0.34
2034	1.49	1.65	1.44	1.35	0.29	0.24	0.49	0.34
2035	1.49	1.65	1.45	1.35	0.29	0.24	0.49	0.34
2036	1.50	1.65	1.45	1.35	0.29	0.24	0.49	0.34
2037	1.50	1.66	1.45	1.35	0.29	0.24	0.49	0.34
2038	1.50	1.66	1.45	1.35	0.30	0.24	0.50	0.34
2039	1.50	1.66	1.45	1.35	0.30	0.24	0.50	0.34
2040	1.50	1.66	1.45	1.35	0.30	0.24	0.50	0.35
2041	1.50	1.66	1.45	1.35	0.30	0.24	0.50	0.35
2042	1.50	1.66	1.45	1.35	0.31	0.24	0.50	0.35
2043	1.51	1.66	1.45	1.35	0.31	0.24	0.50	0.35
2044	1.51	1.66	1.45	1.35	0.31	0.24	0.50	0.35
2045	1.51	1.67	1.45	1.34	0.31	0.24	0.50	0.35
2046	1.51	1.67	1.45	1.34	0.31	0.25	0.50	0.35
2047	1.51	1.67	1.45	1.34	0.32	0.25	0.50	0.35
2048	1.51	1.67	1.46	1.34	0.32	0.25	0.51	0.35
2049	1.51	1.67	1.46	1.34	0.32	0.25	0.51	0.35
2050	1.51	1.67	1.46	1.34	0.32	0.25	0.51	0.35
2051	1.52	1.67	1.46	1.34	0.32	0.25	0.51	0.35
2052	1.52	1.67	1.46	1.34	0.33	0.25	0.51	0.35
2053	1.52	1.67	1.46	1.33	0.33	0.25	0.51	0.35
2054	1.52	1.67	1.46	1.33	0.33	0.25	0.51	0.35
2055	1.52	1.68	1.46	1.33	0.33	0.25	0.51	0.35
2056	1.52	1.68	1.46	1.33	0.33	0.25	0.51	0.35
2057	1.52	1.68	1.46	1.33	0.34	0.25	0.51	0.35
2058	1.52	1.68	1.46	1.33	0.34	0.25	0.51	0.35
2059	1.52	1.68	1.46	1.33	0.34	0.25	0.51	0.35
2060	1.52	1.68	1.46	1.32	0.34	0.25	0.52	0.35

Table 5.7. The annual summer and winter values of RD parameters for years 2027 to 2060

	RD-Summer (mm)				RD-Winter (mm)			
	Subwatersheds				Subwatersheds			
Year	**1**	**2**	**3**	**4**	**1**	**2**	**3**	**4**
2027	820	842	810	779	675	697	660	615
2028	822	843	810	779	678	699	661	615
2029	823	844	810	779	682	700	662	616
2030	824	845	810	778	685	702	662	616
2031	826	845	810	778	688	703	663	616
2032	827	846	810	777	691	704	664	617
2033	829	847	810	777	694	706	664	617
2034	830	848	810	776	697	707	665	618
2035	831	848	810	776	700	708	666	618
2036	833	849	810	776	703	710	667	618
2037	834	850	810	775	705	711	667	619
2038	835	850	810	775	708	713	668	619
2039	836	851	810	774	711	714	669	619
2040	838	852	811	774	714	715	669	620
2041	839	853	811	774	717	716	670	620
2042	840	853	811	773	719	718	671	620
2043	841	854	811	773	722	719	671	621
2044	843	855	811	772	725	720	672	621
2045	844	855	811	772	727	722	673	621
2046	845	856	811	772	730	723	673	622
2047	846	857	811	771	732	724	674	622
2048	847	857	811	771	735	726	675	622
2049	848	858	811	770	737	727	675	623
2050	849	859	811	770	740	728	676	623
2051	851	859	811	770	742	729	677	623
2052	852	860	811	769	744	731	677	624
2053	853	861	811	769	747	732	678	624
2054	854	861	811	769	749	733	679	624
2055	855	862	811	768	751	734	679	625
2056	856	863	811	768	754	736	680	625
2057	857	863	811	767	756	737	681	625
2058	858	864	811	767	758	738	681	625
2059	859	865	811	767	760	739	682	626
2060	860	865	811	766	763	740	683	626

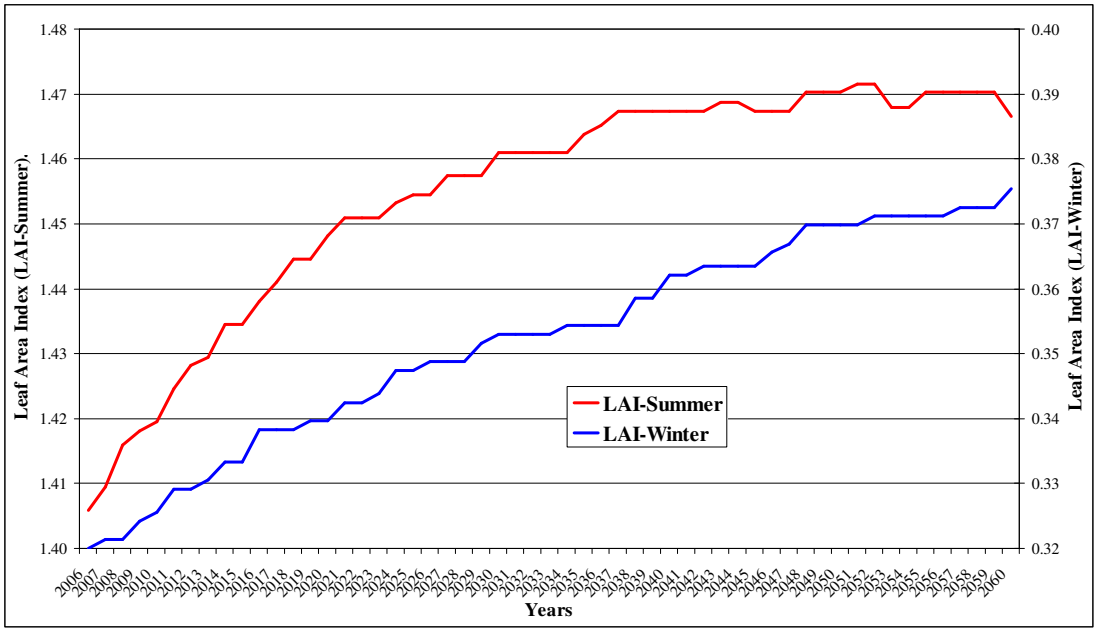

Figure 5.20. Average summer and winter LAI values for years 2006 to 2060

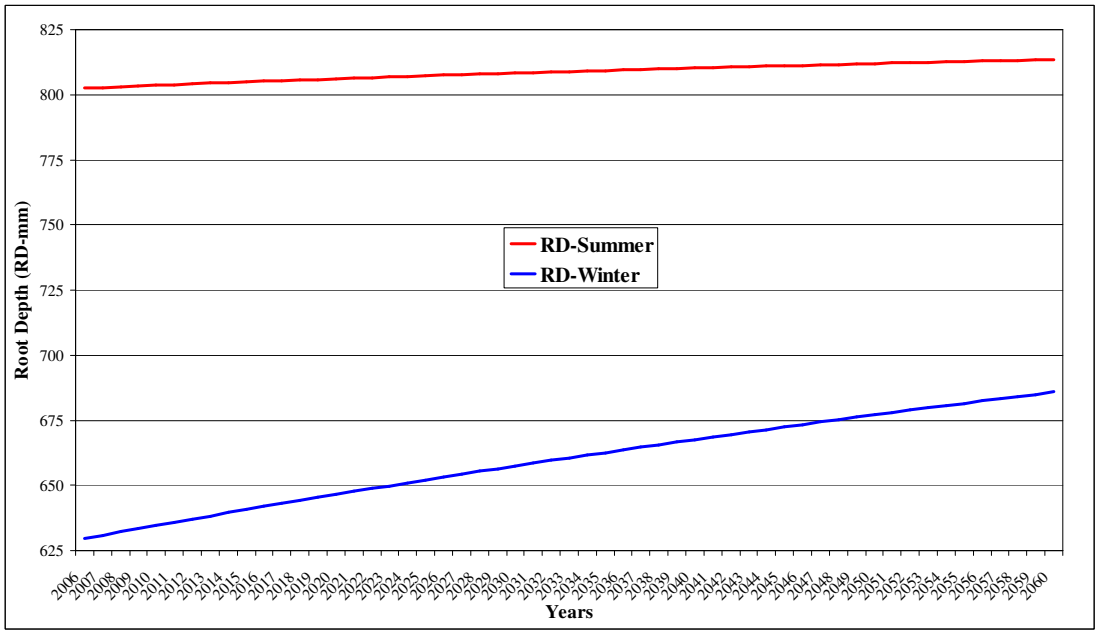

Figure 5.21. Average summer and winter RD values for years 2006 to 2060

The average summer LAI parameter values are predicted to increase slightly while the average summer RD parameter values are predicted to remain almost constant. The values of the subwatershed 4 balance the average of the entire watershed values. On the other

hand, an apparent increase in the winter RD values and a slight increase in the winter LAI values are predicted.

The generated mean annual precipitation is predicted to be 1054 mm for the 34-year period between 2027 and 2060. For this period, the maximum and minimum annual precipitation is 1443 mm and 631 mm. The generated mean annual temperature is 11.3°C. As mentioned in Section 5.2, the generated mean annual precipitation is predicted to be 1001 mm for the 21-year period between 2006 and 2026 with the maximum and minimum annual precipitation of 1287 mm and 692 mm. The generated mean annual temperature is 10.5°C for this period.

Based on the computed LAI and RD values the water budget for the watershed was simulated using the hydrodynamics model. The monthly water balance for the 34 years beyond the base case scenario (i.e., for years 2027 to 2060) is presented in Figure 5.22. The annual water balance for the 55 years between 2006 and 2060 is shown in Figure 5.23.

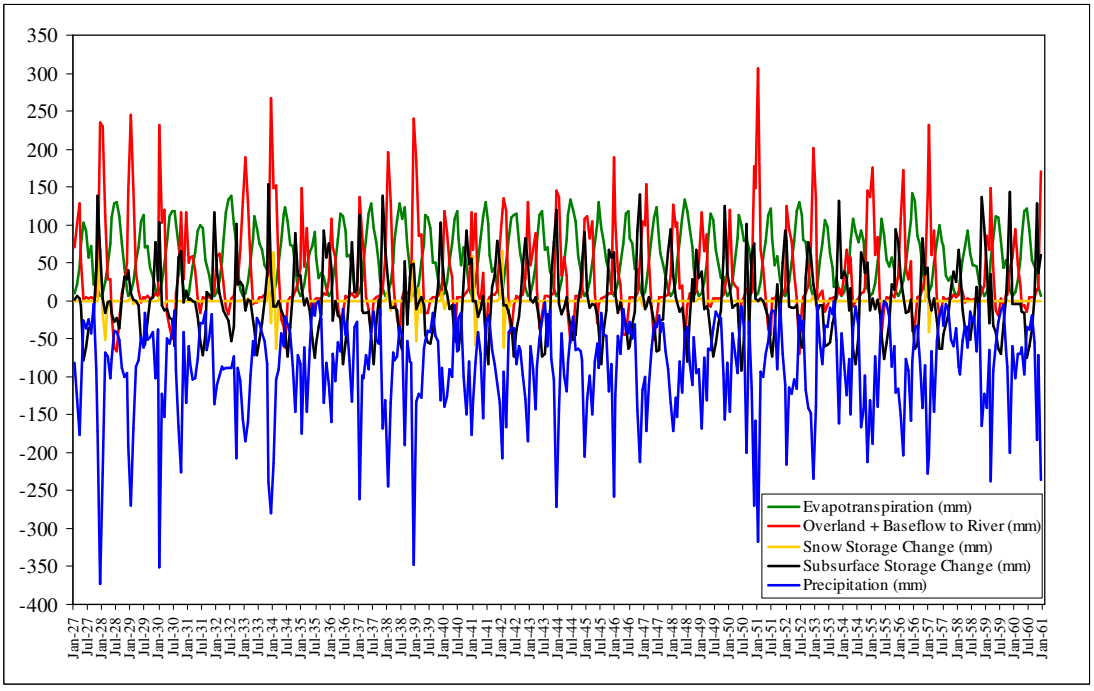

Figure 5.22. Simulated monthly water balance for years 2027 to 2060

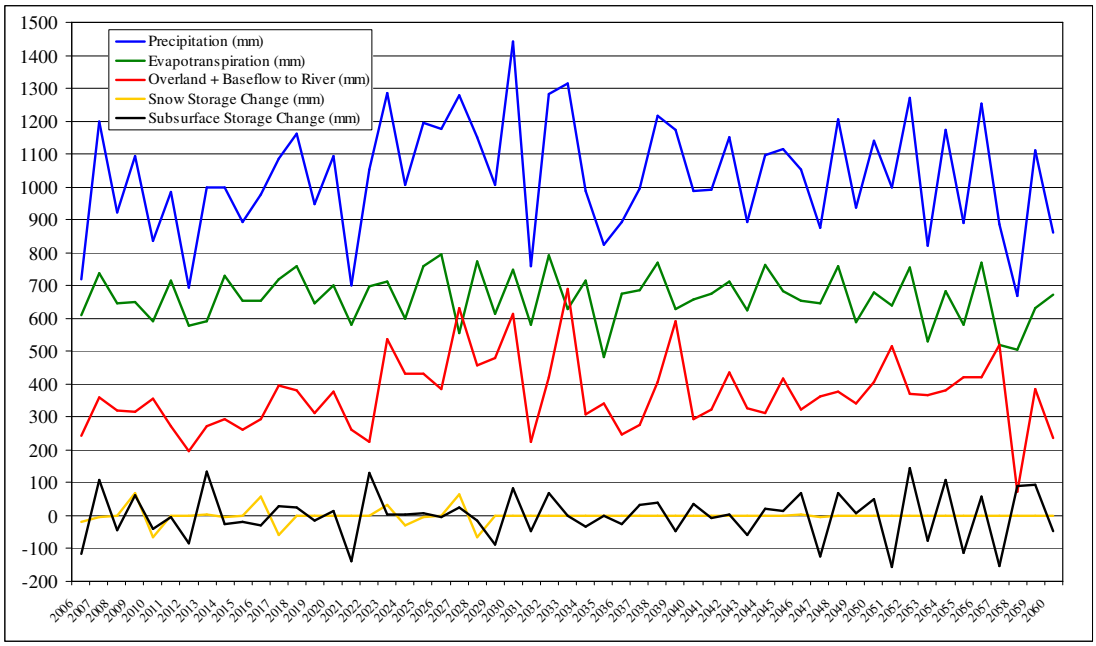

Figure 5.23. Simulated annual water balance for years 2006 to 2060

The results indicate that the average annual evapotranspiration is predicted to be almost 62.5% of the total precipitation while the average annual river flow is predicted to be 37.5% of the total precipitation. For the base case simulation covering the years 2006 to 2026, the fraction of evapotranspiration and river flow are predicted to be 67% and 33%, respectively. Although the land use parameters; the LAI and RD increased in three subwatersheds over the 34 years, the increase in the river flow and decrease in the evapotranspiration is attributed to the increment of the mean annual precipitation. The decrease in the summer values of the LAI and RD may have also contributed to this situation.

For the annual balance of 55 years, the annual river flow and annual evapotranspiration values are predicted to approach each other for some years after 2023. The standard deviation for the annual river flow for the 34-year period between 2027 and 2060 is about 1.5 times higher than that of the 21-year period between 2006 and 2026. The standard deviation for the annual evapotranspiration between 2027 and 2060 is about 1.3 times higher than that of 2006 and 2026. The increase in the standard deviation indicates the increasing irregularity in the water balance. Less snow storage changes are predicted to occur after 2030 due to the increasing temperature (Figure 5.1).

The volumetric moisture content change between 2027 and 2060 in the unsaturated zone at the downstream discharge point of the watershed is shown in Figure 5.24. The change is predicted to occur only within the 3 meters depth from soil surface since the point is at almost the lowest altitude. However, the summer moisture content of the topsoil is predicted to drop down to 5%. The soil moisture content almost does not drop below 15% below the depth of 1 meter. The maximum (saturated) soil moisture content is the maximum porosity of that soil which alters between 45% and 52% within the watershed. The situation is almost the same as the base case between 2005 and 2026.

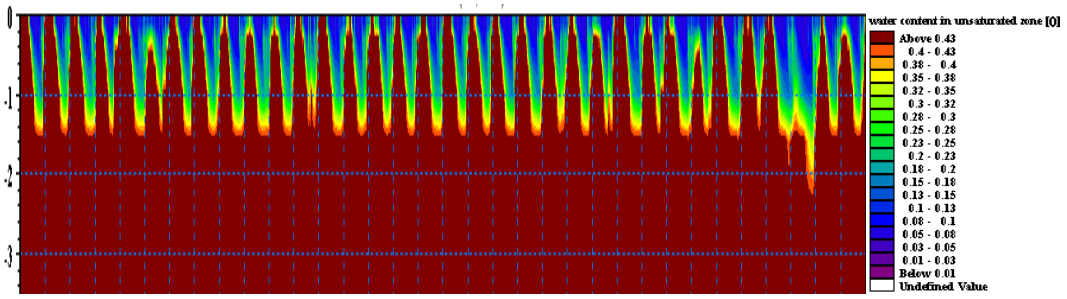

Figure 5.24. The water content change in the unsaturated zone between 2027 and 2060

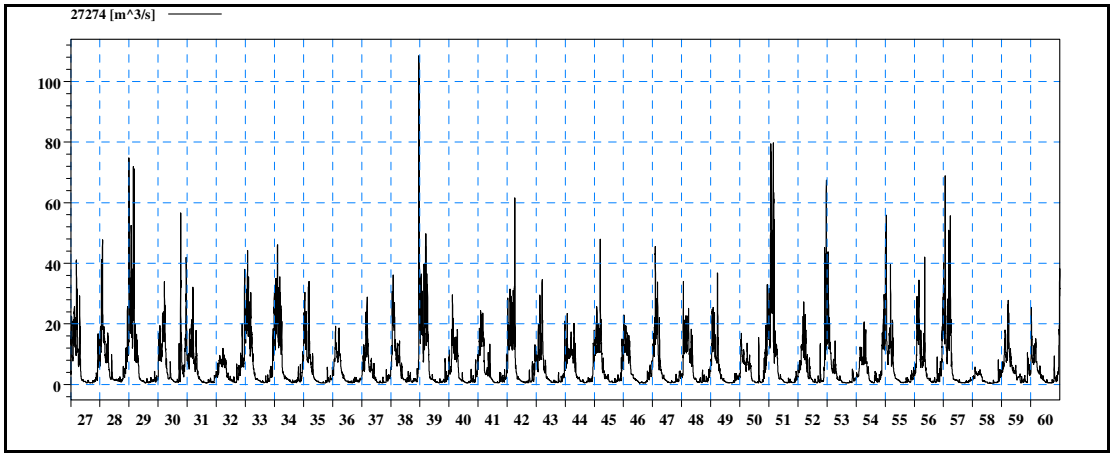

Figure 5.25. Daily discharge of the stream between 2027 and 2060

The daily discharge at the downstream end of the stream is presented in Figure 5.25. The average daily discharge is predicted to be almost 5.74 m^3/s for the period between 2027 and 2060. According to the simulation of the discharge for the ultimate cross section of the stream, the average daily discharge is 5.59 m^3/s for the period between 1986 and 2006 and 5.00 m^3/s for the period between 2006 and 2026. This situation indicates that the

stream flow is predicted to decrease in the coming 21 years and increase in the following 34 years.

Figure 5.26 shows the annual discharge values for the 55 years between 2006 and 2060. The annual discharges are predicted to fluctuate more after 2020. In other words, high and low values of discharges are predicted to occur in the years following 2020.

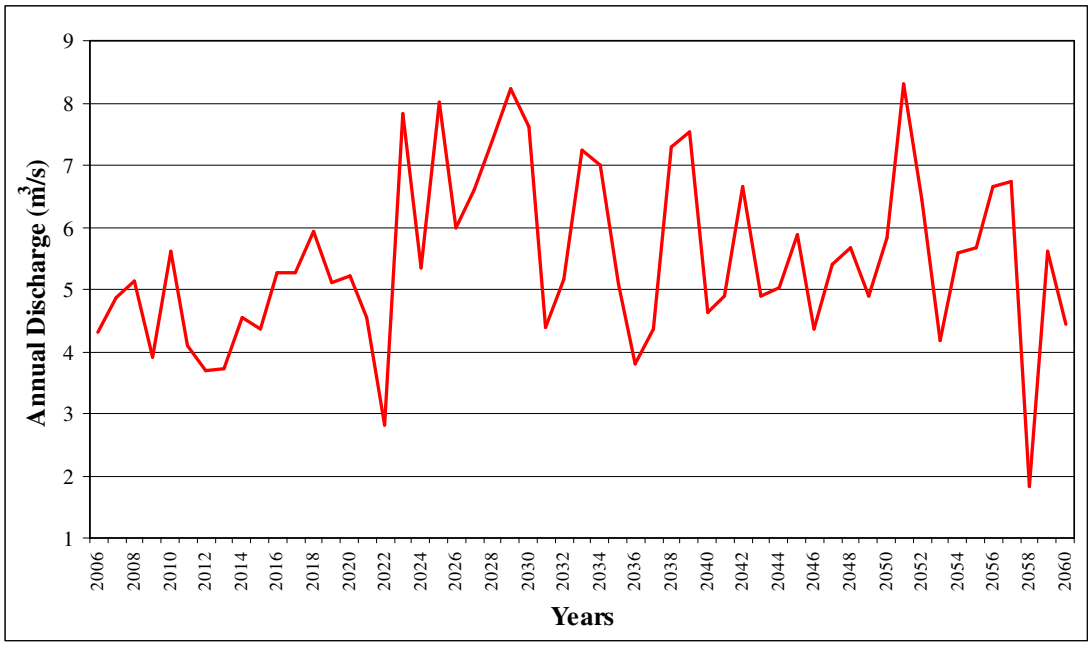

Figure 5.26. Annual discharge values between 2006 and 2060

Over the 34 years between 2027 and 2060, the maximum and minimum annual discharges are predicted to be 8.31 m^3/s and 1.84 m^3/s respectively. The maximum and minimum daily discharges are predicted to be 109.58 m^3/s and 0.35 m^3/s respectively. The highest daily discharge is predicted to occur in February with monthly average of 15.08 m^3/s. The lowest daily discharge is predicted to occur in August with monthly average of 0.89 m^3/s. These long-term extreme annual and daily discharges together with the extreme annual and daily discharges and standard deviation of the base-case simulation between 2006 and 2026 are displayed in Table 5.8.

Table 5.8. Extreme annual and daily discharges for the base case and long-term simulations

	Base Case (2006-2026)	**Long-term (2027-2060)**
Mean Annual Precipitation (mm)	1001	1054
Mean Annual Temperature (°C)	10.5	11.3
Average Daily Discharge (m^3/s)	5.00	5.74
Maximum Annual Discharge (m^3/s)	7.89	8.31
Minimum Annual Discharge (m^3/s)	2.80	1.84
Annual Standard Deviation (m^3/s)	1.23	1.41
Maximum Daily Discharge (m^3/s)	85.12	109.58
Minimum Daily Discharge (m^3/s)	0.68	0.35
Daily Standard Deviation (m^3/s)	5.92	7.61

The long-term simulation is predicted to have higher maximum annual discharge and lower minimum annual discharge than the base case simulation. Moreover, higher maximum daily discharge and lower minimum daily discharge is predicted for the long-term simulation. The higher annual and daily standard deviation values indicate the irregularity in the discharges for the long-term simulation.

It was assumed that a daily river discharge below 1.0 m^3/s indicated the low discharge. The low river discharge is predicted mostly in the month of August followed by July and September. Over the 34-year period between 2027 and 2060, 72.5% of the summer months (July, August and September) are predicted to have low discharge. October, June and November in order are the other months which are predicted to suffer low discharges. It was also assumed that the daily river discharge above 20 m^3/s indicated the high discharge. Figure 5.27 presents the percentages of the days within the year which are predicted to experience low and high discharge.

The percentages of the low and high daily discharges are predicted to increase particularly for the period between 2030 and 2060. Along this period, the high/low extremes are more likely to occur compared to the previous years.

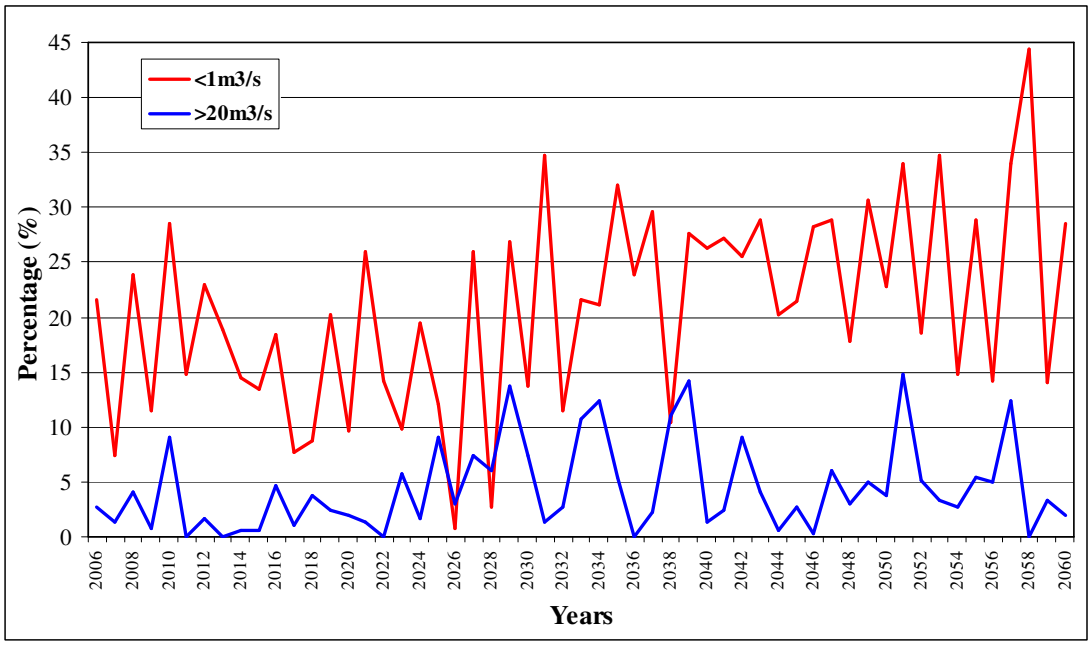

Figure 5.27. Percentage of the low and high daily discharges between 2006 and 2060

5.6. Summary

For the 21-year period between 2006 and 2026, six simulations with the land use model generated the summer and winter values of the two significant parameters; LAI and RD for the hydrodynamics model. The average summer LAI values of the agriculture to forest, deciduous and mixed to coniferous, coniferous and deciduous to mixed and coniferous and mixed to deciduous conversion scenarios increase (Figure 5.7). For the base case and the forest to agriculture conversion scenarios, the summer LAI values initially increase and then decrease (Figure 5.7). The average winter LAI values of the base case, agriculture to forest, deciduous and mixed to coniferous and coniferous and deciduous to mixed conversion scenarios increase (Figure 5.8). For the forest to agriculture and coniferous and mixed to deciduous conversion scenarios, the winter LAI values initially decrease (Figure 5.8). The average summer and winter RD values increase for the agriculture to forest conversion scenario and decrease for the forest to agriculture conversion scenario (Figures 5.9 and 5.10). The average summer and winter RD values of the base case scenario, deciduous and mixed to coniferous, coniferous and deciduous to mixed and coniferous and mixed to deciduous conversion scenarios almost remain constant (Figures 5.9 and 5.10). The increasing trend of the winter LAI and RD values for the base

case scenario continues for the prolonged 34-year period. However, the summer LAI and RD values tend to stabilize in future.

For the six scenario simulations of the 21-year period, the average discharge is predicted to range between 4.54 m^3/s and 5.19 m^3/s where the lowest is for the agriculture to forest conversion scenario and the highest is for the coniferous and deciduous conversion to mixed scenario. The evapotranspiration ratio is predicted to range between 66.2% and 70.8% where the lowest is for the coniferous and deciduous conversion to mixed scenario and the highest is for the agriculture to forest conversion scenario. When the agricultural areas are converted to the forest, the area of the forest and consequently the average summer and winter LAI and RD values highly increase leading to low average discharge and high evapotranspiration. The conversion of the coniferous and deciduous stands to mixed stands results initial increase in the summer and winter LAI values and constant summer and winter RD values. Then a balance forms between these summer and winter values balancing the evaporation and transpiration processes.

The maximum daily discharge with 88.3 m^3/s for the coniferous and deciduous stands conversion to mixed stand scenario and minimum daily discharge with 0.56 m^3/s for the agriculture to forest conversion are predicted. The monthly average discharges are predicted to be highest in February and lowest in August for all the six scenarios. However, the monthly evapotranspiration ratio is predicted to be highest in late spring (May and June) and lowest in winter (December and January). The scenario of agriculture conversion to forest is the most disadvantageous from the point of the low discharge. The low discharge which is assumed to be below 1 m^3/s is predicted for almost 52% of the dry summer months (August, September and July). On the other hand, low is charge is predicted only for the 27% of the dry summer months.

The mean annual precipitation and temperature, average daily discharge, are predicted to increase for the long-term simulation over the 34-year period compared to the base case simulation over the 21-year period. The higher standard deviation in the annual and daily discharges for the long term indicates the high possibility of the discharge irregularity.

6. CONCLUSIONS AND RECOMMENDATIONS

The mesoscale Bartın spring watershed is draining into a spring water reservoir which is supplying the water demand of the city centers of Bartın, Amasra and İnkumu. An integrated land use-hydrodynamics model was developed to estimate the actual water budget and to simulate the future possible water yield capacity of the watershed. The future simulations consider the effect of different land use scenarios and the effect of long term global climatic change on the water balance of the watershed.

Few published hydrological studies have investigated the impact of land use on the water resources considering both the spatial and the temporal dynamics. Most of these studies typically define empirical aggregated values of the LAI and RD without simulating land use change processes and temporal dynamics. The main novelty of this study is that it couples a land use model that simulates the natural and anthropogenic transformations between the land uses to a spatially distributed hydrodynamics model.

A series of simulations were first conducted to validate the integrated land use-hydrodynamics model and to assess its sensitivity to key parameters. The validity of the land use dynamics model is evaluated by applying structure-oriented behavior tests, namely: extreme condition, behavior sensitivity and phase relationship tests. The natural dynamics of the coniferous stand groups was subjected to the extreme condition of “no regrowth of the coniferous seedlings”. This resulted in a continuing increase in the handicapped stands and decline in the other stands. The sensitivity of the coniferous natural dynamics to the model parameters; maturation time, degradation time and regeneration time was tested by sensitivity tests. The dynamics of the coniferous stands is highly sensitive to these parameters. Also an inverse phase relationship between the handicapped coniferous stand and the dense mature coniferous stand (M Conf 3) is observed. These three structure-oriented behavior tests indicate that the land use dynamics model represents the time lags in transition between different forest stand groups. The model was calibrated for anthropogenic conversions between agricultural areas, forest areas, forest open spaces and settlements for the years from 1986 to 2006.

The land use model generates two key land use parameters; Leaf Area Index (LAI) and Root Depth (RD) that are fed into the hydrodynamics model. The LAI for different stand groups was measured in the field while the RD was treated as a calibration parameter. The estimated mean LAI value of the forest stands present in the watershed ranged between 0.74 and 2.40. The relatively low values of the LAI may particularly be due to the physical characteristics of the watershed such as the steep topography and shallow soil depth.

The hydrodynamics model was calibrated for the model parameters: RD, vertical and horizontal saturated hydraulic conductivity, threshold melting temperature and air temperature. The calibration target for the hydrodynamics model was the river discharge at the downstream end of the study area observed for the years 1986 and 1987. The best agreement between the observed and simulated river discharges was obtained with the simulation with seasonal RD values, moderate vertical and horizontal saturated hydraulic conductivity values (5×10^{-8} and 5×10^{-7} respectively), threshold melting temperature of 0°C and modified air temperature are the most consistent with the observed discharge data. The Mean Error (ME), correlation coefficients R and R^2 for this optimal simulation are 0.01 m^3/s, 0.72 and 0.52 respectively.

The calibrated integrated model was run as a base case for the 20 years between 1986 and 2006. The average daily river discharge is predicted to be 5.59 m^3/s. The stream flow and the evapotranspiration are predicted to be 64.5% and 34.5% of the total precipitation.

The sensitivity of the hydrodynamics model to land use was analyzed by assuming the watershed is covered completely by agriculture, coniferous stand (M Conf 3), deciduous stand (YM Decd 3) and mixed stand (Y Conf M Decd 3), respectively. The highest and lowest river discharges are predicted for agriculture and deciduous stand respectively. On the other hand, the evapotranspiration is predicted to be highest and lowest for deciduous stand and agriculture, respectively. This indicates that the agricultural area leads to higher water yield whereas the deciduous stand leads to lower water yield in the watershed.

The sensitivity of the hydrodynamics model to the two key land use parameters; LAI and RD was assessed. The LAI values 1, 2, 3, 5, 7 and 10 were tested with the RD values

of 500 and 1000 mm. Model results indicate that the ratio of the evapotranspiration increases with the increasing LAI up to a value of 3. The hydrodynamics model becomes almost insensitive to the LAI for higher values. The RD value of 1000 mm leads to higher evapotranspiration than the value of 500 mm.

The sensitivity of the hydrodynamics model to the heterogeneity of the saturated hydraulic conductivity values at depths of 3 m and 12.5 m was evaluated. The discharge difference between the calibrated model and the heterogeneous saturated hydraulic conductivity values of the 3 m depth is slightly lower than the heterogeneous saturated hydraulic conductivity values of the 12.5 m depth. Compared to the impact of the land use parameters, the hydrodynamics model is not sensitive to the heterogeneity of the saturated hydraulic conductivity.

To evaluate the impact of land use on the water budget, the integrated land use-hydrodynamics model was run for different land use scenarios for the 21-year period between 2006 and 2026. In addition to the base case scenario which assumes no change in the land use practices, five scenarios were considered: Conversion from agriculture to forest, forest to agriculture, deciduous and mixed to coniferous, coniferous and deciduous to mixed and coniferous and mixed to deciduous. For the base case simulation, the average daily river discharge is predicted to be 5.00 m^3/s while the evapotranspiration is predicted to be 67% of annual precipitation. Compared to the values predicted for the period from 1986 to 2006, the average river discharge is predicted to decrease and evapotranspiration ratio is predicted to increase in the years from 2006 to 2026.

Results of these future simulations indicate that the highest average daily river discharge is predicted for the scenario of coniferous and deciduous stands conversion to mixed stands. It is predicted to be the lowest for the scenario of agricultural areas conversion to forest. Evapotranspiration, on the other hand, is minimum for the scenario of coniferous and deciduous stands conversion to mixed stands and maximum for the scenario of agricultural areas conversion to forest. The difference is attributed to differences in the summer and winter LAI and RD values for these six scenarios.

It is predicted that almost 1/3 of all the scenario simulations have a mean daily discharge range between 0.5 m^3/s and 1.5 m^3/s. The scenario of agricultural areas to forest conversion is predicted to have the highest percentage of this range. The monthly averages of the mean daily discharges are predicted to be highest in February and lowest in August for all the scenario simulations. However the monthly evapotranspiration ratio is predicted to be highest in June and lowest in December.

The scenario of coniferous and deciduous stands conversion to mixed stands is predicted to have the highest maximum daily discharge with about 88 m^3/s. Flooding is more likely to occur for this scenario. The scenario of coniferous and mixed stands conversion to deciduous is predicted to have the lowest maximum discharge with about 47 m^3/s. Flooding is less likely to occur for this scenario. The maximum daily discharges for the base case, agriculture to forest, forest to agriculture and deciduous and mixed to coniferous conversion scenarios are predicted to be about 85 m^3/s, 59 m^3/s, 72 m^3/s and 75 m^3/s respectively. The minimum daily discharges for all the scenarios are predicted to be around 0.67 m^3/s except the scenario of agricultural areas conversion to forest which is predicted to be 0.59 m^3/s.

The average daily discharge below 1 m^3/s was assumed to be an indicator of low river discharge. The summer months August, September and July are predicted to be the driest months respectively. The scenario of agricultural areas conversion to forest is predicted to yield the highest frequency (about 52%) of low discharge in the summer months. On the other hand, the scenario of coniferous and deciduous conversion stands conversion to mixed stands is predicted to yield the lowest frequency (about 27%) of low discharge in the summer months.

To evaluate the effect of global climate change on the water budget, a long term simulation was conducted by extending the base case simulation for 34 additional years to 2060. Based on the A2 climate scenario (Bates et al., 2008), the mean annual temperature predicted with the RegCM3 model is expected to increase by 7.6% over the 55 year period between 2006 and 2060. On the other hand, slightly increasing precipitation is also predicted. The results of the integrated land use-hydrodynamics model indicate that the average daily river discharge and the evapotranspiration ratio are predicted to be 5.74 m^3/s

and 62.5% respectively. Hence, the river discharge is predicted to increase and evapotranspiration ratio is predicted to decrease in the future 34 years.

For the future 34 years, the maximum and minimum daily discharges are predicted to be about 110 m^3/s and 0.35 m^3/s which are respectively higher and lower than the maximum and minimum values predicted for the base case simulation. The maximum and minimum annual discharges are predicted to be 8.3 m^3/s and 1.8 m^3/s indicating a wide range between the years.

Almost 73% of the driest summer months (August, July and September) are predicted to suffer low discharge (less than 1 m^3/s). The percentage is quite high compared to the previous base case simulation. Besides these driest summer months, higher frequency of low discharge is also predicted to occur in October, June and November but in lower percentages.

Analysis of the results also shows that an irregular discharge regime is predicted to occur for the future 34 years between 2027 and 2060. The reason for such a discharge regime with more extreme values is the lower storage capacity due to decreasing snow and more extreme precipitation ranging between 631 mm and 1443 mm. Consequently, extreme conditions such as flooding and low discharge are more likely to occur.

This study demonstrates the dependence of the water balance on the land use dynamics within the watershed. The results of this analysis can be considered as a step towards the development of a fully integrated model that can be used by water authorities and policy makers for the sustainable development of the Bartın spring watershed. To fully achieve this goal, the model must be expanded to include additional modules such as socio-economic, ecological and environmental components. Specific recommendations for future studies can include:

- The integration of the two models is one dimensional; the LAI and RD parameter values generated with the land use model are supplied to the hydrodynamics model. However, the results generated by the hydrodynamics model may influence the land use model parameters. For example, the water content in the soil is one of the

significant outputs of the hydrodynamics model which can alter the maturation, degradation and regeneration time parameters of the land use model. Fully integrated models which consider the feedbacks from the hydrodynamics model to the land use model and the response to these feedbacks can be developed.

- The developed integrated land use-hydrodynamics model simulates the land use transformation and the hydrological processes in the Bartın spring watershed. In reality, these transformations and processes are spatially distributed. However, the spatial distribution of the current integrated model is partial. The level of the spatial distribution can be increased by applying some modifications both to the land use dynamics model and hydrodynamics model. The land use model can be disaggregated by increasing the number of the subwatersheds so that the impact of the different land uses could better be represented in the hydrodynamics model. The disaggregation level of this land use dynamics model may be defined according to the necessities of the possible modeling studies. The spatial resolution of the integrated model can also be improved by developing dynamic land use models which are highly compatible with the Geographical Information Systems (GIS). Thus, each geographical unit may account for the generated land use parameters improving the accuracy of the integrated model results.

- The increment of the topographic map resolution may be incorporated into the model to simulate additional hydrological processes and events within the watershed such as depression formation, ponding and flooding. In particular, the redefinition of the stream cross sections based on actual elevation measurements would allow for analysis of floods within a single modeling framework in conjunction with land use dynamics and water budget calculations.

- Evapotranspiration and snow accumulation and melting are two processes that strongly influence the water budget. Both of these processes are directly dependent on the temperature. By incorporating temperature variations within the watershed, it would be possible to more accurately simulate these two processes.

- The developed model extends vertically to the rock layer which varies in depth from 2 to 30 m from the surface. Future work could focus on extending the boundaries of the model both horizontally to include other watersheds within the region as well as vertically to include the karstic subsurface geology underlying the developed model. For the vertical extension of the model, detailed geologic studies must be conducted to identify and characterize the karstic structure and how it interacts with the surface and subsurface hydrology in the region.

- As the results of this modeling effort show, evapotranspiration is a major component of the overall water budget of the watershed. An important parameter controlling the evapotranspiration is the RD. While the present study treats the RD as a calibration parameter, future research could focus on developing more accurately the dynamic variations of this parameter. For example, the RD of the stand groups can be measured by excavating sample root profiles in the soils of the stand groups and these results can be incorporated into the model.

- The integrated model focuses on the quantity of water rather than its quality. The quality of water is critical parameter since the water is used also for the drinking purpose. Therefore, the integrated model may be coupled with water quality models which simulate the contaminant and sediment transport processes within the watershed.

- Sustainable watershed management concept involves the detailed representation and modeling of the socio-economic, ecological and environmental components together with the physical components of the watershed. Socio-economic components consist of administrators, villagers, agricultural practices whereas the ecological components include all the flora and fauna within the watershed. Quality and quantity of the surface water resources such as streams and subsurface water resources such as karstic aquifer, irrigation practices and fertilizer applications constitute the environmental components. Therefore, new modeling efforts which intend to propose sustainable watershed management options for the Bartın spring watershed must account for the representation of the intra-relations and interrelations of these components.

REFERENCES

Ahmad, S., Simonovic, S.P., 2004. Spatial System Dynamics: New approach for simulation of water resources systems. Journal of Computing in Civil Engineering, 18, 331-340.

Bartın Valiliği Çevre ve Orman İl Müdürlüğü, 2003. Bartın İli Çevre Durum Raporu 2003, Bartın Çevre ve Orman İl Müdürlüğü Yayınları, Bartın.

Barlas, Y., 1996. Formal aspects of model validity and validation in system dynamics. System Dynamics Review, 12, 183-210.

Barlas, Y., 2002. System Dynamics: Systemic feedback modeling for policy analysis. In Knowledege for Sustainable Development-An Insight into the Encyclopedia of Life Support Systems, 1131-1175. UNESCO-Eolss Publishers, U.K.

Bates, B.C., Kundzewicz, Z.W., Wu S., Palutikof, J.P., 2008. Climate change and water. Technical paper of the Intergovernmental Panel on Climate Change (I.P.C.C.), Geneva.

Beighly, R.E., Moglen, G.E., 2002. Trend assessment in rainfall-runoff behavior in urbanizing watersheds. Journal of Hydrologic Engineering, 7, 27-34.

Berterretche, M., Hudak, A.T., Cohen, W.B., Maiersperger, T.K., Gower, S.T., Dungan, J., 2005. Comparison of regression and geostatistical methods for mapping Leaf Area Index (LAI) with Landsat ETM+ data over a boreal forest. Remote Sensing and Environment, 96, 49-61.

Boegh, E., Thorsen, M., Butts, M.B., Hansen, S., Christiansen, J.S., Abrahamsen, P., Hasager, C.B., Jensen, N.O., van der Keur, P., Refsgaard, J.C., Schelde, K., Soegaard, H., Thomsen, A., 2004. Intercorporating remote sensing data in physically based distributed agro-hydrological modeling. Journal of Hydrology, 287, 279-299.

Bouyoucos, G.J., 1936. Directions for making mechanical analysis of soils by the Hydrometer Method, Soil Science, 42, 225-229.

Bozkurt, D., Şen, Ö.L., Turuncoğlu, U.U., Karaca, M., Dalfes, H.N., 2008. Regional climate change projections for Eastern Mediterranean: Preliminary results, EGU General Assembly, Vienna, 13-18 April 2008, 10.

Buytaert, W., Iniguez, V., De Bievre, B., 2007. The effects of afforestation and cultivation on water yield in the Andean Paramo. Forest Ecology and Management, 251, 22-30.

Carsel, R.F., Parrish. R.S., 1988. Developing joint probability distributions of soil water retention characteristics. Water Resources Research, 24, 755-769.

Chaves, J., Neill, C., Germer, S., Neto, S.G., Krusche, A., Elsenbeer, H., 2008. Land management impacts on runoff sources in small Amazon watersheds. Hydrological Processes, 22, 1766-1775.

Chen J.M., Cihlar, J., 1995. Quantifying the effect of canopy architecture on optical measurements of leaf area index using two gap size analysis methods. Transactions in Geoscience and Remote Sensing, 33, 777-787.

Chen, J.M., 1996. Optically based methods for measuring seasonal variation of leaf area index in boreal coniferous stands. Agricultural and Forest Meteorology, 80, 2-4, 135-163.

Choi, W., Deal, B.M., 2008. Assessing hydrological impact of potential land use change through hydrological and land use change modeling for the Kishwaukee River basin (USA). Journal of Environmental Management, 88, 1119-1130.

Chow, V.T., Maidment, D.R., Mays, L.W., 1988. Applied Hydrology, McGraw-Hill Publications, Singapore.

Cohen, W.B., Maiersperger, T.K., Yang, Z., Gower, S.T., Turner, D.P., Ritts, W.D., Berterretche, M., Running, S.W., 2003. Comparison of land cover and LAI estimates

derived from ETM+ and MODIS for four sites in North America: a quality assessment of 2000/2001 provisional MODIS products. Remote Sensing and Environment, 88, 233-255.

Costa, M.H., Botta, A., Cardille, J.A., 2003. Effect of large-scale changes in land cover on the discharge of the Tocantins River, Southeastern Amazonia. Journal of Hydrology, 283, 206-217.

Costa-Cabral, M.C., Richey, J.E., Goteti, G., Lettenmaier, D.P., Feldkötter, C., Snidvongs, A., 2008. Landscape structure and use, climate and water movement in the Mekong River basin. Hydrological Processes, 22, 1731-1746.

Cuo, L., Lettenmaier, D.P., Mattheussen, B.V., Storck, P., Wiley, M., 2008. Hydrologic prediction for urban watersheds with the Distributed Hydrology-Soil-Vegetation Model. Hydrological Processes, 22, 4205-4213.

Çepel, N., 1985. Toprak Fiziği, İ.Ü. Orman Fakültesi Yayınları, İstanbul.

Dalfes, N., 2008. Türkiye için İklim Değişikliği Senaryoları, Yayınlanmamış Sonuç Raporu, Proje No. TÜBİTAK-105G015, İstanbul Teknik Üniversitesi Avrasya Yer Bilimleri Enstitüsü.

Danish Hydrualic Institute (DHI), 2005. MIKE SHE User's Guide, Denmark.

Daughtry, C.S.T., 1990. Direct Measurements of Canopy Structure. Remote Sensing Reviews, 5, 45-60.

Deaton, M.L., Winebrake, J.J., 2000. Dynamic Modeling for Environmental Systems, Springer-Verlag Publications, New York.

Debarry, P.A., 2004. Watersheds: Processes, Assessment and Management, John Wiley and Sons Inc., U.S.A.

Demarez, V., Duthoit, S., Baret, F., Weiss, M., Dedieu, G., 2008. Estimation of leaf area indexes of crops with hemispherical photographs. Agricultural and Forest Meteorology, 148, 644-655.

Demetriou, C., Punthakey, J.F., 1999. Evaluating sustainable groundwater management options using the MIKE SHE integrated hydrogeological modeling package. Environmental Modelling & Software, 14, 129-140.

Devlet Meteoroloji İşleri Genel Müdürlüğü (D.M.İ.), 2007. Günlük Meteorolojik Veriler, Ankara.

Devlet Su İşleri (D.S.İ.) 2001. 2001 Yılı Akım Gözlem Yıllığı, Ankara.

Devore, J., Farnum, N., 1999. Applied Statistics for Engineers and Scientists, Duxbury Press, U.S.A.

Dumlu O., Yalçın, T., Bozkurtoğlu, E., 2006. Yeraltı Suyu Jeolojisi ve Hidroliği, Literatür Kitabevi, İstanbul.

Eijkelkamp Company, 2008. Operating instructions for laboratory permeameter, Netherlands.

Elguindi, N., Bi, X., Giorgi, F., Nagarajan, B., Pal, J., Solmon, F., Rauscher, S., Zakey, A., 2007. User's Guide for RegCM Version 3.1, Italy.

Elshorbagy, A., Jutla, A., Barbour, L., Kells, J., 2005. System dynamics approach to assess the sustainability of reclamation of disturbed watersheds. Canadian Journal of Civil Engineering, 32, 144-158.

Erol, O., 2004. Genel Klimatoloji, Çantay Kitabevi, İstanbul.

ESRI, 2005. Arc GIS 9, What is Arc GIS 9.1?, U.S.A.

Fang, H., Liang, S., Townshend, J.R., Dickinson, R.E., 2008. Spatially and temporally continuous LAI data sets based on an integrated filtering method: Examples from North America. Remote Sensing & Environment, 112, 75-93.

Fang, H., Liang, S., 2005. A hybrid inversion method for mapping leaf area index from MODIS data: experiments and application to broadleaf and needleleaf canopies. Remote Sensing and Environment, 94, 405-424.

Fernandez, J.M., Selma, M.A.E., 2004. The dynamics of water scarcity on irrigated landscapes: Mazarron and Aguilas in south-eastern Spain. System Dynamics Review, 20, 117-137.

Fleischbein, K., Wilcke, W., Valarenzo, C., Zech, W., Knoblich, K., 2006. Water budgets of three small catchments under montane forest in Ecuador: Experimental and modelling approach. Hydrological Processes, 20, 2491-2507.

Ford, A., 1999. Modeling the Environment, Island Press, U.S.A.

Frazer, G.W., Fournier, R.A., Trofymow, J.A., Hall, R.J., 2001. A comparison of digital and fisheye photography for analysis of forest canopy structure and gap light transmission. Agricultural and Forest Meteorology, 109, 249-263.

Freeze, R.A., Cherry, J.A., 1979. Groundwater, Prentice Hall, Inc., U.S.A.

Genç, M., 2004. Silvikültürün Temel Esasları, Süleyman Demirel Üniversitesi Basımevi, Isparta.

Gupta, P.K., Singh, R., Raghuwanshi, N.S., Dutta, S., Panigrahy, S., 2008. Effect of remotely sensed data on the performance of a distributed hydrological model: Case Study. Journal of Hydrologic Engineering, 13, 939-947.

Gülçur, F., 1974. Toprağın Fiziksel ve Kimyasal Analiz Metodları, İ.Ü. Orman Fakültesi Yayınları, İstanbul.

Güneralp, B., Barlas, Y., 2003. Dynamic modelling of a shallow freshwater lake for ecological and economic sustainability. Ecological Modelling, 167, 115-138.

Hale, S.E., Edwards, C., 2002. Comparison of film and digital hemispherical photography across a wide range of canopy densities. Agricultural and Forest Meteorology, 112, 51-56.

Henriksen, H.J., Troldborg, L., Nyegaard, P., Sonnenberg, T.O., Refsgaard, J.C., Madsen, B., 2003. Methodology for construction, calibration and validation of a national hydrological model for Denmark. Journal of Hydrology, 280, 52-71.

High Performance Systems Inc. (H.P.S.), 2001. Tutorial and technical documentation of Stella 7.0.1, Honover.

Islam, N., Wallender, W.W., Mitchell, J., Wicks, S., Howitt, R.E., 2006. A comprehensive experimental study with mathematical modeling to invesatigate the effects of cropping practices on water balance variables. Agricultural Water Management, 82, 129-147.

İller Bankası Genel Müdürlüğü, 1985. Bartın-Amasra İçmesuyu Projesi Açıklama Raporu, Ankara.

İller Bankası 18. Bölge Müdürlüğü, 1998. Bartın (Merkez) Belediyesi Hidrolojik-Hidrojeolojik Ek Etüd Raporu, Kastamonu.

Jayatilaka, C.J., Storm, B., Mudgway, L.B., 1998. Simulation of water flow on irrigation bay scale with MIKE SHE. Journal of Hydrology, 208, 108-130.

Jonckheere, I., Fleck, S., Nackaerts, K., Muys, B., Coppin, P., Weiss, M., Baret, F., 2004. Review of methods for in situ leaf area index determination Part I. Theories, sensors and hemispherical photography. Agricultural and Forest Meteorology, 121, 19-35.

Jury, W.A., and Horton, R., 2004. Soil Physics, John Wiley and Sons Inc., U.S.A.

Kalıpsız, A., 1998. Orman Hasılatı Bilgisi, İ.Ü. Orman Fakültesi Yayınları, İstanbul.

Kantarcı, M.D., 2000. Toprak İlmi, İ.Ü. Orman Fakültesi Yayınları, İstanbul.

Karabük İl Özel İdaresi, 2006. Karabük İli Köyleri Sondaj Kuyu Logu Raporları, Karabük.

Karvonen, T., Koivusalo, H., Jauhiainen, M., Palko, J., Weppling, K., 1999. A hydrological model for predicting runoff from different land use areas. Journal of Hydrology, 217, 253-265.

Kim, S.J., Kwon, H.J., Park, G.A., Lee, M.S., 2005. Assessment of land use impact on stream flow via a grid-based modeling approach including paddy fields. Hydrological Processes, 19, 3801-3817.

Kristensen, K.J., Jensen, S.E., 1975. A model for estimating actual evapotranspiration from potential transpiration. Nordic Hydrology, 6, 70-88.

Lambin, E.F., Modelling Land Use Change, Finding Simplicity in Complexity. In Wainwright, J., Mulligan, M. (Eds.), Environmental Modelling, 245-254, John Wiley & Sons, Ltd., England.

Linsley, R.K., Kohler, M.A., Paulhus, J.L.H., 1975. Hydrology for Engineers, McGraw-Hill Publications, U.S.A.

Liu, Y.B., Gebremeskel, S., De Smedt, F., Hoffmann, L., Pfister, L., 2006. Predicting storm runoff from different land use classes using a Geographical Information System based distribution model. Hydrological Processes, 20, 533-548.

Liu, H.L., Chen, X., Bao, A.M., Wang, L., 2007. Investigation of groundwater response to overland flow and topography using a coupled MIKE SHE/MIKE 11 modeling system for an arid watershed. Journal of Hydrology, 347, 448-459.

Luijten, J.C., Jones, J.W., Knapp, E.B., 2000. Dynamic Modelling of Strategic Water Availability in the Cabuyal River, Colombia: The impact of land cover change on the hydrological balance. Advances in Environmental Monitoring and Modelling, 1, 36-60.

Maden Tetkik Arama Genel Müdürlüğü (M.T.A.), 2002. Zonguldak F-29 Paftası Jeoloji Haritası ve Raporları, Ankara.

Madsen, H., 2003. Parameter estimation in distributed hydrological catchment modeling using automatic calibration with multiple objectives. Advances in Water Resources, 26, 205-216.

McMichael, C.E., Hope, A.S., 2007. Predicting streamflow response to fire-induced landcover change: Implications of parameter uncertainty in the MIKE SHE model. Journal of Environmental Management, 84, 245-256.

Mernild, S.H., Hasholt, B., Liston, G.E., 2008. Climatic control on river discharge simulations, Zackenberg River drainage basin, northeast Greenland. Hydrological Processes, 22, 1932-1948.

Molina, A., Govers, G., Vanacker, V., Poesen, J., Zeelmaekers, E., Cisneros, F., 2007. Runoff generation in a degraded Andean ecosystem: Interaction of vegetation cover and land Use. CATENA, 71, 357-370.

Nobis, M., Hunziker, U., 2005. Automatic thresholding for hemispherical canopy-photographs based on edge detection. Agricultural and Forest Meteorology, 128, 243-250.

North, M., Chen, J., Oakley, B., Song, B., Rudnicki, M., Gray, A., Innes, J., 2004. Forest Science, 50, 299-311.

Notter, B., MacMillan, L., Viviroli, D., Weingartner, R., Liniger, H.P., 2007. Impacts of environmental change on water resources in the Mt. Kenya region. Journal of Hydrology, 343, 266-278.

Orman Genel Müdürlüğü (O.G.M.), 2006. Ulus Orman İşletme Müdürlüğü Orman Amenajman Planları, Ankara.

Özhan, S., 2004. Havza Amenajmanı, İ.Ü. Orman Fakültesi Yayınları, İstanbul.

Öztürk, M., Saysel, A.K., Copty, N., Aydın, A., 2007. A GIS Based Dynamic Land Use Model for Bartın-Ulupınar Waterhed Management, International Congress of River Basin Management, Antalya, 22-24 March 2007, 2, 207-219.

Penman, H.L., 1948. Natural evaporation from open water, bare soil and grass. Proc. Phil. Trans., 330, 399-404.

Pisek, J., Chen, J.M., 2007. Comparison of MODIS and VEGETATION global LAI products over four BigFoot sites in North America. Remote Sensing and Environment, 109, 81-94.

Powersim Corporation, 1996. Powersim 2.5 Reference Manual, Norway.

Priestly, C.H.B. and Taylor, R.J., 1972. On the assessment of surface heat flux and evaporation using large scale parameters. Mon. Wea. Rev., 100, 81-92.

Refsgaard, J.C., Storm, B., 1995. MIKE SHE. In Singh, V.P. (Eds.), Computer Models of Watershed Hydrology, 809-846, Water Resources Publications, U.S.A.

Refsgaard, J.C., 1997. Parameterisation, calibration and validation of distributed hydrological models. Journal of Hydrology, 198, 69-97.

Raudkivi, A.J., 1979. Hydrology: An Advanced Introduction to Hydrological Processes and Modelling, Pergamon Press Publications, England.

Saatçioğlu, F., 1976. Silvikültür I-Silvikültürün Biyolojik Esasları ve Prensipleri, İ.Ü. Orman Fakültesi Yayınları, İstanbul.

Sahoo, G.B., Ray, C., De Carlo, E.H., 2006. Calibration and validation of a physically distributed hydrological model, MIKE SHE, to predict streamflow at high frequency in a flashy mountainous Hawaii stream. Journal of Hydrology, 327, 94-109.

Saysel, A.K., Barlas, Y., 2001. A dynamic model of salinization on irrigated lands. Ecological Modeling, 139, 177-199.

Schleppi, P., Conedera, M., Sedivy, I., Thimonier, A., 2007. Correcting non-linearity and slope effects in the estimation of the leaf area index of forests from hemispherical photographs. Agricultural and Forest Meteorology, 144, 236-242.

Shabanov, N.V., Huang, D., Yang, W., Tan, B., Knyazikhin, Y., Myneni, R.B., Ahl, D.E., Gower, S.T., Huete, A.R., Aragao, L.E.O.C., Shimabukuro, Y.E., 2005. Analysis and optimization of the MODIS Leaf Area Index algorithm retrievals over broadleaf forests. Transactions in Geoscience and Remote Sensing, 43, 1855-1865.

Simonovic, S.P., 2002. World water dynamics: Global modeling of water resources. Journal of Environmental Management, 66, 249-267.

Simonovic, S.P., Rajasekaram V., 2004. Integrated analyses of Canada's water resources: A system dynamics model. Canadian Water Resources Journal, 29, 223-250.

Siriwardena, L., Finlayson, B.L., Mcmahon, T.A., 2006. The impact of land use change on catchment hydrology in large catchments: The Comet River, Central Queensland, Australia. Journal of Hydrology, 326, 199-214.

Singh, R., Subramanian, K., Refsgaard, J.C., 1999. Hydrological modeling of a small watershed using MIKE SHE for irrigation planning. Agricultural Water Management, 41, 149-166.

Singh, V.P., Frevert, D.K. (Eds.), 2006, Watershed Models, CRS Press, Taylor and Francis Group, U.S.A.

Stave, K.A., 2002. A system dynamics model to facilitate public understanding of water management options in Las Vegas, Nevada. Journal of Environmental Management, 67, 303-313.

Sun, G., Riekerk, H., Comerford, N.B., 1998. Modeling the hydrologic impacts forest harvesting on Florida Flatwoods. Journal of The American Water Resources Association, 34, 843-854.

Tarım ve Köyişleri Bakanlığı, Araştırma ve Planlama Koordinatörlüğü (A.P.K.) Daire Başkanlığı, 2005. Sayısal toprak haritaları, Ankara.

Thanapakpawin, P., Richey, J., Thomas, D., Rodda, S., Campbell, B., Logsdon, M., 2006. Effects of landuse change on the hydrologic regime of the Mae Chaem River basin, NW Thailand. Journal of Hydrology, 234, 215-230.

Thompson, J.R., Sorensen, H.R., Gavin, H., Refsgaard, A., 2004. Application of the coupled MIKE SHE/MIKE 11 modelling system to a lowland wet grassland in Southeast England. Journal of Hydrology, 293, 151-179.

Thornthwaite, C.W., 1948. An approach towards a rational classification of climate. Geographical Review, 38, 55-94.

Tidwell, V.C., Passell, H.D., Conrad, S.H., Thomas, R.P., 2004. System dynamics modeling for community-based water planning: Application to the Middle Rio Grande. Aquatic Sciences, 66, 357-372.

Turan, B., 2002. Obtaining Inundation Maps by GIS and Hydrologic-Hydraulic Model Integration, Ph.D. Thesis, Middle East Technical University.

Turoğlu, H., Özdemir, H., 2005. Bartın'da Sel ve Taşkınlar: Sebepler, Etkiler, Önleme ve Zarar Azaltma Önerileri, Çantay Yayınevi, İstanbul.

Usul, N., 2001. Engineering Hydrology, M.E.T.U. Press, Ankara.

Van Genuchten, M.T., 1980. A closed-form equation for predicting the hydraulic conductivity of unsaturated soils. Soil Sci. Soc. Am. J., 44, 892-898.

VanShaar, J.R., Haddeland, I., Lettenmaier, D.P., 2002. Effects of land-cover changes on the hydrological response of interior Columbia River basin forested catchments. Hydrological Processes, 16, 2499-2520.

Vazquez, R.F., Feyen, J., 2007. Assessment of the effects of DEM gridding on the predictions of basin runoff using MIKE SHE and a modeling resolution of 600 m. Journal of Hydrology, 334, 73-87.

Ventana Systems, 1996. Vensim User's Guide, version 1.62, U.S.A.

Wang, S., Kang, S., Zhang, L., Li, F., 2008. Modelling hydrological response to different land-use and climate change scenarios in the Zamu River basin of northwest China. Hydrological Processes, 22, 2502-2510.

Ward R.C., Robinson, M., 2000. Principles of Hydrology, McGraw-Hill Publications, London.

Wei, X., Liu, S., Zhou, G., Wang, C., 2005. Hydrological Processes in major types of Chinese forest. Hydrological Processes, 19, 63-75.

Welles, J.M., Cohen, S., 1996. Canopy structure measurement by gap fraction analysis using commercial instrumentation. Journal of Experimental Botany, 47, 1335-1342.

Wilson, J.W., 1960. Inclined point quadrats. New Phytologist, 59, 1-7.

Wissmar, R.C., Timm, R.K., Logsdon, M.G., 2004. Effects of changing forest and impervious and covers on discharge characteristics of watersheds. Environmental Management, 34, 91-98.

Yalçın, T., 1992. Penman yöntemi kullanılarak potansiyel buharlaşmanın hesaplanması için bilgisayar programı. MJKM Bül., 13, 114-122.

Yan J.J., K.R. Smith, 1994. Simulation of integrated surface water and ground water systems - model formulation. Water Resources Bulletin, 30, 1-12.

Yue, S., Hashino, M., 2005. Statistical interpretation of the impact of forest growth on stream flow of the Sameura Basin, Japan. Environmental Monitoring and Assessment, 104, 369-384.

Xu, Z.X., Takeuchi K., Ishidaira H., Zhang, X.W. 2002. Sustainability analysis for Yellow River water resources using the system dynamics approach. Water Resources Management, 16, 239-261.

Zhang, Y.K., Schilling, K.E., 2006. Increasing stream flow and baseflow in Mississippi River since the 1940s: Effect of land use change. Journal of Hydrology, 324, 412-422.

Zhang, Z., Wang, S., Sun, G., McNulty, S.G., Zhang, H., Li, J., Zhang, M., Klaghofer, E., Strauss, P., 2008. Evaluation of the MIKE SHE model for Application in the Loess Plateau, China. Journal of the American Water Resources Association, 44-5, 1108-1120.

APPENDIX A: PENMAN MONTHLY WATER BUDGET OF THE WATERSHED

Table A.1. Water budget of 1986

MONTHS	1	2	3	4	5	6	7	8	9	10	11	12	Σ
PRECIPITATION (P), (mm)	110.3	64.0	22.2	48.7	77.2	73.7	20.6	0.0	20.0	40.8	99.3	110.5	687.3
POTENTIAL EVAPOTRANSPIRATION (E_P), (mm)	11.5	26.2	54.6	103.9	117.4	156.3	171.2	154.1	93.6	46.9	15.1	6.1	956.8
P - E_P (mm)	98.8	37.8	-32.4	-55.2	-40.2	-82.6	-150.6	-154.1	-73.6	-6.1	84.3	104.4	–
RESERVED WATER (R), (mm)	100.0	100.0	67.6	12.4	0.0	0.0	0.0	0.0	0.0	0.0	84.3	100.0	–
ACTUAL EVAPOTRANSPIRATION (E_A), (mm)	11.5	26.2	54.6	103.9	89.6	73.7	20.6	0.0	20.0	40.8	15.1	6.1	462.2
WATER DEFICIT (mm)	0.0	0.0	0.0	0.0	27.7	82.6	150.6	154.1	73.6	6.1	0.0	0.0	494.7
EXCESS WATER (mm)	98.8	37.8	0.0	0.0	0.0	0.0	0.0	0.0	0.0	0.0	0.0	88.6	225.2
OVERLAND FLOW (mm)	71.5	54.7	27.3	13.7	6.8	3.4	1.7	0.9	0.4	0.2	0.1	44.3	225.1
PRECIPITATION-OVERLAND FLOW (mm)	38.8	9.4	-5.1	35.0	70.4	70.3	18.9	-0.9	19.6	40.6	99.2	66.2	462.2

Table A.2. Water budget of 1987

MONTHS	1	2	3	4	5	6	7	8	9	10	11	12	Σ
PRECIPITATION (P), (mm)	197.1	30.8	55.1	68.0	53.4	50.0	28.6	56.8	0.8	87.9	53.1	198.0	879.6
POTENTIAL EVAPOTRANSPIRATION (E_P), (mm)	13.1	26.5	52.6	83.4	123.1	158.6	175.4	136.7	94.0	50.0	17.6	9.5	940.4
P - E_P (mm)	184.0	4.3	2.5	-15.4	-69.7	-108.6	-146.8	-79.9	-93.2	37.9	35.5	188.5	–
RESERVED WATER (R), (mm)	100.0	100.0	100.0	84.6	14.9	0.0	0.0	0.0	0.0	37.9	73.8	100.0	–
ACTUAL EVAPOTRANSPIRATION (E_A), (mm)	13.1	26.5	52.6	83.4	123.2	64.9	28.6	56.8	0.8	50.0	17.6	9.5	526.9
WATER DEFICIT (mm)	0.0	0.0	0.0	0.0	0.0	93.7	146.8	79.9	93.2	0.0	0.0	0.0	413.5
EXCESS WATER (mm)	184.0	4.3	2.5	0.0	0.0	0.0	0.0	0.0	0.0	0.0	0.0	162.3	353.1
OVERLAND FLOW (mm)	132.6	68.4	35.5	17.7	8.9	4.4	2.2	1.1	0.6	0.3	0.1	81.2	353.0
PRECIPITATION-OVERLAND FLOW (mm)	64.5	-37.6	19.6	50.3	44.5	45.6	26.4	55.7	0.3	87.6	53.0	116.8	526.6

Table A.3. Water budget of 1988

MONTHS	1	2	3	4	5	6	7	8	9	10	11	12	Σ
PRECIPITATION (P), (mm)	65.7	45.4	111.8	82.9	76.2	110.3	70.7	36.5	82.5	132.2	184.6	152.3	1151.1
POTENTIAL EVAPOTRANSPIRATION (E_P), (mm)	11.7	26.4	57.3	80.8	120.5	148.6	172.4	148.2	88.9	43.2	17.4	8.9	924.4
P - E_P (mm)	54.0	19.0	54.5	2.1	-44.3	-38.3	-101.7	-111.7	-6.4	89.0	167.2	143.4	–
RESERVED WATER (R), (mm)	100.0	100.0	100.0	100.0	55.7	17.4	0.0	0.0	0.0	89.0	100.0	100.0	–
ACTUAL EVAPOTRANSPIRATION (E_A), (mm)	11.7	26.4	57.3	80.8	120.5	148.6	88.1	36.5	82.5	43.2	17.4	8.9	722.0
WATER DEFICIT (mm)	0.0	0.0	0.0	0.0	0.0	0.0	84.3	111.7	6.4	0.0	0.0	0.0	202.5
EXCESS WATER (mm)	54.0	19.0	54.5	2.1	0.0	0.0	0.0	0.0	0.0	0.0	156.2	143.4	429.1
OVERLAND FLOW (mm)	82.4	50.7	52.6	27.3	13.7	6.8	3.4	1.7	0.9	0.4	78.1	110.7	428.7
PRECIPITATION-OVERLAND FLOW (mm)	-16.7	-5.3	59.2	55.6	62.5	103.5	67.3	34.8	81.6	131.8	106.5	41.6	722.4

Table A.4. Water budget of 1989

MONTHS	1	2	3	4	5	6	7	8	9	10	11	12	Σ
PRECIPITATION (P), (mm)	48.8	60.0	34.2	9.1	61.1	109.4	48.0	11.5	114.2	174.0	191.0	71.5	932.8
POTENTIAL EVAPOTRANSPIRATION (E_P), (mm)	9.1	26.3	59.7	96.3	129.4	153.6	170.3	147.6	82.3	48.9	17.0	3.5	944.0
P - E_P (mm)	39.7	33.7	-25.5	-87.2	-68.3	-44.2	-122.3	-136.1	31.9	125.1	174.0	68.0	–
RESERVED WATER (R), (mm)	100.0	100.0	74.5	0.0	0.0	0.0	0.0	0.0	31.9	100.0	100.0	100.0	–
ACTUAL EVAPOTRANSPIRATION (E_A), (mm)	9.1	26.3	59.7	83.6	61.1	109.4	48.0	11.5	82.3	48.9	17.0	3.5	560.3
WATER DEFICIT (mm)	0.0	0.0	0.0	12.7	68.3	44.2	122.3	136.1	0.0	0.0	0.0	0.0	383.6
EXCESS WATER (mm)	39.7	33.7	0.0	0.0	0.0	0.0	0.0	0.0	0.0	57.0	174.0	68.0	372.5
OVERLAND FLOW (mm)	62.2	48.0	24.0	12.0	6.0	3.0	1.5	0.8	0.4	28.5	101.3	84.6	372.1
PRECIPITATION-OVERLAND FLOW (mm)	-13.4	12.1	10.2	-2.9	55.1	106.4	46.5	10.8	113.8	145.5	89.8	-13.1	560.7

Table A.5. Water budget of 1990

MONTHS	1	2	3	4	5	6	7	8	9	10	11	12	Σ
PRECIPITATION (P), (mm)	53.4	52.7	36.0	86.5	62.9	84.8	3.0	11.5	114.5	99.0	132.0	121.5	857.8
POTENTIAL EVAPOTRANSPIRATION (E_P), (mm)	9.0	26.5	64.9	87.0	131.9	159.7	170.8	151.1	90.0	51.1	15.7	3.2	961.0
P - E_P (mm)	44.4	26.2	-28.9	-0.5	-69.0	-74.9	-167.8	-139.6	24.5	47.9	116.3	118.3	–
RESERVED WATER (R), (mm)	100.0	100.0	71.1	70.5	1.5	0.0	0.0	0.0	24.5	72.4	100.0	100.0	–
ACTUAL EVAPOTRANSPIRATION (E_A), (mm)	9.0	26.5	64.9	87.1	132.0	86.3	3.0	11.5	90.0	51.1	15.7	3.2	580.2
WATER DEFICIT (mm)	0.0	0.0	0.0	0.0	0.0	73.4	167.8	139.6	0.0	0.0	0.0	0.0	380.8
EXCESS WATER (mm)	44.4	26.2	0.0	0.0	0.0	0.0	0.0	0.0	0.0	0.0	88.7	118.3	277.6
OVERLAND FLOW (mm)	62.9	44.6	22.3	11.1	5.6	2.8	1.4	0.7	0.4	0.2	44.3	81.3	277.4
PRECIPITATION-OVERLAND FLOW (mm)	-9.5	8.2	13.7	75.4	57.3	82.0	1.6	10.8	114.2	98.8	87.7	40.2	580.4

Table A.6. Water budget of 1991

MONTHS	1	2	3	4	5	6	7	8	9	10	11	12	Σ
PRECIPITATION (P), (mm)	57.0	115.5	29.5	121.3	133.7	217.4	96.5	15.5	125.6	113.8	48.5	73.5	1147.8
POTENTIAL EVAPOTRANSPIRATION (E_P), (mm)	10.0	24.8	49.2	78.1	115.6	145.0	169.4	147.0	87.9	51.3	17.6	8.7	904.6
P - E_P (mm)	47.0	90.7	-19.7	43.2	18.1	72.4	-72.9	-131.5	37.7	62.5	30.9	64.8	–
RESERVED WATER (R), (mm)	100.0	100.0	80.3	100.0	100.0	100.0	27.1	0.0	37.7	100.0	100.0	100.0	–
ACTUAL EVAPOTRANSPIRATION (E_A), (mm)	10.0	24.8	49.2	78.1	115.6	145.0	169.4	42.6	87.9	51.3	17.6	8.7	800.2
WATER DEFICIT (mm)	0.0	0.0	0.0	0.0	0.0	0.0	0.0	104.4	0.0	0.0	0.0	0.0	104.4
EXCESS WATER (mm)	47.0	90.7	0.0	23.5	18.1	72.4	0.0	0.0	0.0	0.2	30.9	64.8	347.6
OVERLAND FLOW (mm)	43.6	67.1	35.6	29.5	28.3	48.1	24.1	12.0	6.0	0.1	15.5	40.2	350.1
PRECIPITATION-OVERLAND FLOW (mm)	13.4	48.4	-6.1	91.8	105.4	169.3	72.5	3.5	119.6	113.7	33.0	33.3	797.7

Table A.7. Water budget of 1992

MONTHS	1	2	3	4	5	6	7	8	9	10	11	12	Σ
PRECIPITATION (P), (mm)	131.8	180.5	76.0	73.7	9.2	62.5	77.5	0.0	18.5	149.5	203.5	137.5	1120.2
POTENTIAL EVAPOTRANSPIRATION (E_P), (mm)	12.1	24.6	51.3	90.5	128.2	138.6	152.1	156.5	86.7	52.3	16.3	5.7	914.9
P - E_P (mm)	119.7	155.9	24.7	-16.8	-119.0	-76.1	-74.6	-156.5	-68.2	97.2	187.2	131.8	–
RESERVED WATER (R), (mm)	100.0	100.0	100.0	83.2	0.0	0.0	0.0	0.0	0.0	97.2	100.0	100.0	–
ACTUAL EVAPOTRANSPIRATION (E_A), (mm)	12.1	24.6	51.4	90.5	92.4	62.5	77.5	0.0	18.5	52.3	16.3	5.7	503.6
WATER DEFICIT (mm)	0.0	0.0	0.0	0.0	35.8	76.1	74.6	156.5	68.2	0.0	0.0	0.0	411.3
EXCESS WATER (mm)	119.7	155.9	24.7	0.0	0.0	0.0	0.0	0.0	0.0	0.0	184.5	131.8	616.6
OVERLAND FLOW (mm)	115.9	135.9	80.3	40.1	20.1	10.0	5.0	2.5	1.3	0.6	92.3	112.0	616.0
PRECIPITATION-OVERLAND FLOW (mm)	15.9	44.6	-4.3	33.6	-10.9	52.5	72.5	-2.5	17.2	148.9	111.3	25.5	504.2

Table A.8. Water budget of 1993

MONTHS	1	2	3	4	5	6	7	8	9	10	11	12	Σ
PRECIPITATION (P), (mm)	86.0	78.4	52.1	70.0	67.7	76.6	5.1	120.4	27.9	22.5	74.5	102.5	783.7
POTENTIAL EVAPOTRANSPIRATION (E_P), (mm)	9.3	26.0	58.0	87.2	111.2	160.4	169.1	145.4	96.3	56.5	16.7	3.6	939.7
P - E_P (mm)	76.7	52.4	-5.9	-17.2	-43.5	-83.8	-164.0	-25.0	-68.4	-34.0	57.8	98.9	–
RESERVED WATER (R), (mm)	100.0	100.0	94.1	77.0	33.5	0.0	0.0	0.0	0.0	0.0	57.8	100.0	–
ACTUAL EVAPOTRANSPIRATION (E_A), (mm)	9.3	26.0	58.0	87.2	111.2	110.1	5.1	120.4	27.9	22.5	16.7	3.6	598.0
WATER DEFICIT (mm)	0.0	0.0	0.0	0.0	0.0	50.3	164.0	25.0	68.4	34.0	0.0	0.0	341.7
EXCESS WATER (mm)	76.7	52.4	0.0	0.0	0.0	0.0	0.0	0.0	0.0	0.0	0.0	56.7	185.7
OVERLAND FLOW (mm)	52.5	52.4	26.2	13.1	6.6	3.3	1.6	0.8	0.4	0.2	0.1	28.3	185.6
PRECIPITATION-OVERLAND FLOW (mm)	33.5	26.0	25.9	56.9	61.1	73.3	3.5	119.6	27.5	22.3	74.4	74.2	598.1

Table A.9. Water budget of 1994

MONTHS	1	2	3	4	5	6	7	8	9	10	11	12	Σ
PRECIPITATION (P), (mm)	58.7	40.5	36.4	29.7	65.0	59.2	1.5	93.9	9.6	112.6	200.0	170.4	877.5
POTENTIAL EVAPOTRANSPIRATION (E_P), (mm)	11.4	25.7	59.4	105.1	147.0	166.0	180.2	147.5	111.5	59.0	17.3	5.9	1036.0
P - E_P (mm)	47.3	14.8	-23.0	-75.4	-82.0	-106.8	-178.7	-53.6	-101.9	53.6	182.7	164.5	–
RESERVED WATER (R), (mm)	100.0	100.0	77.0	1.6	0.0	0.0	0.0	0.0	0.0	53.6	100.0	100.0	–
ACTUAL EVAPOTRANSPIRATION (E_A), (mm)	11.4	25.7	59.4	105.1	66.6	59.2	1.5	93.9	9.6	59.1	17.3	5.9	514.6
WATER DEFICIT (mm)	0.0	0.0	0.0	0.0	80.4	106.8	178.7	53.6	101.9	0.0	0.0	0.0	521.4
EXCESS WATER (mm)	47.3	14.8	0.0	0.0	0.0	0.0	0.0	0.0	0.0	0.0	136.3	164.5	362.9
OVERLAND FLOW (mm)	81.8	48.3	24.2	12.1	6.0	3.0	1.5	0.8	0.4	0.2	68.1	116.3	362.7
PRECIPITATION-OVERLAND FLOW (mm)	-23.1	-7.8	12.2	17.6	59.0	56.2	0.0	93.1	9.2	112.4	131.9	54.1	514.8

Table A.10. Water budget of 1995

MONTHS	1	2	3	4	5	6	7	8	9	10	11	12	Σ
PRECIPITATION (P), (mm)	130.9	35.8	120.0	81.6	38.5	156.2	199.5	40.6	62.1	67.0	184.5	107.1	1223.8
POTENTIAL EVAPOTRANSPIRATION (E_P), (mm)	11.7	28.1	58.2	92.5	134.2	163.8	164.0	148.7	94.0	51.0	16.2	6.1	968.5
P - E_P (mm)	119.2	7.7	61.8	-10.9	-95.7	-7.6	35.5	-108.1	-31.9	16.0	168.3	101.0	–
RESERVED WATER (R), (mm)	100.0	100.0	100.0	89.1	0.0	0.0	35.5	0.0	0.0	16.0	100.0	100.0	–
ACTUAL EVAPOTRANSPIRATION (E_A), (mm)	11.7	28.1	58.2	92.5	127.6	156.2	164.0	76.1	62.1	51.0	16.2	6.1	849.8
WATER DEFICIT (mm)	0.0	0.0	0.0	0.0	6.7	7.6	0.0	72.6	31.9	0.0	0.0	0.0	118.7
EXCESS WATER (mm)	119.2	7.7	61.8	0.0	0.0	0.0	0.0	0.0	0.0	0.0	84.3	101.0	374.0
OVERLAND FLOW (mm)	95.4	51.5	58.7	29.3	14.7	7.3	3.7	1.8	0.9	0.5	42.2	71.6	377.6
PRECIPITATION-OVERLAND FLOW (mm)	35.5	-15.7	61.3	52.3	23.8	148.9	195.8	38.8	61.2	66.5	142.3	35.5	846.2

Table A.11. Water budget of 1996

MONTHS	1	2	3	4	5	6	7	8	9	10	11	12	Σ
PRECIPITATION (P), (mm)	44.3	70.2	72.2	71.0	48.3	42.1	11.3	0.0	200.8	92.4	137.1	148.6	938.3
POTENTIAL EVAPOTRANSPIRATION (E_P), (mm)	11.3	26.3	47.3	89.8	148.1	158.0	185.8	150.8	79.7	49.5	13.4	10.9	970.8
P - E_P (mm)	33.0	43.9	24.9	-18.8	-99.8	-115.9	-174.5	-150.8	121.1	42.9	123.7	137.7	–
RESERVED WATER (R), (mm)	100.0	100.0	100.0	81.2	0.0	0.0	0.0	0.0	100.0	100.0	100.0	100.0	–
ACTUAL EVAPOTRANSPIRATION (E_A), (mm)	11.3	26.3	47.3	89.8	129.5	42.1	11.3	0.0	79.7	49.5	13.4	10.9	511.0
WATER DEFICIT (mm)	0.0	0.0	0.0	0.0	18.6	115.9	174.5	150.8	0.0	0.0	0.0	0.0	459.8
EXCESS WATER (mm)	33.0	43.9	24.9	0.0	0.0	0.0	0.0	0.0	21.2	42.9	123.7	137.7	427.3
OVERLAND FLOW (mm)	69.7	56.8	40.9	20.4	10.2	5.1	2.6	1.3	10.8	26.7	75.2	106.5	426.2
PRECIPITATION-OVERLAND FLOW (mm)	-25.4	13.4	31.3	50.6	38.1	37.0	8.8	-1.3	190.0	65.7	61.9	42.2	512.1

Table A.12. Water budget of 1997

MONTHS	1	2	3	4	5	6	7	8	9	10	11	12	Σ
PRECIPITATION (P), (mm)	95.1	109.2	97.6	129.7	27.4	90.3	104.1	252.8	23.9	160.7	40.9	143.2	1274.9
POTENTIAL EVAPOTRANSPIRATION (E_P), (mm)	11.8	25.5	53.5	75.1	134.6	154.3	169.9	128.0	87.3	46.3	15.7	7.9	910.0
P - E_P (mm)	83.3	83.7	44.1	54.6	-107.2	-64.0	-65.8	124.8	-63.4	114.4	25.2	135.3	–
RESERVED WATER (R), (mm)	100.0	100.0	100.0	100.0	0.0	0.0	0.0	100.0	36.6	100.0	100.0	100.0	–
ACTUAL EVAPOTRANSPIRATION (E_A), (mm)	11.8	25.5	53.5	75.1	127.4	90.3	104.1	128.0	87.3	46.3	15.7	7.9	773.0
WATER DEFICIT (mm)	0.0	0.0	0.0	0.0	7.2	64.0	65.9	0.0	0.0	0.0	0.0	0.0	137.0
EXCESS WATER (mm)	83.3	83.7	44.1	54.6	0.0	0.0	0.0	24.8	0.0	50.9	25.2	135.3	501.9
OVERLAND FLOW (mm)	81.8	82.8	63.4	59.0	29.5	14.8	7.4	16.1	8.0	25.5	25.3	80.3	493.9
PRECIPITATION-OVERLAND FLOW (mm)	13.3	26.4	34.2	70.7	-2.1	75.6	96.7	236.7	15.9	135.2	15.6	62.9	781.0

Table A.13. Water budget of 1998

MONTHS	1	2	3	4	5	6	7	8	9	10	11	12	Σ
PRECIPITATION (P), (mm)	158.0	168.1	128.8	52.0	254.2	58.7	58.4	0.0	157.1	129.2	64.6	72.0	1301.1
POTENTIAL EVAPOTRANSPIRATION (E_P), (mm)	9.6	27.1	52.8	93.0	105.7	162.4	184.2	170.8	98.1	55.0	18.1	6.8	983.8
P - E_P (mm)	148.4	141.0	76.0	-41.0	148.5	-103.7	-125.8	-170.8	59.0	74.2	46.5	65.2	–
RESERVED WATER (R), (mm)	100.0	100.0	100.0	59.0	100.0	0.0	0.0	0.0	59.0	100.0	100.0	100.0	–
ACTUAL EVAPOTRANSPIRATION (E_A), (mm)	9.6	27.1	52.8	93.0	105.8	158.7	58.4	0.0	98.1	55.0	18.1	6.8	683.5
WATER DEFICIT (mm)	0.0	0.0	0.0	0.0	0.0	3.7	125.8	170.8	0.0	0.0	0.0	0.0	300.4
EXCESS WATER (mm)	148.4	141.0	76.0	0.0	107.5	0.0	0.0	0.0	0.0	33.2	46.5	65.2	617.7
OVERLAND FLOW (mm)	98.4	119.7	97.8	48.9	78.2	39.1	19.6	9.8	4.9	16.6	31.5	48.4	612.8
PRECIPITATION-OVERLAND FLOW (mm)	59.6	48.4	31.0	3.1	176.0	19.6	38.9	-9.8	152.2	112.6	33.1	23.6	688.3

Table A.14. Water budget of 1999

MONTHS	1	2	3	4	5	6	7	8	9	10	11	12	Σ
PRECIPITATION (P), (mm)	46.1	155.8	72.0	24.3	55.7	134.3	3.2	82.2	38.2	106.7	224.0	102.9	1045.4
POTENTIAL EVAPOTRANSPIRATION (E_P), (mm)	11.3	26.2	55.6	89.8	126.9	161.9	177.2	150.8	92.2	50.5	16.5	7.4	966.3
P - E_P (mm)	34.8	129.6	16.4	-65.5	-71.2	-27.6	-174.0	-68.6	-54.0	56.2	207.5	95.5	–
RESERVED WATER (R), (mm)	100.0	100.0	100.0	34.5	0.0	0.0	0.0	0.0	0.0	56.2	100.0	100.0	–
ACTUAL EVAPOTRANSPIRATION (E_A), (mm)	11.3	26.2	55.6	89.8	90.2	134.3	3.2	82.2	38.2	50.5	16.5	7.4	605.5
WATER DEFICIT (mm)	0.0	0.0	0.0	0.0	36.8	27.6	174.0	68.6	54.0	0.0	0.0	0.0	360.9
EXCESS WATER (mm)	34.8	129.6	16.4	0.0	0.0	0.0	0.0	0.0	0.0	0.0	163.7	95.5	440.0
OVERLAND FLOW (mm)	61.7	95.7	56.0	28.0	14.0	7.0	3.5	1.8	0.9	0.4	81.9	88.7	439.5
PRECIPITATION-OVERLAND FLOW (mm)	-15.6	60.2	16.0	-3.7	41.7	127.3	-0.3	80.5	37.3	106.3	142.1	14.2	605.9

Table A.15. Water budget of 2000

MONTHS	1	2	3	4	5	6	7	8	9	10	11	12	Σ
PRECIPITATION (P), (mm)	122.9	87.8	137.1	118.5	51.7	139.0	27.3	170.3	81.3	101.1	4.5	67.0	1108.5
POTENTIAL EVAPOTRANSPIRATION (E_P), (mm)	10.4	25.7	53.3	91.1	122.8	153.0	171.3	147.5	91.3	49.2	17.3	7.1	939.9
P - E_P (mm)	112.5	62.1	83.8	27.4	-71.1	-14.0	-144.0	22.8	-10.0	51.9	-12.8	59.9	–
RESERVED WATER (R), (mm)	100.0	100.0	100.0	100.0	28.9	14.9	0.0	22.8	12.9	64.8	52.0	100.0	–
ACTUAL EVAPOTRANSPIRATION (E_A), (mm)	10.4	25.7	53.3	91.1	122.8	153.1	42.2	147.5	91.3	49.2	17.3	7.1	810.8
WATER DEFICIT (mm)	0.0	0.0	0.0	0.0	0.0	0.0	129.1	0.0	0.0	0.0	0.0	0.0	129.1
EXCESS WATER (mm)	112.5	62.1	83.8	27.4	0.0	0.0	0.0	0.0	0.0	0.0	0.0	11.9	297.7
OVERLAND FLOW (mm)	59.2	60.7	72.2	49.8	24.9	12.5	6.2	3.1	1.6	0.8	0.4	6.0	297.3
PRECIPITATION-OVERLAND FLOW (mm)	63.7	27.1	64.9	68.7	26.8	126.6	21.1	167.2	79.7	100.3	4.1	61.0	811.2

Table A.16. Water budget of 2001

MONTHS	1	2	3	4	5	6	7	8	9	10	11	12	Σ
PRECIPITATION (P), (mm)	0.0	79.0	87.5	58.5	87.5	63.4	12.5	0.0	102.0	64.0	148.5	190.1	893.0
POTENTIAL EVAPOTRANSPIRATION (E_P), (mm)	11.4	26.3	58.1	88.9	122.9	153.2	176.7	148.3	93.5	48.8	17.0	6.7	951.8
P - E_P (mm)	-11.4	52.7	29.4	-30.4	-35.4	-89.8	-164.2	-148.3	8.5	15.2	131.5	183.4	–
RESERVED WATER (R), (mm)	88.6	100.0	100.0	69.6	34.1	0.0	0.0	0.0	8.5	23.7	100.0	100.0	–
ACTUAL EVAPOTRANSPIRATION (E_A), (mm)	11.4	26.3	58.1	88.9	123.0	97.5	12.5	0.0	93.5	48.8	17.0	6.7	583.7
WATER DEFICIT (mm)	0.0	0.0	0.0	0.0	0.0	55.6	164.2	148.3	0.0	0.0	0.0	0.0	368.2
EXCESS WATER (mm)	0.0	41.3	29.4	0.0	0.0	0.0	0.0	0.0	0.0	0.0	55.2	183.4	309.3
OVERLAND FLOW (mm)	52.8	47.0	38.2	19.1	9.1	4.8	2.4	1.2	0.6	0.3	27.6	105.5	308.6
PRECIPITATION-OVERLAND FLOW (mm)	-52.8	32.0	49.3	39.4	78.4	58.6	10.1	-1.2	101.4	63.7	120.9	84.6	584.5

Table A.17. Water budget of 2002

MONTHS	1	2	3	4	5	6	7	8	9	10	11	12	Σ
PRECIPITATION (P), (mm)	97.6	47.9	48.7	85.0	28.2	147.6	118.4	74.6	77.3	128.1	55.6	44.7	953.7
POTENTIAL EVAPOTRANSPIRATION (E_P), (mm)	9.8	27.4	60.3	86.6	142.1	159.1	175.6	136.7	92.5	51.8	15.7	4.5	962.1
P - E_P (mm)	87.8	20.5	-11.6	-1.6	-113.9	-11.5	-57.2	-62.1	-15.2	76.3	39.9	40.2	–
RESERVED WATER (R), (mm)	100.0	100.0	88.4	86.7	0.0	0.0	0.0	0.0	0.0	76.3	100.0	100.0	–
ACTUAL EVAPOTRANSPIRATION (E_A), (mm)	9.8	27.4	60.3	86.7	114.9	147.6	118.4	74.6	77.3	51.8	15.7	4.5	789.1
WATER DEFICIT (mm)	0.0	0.0	0.0	0.0	27.1	11.5	57.2	62.1	15.2	0.0	0.0	0.0	173.0
EXCESS WATER (mm)	87.8	20.5	0.0	0.0	0.0	0.0	0.0	0.0	0.0	0.0	16.1	40.2	164.6
OVERLAND FLOW (mm)	56.0	38.2	19.1	9.6	4.8	2.4	1.2	0.6	0.3	0.2	8.1	24.1	164.5
PRECIPITATION-OVERLAND FLOW (mm)	41.6	9.7	29.6	75.4	23.4	145.2	117.2	74.0	77.0	128.0	47.5	20.6	789.3

Table A.18. Water budget of 2003

MONTHS	1	2	3	4	5	6	7	8	9	10	11	12	Σ
PRECIPITATION (P), (mm)	151.3	65.2	81.1	45.8	16.9	0.0	69.9	11.8	64.0	84.4	96.5	104.4	791.3
POTENTIAL EVAPOTRANSPIRATION (E_P), (mm)	13.9	24.9	55.6	83.7	151.3	176.6	162.8	153.7	81.3	49.2	15.9	4.7	973.4
P - E_P (mm)	137.4	40.3	25.5	-37.9	-134.4	-176.6	-92.9	-141.9	-17.3	35.2	80.6	99.7	–
RESERVED WATER (R), (mm)	100.0	100.0	100.0	62.1	0.0	0.0	0.0	0.0	0.0	35.3	100.0	100.0	–
ACTUAL EVAPOTRANSPIRATION (E_A), (mm)	13.9	24.9	55.6	83.7	79.0	0.0	69.9	11.8	64.0	49.2	15.9	4.7	472.5
WATER DEFICIT (mm)	0.0	0.0	0.0	0.0	72.2	176.6	92.9	141.9	17.3	0.0	0.0	0.0	500.9
EXCESS WATER (mm)	137.4	40.3	25.5	0.0	0.0	0.0	0.0	0.0	0.0	0.0	15.9	99.7	318.8
OVERLAND FLOW (mm)	95.6	68.0	46.7	23.4	11.7	5.8	2.9	1.5	0.7	0.4	7.8	53.8	318.3
PRECIPITATION-OVERLAND FLOW (mm)	55.7	-2.8	34.4	22.4	5.2	-5.8	67.0	10.3	63.3	84.0	88.7	50.6	473.0

Table A.19. Water budget of 2004

MONTHS	1	2	3	4	5	6	7	8	9	10	11	12	Σ
PRECIPITATION (P), (mm)	133.0	172.6	107.5	40.3	59.9	126.9	17.3	192.3	36.2	30.8	108.8	100.8	1126.4
POTENTIAL EVAPOTRANSPIRATION (E_P), (mm)	11.5	24.8	59.3	89.3	131.0	150.1	181.0	132.7	97.1	55.3	17.0	4.0	953.2
P - E_P (mm)	121.5	147.8	48.2	-49.0	-71.1	-23.2	-163.7	59.6	-60.9	-24.5	91.8	96.8	–
RESERVED WATER (R), (mm)	100.0	100.0	100.0	51.0	0.0	0.0	0.0	59.6	0.0	0.0	91.8	100.0	–
ACTUAL EVAPOTRANSPIRATION (E_A), (mm)	11.5	24.8	59.3	89.3	110.9	126.9	17.3	132.7	95.8	30.8	17.0	4.0	720.3
WATER DEFICIT (mm)	0.0	0.0	0.0	0.0	20.1	23.2	163.7	0.0	1.4	24.5	0.0	0.0	232.9
EXCESS WATER (mm)	121.5	147.8	48.2	0.0	0.0	0.0	0.0	0.0	0.0	0.0	0.0	88.6	406.1
OVERLAND FLOW (mm)	82.9	115.4	81.8	40.9	20.4	10.2	5.1	2.6	1.3	0.6	0.3	44.3	405.8
PRECIPITATION-OVERLAND FLOW (mm)	50.1	57.3	25.7	-0.6	39.5	116.7	12.2	189.7	34.9	30.2	108.5	56.5	720.6

Table A.20. Water budget of 2005

MONTHS	1	2	3	4	5	6	7	8	9	10	11	12	Σ
PRECIPITATION (P), (mm)	129.0	51.8	133.7	114.6	47.1	160.3	53.7	1.6	85.6	173.8	117.6	92.4	1161.2
POTENTIAL EVAPOTRANSPIRATION (E_P), (mm)	11.2	26.1	56.0	86.4	125.2	155.1	175.0	147.3	92.0	46.1	18.1	6.5	945.0
P - E_P (mm)	117.8	25.7	77.7	28.2	-78.1	5.2	-121.3	-145.7	-6.4	127.7	99.5	85.9	–
RESERVED WATER (R), (mm)	100.0	100.0	100.0	100.0	22.0	27.1	0.0	0.0	0.0	100.0	100.0	100.0	–
ACTUAL EVAPOTRANSPIRATION (E_A), (mm)	11.2	26.1	56.0	86.4	125.2	155.1	80.8	1.6	85.6	46.1	18.1	6.5	698.8
WATER DEFICIT (mm)	0.0	0.0	0.0	0.0	0.0	0.0	94.2	145.7	6.4	0.0	0.0	0.0	246.3
EXCESS WATER (mm)	117.8	25.7	77.7	28.2	0.0	0.0	0.0	0.0	0.0	27.7	99.5	85.9	462.5
OVERLAND FLOW (mm)	94.5	60.1	68.9	48.6	24.3	12.1	6.1	3.0	1.5	13.9	56.7	71.3	460.9
PRECIPITATION-OVERLAND FLOW (mm)	34.5	-8.3	64.8	66.1	22.8	148.2	47.6	-1.4	84.1	159.9	60.9	21.1	700.3

Table A.21. Water budget of 2006

MONTHS	**1**	**2**	**3**	**4**	**5**	**6**	**7**	**8**	**9**	**10**	**11**	**12**	**Σ**
PRECIPITATION (P), (mm)	97.9	146.0	58.1	2.5	41.7	66.6	3.5	2.0	96.1	61.9	179.9	69.0	825.2
POTENTIAL EVAPOTRANSPIRATION (E_P), (mm)	11.5	25.7	56.4	89.6	128.0	160.2	170.1	153.6	90.4	49.7	15.0	2.7	952.9
P - E_P (mm)	86.4	120.3	1.7	-87.1	-86.3	-93.6	-166.6	-151.6	5.7	12.2	164.9	66.3	–
RESERVED WATER (R), (mm)	100.0	100.0	100.0	12.9	0.0	0.0	0.0	0.0	5.7	17.9	100.0	100.0	–
ACTUAL EVAPOTRANSPIRATION (E_A), (mm)	11.5	25.7	56.4	89.6	54.6	66.6	3.5	2.0	90.4	49.7	15.0	2.7	467.7
WATER DEFICIT (mm)	0.0	0.0	0.0	0.0	73.4	93.6	166.6	151.6	0.0	0.0	0.0	0.0	485.2
EXCESS WATER (mm)	86.4	120.3	1.8	0.0	0.0	0.0	0.0	0.0	0.0	0.0	82.8	66.3	357.5
OVERLAND FLOW (mm)	70.1	95.2	48.5	24.2	12.1	6.1	3.0	1.5	0.8	0.4	41.4	53.8	357.1
PRECIPITATION-OVERLAND FLOW (mm)	27.8	50.8	9.6	-21.7	29.6	60.5	0.5	0.5	95.3	61.5	138.5	15.2	468.1

APPENDIX B: LAND USE CHANGE BETWEEN 1986 AND 2006

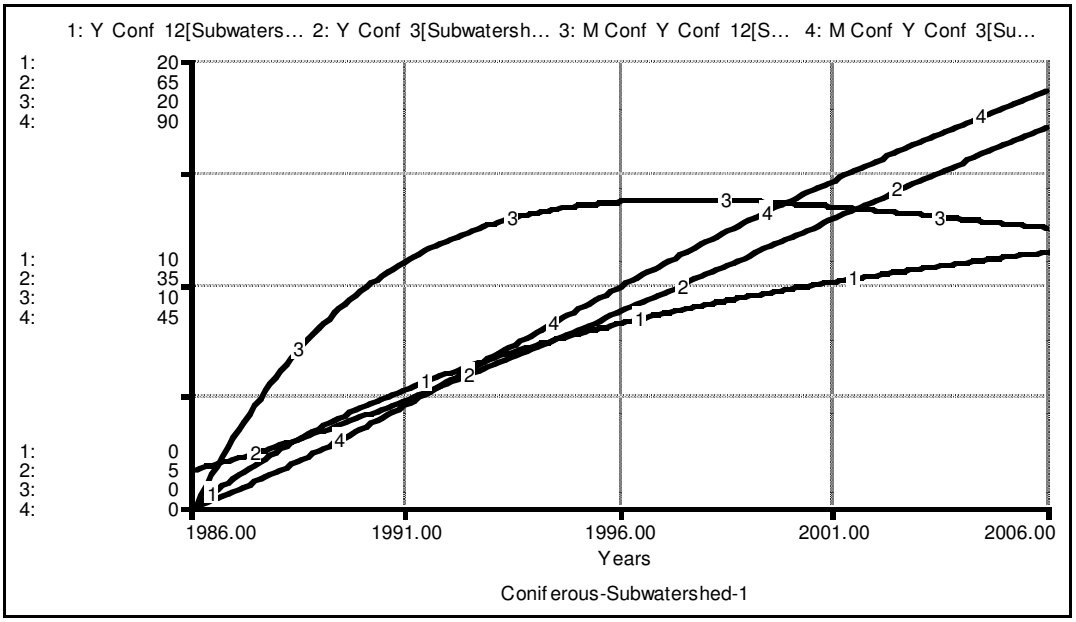

Figure B.1. Simulation of the young coniferous stands, Subwatershed 1

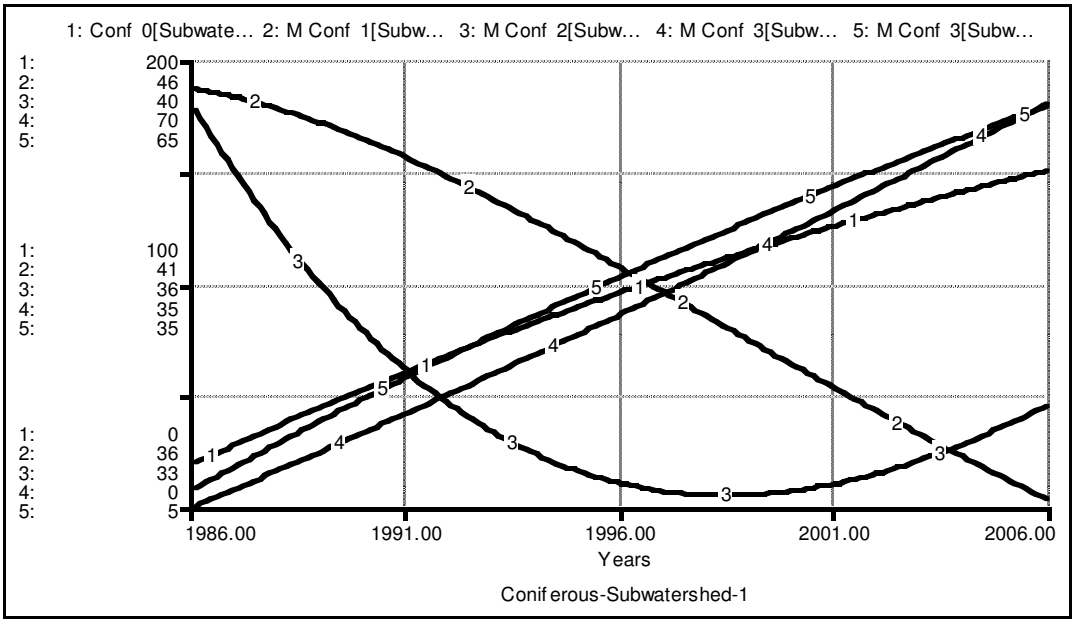

Figure B.2. Simulation of the mature coniferous stands, Subwatershed 1

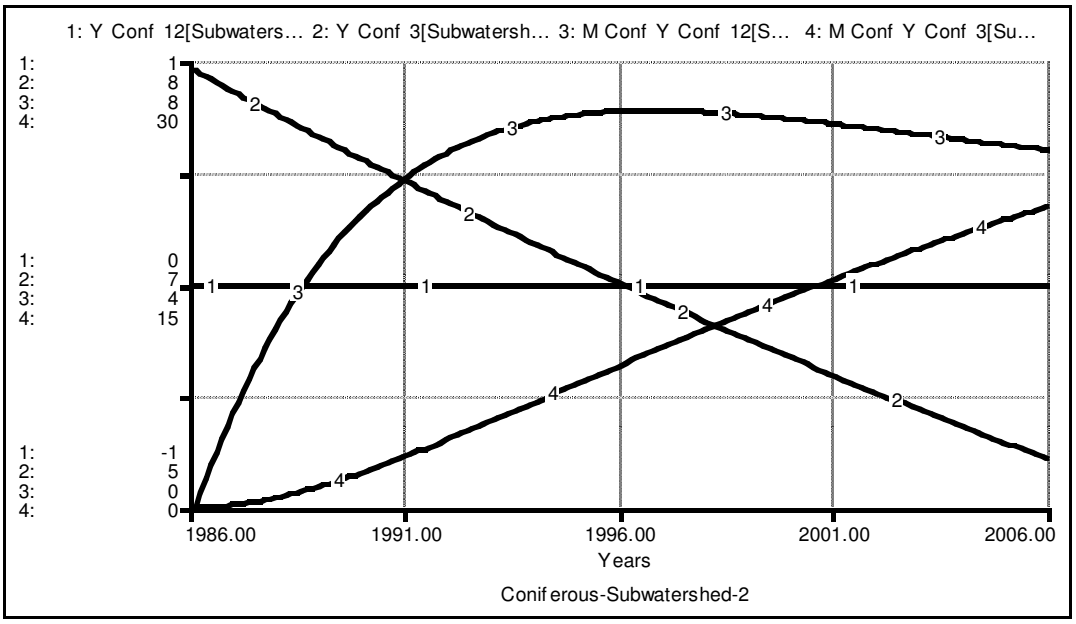

Figure B.3. Simulation of the young coniferous stands, Subwatershed 2

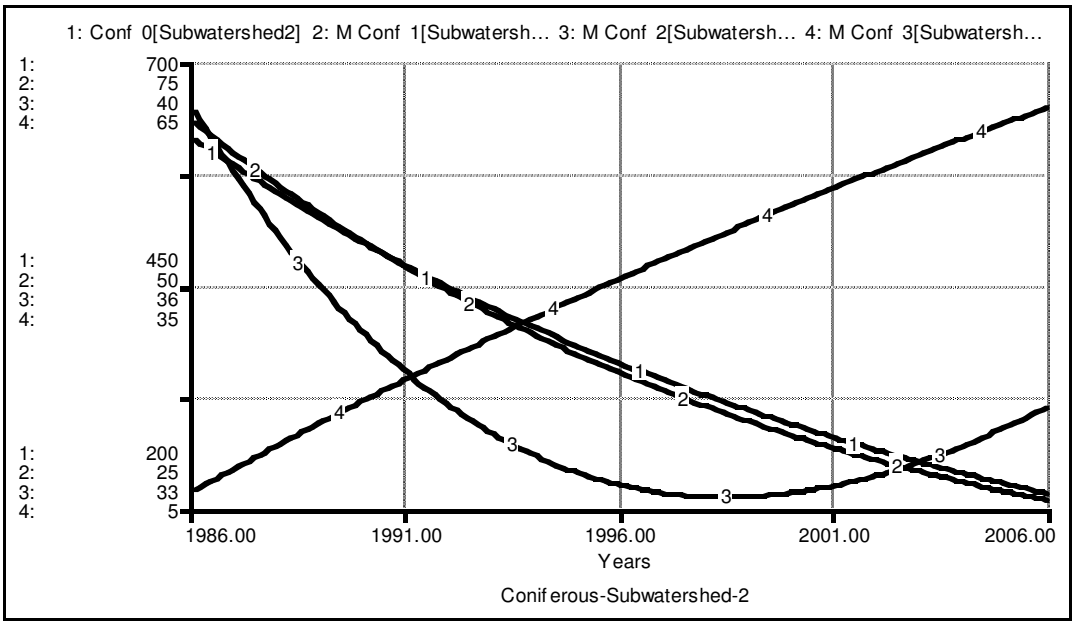

Figure B.4. Simulation of the mature coniferous stands, Subwatershed 2

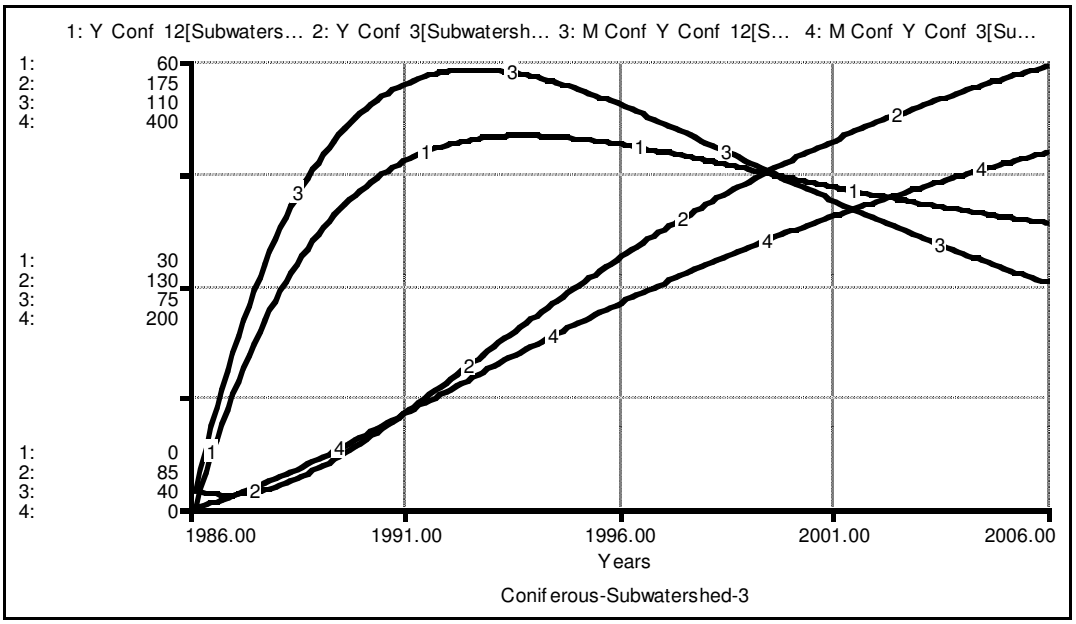

Figure B.5. Simulation of the young coniferous stands, Subwatershed 3

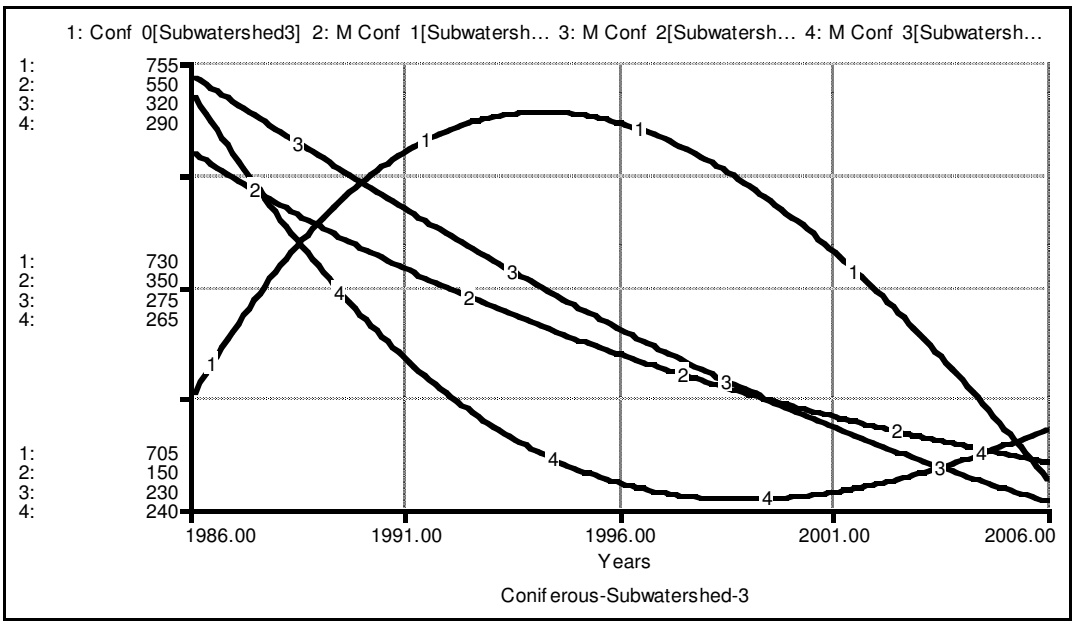

Figure B.6. Simulation of the mature coniferous stands, Subwatershed 3

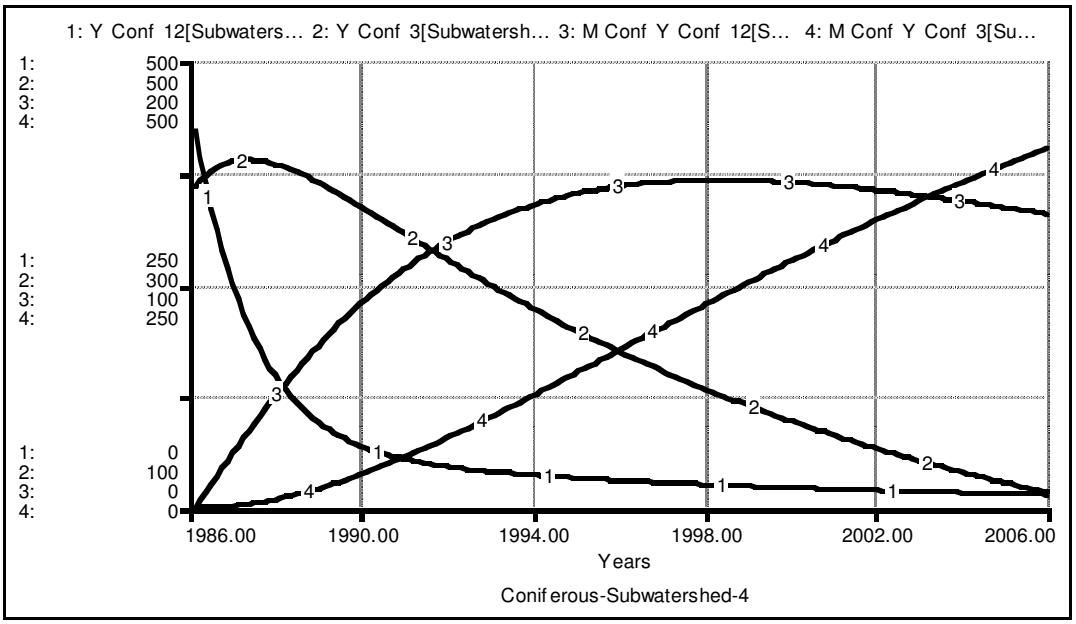

Figure B.7. Simulation of the young coniferous stands, Subwatershed 4

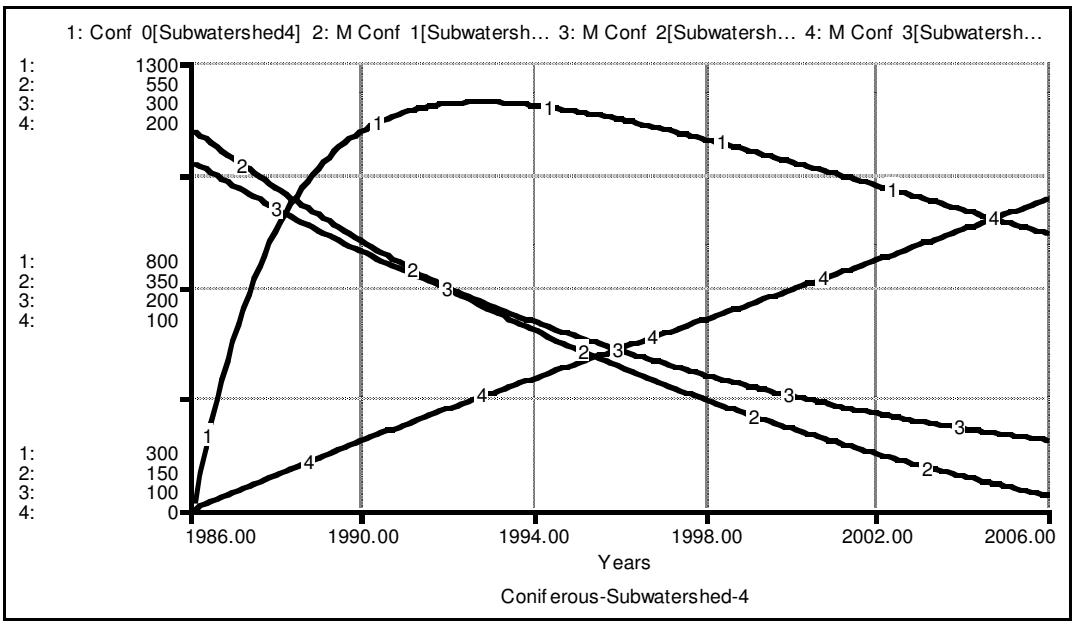

Figure B.8. Simulation of the mature coniferous stands, Subwatershed 4

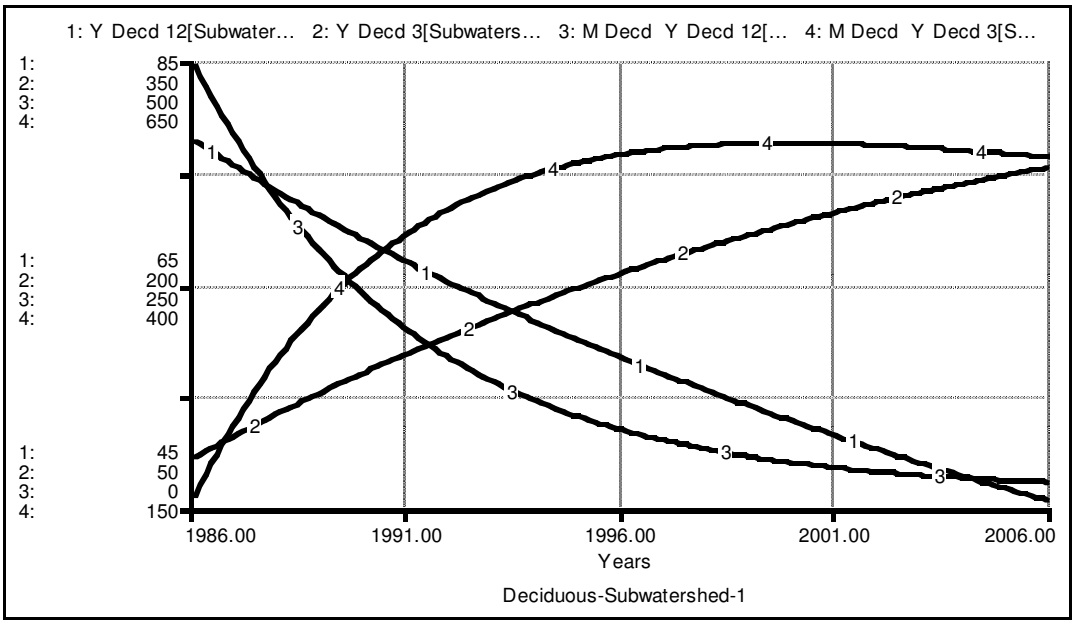

Figure B.9. Simulation of the young deciduous stands, Subwatershed 1

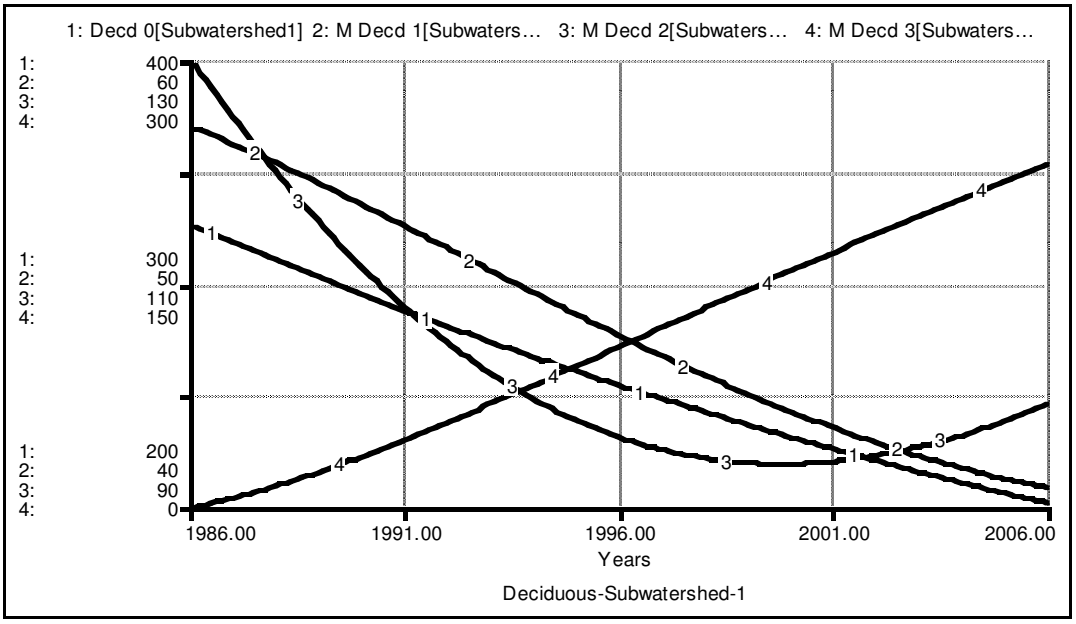

Figure B.10. Simulation of the mature deciduous stands, Subwatershed 1

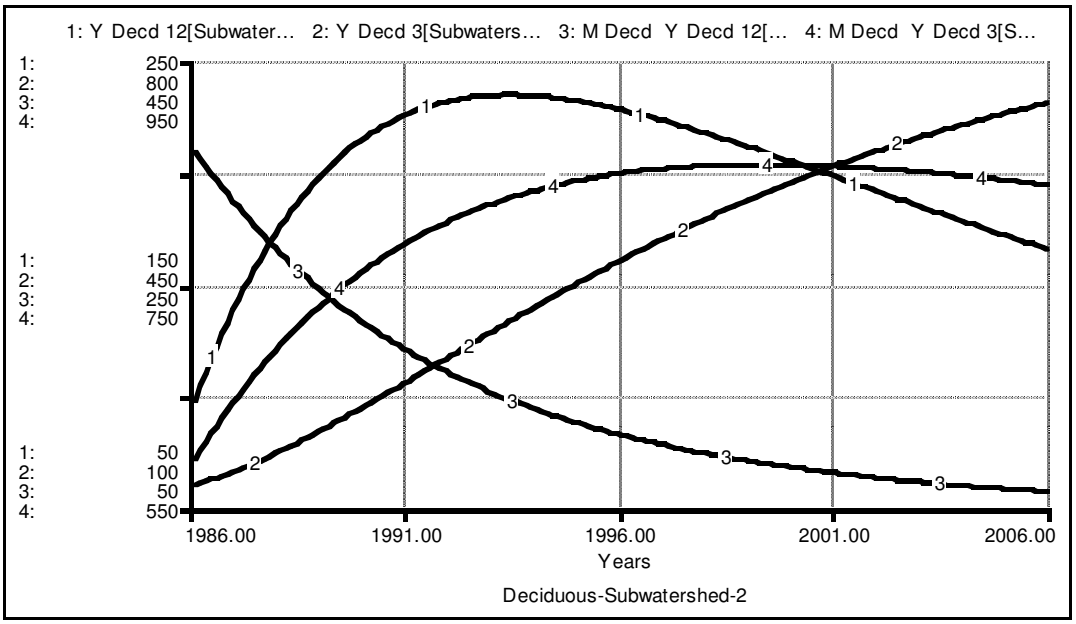

Figure B.11. Simulation of the young deciduous stands, Subwatershed 2

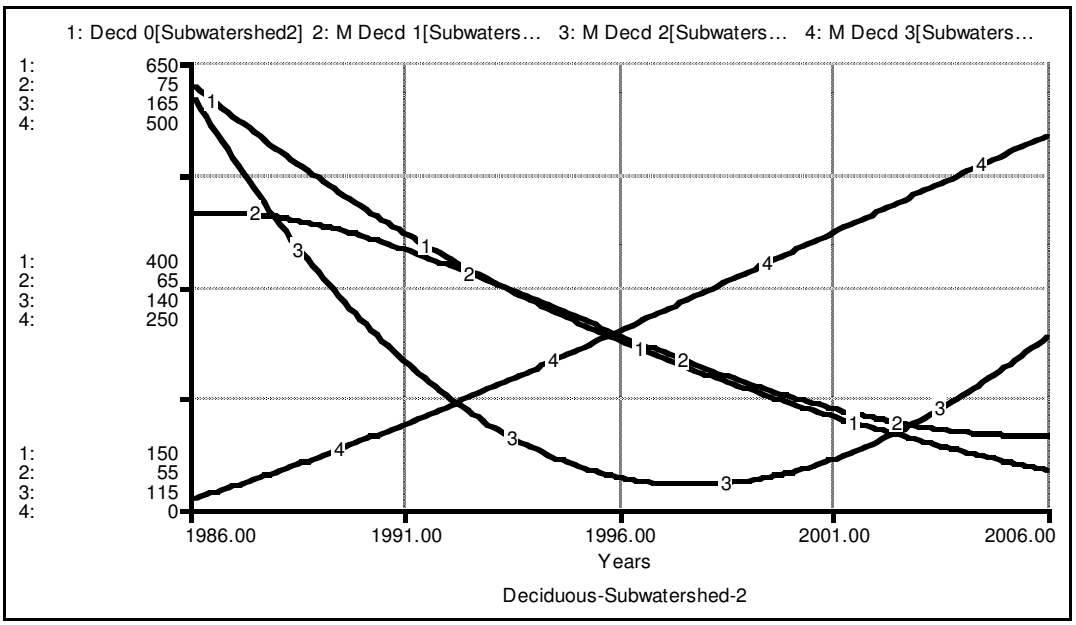

Figure B.12. Simulation of the mature deciduous stands, Subwatershed 2

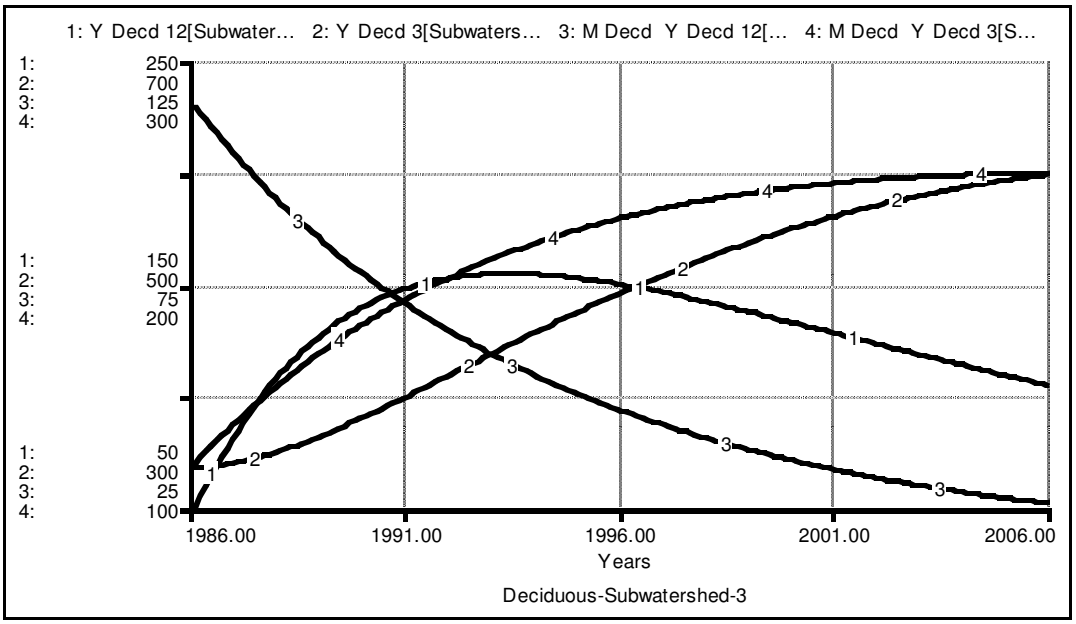

Figure B.13. Simulation of the young deciduous stands, Subwatershed 3

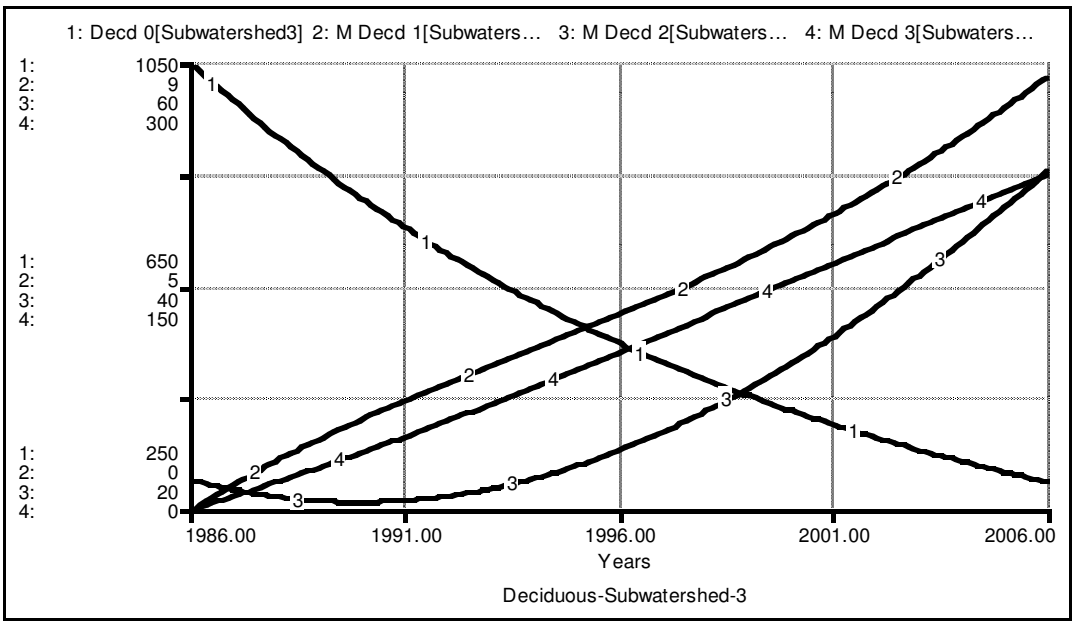

Figure B.14. Simulation of the mature deciduous stands, Subwatershed 3

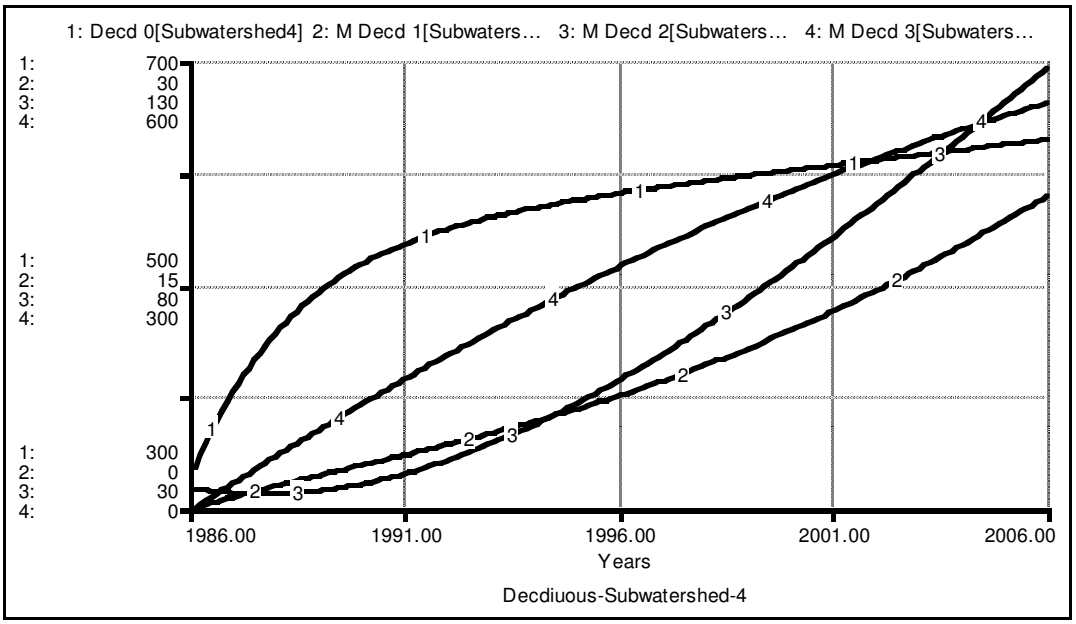

Figure B.15. Simulation of the young deciduous stands, Subwatershed 4

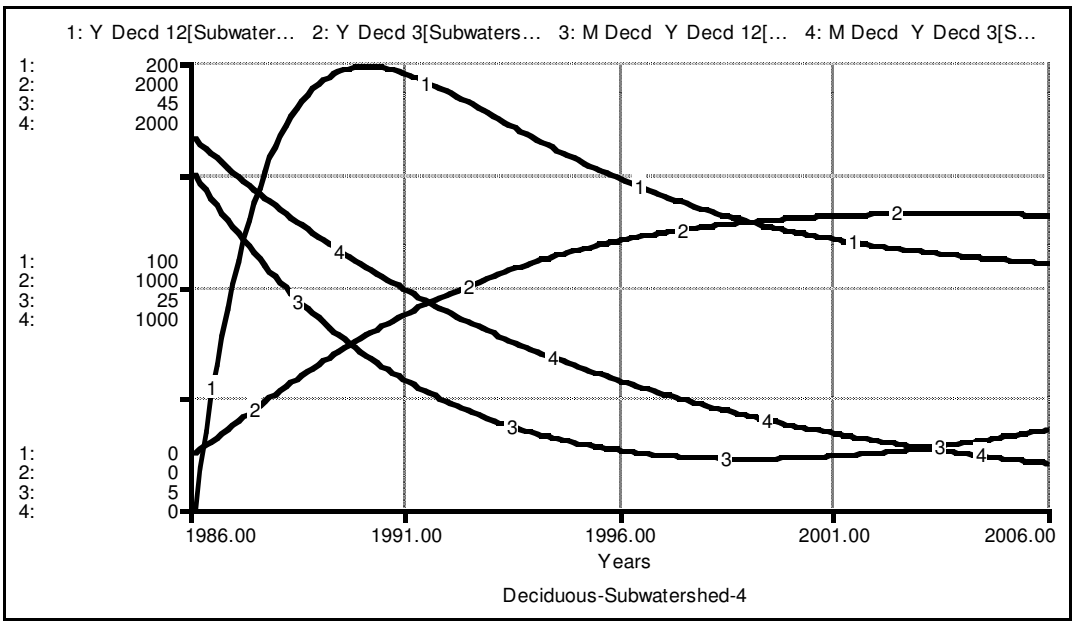

Figure B.16. Simulation of the mature deciduous stands, Subwatershed 4

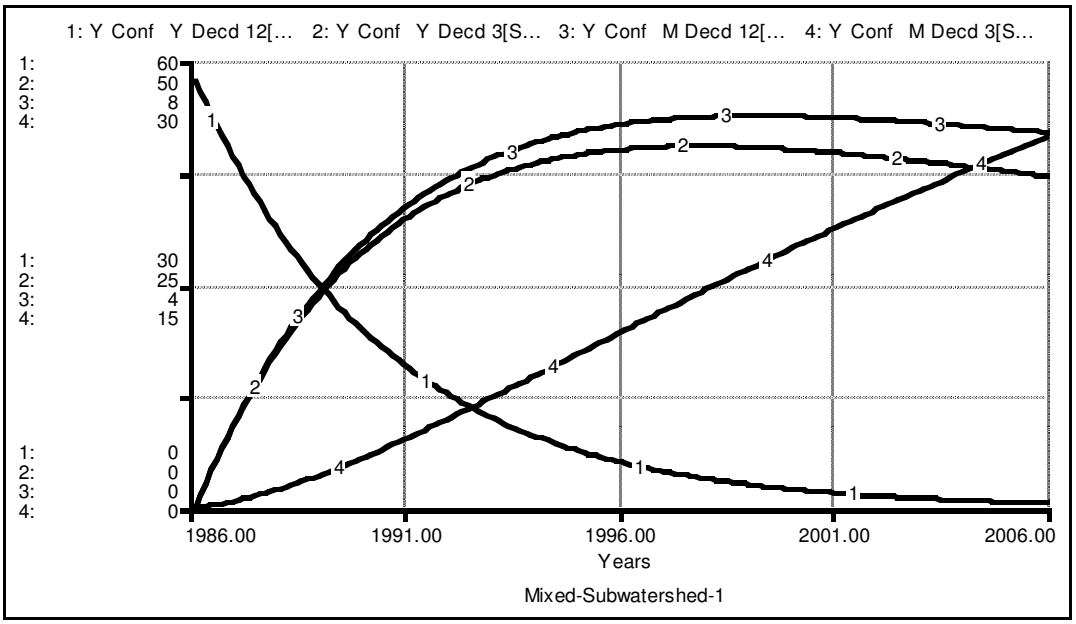

Figure B.17. Simulation of the young mixed stands, Subwatershed 1

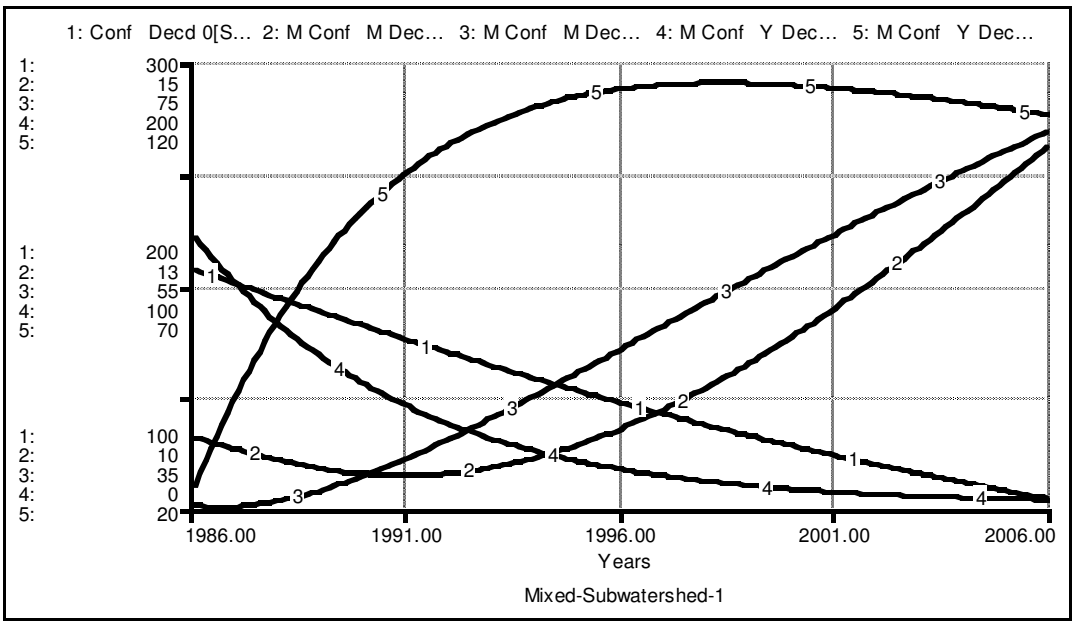

Figure B.18. Simulation of the mature mixed stands, Subwatershed 1

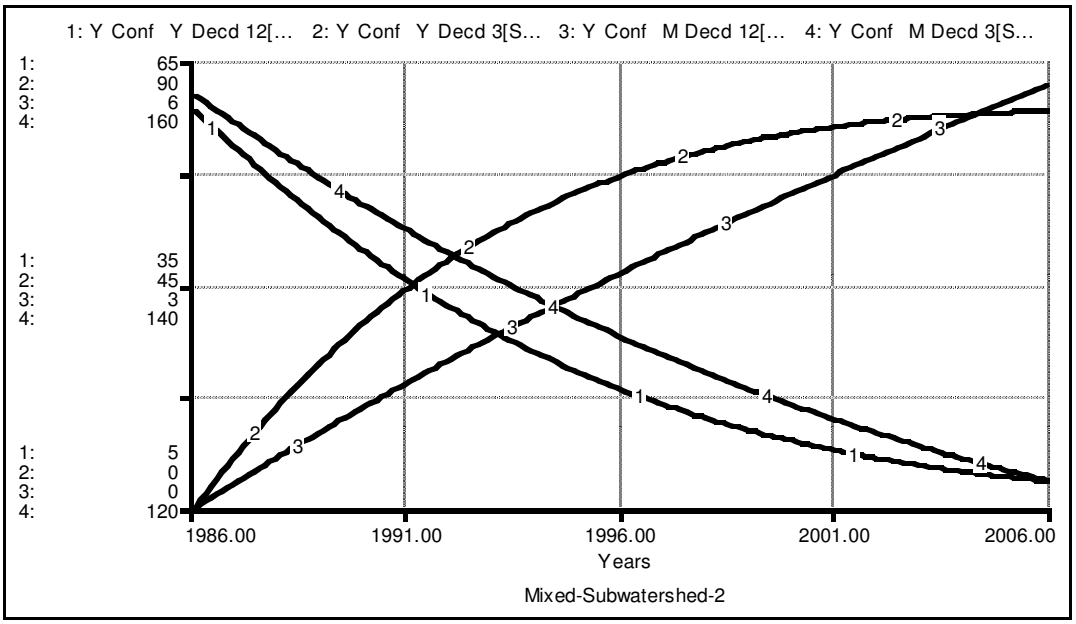

Figure B.19. Simulation of the young mixed stands, Subwatershed 2

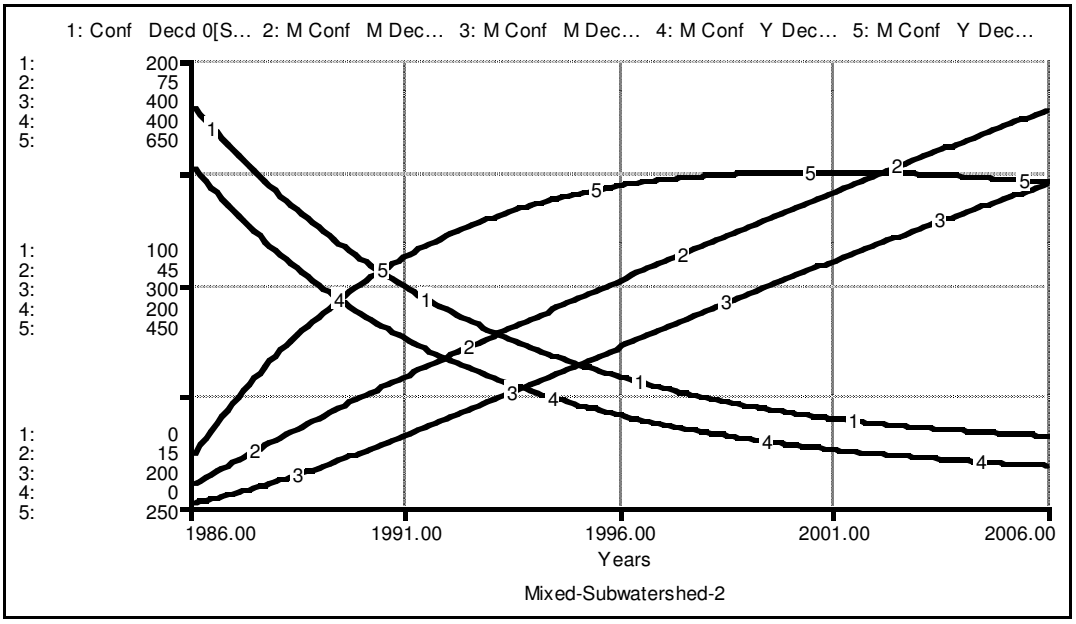

Figure B.20. Simulation of the mature mixed stands, Subwatershed 2

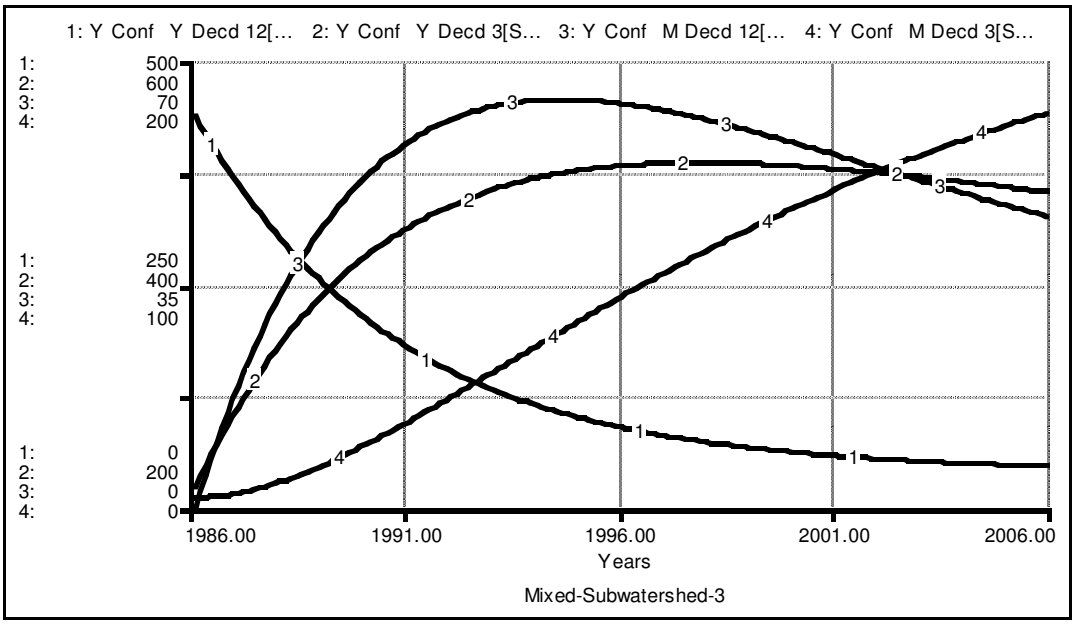

Figure B.21. Simulation of the young mixed stands, Subwatershed 3

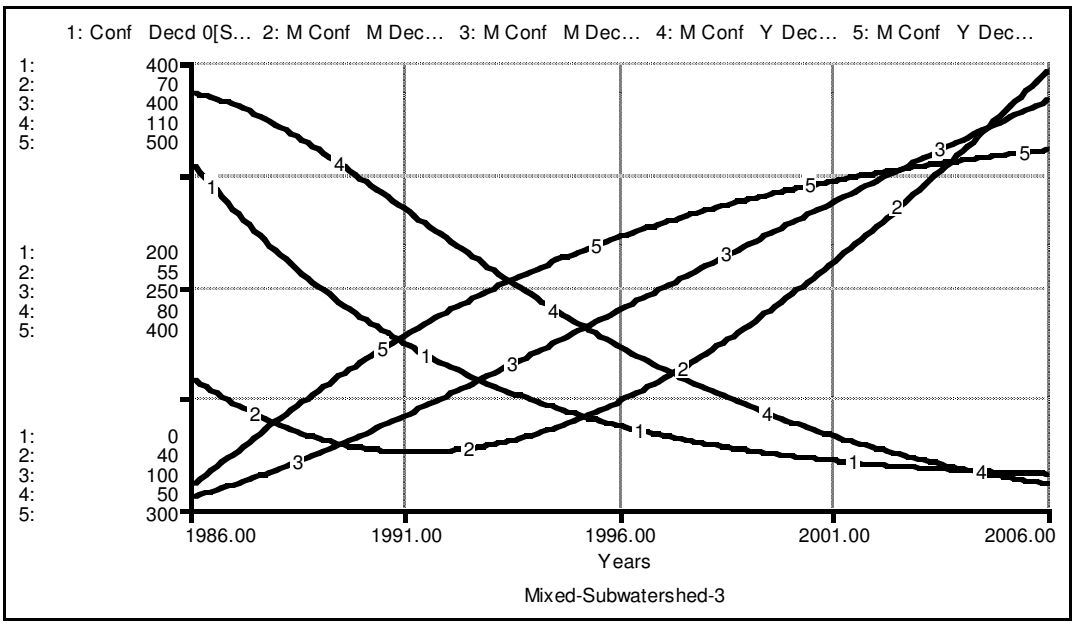

Figure B.22. Simulation of the mature mixed stands, Subwatershed 3

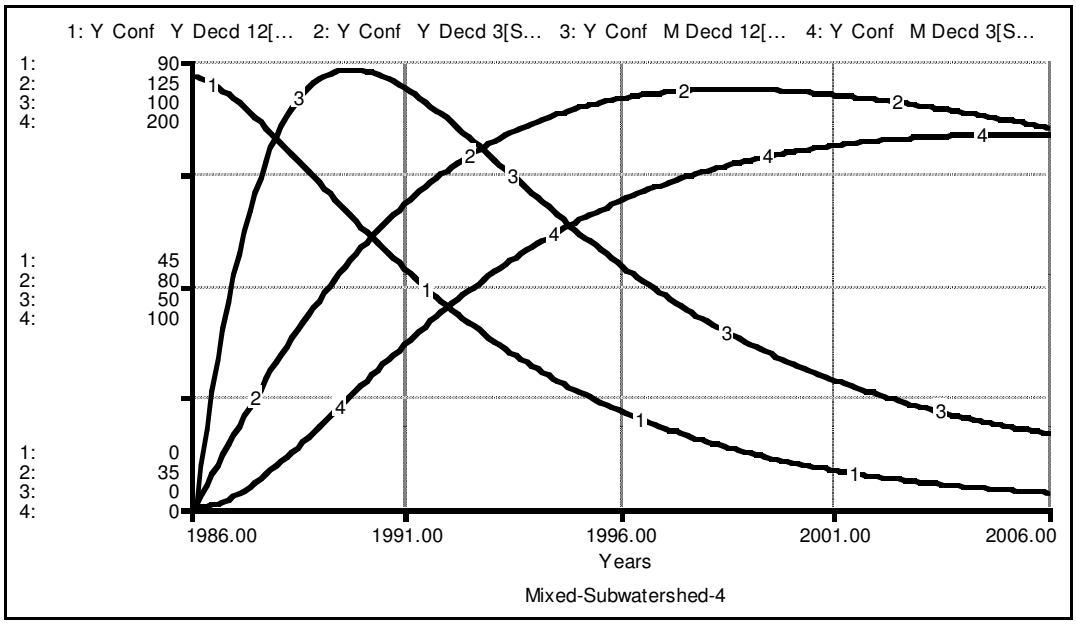

Figure B.23. Simulation of the young mixed stands, Subwatershed 4

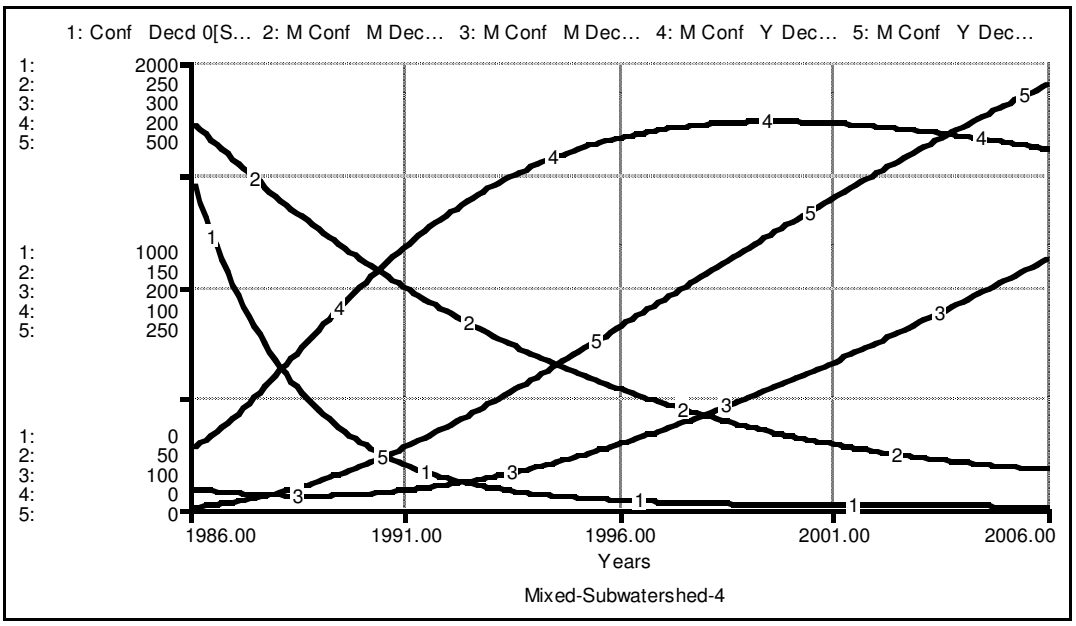

Figure B.24. Simulation of the mature mixed stands, Subwatershed 4

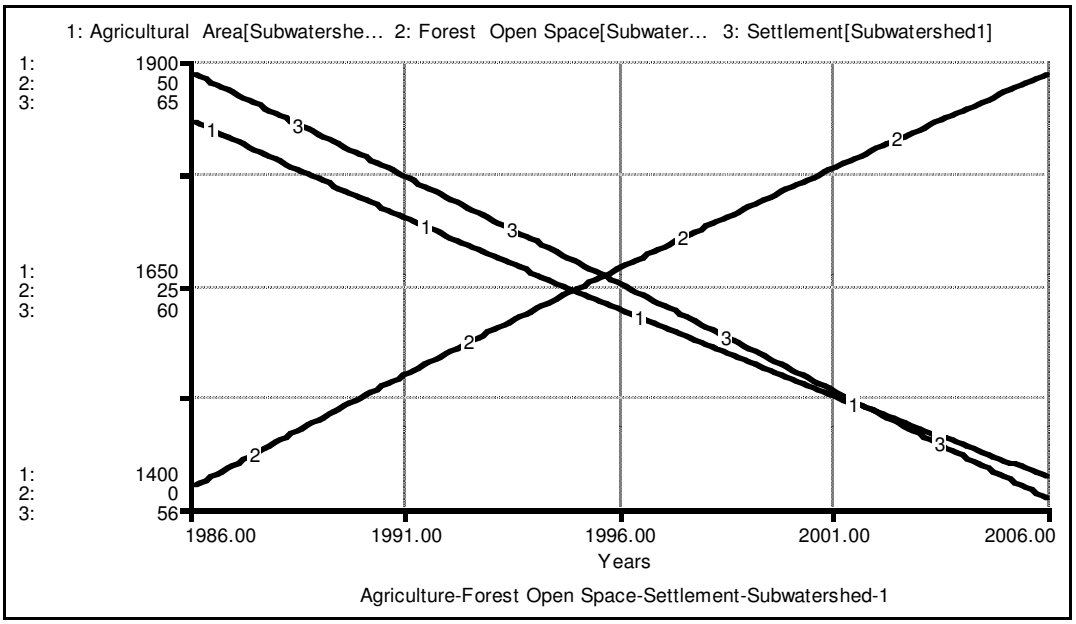

Figure B.25. Simulation of the agricultural area, forest open space and settlement, Subwatershed 1

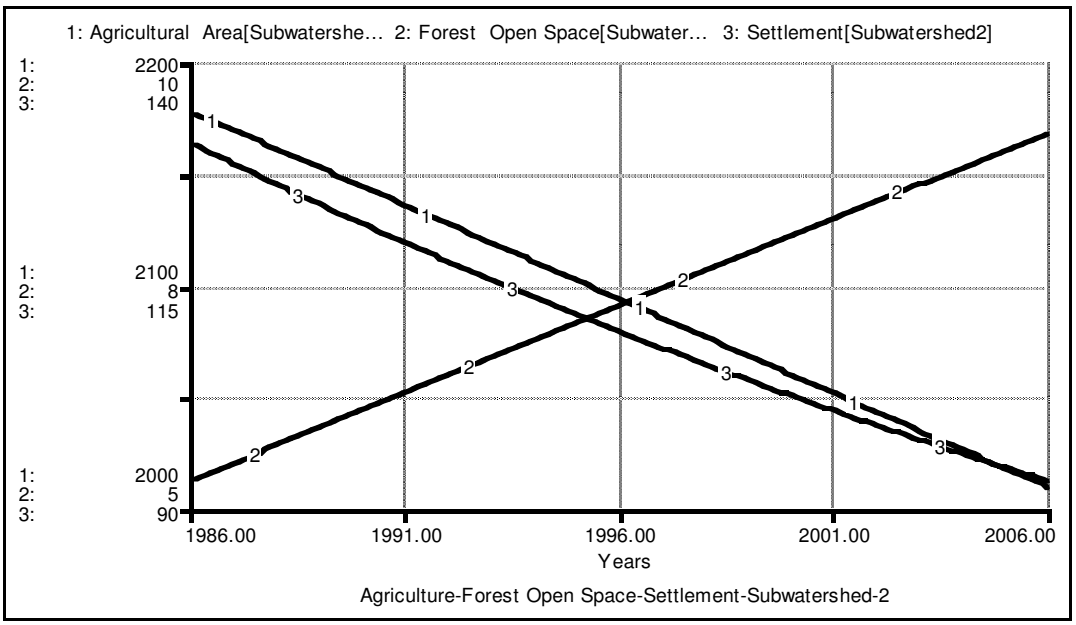

Figure B.26. Simulation of the agricultural area, forest open space and settlement, Subwatershed 2

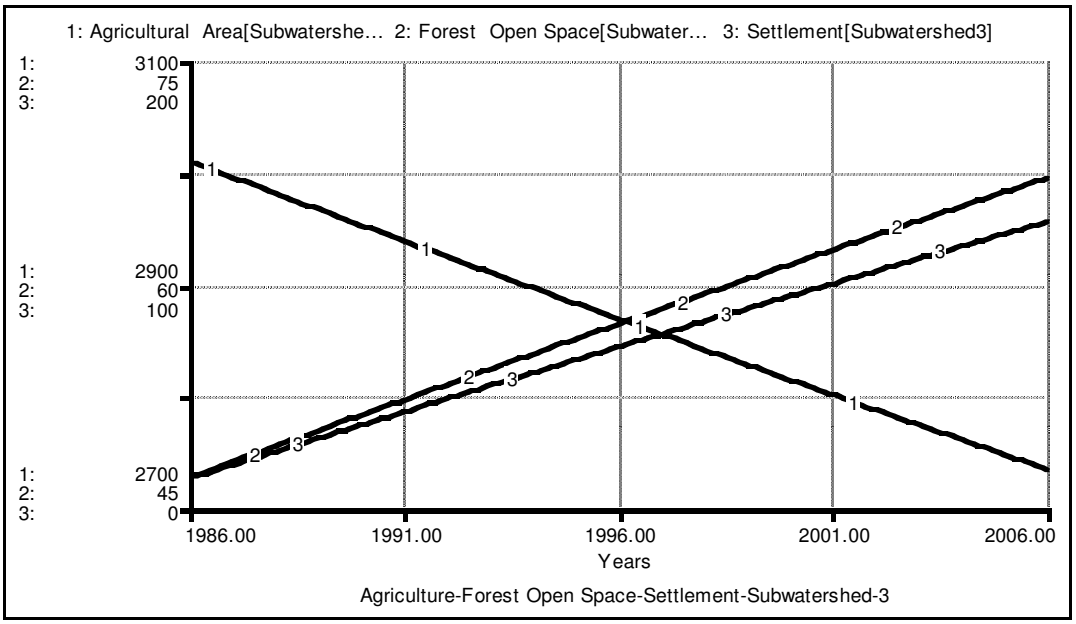

Figure B.27. Simulation of the agricultural area, forest open space and settlement, Subwatershed 3

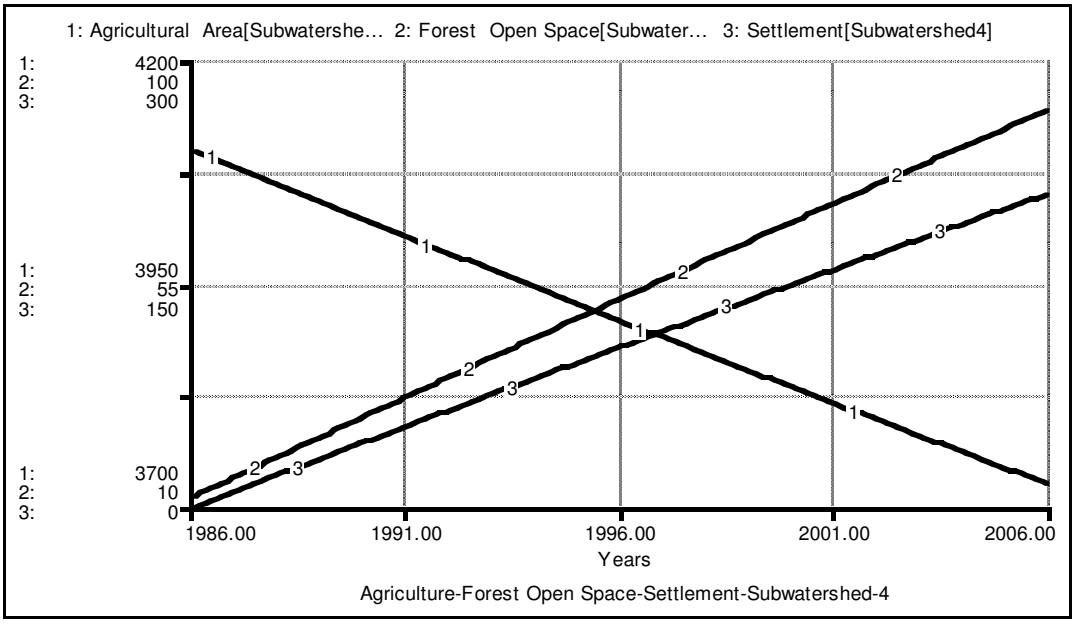

Figure B.28. Simulation of the agricultural area, forest open space and settlement, Subwatershed 4